Platinum-group mineralogy of PGE-Au placers of the southern Far East, Russia

Dissertation
for acquisition of a degree of Doctor in Natural Sciences

presented by
Galina G. Shcheka
from Moscow (Russia)

Approved by
the Faculty of Mathematics and Natural Sciences of
Technical University of Clausthal

Day of examination:
31 March 2005

Platingruppen-Mineralogie von PGE-Gold-Seifen im südlichen Fernen Osten von Russland

Dissertation
zur Erlangung des Grades eines Doktors der Naturwissenschaften

vorgelegt von
Galina G. Shcheka
aus Moskau (Russland)

Genehmigt von der
Mathematisch-Naturwissenschaftlichen Fakultät
der Technischen Universität Clausthal

Tag der mündlichen Prüfung:
31. März 2005

This dissertation was undertaken at the Economic Geology Group of the Institute of Mineralogy and Mineral Resources of Technical University of Clausthal.

Dean: Prof. Dr. D. Mayer
Supervisor: Prof. Dr. B. Lehmann
Co-supervisor: Prof. Dr. K. Mengel

Die vorliegende Arbeit wurde an der Abteilung Lagerstättenforschung des Instituts für Mineralogie und Mineralische Rohstoffe der Technischen Universität Clausthal angefertigt.

Dekan: Prof. Dr. D. Mayer
Referent: Prof. Dr. B. Lehmann
Korreferent: Prof. Dr. K. Mengel

ACKNOWLEDGEMENTS

I am particularly grateful to Prof. Bernd Lehmann for kind supervision of this dissertation, which demanded from him a lot of patience, endurance, self-restrain and time.

Prof. Kurt Mengel is sincerely thanked for his acceptance to review my thesis.

Deep appreciation is given to Klaus Hermann, who was alongside all these years and managed to carry out excellent technical support during electron microprobe analysis. To make this research without his help would have been not possible. At the beginning of the study, Dr. Karsten Gömann had also taken part in microprobe survey and is very thanked for.

I am very thankful to the staff of the Institute of Mineralogy and Mineral Resources, TU Clausthal, for their friendly relationship and readiness to help, namely
Dr. Eike Gierth for the help with ore microscopy;
Ulf Hemmerling for sample preparation;
Fred Türck for computer assistance and
Helga Vollbrecht for organizational and moral support.

I also greatly acknowledge Frank Sandhagen (Geological Institute, Clausthal) for help with scanning electron microscopy;
Dr. Alex Wallianos (Max-Planck Institute for Nuclear Physics, Heidelberg) for providing the proton induced X-ray analysis;
Drs. Anna Bieniok and Dan Topa (Institute of Mineralogy, Salzburg) for the help with X-ray diffraction analysis;
Gilles Laflamme (CANMET, Ottawa) for some control microprobe analyses;
Alexandr A. Vrzhosek, Prof. Sergey A. Shcheka, Prof. Sergey V. Vysotskiy and Dr. Alexandr N. Solianik (Far East Geological Institute, Vladivostok) for providing sample material and helpful remarks on some parts of the dissertation.

Galina G. Shcheka

TABLE OF CONTENTS

0 ABSTRACT

Platinum placer deposits associated with zoned ultramafic intrusions (Uralian-/Alaskan-type complexes with dunitic core and clinopyroxenite rim) are historically of great economic importance and are currently regaining in interest due to new discoveries in the Russian Far East. Heavy-mineral concentrates from five PGE-Au placers were studied for their magmatic (primary) platinum-group minerals (PGM) and their alteration (secondary) products. These placers are: Zolotaya, Fadeevka, and Kedrovka in the Paleozoic foldbelt of southern Primorye, and Darya and Kondyor in the Archean Aldan Shield, Siberian Platform, Khabarovskiy Krai. The placers are mostly derived from Paleozoic/Mesozoic multiple intrusion complexes of Uralian/Alaskan-type with late alkaline felsic intrusions.

The detailed PGM mineralogy of the Zolotaya and Fadeevka river placers is based on more than 150 hand-picked mineral grains from alluvial heavy-mineral concentrates. The dominant PGM phase is Pt-Fe alloy, with the remainder consisting of Os-Ir (+Pt+Ru) alloys. A broad spectrum of PGE-bearing sulfides, sulfarsenides, arsenides, tellurides, bismuthides, antimonides, and Au-bearing alloy occurs as inclusions or rims within/on the PGE alloy phases. Multiphase inclusion assemblages (predominantly sulfides) in the alloy matrix are of likely primary origin; whereas rims and replacement aggregates are formed by hydrothermal overprint. This hydrothermal overprint assemblage is represented by cooperite [PtS], sperrylite [$PtAs_2$], kashinite [$(Ir,Rh)_2S_3$], $(Rh,Pt)_3S_4$ phase, cuprorhodsite-cuproiridsite-malanite group [$CuRh_2S_4$-$CuIr_2S_4$-$CuPt_2S_4$], minerals of the platarsite-hollingworthite-irarsite solid solution [$Pt(As,S)_2$-$Rh(As,S)_2$-$Ir(As,S)_2$)], stumpflite [Pt(Sb,Bi)], mertieite-II [Pd_8Sb_3], Sb-bearing irarsite [IrAs(Sb)S], Ir(Pt)Te(As,Sb) phase, tolovkite [IrSbS], maslovite [PtTeBi], $(Ir,Os)_7As_3$, $(Ir,Os)_2As_3$, IrAsSb phase, and Au-Ag alloy. Geological, mineralogical and chemical observations point to a connection of the Zolotaya and Fadeevka placers to Late Permian dunite-hornblendite-gabbro intrusions of Uralian/Alaskan-type. Particularly, the composition of chromite from heavy-mineral concentrates and from inclusions within PGM from the Zolotaya placer is typical of Uralian/Alaskan-type intrusions, i.e., high chromium and iron content at relatively low titanium content.

First mineralogical and chemical data on a new PGM discovery at the Kedrovka river placer are based on samples from a field expedition in summer 2000. The preliminary examination of the PGM association shows the absence of Pt-Fe alloys and refractory PGE as major PGM phases, and a spinel composition which excludes an origin from Uralian-/Alaskan-type intrusions. The alluvial PGM of the Kedrovka River are probably derived from Paleozoic ophiolites.

The study of PGM occurrences in the Aldan Shield is focused on a particular mineralogical feature, i.e. the occurrence of exotic euhedral coarse-grained Pt-Fe alloy (up to several cm large)

and other PGM, together with gold mineralization. The best documented example is the alluvial Kondyor PGE-Au deposit, located within a Mesozoic alkaline ultramafic ring complex. The Pt-Fe alloy macrocrystals have unusual trace-element composition, i.e. very low in PGE other than the main mineral component, and elevated contents of Sb and Sn, as derived from electron microprobe and reconnaissance proton microprobe analysis. The Pt-Fe alloy phases occur in association with a complex reaction mineral assemblage composed of Pd- and Pt-bearing antimonides, arsenides, bismuthides, tellurides, sulfides and intermetallic compounds with Au, Cu, Pb, Sn, Hg.

A heavy-mineral concentrate from the Darya river, 75 km SW of Kondyor, yielded a similar PGM assemblage, with the first occurrence of a macrocrystal assemblage composed of ferroan platinum, plus idiomorphic crystals (mm size) of cooperite and mertieite-II. The origin of the unique macrocrystals from the Kondyor and Darya deposits is little understood, and may be related to late-magmatic hydrous overprint.

1 INTRODUCTION

Platinum was discovered in the early 18th century during colonial gold panning in the Choco province of Colombia. The metal resembled native silver and was called "little silver" ("platina" from Spanish "plata" = silver). However, platinum was apparently known for much longer time, as artefacts from ancient Egypt, and the Roman and Inca cultures suggest. The first published reference to platinum was made in 1748 by Don Antonio de Ulloa y Gracia de la Torre, in the description of a journey to Peru, where he mentioned "*Platino del Pinto*", which occurs together with gold in gravels of the river Pinto, New Granada (now Colombia) in South America. The English physicist Sir William Watson described it in 1750 as a new "semi-metal or metalloid". The subsequent study of platinum-bearing samples in the early 19th century identified a complex mixture of several similar metals, namely platinum, osmium, iridium, ruthenium, rhodium, and palladium, which all together constitute the platinum-group elements (PGEs).

Large alluvial platinum deposits were discovered in the central Ural Mountains in 1823, which soon became the world's dominant source of platinum until the end of the 1920s. About 300 t of PGE were produced in about 100 years (Vysotskiy 1925), which corresponds to less than the annual PGE mine production of today.

Placer PGE deposits were slowly replaced by primary PGE deposits, when the "Merensky Reef" in the Bushveld Complex (South Africa), and the Norilsk district (Russia) were discovered and developed in the late 1920s to 1940s. Industrial demand for PGE was very limited until about 30 years ago when autocatalysts were first developed. The autocatalyst market currently dominates the demand for palladium (70-80 %) and rhodium (90 %), and uses about 40 % of the platinum produced. Platinum has also become important in jewellery, where another 40 % of the Pt production is used. The remainder has a wide range of modern industrial applications, with possibly the fuel-cell technology the most important future market. The other PGEs (Os, Ir, Ru) are produced in very limited quantities (a few tons to a few tens of tons per year), and have mainly applications in high-strength high-temperature superalloys.

The current PGE market is dominated by only two major areas of production, both characterized by extensive continental mafic-ultramafic magmatism and PGE enrichment in immiscible sulfide melt:

(1) Noril'sk district, Siberia, Russia: The massive sulfide ore of the Norilsk district, with the Oktyabrsky mine the most important, has a resource tonnage of about 1 Gt with around 10 g/t

PGE (Pd/Pt 3-4), 1.8 % Ni and 3.0 % Cu, and produces currently about 20 % of the world's nickel, as well as 60 % of Pd and 20 % Pt (Yakubchuk and Nikishin 2004; Johnson Matthey 2004). The Ni-Cu-PGE mineralization occurs in 250-Ma-old mafic intrusions which are rift-controlled feeders to the Permo-Triassic flood basalts of the Siberian superplume province (Yakubchuk and Nikishin 2004).

(2) Bushveld complex, South Africa: 75 % of the world's Pt production and 30 % of Pd production is from magmatic ore in the 2-Ga-old Bushveld layered mafic intrusion. PGE mineralization is bound to several chromite-rich orthopyroxene-plagioclase horizons within the gabbro sequence of the "Critical Zone", with the "Merensky Reef" the most well known (about 5-10 g/t PGE (Pd/Pt 0.5).

About 5 % of the current Russian PGE production is from placers discovered and developed in the 1980s only. These placers are in the Russian Far East, with the Kondyor alluvial mine (3-4 t Pt/year) in the Aldan Shield, and the Koryak alluvial mine (about 2 t Pt/year) on the Kamchatka Peninsula (Johnson Matthey 2004).

The mineralogy and geological background of PGE placers is distinctly different from the primary magmatic sulfide-bound PGE mineralization of the Noril'sk or Bushveld type. PGE placers are dominated by platinum in the mineralogical form of ferroplatinum alloy, i.e. sulfides are absent or rare. This reflects the primary magmatic mineralogy of the source rocks, which are also distinctly different from layered mafic intrusions or feeder intrusions of flood basalts. Platinum placers are mainly associated with Paleozoic/Mesozoic zoned ultramafic intrusions of the so-called "Uralian/Alaskan-type". Uralian/Alaskan complexes world-wide display a concentrical zoning pattern with ultramafic-mafic rock units, are often pipe-like with less than 80 km^2 in size, and occur either in an anorogenic setting within stable platforms, i.e. no deformation (Aldan Shield: Kondyor, Inagli), or in mobile belts and then are more or less deformed and tectonically dismembered (Urals, Tulameen, Alaska, Ethiopia, Colombia).

Some main features of Uralian/Alaskan complexes are (Taylor 1967; Johan 2002):

- Dunite core and clinopyroxenite rim
- General absence of orthopyroxene and plagioclase
- Highly magnesian olivine in dunites (Fo_{93})
- Clinopyroxenite composition is exclusively that of diopside

- Occurrence of chromite exclusively in dunite, either as accessory mineral or in local segregations (“schlieren”)
- High magnetite content (15-20 vol.% of the rock)
- The PGE mineralogy is dominated by Pt-Fe alloy, and PGE-sulfur compounds are rare.

The mineralogy implies that Uralian/Alaskan-type intrusions are characterized by low sulfur and high oxygen fugacity. It should be noted that both mineralogical and petrological information on Uralian/Alaskan-type intrusions and their PGE mineralization is scanty. In particular, information on PGE mineralization in Russia was and is still largely confidential.

This dissertation is a contribution to the mineralogical investigation of Russian PGE placer deposits, and is focused on the detailed mineralogical description of platinum-group minerals (PGM) in five placer occurrences of the Russian Far East. Three PGE occurrences (Zolotaya, Fadeevka, and Kedrovka) are located in the Paleozoic foldbelt of southern Primorye. The other two PGE occurrences are Darya and Kondyor in the Archean Aldan Shield on the Siberian Platform, Khabarovskiy Krai. All placer deposits are in areas of Uralian/Alaskan-type intrusive magmatism followed by alkaline felsic magmatism. A recurring feature of the PGE mineralogy is the association with gold, which may be related to this later felsic overprint. The goal of this thesis is to provide and to systematize data on the PGMs in these occurrences. The state of knowledge on the placers studied is very variable. While the important Kondyor deposit had a number of earlier studies, data on the Fadeevka and Darya placers were very preliminary only, and there were no data on Zolotaya. The discovery of the Kedrovka placer was during this study, and PGM are first confirmed here.

The study of the placers presented in this dissertation is not based on own exploration/field work, but depends on the availability of samples from previous expeditions/exploration campaigns. The sample material is from the mineralogical collections of the Far East Geological Institute in Vladivostok, particularly the Nekrasov collection, and from individual research campaigns. Some of the results have been published in international journals:

Shcheka, G.G., Solianik, A.N., Lehmann B., Bieniok, A., Amthauer, G., Topa, D., Laflamme, J.H.G. (2004): Euhedral crystals of ferroan platinum, cooperite and mertieite-II from alluvial sediments of the Darya river, Aldan Shield, Russia. *Mineral. Mag.*, **68**, 871-885.

Shcheka, G.G., Lehmann B., Gierth, E., Gömann, K., Wallianos, A. (2004): Macrorystals of Fe-Pt alloy from the Kondyor PGE placer deposit, Khabarovskiy Kray, Russia: Trace element content, mineral inclusions, and reaction assemblages. *Can. Mineral.,* **42**, 601-617.

Shcheka, G.G., Vrzhosek, A.A., Lehmann, B., Tolstykh, N.D. (2004): Associations of platinum-group minerals from the Zolotaya gold placer, Primorye, Russian Far East. *Can. Mineral*., **42**, 583-599.

2 ANALYTICAL METHODS

Grains of PGM and associated minerals were picked from heavy mineral concentrates and studied by optical, microchemical and structural methods.

Ore microscopy, scanning electron analysis and electron-microprobe analysis with wavelength-dispersive and energy-dispersive X-ray spectrometry (EDS) were done at Technical University of Clausthal, Germany, with additional microanalysis done at CANMET, Ottawa. The proton-induced X-ray emission (PIXE) analysis was done at the Heidelberg Max-Planck Institute of Nuclear Physics. X-ray analysis and single crystal X-ray analysis were carried out at the Institute of Earth Sciences, University of Tübingen, Germany, and at the Institute of Mineralogy, University of Salzburg, Austria.

The most important instrument in this study was the electron microprobe CAMECA SX100 at Technical University of Clausthal. Several programs for different groups of minerals were applied during the years of research. Generally, the PGM were analyzed at 20 kV, with a beam current of 20 nA and a beam 1 μm across. The counting time varied from 10 to 30 s. The concentration of nineteen elements was determined using the following standards: FeS_2, $CuFeS_2$, PbTe, SnO_2, InSb, InAs, HgTe, and pure platinum, iridium, osmium, ruthenium, rhodium, palladium, silver, bismuth, antimony, gold, nickel, cobalt, iron and copper. The X-ray Kα-lines were used for Ni, Co, Fe; Lα for Ru, Rh, Sn, Sb, Te, Au, Pt, Ir, Cu; $Lβ_1$ for Pd and Ag; and Mα for Os, Pb, Bi. The Pd Lα instead of the Pd Lβ line was used for the measurement of silver-bearing minerals in order to avoid the overlap of PdLβ and AgLα peaks. The Pd-bearing oxygenated compounds were studied using the following X-ray lines: Kα for Cu, Fe, As, and O; Lα for Pd, Pt, Sn, Sb, Te, Hg, and Bi with SnO_2 as a standard for oxygen measurement, and the difference in between the analytical total and 100 % was taken as a qualitative indication of the presence of water.

The following detection limits were obtained (in wt.%): 0.15 for Os, 0.15 for Ir, 0.16 for Ru, 0.12 for Rh, 0.24 for Pd, 0.27 for Pt, 0.27 for Au, 0.32 for Ag, 0.23 for Pb, 0.04 for Fe, 0.02 for Ni, 0.09 for Cu, 0.03 for Co, 0.18 for Bi, 0.08 for Sb, 0.08 Sn, 0.09 for Te, 0.05 for As, 0.06 for S, and 0.11 for O.

Oxides and silicates were analyzed for twelve elements using the following standards: kaersutite, Cr_2O_3 (synthetic), TiO_2, sphalerite, Fe_2O_3 (synthetic), rhodonite, forsterite (San Carlos), albite. The SiKα, KKα, CaKα, CrKα, TiKα, SKα, FeKα, MnKα, ZnKα, NaKα, MgKα, AlKα lines were used. The Kα line of oxygen and the YAG synthetic compound have been used as standard

for oxygen in the analysis of a bismuth oxide phase. Data reduction was done by the Pouchou-Pichoir method.

Supplementary analyses in Canada were done on a JEOL 733 electron microprobe operated at 20 kV, with a specimen current (cup reading) of 20 nA. The following X-ray lines (and standards) were used: PdLα ($Pd_{11}Sb_2As_2$); CuKα, NiKα, IrLα, TeLα, and BiMα (metals); SbLα (Pd_8Sb_3); AsLα (InAs); PtLα and FeKα (PtFe). Counting time was of the order of 40 s for the minor and trace elements, and raw data corrections by ZAF were applied.

Proton-induced X-ray emission (PIXE) analysis was done at the Heidelberg nuclear microprobe (Traxel et al. 1995) using incident protons at energies of 2.2 MeV and beam currents from 20 pA up to 300 pA. Calibration was done with pure elements and was checked with a number of international glass standards (Wallianos et al. 1997; Jochum et al. 2000). For data reduction, the GUPIX software was used (Maxwell et al. 1989, 1995).

3 PLATINUM-GROUP MINERALOGY OF THE ZOLOTAYA AND FADEEVKA PGE-Au PLACERS, PRIMORYE

3.1 INTRODUCTION

Platinum-group minerals (PGM) in southwestern Primorye (Fig. 1) were discovered at the end of the 19th century during gold placer mining on the territory of the Sof'e-Alexeevskoe Cossacks.

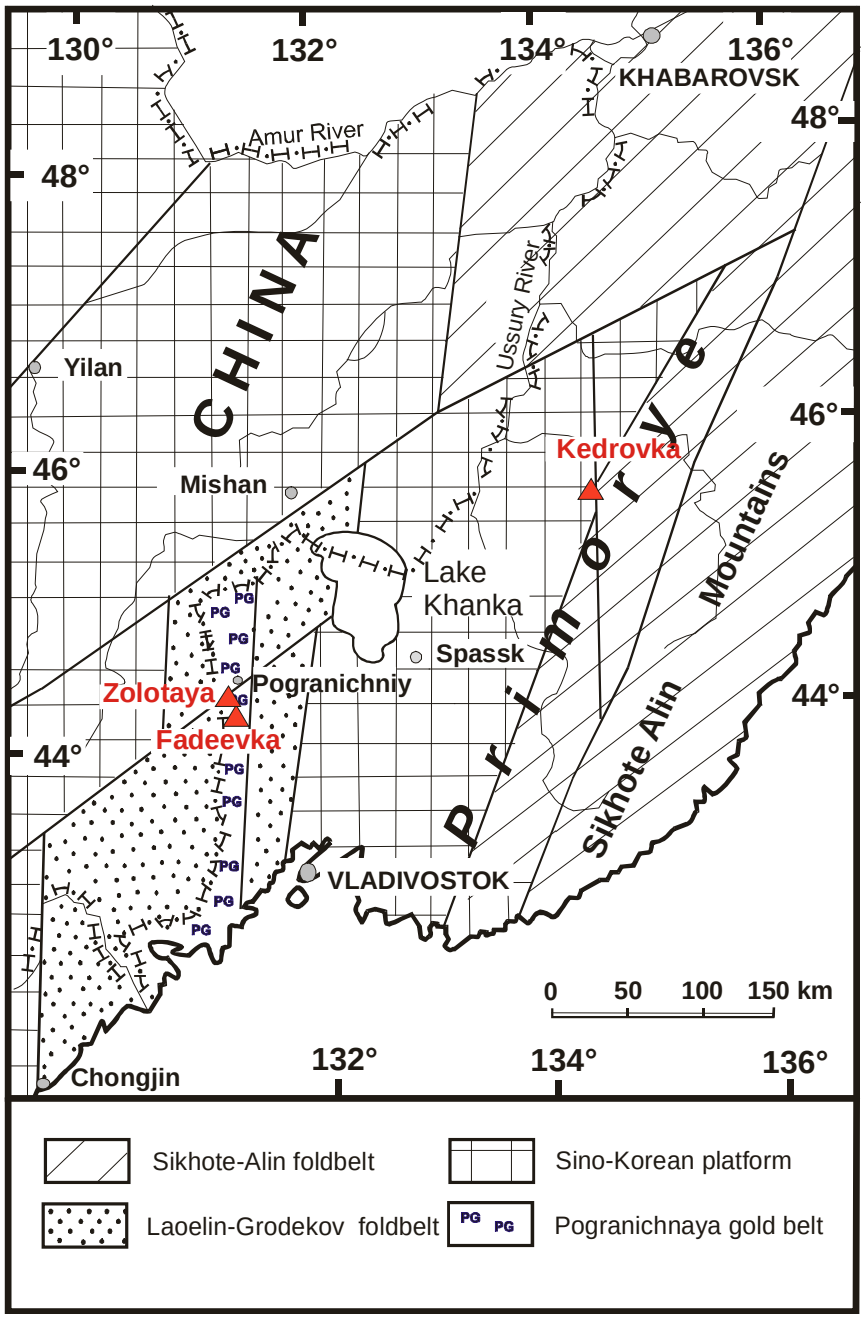

Fig. 1. *Location map of the PGE-bearing gold placers of Zolotaya, Fadeevka and Kedrovka rivers in Primorye, Russian Far East. Map simplified after Shcheka et al. (2001).*

In 1900-1912, exploration for gold was carried out at four fields: Zolotaya and Baykal river (former Dzhunikha) valleys and their northern tributaries (Annert 1928). In 1931, S.G. Vaulin, mining engineer with the "Dal'zoloto" company, evaluated the platinum potential. He confirmed the presence of small amounts of PGM in the gold placers (up to 3 mg PGE/m^3) and noted the occasional occurrence of nuggets with a weight of more than 50 mg. Only about sixty years later, the composition and secondary transformation of the PGM from the Fadeevka placer were studied by researchers from the Far East Geological Institute in Vladivostok (Shcheka et al. 1991).

The present chapter gives a description of the primary and secondary PGM mineralization, based on sample material from heavy-mineral concentrates of the Zolotaya river. Chromian spinels were analyzed both from the Zolotaya and Fadeevka River placers.

3.2 GEOLOGICAL SETTING OF ZOLOTAYA AND FADEEVKA RIVER PLACERS

The Zolotaya and Fadeevka rivers are located in the Pogranichnaya gold belt, which is part of the southern Laoelin-Grodekov foldbelt, Primorye (Figs. 1, 2). The foldbelt has N-S strike and stretches along the China-Russia border, southwest of Lake Khanka. This area represents an island-arc terrane that accreted to the west of the Sino-Korean platform during the Late Paleozoic (Khanchuk et al. 1996). The stratigraphic sequence of the study area consists of an Early Paleozoic basement of sericite-chlorite schist overlain by Permian black shale. Late Permian folding and thrusting were accompanied by basic to ultrabasic magmatism, followed by extensive granitic magmatism. Shallow gabbroic sills and stocks and granitic rocks with dominantly albitized granophyric granites (granodiorite-granite complex) are comagmatic with metabasaltic volcanism (spilite-keratophyre series). A differentiated dunite-hornblendite-gabbro complex, associated with magmatic copper-nickel sulfide mineralization, intrudes the Permian black shale. Cortlandite and hornblendite (with orthopyroxene) rich in high-aluminum hornblende (replacing ortho- and clinopyroxene) are the most common rock units. This complex is concentrically zoned and is regarded as of Uralian/Alaskan-type (Shcheka et al. 1990). A large part of it was intruded by Late Permian granites and now occurs as xenoliths and large blocks (roof pendants) within the granitic rocks. Larger occurrences are in the upper Baykal valley and in the upper reaches of the Kamenuska river west of Veranda mountain (Fig. 2). The hornblendite suite of the dunite-hornblendite-gabbro complex has a composition similar to peridotites and hornblende-rich pyroxenites of the zoned ultrabasic intrusions of southwestern Alaska (Taylor and Noble 1969;Himmelberg and Loney 1995).

A minor amount of hornblendite is also present in some concentrically zoned massifs of the

Uralian Platinum Belt (Ivanov 1997). All above-mentioned massifs have similar petrochemical and mineralogical characteristics, although the proportion of hornblende-bearing ultrabasic rocks in individual intrusive complexes is highly variable.

The Permian black shale hosts a number of quartz veins with pyrite-arsenopyrite-gold which formed in connection with the felsic intrusions, and which are thought to be the source of the alluvial gold placers (Shcheka et al. 1991). The alluvial gold from the Zolotaya river consists of dominantly (1) low-silver Au-Ag alloy with <8 wt.% Ag, and (2) high-silver Au-Ag alloy with up to 25 wt.% Ag. Occasionally, a complex Au-Ag-Hg-Pd alloy occurs with up to 8 wt.% Pd and 4 wt.% Hg. The palladium component in this variant is thought to be related to remobilization from dunitic rocks during the wide-spread felsic magmatism (Molchanov et al. 2001).

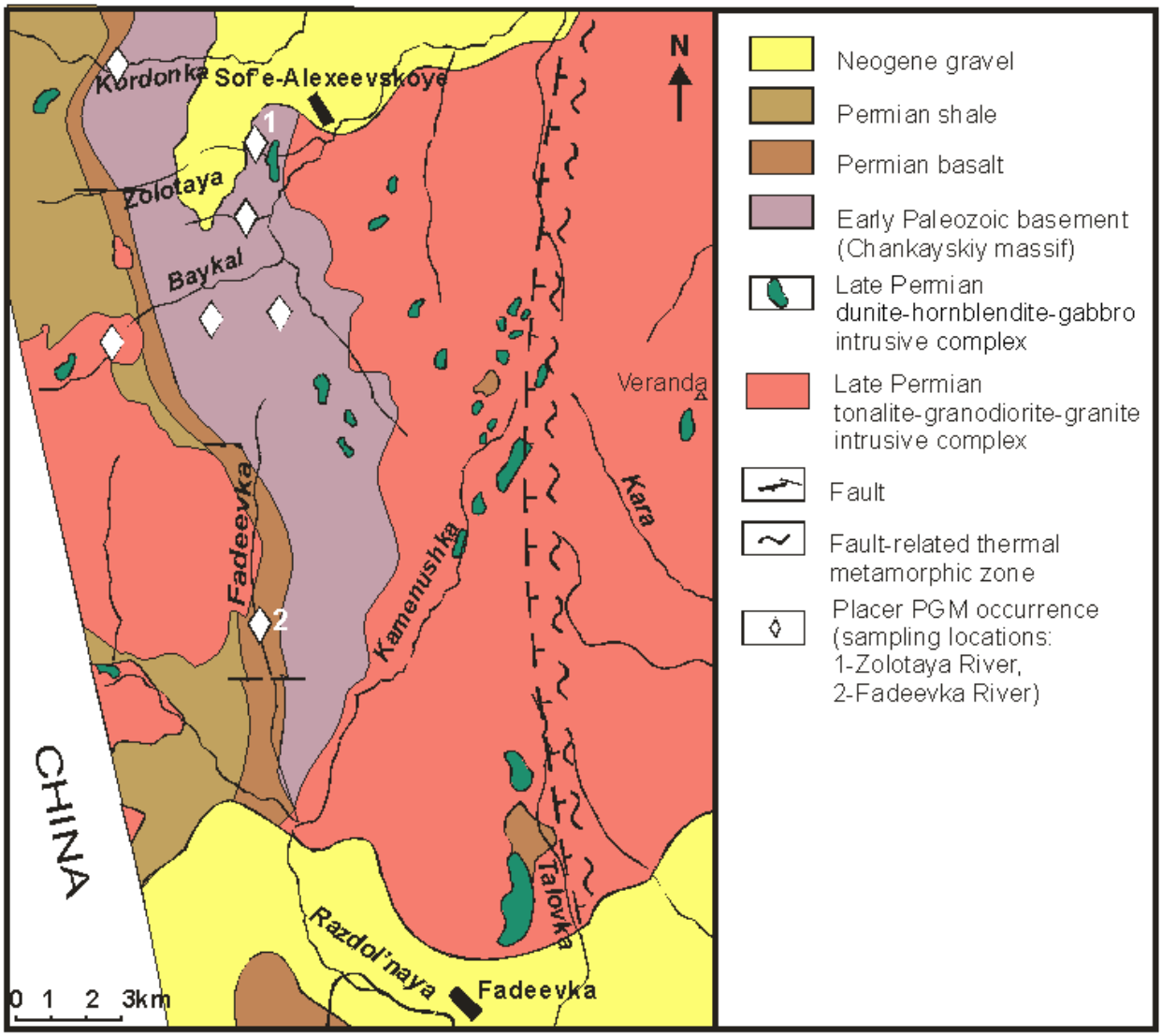

Fig. 2. *Geological sketch map of the study area.*

3.3 SOURCE OF THE PGM FROM ZOLOTAYA AND FADEEVKA RIVER PLACERS

The earlier study of PGM and associated minerals from the Fadeevka river placer suggested that the PGM mineralization is related to the dunite-hornblendite-gabbro complex (Shcheka et al. 1991). Since then, it was found that black shales could also be a source of PGM. The chemical composition of chromian spinel is often used for both the petrogenetic characterization of basic-ultrabasic magmatic complexes and their related mineralization (e.g., Barnes and Roeder 2001). We studied the chromian spinel from the Fadeevka and Zolotaya placers both as inclusions in PGM and in individual chromian spinel in heavy mineral concentrates, and compared it to chromian spinel from the Late Permian dunite-hornblendite-gabbro complex within the same area. All three sample groups studied have a similar compositon suggesting a common source (Table 1).

TABLE 1. CHEMICAL COMPOSITION OF CHROMIAN SPINEL (WT.%).

No		TiO_2	Al_2O_3	Cr_2O_3	Fe_2O_3	FeO	MnO	MgO	ZnO	Σ	φ	*f*	*f'*
1	Inclusions in PGM	0.23	9.88	58.33	3.11	15.38	-	11.67	0.18	98.78	79.8	46.7	15.4
2	grains (Zolotaya	0.19	5.52	60.61	6.38	16.08	0.42	10.79	n.a.	99.99	88.1	53.1	26.3
3	and Fadeevka)	0.30	8.94	54.36	6.79	20.69	0.43	8.11	n.a.	99.62	80.3	65.0	22.8
4	Chromian spinel	-	7.21	62.15	3.83	11.57	-	14.13	-	98.89	85.5	37.3	23.0
5	in heavy-mineral	-	6.01	60.45	4.39	21.55	0.23	7.17	0.20	100.00	87.1	66.6	15.5
6	concentrate	0.21	9.58	58.36	3.51	17.68	0.18	10.40	-	99.92	80.3	52.9	15.1
7	(Zolotaya river)	-	4.61	57.84	5.83	26.30	0.43	3.38	0.46	98.85	89.4	83.9	16.6
8		0.25	6.38	57.04	7.34	22.42	0.26	6.89	0.13	100.71	85.7	70.2	22.8
9		0.25	9.90	54.64	6.15	18.39	0.23	9.71	-	99.27	78.7	58.0	23.1
10		0.26	10.60	52.71	7.43	19.54	0.18	9.21	-	99.93	76.9	61.5	25.5
11		0.24	11.62	51.63	6.79	19.11	0.20	9.32	0.14	99.05	74.9	60.3	24.2
12	Chromian spinel	0.07	3.91	59.95	6.29	23.34	0.52	5.71	n.a.	99.79	91.1	74.0	19.5
13	in heavy-mineral	0.08	8.15	58.39	3.45	21.49	0.48	7.64	n.a.	99.69	82.8	64.7	11.5
14	concentrate	0.12	6.93	58.00	5.88	20.32	0.42	8.10	n.a.	100.07	84.9	63.4	19.7
15	(Fadeevka river)	0.12	8.10	54.32	6.81	22.72	0.43	6.77	n.a.	99.28	81.8	71.0	20.4
16		0.21	12.95	48.59	7.57	23.48	0.40	6.73	n.a.	99.93	71.6	71.6	22.5
17	Chromian spinel	0.43	6.36	55.39	7.03	23.78	1.09	5.05	0.77	99.90	85.3	77.0	21.0
18	in dunite and	0.30	9.93	54.73	2.96	26.05	0.92	4.35	n.a.	99.25	78.7	78.7	9.3
19	hornblendite	0.61	7.71	52.52	9.34	20.62	0.92	7.76	n.a.	99.48	81.2	67.8	28.9
20		0.28	6.72	57.06	4.17	26.35	0.67	3.96	n.a.	99.19	85.0	81.0	12.4
21		0.46	11.84	48.43	6.55	28.24	0.68	3.14	0.54	99.88	73.3	85.9	17.2

Note: φ = Cr/(Cr+Al) at.%; *f* = Fe/(Fe+Mg) at.%; $f' = Fe^{3+}/(Fe^{3+}+Fe^{2+})$ at.%; Fe^{3+} calculated based on mineral stoichiometry; n.a.- not analyzed; - not detected

The chromian spinel has high chromium, low titanium content and low oxidation state. The plot of $Fe^{3+}/(Cr^{3+}+Fe^{3+}+Al^{3+})$ *vs* $Cr^{3+}/(Cr^{3+}+Fe^{3+}+Al^{3+})$ for chromian spinel from the Zolotaya and Fadeevka areas shows a compositional field similar to Uralian/Alaskan-type occurrences and different from the ophiolitic trend (Fig. 3).

The composition of an olivine inclusion (Fo_{91}) within a PGM grain is similar to olivine in dunite and further confirms the connection of PGM mineralization from Zolotaya river to the dunite-hornblendite-gabbro intrusions.

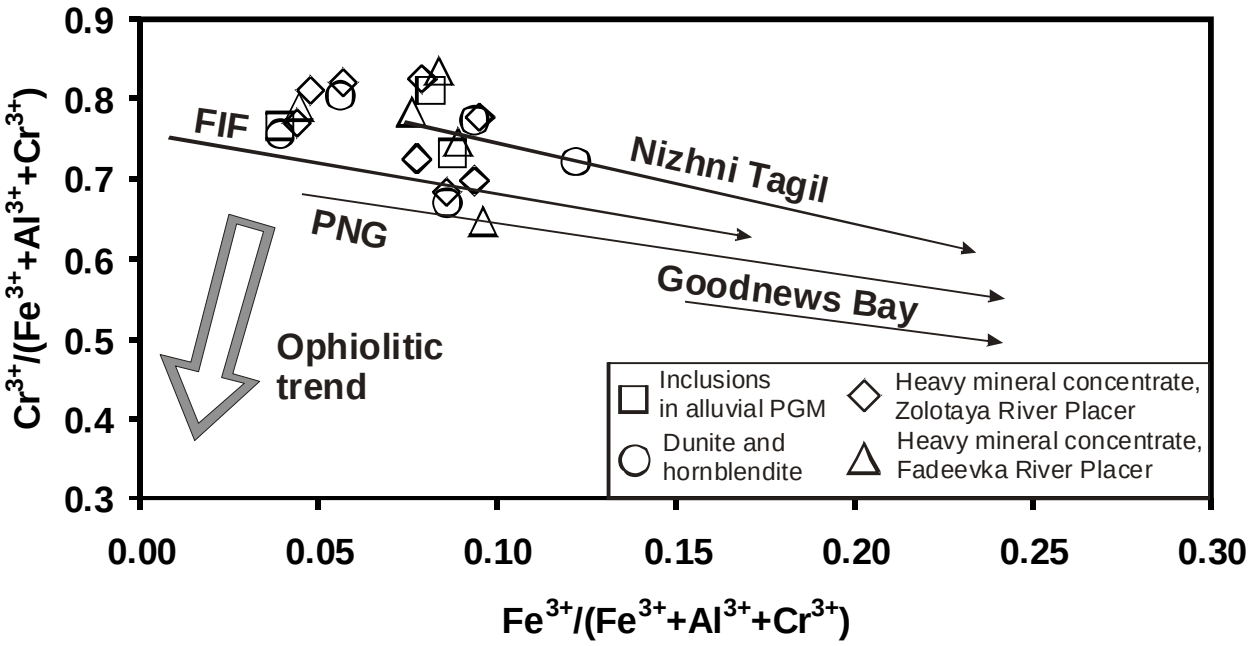

Fig. 3. *Plot of $Fe^{3+}/(Cr^{3+}+Fe^{3+}+Al^{3+})$ vs $Cr^{3+}/(Cr^{3+}+Fe^{3+}+Al^{3+})$ for chromian spinel from the Zolotaya and Fadeevka areas. Evolution trends for the Nizhni Tagil, Fifield (FIF), Goodnews Bay and Papua New Guinea (PNG) Uralian/Alaskan-type chromian spinels as well as for ophiolitic chromitites according to Johan (2002).*

3.4 PGM ASSOCIATIONS OF THE ZOLOTAYA RIVER PLACER

About 40 grains of PGM from the Zolotaya gold placer have been studied by electron-microprobe analysis. Ninety percent of the grains consist of a Pt-Fe alloy; the remainder is Os-Ir-Ru-Pt alloy. Other PGM occur as inclusions or rims within the main alloy phases. The PGM grain size seldom exceeds 2 mm (maximum is 4.4 mm across) and normally varies from 0.2 up to 1.4 mm. The grain shape is isometric or tabular, commonly irregular and angular. Usually, the PGM are poorly rounded, with euhedral outlines preserved, which indicates relatively little transport. Occasionally, PGM are intergrown with silicates, such as forsterite, quartz, chamosite, white mica, and clay minerals.

3.4.1 Primary Pt-Fe alloy

The Pt content in Pt-Fe alloy varies from 80.0 up to 91.8 wt.% (Table 2, Fig. 4). The most common minor elements are rhodium (from 0.55 up to 2.51 wt.%) and palladium (up to

1.07wt.%). Some grains are rich in iridium (up to 7.14 wt.%). Copper ranges from 0.26 up to 1.12 wt.%, and was found in all grains analyzed.

TABLE 2. SELECTED ANALYSES OF Pt-Fe ALLOY OF THE ZOLOTAYA RIVER

No	1	2	3	4	5	6	7	8	9	10	11
Sample	ZL34/1	ZL-1/1	ZL32/1	ZL32/3	ZL32/2	ZL-1/14/2	ZL34/5	ZL-37/1	Zl14	Zl25-5	ZL30/1
wt.%											
Os	1.59	1.84	0.64	0.71	0.65	0.57	2.07	0.11	-	-	0.26
Ru	0.13	0.21	0.08	-	-	0.11	0.20	-	-	-	-
Rh	1.12	1.14	2.08	2.51	2.05	1.58	0.55	1.43	1.73	1.36	2.24
Pd	0.31	-	0.46	0.57	-	1.07	-	0.94	-	0.26	0.58
Pt	90.79	91.77	89.79	88.86	89.68	89.53	88.61	88.87	83.47	80.00	80.96
Ir	-	-	-	-	-	1.26	-	-	3.72	7.14	3.90
Ni	0.09	0.18	0.06	0.07	0.05	0.09	0.07	0.03	0.06	0.28	0.29
Fe	4.05	4.66	5.71	5.62	5.64	5.48	5.76	7.96	8.95	9.20	10.22
Cu	0.37	0.30	0.56	0.67	0.61	1.12	0.77	0.77	0.37	0.26	0.57
Total	98.45	100.10	99.38	99.01	98.68	100.81	98.03	100.11	98.30	98.50	99.02
at.%											
Os	1.47	1.65	0.56	0.62	0.57	0.49	1.85	0.09	-	-	0.21
Ru	0.23	0.36	0.13	-	-	0.18	0.34	-	-	-	-
Rh	1.91	1.90	3.36	4.06	3.35	2.51	0.91	2.19	2.66	2.08	3.29
Pd	0.51	-	0.72	0.89	-	1.64	-	1.39	-	0.38	0.82
Pt	81.83	80.49	76.58	75.75	77.33	74.96	77.13	71.85	67.79	64.43	62.80
Ir	-	-	-	-	-	1.07	-	-	3.07	5.84	3.07
Ni	0.27	0.52	0.17	0.20	0.14	0.25	0.20	0.08	0.16	0.75	0.75
Fe	12.75	14.28	17.01	16.73	16.99	16.03	17.51	22.48	25.39	25.88	27.69
Cu	1.02	0.81	1.47	1.75	1.61	2.88	2.06	1.91	0.92	0.64	1.36
Total	100	100	100	100	100	100	100	100	100	100	100

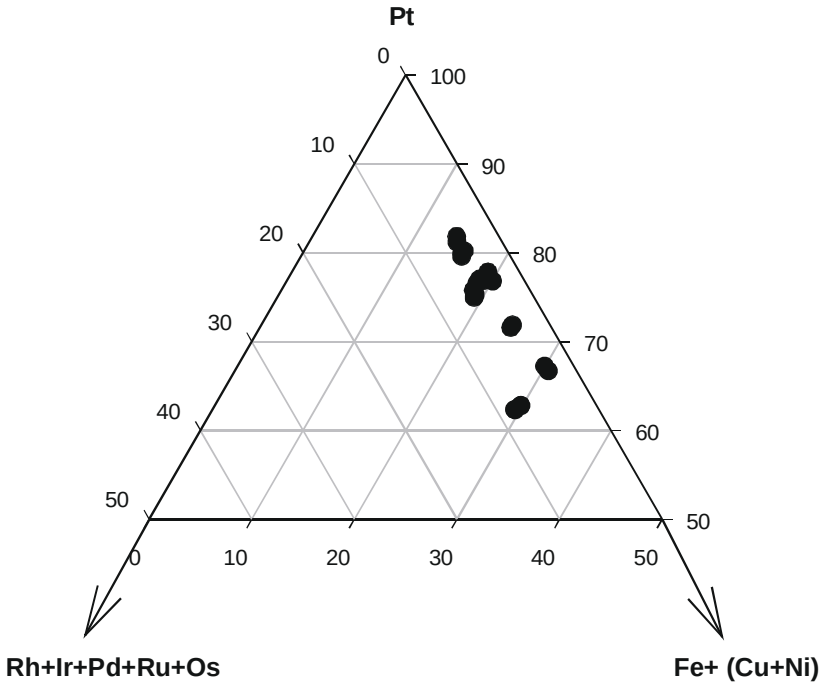

Fig. 4. *Composition of Pt-Fe alloy from the Zolotaya river placer (at.%).*

TABLE 3. SELECTED ANALYSES OF Os-Ir-Ru-Pt ALLOY OF THE ZOLOTAYA RIVER

No	1	2	3	4	5	6	7	8	9	10	11	12
Sample	ZL34/6	ZL34/8	ZL30/11	ZL2/3	ZL1/6/7	ZL25-3	ZL1m	ZL1/6/8	ZL2/1n	ZL1/6/3	ZL1/6/2	ZL22/3n
wt.%												
Os	94.63	92.30	69.41	60.01	47.55	60.03	32.65	32.14	30.27	24.69	22.98	1.93
Ru	-	1.01	0.16	4.65	13.83	4.45	2.88	18.27	4.25	13.94	13.28	10.76
Rh	-	0.22	1.18	1.64	1.14	0.61	0.74	1.39	5.32	2.20	2.63	2.98
Pd	-	-	-	0.55	-	0.36	-	-	1.70	-	-	1.32
Pt	3.43	7.21	1.03	-	2.79	-	5.20	1.36	12.03	10.68	12.93	18.47
Ir	-	0.73	25.68	32.15	33.65	34.31	58.03	45.67	44.99	47.15	46.39	60.22
Fe	0.11	0.06	0.07	-	0.14	-	0.09	0.14	0.24	0.79	0.62	0.04
Cu	0.05	0.09	-	-	-	-	0.14	-	-	0.17	0.17	2.17
Ni	-	-	-	-	-	-	-	-	-	0.10	0.08	-
Total	98.22	101.62	97.53	99.00	99.10	99.76	99.73	98.97	98.80	99.72	99.00	97.89
at.%												
Os	96.07	89.75	70.43	57.37	42.38	57.65	31.80	27.69	27.97	21.35	20.12	1.69
Ru	-	1.85	0.31	8.37	23.20	8.04	5.28	29.62	7.39	22.70	21.87	17.72
Rh	-	0.40	2.21	2.90	1.88	1.08	1.33	2.21	9.09	3.52	4.26	4.82
Pd	-	-	-	0.94	-	0.62	-	-	2.81	-	-	2.06
Pt	3.40	6.84	1.02	-	2.43	-	4.94	1.14	10.84	9.01	11.04	15.76
Ir	-	0.70	25.79	30.42	29.68	32.61	55.94	38.93	41.14	40.37	40.18	52.15
Fe	0.38	0.20	0.24	-	0.43	-	0.30	0.41	0.76	2.33	1.85	0.12
Cu	0.15	0.26	-	-	-	-	0.41	-	-	0.44	0.45	5.68
Ni	-	-	-	-	-	-	-	-	-	0.28	0.23	-
Total	100	100	100	100	100	100	100	100	100	100	100	100

Note: S, Pb, Bi, Pd, Sn, Sb, Te, As were not detected; - below detection limit

3.4.2 Primary Os-Ir-Ru-Pt alloy

The grains of Os-Ir-Ru-Pt alloy have an extremely heterogeneous texture and consist of up to four different mineral phases, reflecting various stages of exsolution of the primary solid-solution (Table 3, Fig. 5).

Sample ZL-22 was found to be the most interesting because it allowes to define the composition of the primary grains and to correlate it with the composition of its exsolved products. The grain matrix consists of a micrographic intergrowth of iridium-rich Pt-Fe alloy $[(Pt_{2.47}Ir_{0.17}Rh_{0.05}Pd_{0.01}Ru_{0.01})_{2.71}(Fe_{0.95}Cu_{0.04}Ni_{0.01})_{1.00}]$ and an alloy phase of $Ir_{0.52}Ru_{0.18}Pt_{0.16}Cu_{0.06}Rh_{0.05}Pd_{0.02}Os_{0.02}$ composition (Fig. 6a). Numerous inclusions of cherepanovite (RhAs) and iridarsenite ($IrAs_2$) are located in the matrix. The grain has a homogeneous rim of $Pt_{0.46}Ir_{0.25}Fe_{0.18}Ru_{0.08}Rh_{0.01}Os_{0.01}Cu_{0.01}$with graphic inclusions of cherepanovite with high Ru content (up to 20 wt.%), in association with irarsite [(Ir,Rh,Pt)AsS] (Fig. 6b). We analyzed the matrix of the micrographic grain with a defocused beam (50 μm) in oder to obtain its bulk composition. The composition, $Pt_{0.49}Ir_{0.23}Fe_{0.17}Ru_{0.07}Rh_{0.02}Os_{0.01}Pd_{0.01}$, is nearly identical to that of the rim, suggesting variable degree of exsolution from a homogeneous primary phase for both rim and core.

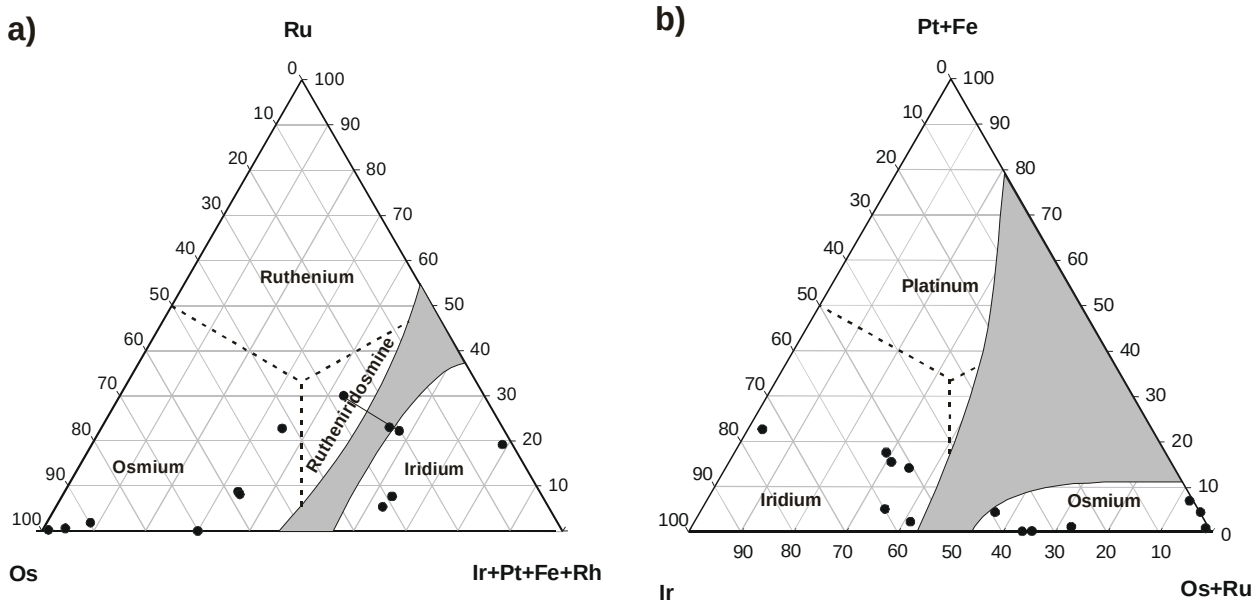

Fig. 5*. Composition of Os-Ir-Ru-Pt alloy* ***a)*** *in the Os-Ru-(Ir+Pt+Fe+Rh) diagram,* ***b)*** *in the Ir-(Os+Ru)-(Pt+Fe) diagram (at.%). Shaded area locates immiscibility gap according to Cabri and Feather (1975).*

Other samples consist of aggregates of (i) zonal intergrowths of ruthenosmiride [$Ir_{0.40}Ru_{0.22}Os_{0.20}Pt_{0.11}Rh_{0.04}Fe_{0.02}$] with two variants of rutheniridosmine, [$Ir_{0.39}Ru_{0.30}Os_{0.28}Rh_{0.02}Pt_{0.01}$] and [$Os_{0.42}Ir_{0.30}Ru_{0.23}Pt_{0.02}Rh_{0.02}$], and iridium-bearing Pt-Fe alloy [$(Pt_{2.10}Ir_{0.16}Rh_{0.09}Ru_{0.01})_{2.36}(Fe_{0.89}Ni_{0.07}Cu_{0.04})_{1.00}$] (sample ZL-1/6), (ii) iridium $Ir_{0.41}Os_{0.28}Pt_{0.11}Rh_{0.09}Ru_{0.07}Pd_{0.03}$ with numerous spotted inclusions of Ir- and Rh-rich Pt-Fe alloy $(Pt_{2.66}Rh_{0.15}Ir_{0.10}Pd_{0.05})_{2.95}(Fe_{0.94}Cu_{0.04}Ni_{0.02})_{1.00}$ and ribbon-like osmium $Os_{0.57}Ir_{0.30}Ru_{0.08}Rh_{0.03}$ (Fig. 6c, sample ZL-2), and (iii) Ir-rich Pt-Fe alloy $(Pt_{2.57}Ir_{0.12}Rh_{0.10})_{2.79}(Fe_{0.96}Cu_{0.04})_{1.00}$ with subhedral inclusions of iridium $Ir_{0.57}Os_{0.26}Pt_{0.08}Rh_{0.06}Ru_{0.02}$ (Fig. 6d, sample ZL-14).

Only one homogeneous grain of iridium with the composition of $Ir_{0.56}Os_{0.32}Ru_{0.06}Pt_{0.05}Rh_{0.01}$ was found. Besides of these mineral associations, there are intergrowths of Pt-Fe alloy with plates of osmium $Os_{0.71}Ir_{0.26}Rh_{0.02}Pt_{0.01}$, and submicrometric inclusions of native osmium $Os_{0.96}Pt_{0.04}$ in Pt-Fe alloy.

On the basis of these observations, the refractory PGM of the Zolotaya placer can be subdivided into three groups: (1) heterogeneous Os-Ir-Ru-Pt grains (most common) formed as a result of breakdown of the solid solution (Fig. 6a,c), (2) Pt-Fe alloy and Os-Ir alloy intergrowths, (3) homogeneous grains.

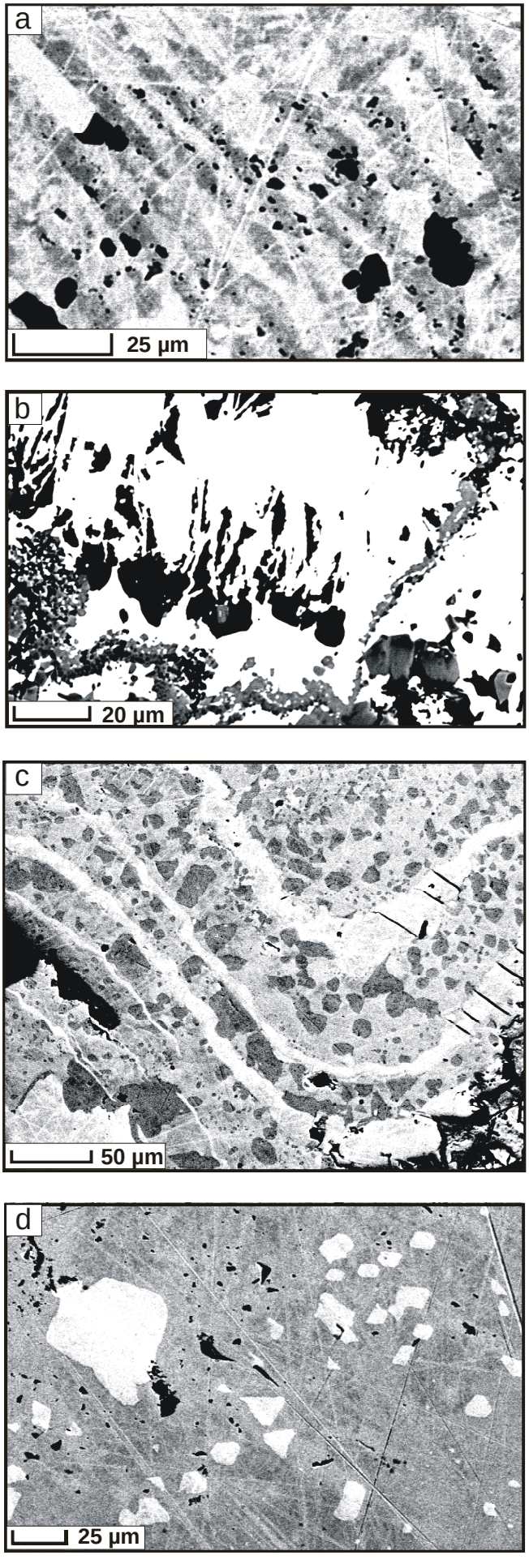

Fig. 6. *Back-scattered electron (BSE) images of different exsolution textures of Ir-Os-Ru-Pt alloy from Zolotaya river.* ***a)*** *Matrix of micrographic intergrowth of Ir-rich Pt-Fe alloy (grey) with Ir-Ru-Pt alloy (white), and cherepanovite inclusions (dark grey). Sample ZL-22.* ***b)*** *Rim zone of Pt-Ir-Fe-Ru alloy (white) with myrmekitic inclusions of Ru-rich cherepanovite (black). Irarsite (dark grey) occurs as reaction rim and on fractures. Sample ZL-22.* ***c)*** *Patchy inclusions of Ir-rich Pt-Fe alloy (dark grey) in iridium matrix (grey) and ribbon-like osmium (white). Sample ZL-2.* ***d)*** *Subhedral inclusions of iridium (white) in Ir-rich Pt-Fe alloy (grey). Sample ZL-14.*

3.4.3 Primary and secondary cooperite [PtS] and cuprorhodsite [$Cu(Rh,Ir)_2S_4$]

Cooperite from the Zolotaya placer occurs in two different varieties. Primary cooperite intergrown with cuprorhodsite and chalcopyrite forms roundish multiphase inclusions in Pt-Fe alloy (Fig. 7).

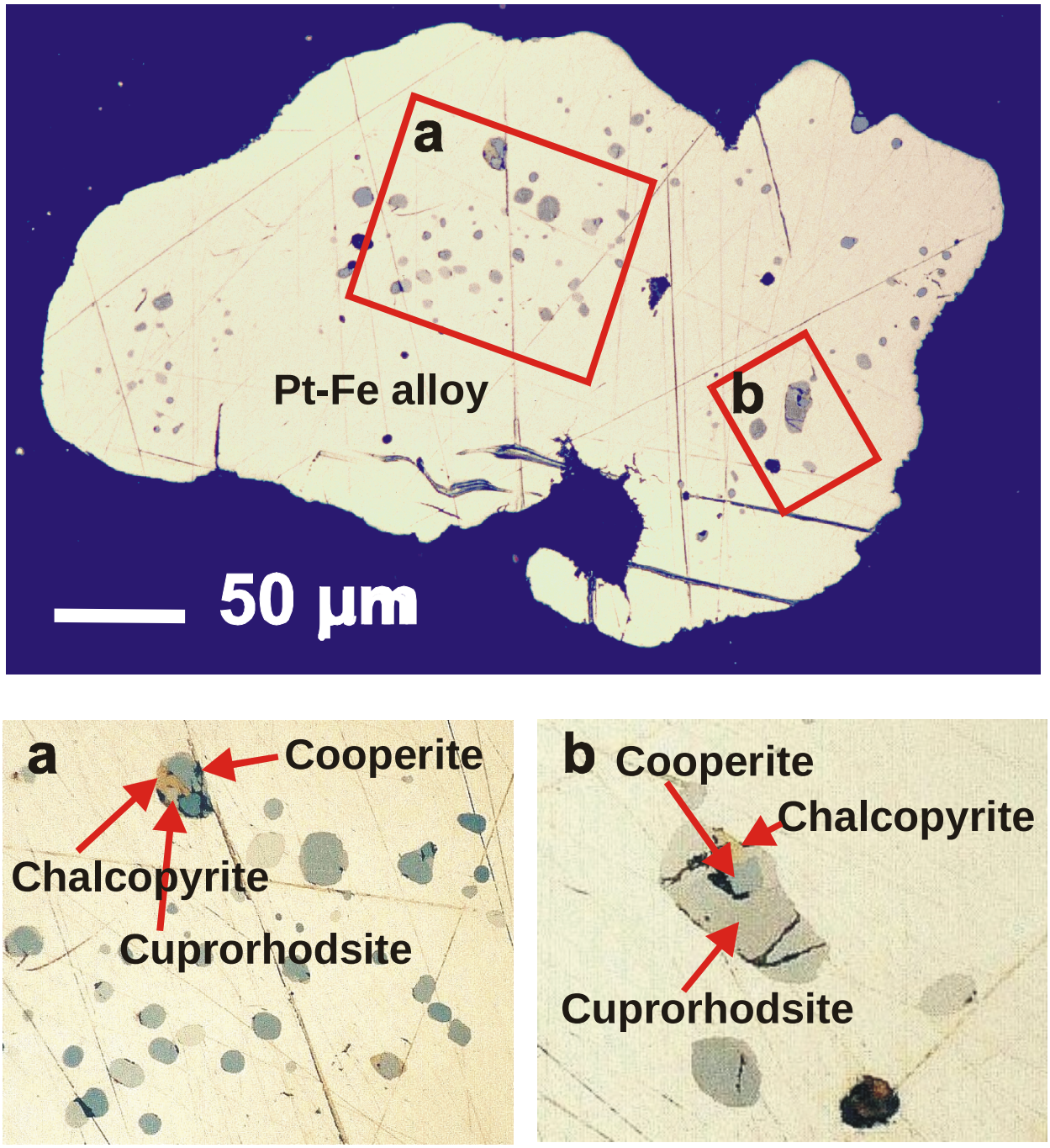

Fig. 7. *Cooperite inclusions in Pt-Fe alloy. Sample ZL-1/7.*

The inclusions do not exceed a size of more than 10-20 μm across. Cuprorhodsite from the multiphase inclusions contains up to 30.8 wt.% Pt, whereas the Ir content does not exceed 0.81 wt.% (Table 4). Chalcopyrite contains up to 5.12 wt.% Pt and 1.13 wt.% Pd.

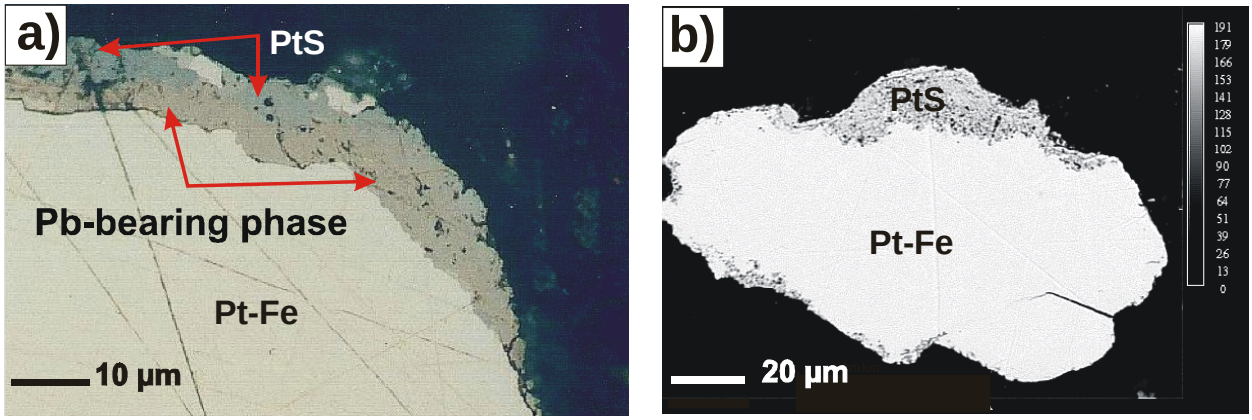

***Fig. 8**. Rim assemblage on Pt-Fe alloy **a)** intergrowth of cooperite with Pb-Ir-Cu-Rh sulfide (xingzhongite or konderite); **b)** cooperite rim.*

Secondary cooperite forms a rim around Pt-Fe grains (Fig. 8).

The distinctive feature of primary cooperite is its palladium content of up to 1.98 wt.%, whereas secondary cooperite commonly has a Pd content below the detection limit and only rarely attains 0.66 wt.% (Table 4).The width of the secondary rim of cooperite reaches up to 50 μm. One of the Pt-Fe grains studied is surrounded by a complex rim, which consists of cooperite intergrown with a Pb-Ir-Cu-Rh sulfide (Table 5, Fig. 8a). The Pb content varies from 1.60 up to 7.54 wt.%. The Pb-bearing phase could be either xingzhongite [$(Ir,Pt)_2(Cu,Pb)S_4$] or konderite [$PbCu_3Rh_8S_{16}$].

In another sample, patchy intergrowth aggregates of cooperite with sperrylite form a several μm-large rim on Pt-Fe alloy. Cooperite contains up to 3.02 wt.% Ir, and both cooperite and sperrylite have up to 1.30 wt.% Rh.

3.4.4 Primary minerals of erlichmanite-laurite solid-solution series [OsS_2-RuS_2]

Members of the erlichmanite-laurite solid-solution series, [OsS_2-RuS_2], occur both in the form of idiomorphic inclusions (up to 15 μm across) in Pt-Fe alloy and as an intergrowth with Os-Ir-Ru-Pt alloy. Pure laurite has been found as an intergrowth with a zoned rutheniridosmine grain. Erlichmanite, with up to 12.1 wt.% Ru (Table 5), occurs as intergrowth with iridium (Fig. 9).

Idiomorphic inclusions of Os-bearing laurite of hexagonal habit (up to 20.2 wt.% Os) occur within Pt-Fe alloy. The euhedral laurite is evidence of the primary formation and subsequent entrapment by Pt-Fe alloy.

TABLE 4. CHEMICAL COMPOSITION OF CUPRORHODSITE, CHEREPANOVITE, IRIDARSENITE, IRARSITE AND COOPERITE FROM THE ZOLOTAYA RIVER

No	1	2	3	4	5	6	7	8
Sample	Zl -1/7/2	Zl -1/7/2/1	ZL22/5	ZL22r	Zl22/6	Zl22-5	ZL33/1	ZL-1/7/3
	$CuRh_2S_4$	$CuRh_2S_4$	RhAs	(Rh,Ru) As	$(Ir,Ru)As_2$	$(Ir,Ru)As_2$	PtS	PtS
wt.%								
S	27.72	27.00	-	-	-	7.50	14.63	14.64
Ru	-	-	4.65	19.15	0.43	-	-	-
Rh	30.54	26.58	47.15	27.42	2.85	5.94	0.41	0.54
Pd	-	-	0.47	-	0.61	-	-	1.98
Sb	-	-	2.87	0.63	0.77	0.16	-	-
Ir	0.71	0.81	7.66	8.03	47.88	46.77	-	-
Pt	25.54	30.80	1.34	2.88	4.07	8.11	84.89	82.80
Au	-	-	-	-	-	0.68	-	-
Fe	2.55	1.77	-	0.07	0.21	0.10	-	-
Cu	11.23	11.85	-	-	-	-	0.10	0.09
As	-	-	36.78	39.60	43.03	27.80	0.09	0.11
Total	98.29	98.81	100.92	97.78	99.85	97.06	100.12	100.16
Formula coefficient *(apfu)*								
S	3.98	3.97	0.00	0.00	0.00	0.74	1.02	1.01
Ru	0.00	0.00	0.09	0.36	0.01	0.00	0.00	0.00
Rh	1.37	1.22	0.86	0.51	0.09	0.18	0.01	0.01
Pd	0.00	0.00	0.01	0.00	0.02	0.00	0.00	0.04
Sb	0.00	0.00	0.04	0.01	0.02	0.00	0.00	0.00
Ir	0.02	0.02	0.07	0.08	0.84	0.77	0.00	0.00
Pt	0.60	0.74	0.01	0.03	0.07	0.13	0.97	0.94
Au	0.00	0.00	0.00	0.00	0.00	0.01	0.00	0.00
Fe	0.21	0.15	0.00	0.00	0.01	0.01	0.00	0.00
Cu	0.83	0.89	0.00	0.00	0.00	0.00	0.00	0.00
As	0.00	0.00	0.92	1.01	1.93	1.17	0.00	0.00
Total	7	7	2	2	3	3	2	2

Note: 1, 2 cuprorhodsite, 3 cherepanovite, 4 cherepanovite-ruthenarsenite solid solution, 5 iridarsenite, 6 irarsite, 7 secondary cooperite, 8 primary cooperite; Bi, Os, Ni, Pb, Bi, Pd, Sn, Te, As were not detected; - below detection limit

3.4.5 Secondary PGE arsenides and sulfarsenides

As-bearing PGM are relatively rare. They are commonly represented by sperrylite and occur as rim phases around grains of Pt-Fe alloy or fill cavities after leached magmatic Os-Ir lamellae in Pt-Fe alloy. There are also inclusions of iridarsenite and irarsite in association with minerals of the cherepanovite-ruthenarsenite solid solution (Table 4).

Minerals of the cherepanovite-ruthenarsenite solid-solution series, RhAs-(Ru,Ni)As, form irregular inclusions (up to 20 μm; Table 4) mainly close or within the rim of heterogeneous grains with lattice-like intergrowth of Ir-bearing Pt-Fe and Ir-Ru-Pt alloy (Fig. 6a). In some cases

cherepanovite occurs as intergrowth with iridarsenite (Ir,Ru,Rh,Pt)As_2. In the rim zone cherepanovite has high Ru content (up to 19.2 wt.%). Probably this phase is an intermediate member of the cherepanovite-ruthenarsenite solid solution. Ru-rich cherepanovite forms graphical intergrowth aggregates with irarsite (Ir,Rh,Pt,Ru)AsS.

TABLE 5. SELECTED ANALYSES OF LAURITE-ERLICHMANITE SOLID SOLUTION SERIES FROM ZOLOTAYA RIVER

No	**1**	**2**	**3**
Sample	**Zl=1/6/10**	**Zl-1/9/3**	**Zl-1 ak/2**
wt.%			
Os	0.69	20.24	47.69
S	38.65	33.34	27.66
Ru	57.12	38.31	12.07
Ir	1.69	2.35	10.12
Rh	1.22	2.07	0.28
Pt	2.49	2.21	0.35
As	-	1.53	-
Total	101.86	100.05	98.17
Formula coefficient *(apfu)*			
Os	0.01	0.2	0.58
S	2	1.96	2.01
Ru	0.94	0.72	0.28
Ir	0.01	0.02	0.12
Rh	0.02	0.04	0.01
Pt	0.02	0.02	0
As	0	0.04	0
Total	3	3	3

Note: No 1 intergrown with zonal rutheniridosmine
No 2 inclusion inside the Pt-Fe grain
No 3 intergrown with iridium grain
Pb, Bi, Pd, Sn, Sb, Te, Ir, Ni, Fe, Cu were not detected; - below detection limit

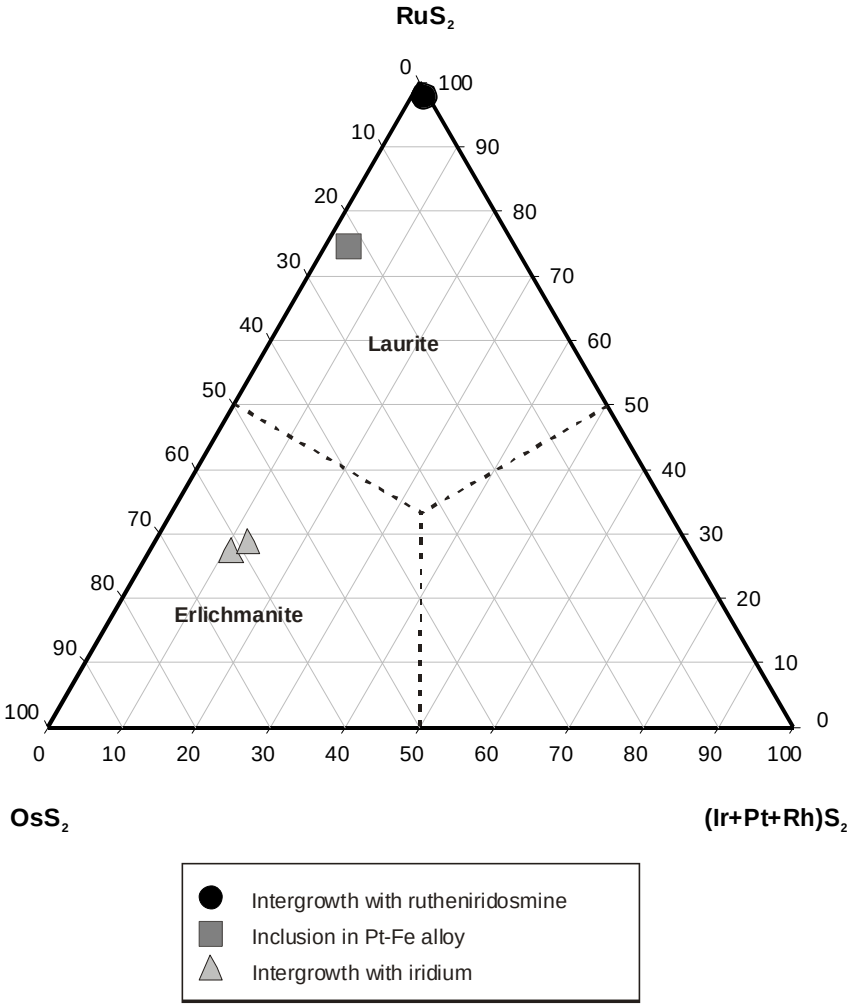

Fig. 9. *Mineral composition of the laurite-erlichmanite solid solution (at.%).*

3.4.6 DISCUSSION

The Zolotaya river placer contains primary (magmatic) and secondary PGM (Table 6). The primary minerals are Pt-Fe alloy, Os-Ir-Ru alloy, cooperite (in multiphase inclusions), laurite, erlichmanite, cuprorhodsite, cherepanovite and iridarsenite. The secondary minerals are distinguished by their occurrence in reaction rims around grains of Pt-Fe alloy and are represented by cooperite, irarsite, platarsite and sperrylite.

Pt-Fe alloy is the main PGM in the Zolotaya River placer. The Fe content (including Ni and Cu) varies from 14 up to 30 at.% which is characteristic of native platinum and ferroan platinum alloy (Cabri and Feather 1975). Its average composition is (n=21): 87.84±3.25 wt.% Pt (73.35±5.89 at.%), 6.88±2.37 wt.% Fe (19.69±5.72 at.%), 0.85±0.73 wt.% Os, 0.09±0.09 wt.% Ru, 1.58±0.65 wt.% Rh, 0.47±0.31 wt.% Pd, 0.67 ±1.42 wt.% Ir, 0.13 wt.% ±0.11 wt.% Ni, and

0.61±0.21 wt.% Cu. The main minor PGE present is rhodium. Pt-Fe alloy of similar composition is typical of Uralian/Alaskan-type deposits (Cabri et al. 1996).

TABLE 6. PGM IN THE ZOLOTAYA RIVER PLACER

Mineral	**Origin**	**Abundance**
Pt-Fe alloy	Magmatic	++++
Os-Ir-Ru alloy	Magmatic	++
Cooperite PtS	1. Magmatic 2. Secondary	+ +++
Laurite RuS_2	Magmatic	+
Erlichmanite $(Os,Rh,Ir)S_2$	Magmatic	+
Cuprorhodsite $CuRh_2S_4$	Magmatic	+
Cherepanovite RhAs	Magmatic (?)	++
(Rh,Ru,Ir)As	Magmatic (?)	++
Iridarsenite $(Ir,Ru)As_2$	Magmatic (?)	++
Irarsite (Ir,Ru)AsS	Secondary	++
Platarsite (Pt,Rh)AsS	Secondary	+
Sperrylite $PtAs_2$	Secondary	+
Konderite/Xingzhongite (?)	Secondary	+

Ir-bearing Pt-Fe alloy forms three different morphological types: (1) lattice-like intergrowths (exsolution fabric) with Ir-Os-Ru-Pt alloy (Fig. 6a), (2) irregular patchy inclusions in Ir-Os-Ru-Pt alloy (Fig. 6c), (3) a grain matrix with subhedral inclusions of iridium (Fig. 6d).

The triangular diagram (Pt+Fe)-(Os+Ru)-(Ir+Rh) of Slansky et al. (1991) allows an estimate of the temperature of formation and was applied to the Uralian/Alaskan-type intrusions of Fifield, Nizhni Tagil and Durance River (Slansky et al. 1991), Inagli (Tolstykh and Krivenko 1997), Salmon River (Tolstykh et al. 2002), and Kondyor and Guli (Malitch and Thalhammer 2002).
The composition of multiphase assemblages from the Zolotaya River is plotted in relation to temperature of formation (Fig. 10). Grain ZL-22 shows the highest temperature of >850^{o}C. Sample ZL-2 shows step-like exsolution with an Ir content corresponding to 800°C.

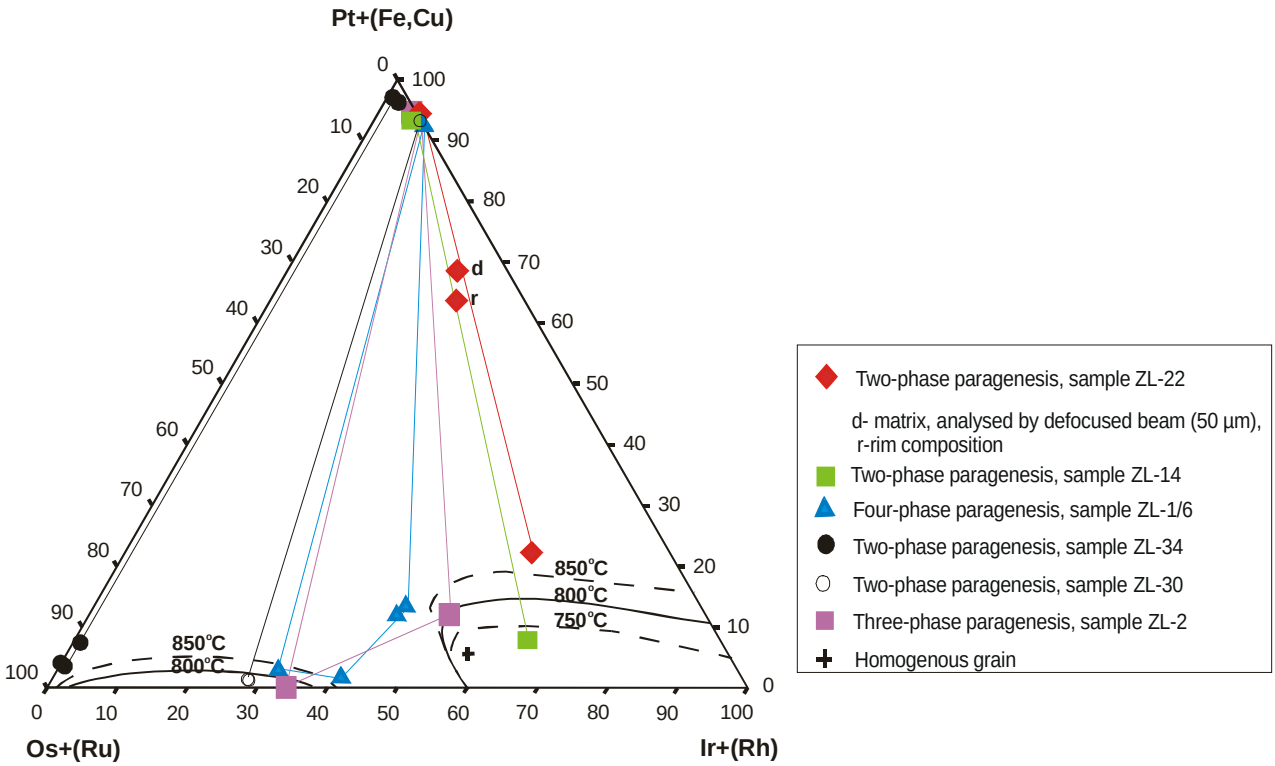

Fig. 10. *Phase diagram of the Pt+(Fe,Cu) – Os+(Ru) – Ir+(Rh) system (Slansky et al. 1991).*

The formation of iridium and Ir-rich Pt-Fe alloy (3.72 wt.% Ir) took place at a temperature slightly below 750°C (sample ZL-14). In sample ZL-1/6, native osmium formed first, followed by phases rich in Ir (at temperatures >850°C).

The textural evidence of the multiphase mineral associations and the interpretation of the compositional data by help of the diagram of Slansky et al. (1991) point to high-temperature formation of the Ir-Os-Ru-Pt alloy similar to that for the Inagli, Kondyor and other Uralian/Alaskan-type intrusions.

Cooperite is the most common PGE sulfide mineral and occurs both as primary inclusion phase enriched in Pd, and as secondary rim phase. The absence of nickel in cooperite from the Zolotaya river placer is typical of Uralian/Alaskan-type deposits.

Cuprorhodsite belongs to the group of PGE-bearing thiospinels, i.e. cuprorhodsite-cuproiridsite-malanite-ferrorhodsite solid solution. These minerals are most abundant in Uralian/Alaskan-type deposits (Cabri et al. 1981; Rudashevskiy et al. 1985a; Nekrasov et al. 1994; Augé et al. 2002; Garuti et al. 2002), but they occur also in ophiolitic complexes (Corrivaux and Laflamme 1990; Augé and Maurizot 1995; Garuti et al. 1995, 1999), and in layered mafic-ultramafic intrusions (Barkov et al. 1997, 2000). The cuprorhodsite-cuproiridsite series shows complete solid-solution, whereas pure malanite is not described in the literature. The cuprorhodsite from the Zolotaya

placer is similar to occurrences in eastern Madagascar, Burma, Borneo, Ecuador, India (Baula), and Russia (Chukotka) (Fig. 11).

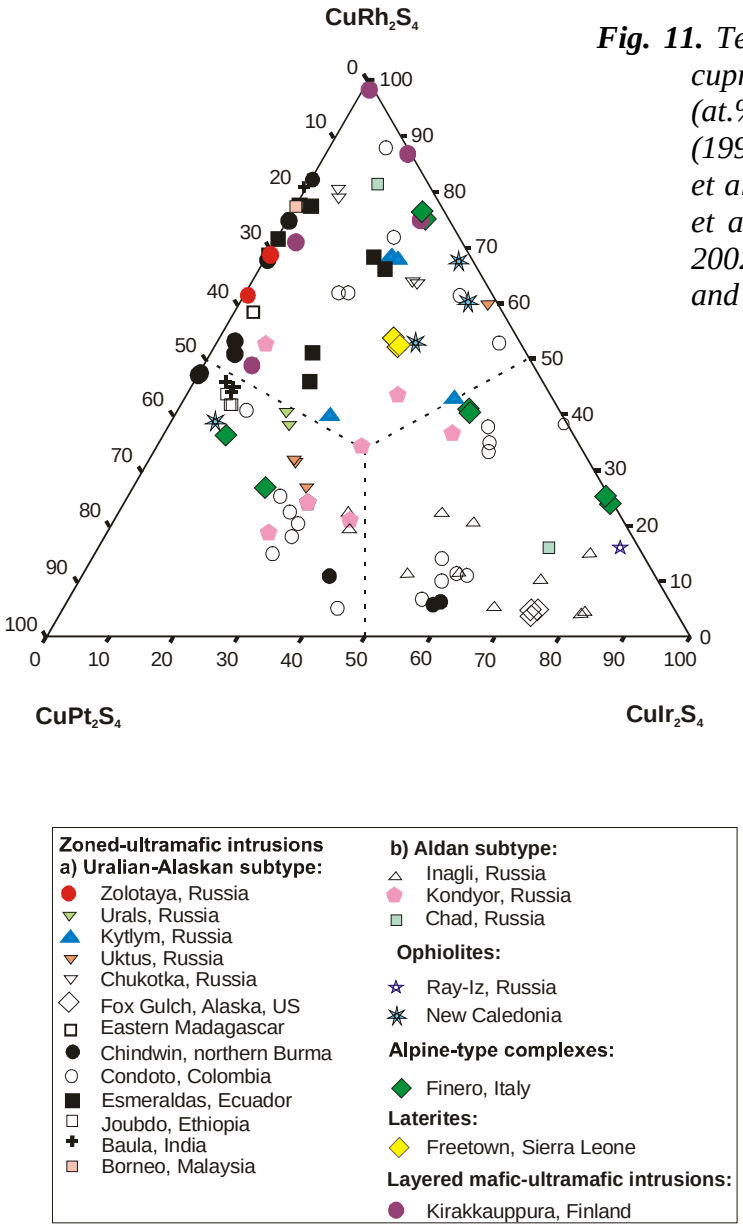

Fig. 11. *Ternary diagram of the cuprorhodsite-cuproiridsite-malanite solid solution (at.%). Data sources: Augé and Legendre (1992); Augé and Maurizot (1995); Augé et al. (2002); Barkov et al. (2002); Cabri et al. (1996); Garuti et al. (1995, 1999, 2002); Nekrasov et al. (1994); Tolstykh and Krivenko (1997).*

In general, the Ir content of minerals of the cuprorhodsite-cuproiridsite solid solution from these occurrences is very low. Judging from the distribution of minerals at the different localities, there is no visible correlation between type of deposit and cuprorhodsite-cuproiridsite-malanite mineral composition. Rather, a compositional control is exerted by the saturation of the ore-forming system in a mineral phase containing Rh, Ir, and/or Pt.

Many studies on PGM in Uralian/Alaskan-type deposits give detailed descriptions of multiphase inclusions. In general, the inclusions consist of base-metal sulfides and (Pd,Pt,Rh) sulfides and tellurides. Pt-Pd mineral assemblages are characteristic of the PGM occurrences of the Durance river, France, and Pustaya river, Kamchatka, Russia (Johan et al. 1990; Tolstykh et al. 2000). Rh-Pd mineral assemblages are more common in Santiago river, Ecuador (Weiser and Schmidt-

Thomé 1993). Rh-bearing minerals are also most typical of multiphase inclusions from the Zolotaya river placer.

Such multiphase inclusions were described also in PGM from the ophiolitic complexes of northwestern Salair, Russia (Tolstykh et al. 1999), Troodos, Cyprus (McElduff and Stumpfl 1990), Kraubath, Austria (Malitch et al. 2001), and Ronda, southern Spain (Torres-Ruiz et al. 1996). The most typical paragenesis of these complexes consists of laurite + (Pt, Ir, Rh, Ni, Fe, Cu)-bearing sulfides and base-metal sulfides (including millerite, NiS). The study of multiphase inclusions leads to the assumption that complex solid-solutions of Pt, Fe, Ir, Rh, Pd, Cu, Ni, Au and S exist at high temperature (Johan et al. 1990). Tolstykh et al. (2000) suggested that these inclusions form from vapor-saturated residual melt in a closed-system situation in gas-rich miaroles.

Minerals of the erlichmanite-laurite solid-solution series vary from pure laurite (in association with ruthenarsenite), through Os-bearing laurite (in association with Pt-Fe alloy) to erlichmanite (in association with iridium). Rhodium is present up to 2.07 wt.%, which is one distinguishing feature of Uralian/Alaskan-type deposits (Johan et al. 1989).

Cherepanovite is a rare mineral. It was first described in the deposits of the Koryaksko-Kamchatskiy Ultrabasic Belt (Rudashevskiy et al. 1985b). Cherepanovite has also been found in New Zealand (Railton and Watters 1990), Tasmania, Australia (Botrill 1993), and the Polar and Southern Urals of Russia (Britvin et al. 1999; Garuti et al. 1999). Cherepanovite occurs in two varieties in the Zolotaya river samples: (1) low in Ru in core zones, (2) high in Ru in rim zones. The high Ru content in the cherepanovite structure suggests that there is a wide range in solid solution between cherepanovite and ruthenarsenite at high temperature.

All mineralogical and chemical observations point to a connection of the Zolotaya and Fadeevka river placers to the Late Permian dunite-hornblendite-gabbro intrusions of Uralian/Alaskan-type. The composition of the chromite from heavy-mineral concentrates and from inclusions within PGM from the Zolotaya placer is typical of Uralian/Alaskan-type intrusions, i.e., high chromium and iron content at relatively low titanium content. The primary PGM are dominated by Pt-Fe alloy (about 90%), and Os-Ir-Ru alloy is subordinate. All other PGM occur as rim or inclusion phases in the primary PGE alloys. Cooperite is impoverished in Ni. Rhodium and Cu are invariably present as minor elements of the Pt-Fe alloy, and the minerals of the laurite-erlichmanite solid solution have an elevated Rh content. Other Rh-bearing minerals present are cuprorhodsite and cherepanovite. The distinct rhodium signature is one of the main features of Uralian/Alaskan-type deposits.

3.5 PGM ASSOCIATION OF FADEEVKA RIVER PLACER

The PGE mineralogy of the Fadeevka river placer was first published in the reconnaissance study by Shcheka et al. (1991). The present chapter gives more detailed data including secondary alteration of primary magmatic minerals. The PGM grains were picked from a heavy mineral concentrate of the Fadeevka river (Fig. 2). Of 109 grains studied, the dominant amount (91 grains) is represented by Pt-Fe alloy, with the rest formed by Os-Ir (+Pt+Ru) alloys. A broad spectrum of PGE-bearing sulfides, sulfarsenides, arsenides, tellurides, bismuthides, antimonides, etc. was found as inclusions or rims within/after Pt-Fe alloy and Os-Ir alloy. One group of minerals (predominantly sulfides) forms multiphase assemblages as inclusions in Pt-Os-Ir and Pt-Fe alloy and is assumed to have a primary origin; the other mineral group occurs as rims and replacement aggregates and is of secondary origin. This group is represented by As-, S-, Sb-, Te-Sn-, Au-, Ag-bearing minerals.

3.5.1 Primary Pt-Fe alloy

Pt-Fe alloy constitutes the most abundant group of PGM found in the Fadeevka river alluvium. These grains vary from 100 μm up to 2-4 mm in size (Fig. 12) with minor-PGE element contents of Pd (up to 2,30 wt.%), Rh (up to 2,65 wt.%), Ir (up to 8,01 wt.%) and Os (up to 2,04 wt.%) (Table 7). The PGE/(Fe+Cu+Ni) ratio varies from 2 to 8 (Fig. 13). Pt-Fe alloy has primary inclusions consisting of laurite-erlichmanite solid solution and multiphase sulfide inclusions.

Inclusions of laurite-erlichmanite solid solution

Minerals of laurite-erlichmanite solid solution occur commonly as inclusions within the Pt-Fe alloy grains, and display compositional zoning (Table 8; Fig. 14). All laurite-erlichmanite inclusions are enriched in Rh (up to 5.80 wt.%) and Ir (up to 10.25 wt.%) and have traces of Pt.

TABLE 7. REPRESENTATIVE CHEMICAL COMPOSITION OF Pt -Fe ALLOY FROM FADEEVKA RIVER

	F2/1	f5.36	F1-1/19	F1-1/12	f5.16	f3.15	F2-2/1	F2-1-9	F1-1/14	F1-1/11	F2-2/4	F1-1/13	FD1.10	F1-1/13
wt.%														
Os	-	-	2.03	0.26	-	-	1.56	0.97	1.40	1.66	2.04	-	0.45	-
Ru	-	-	-	-	-	-	0.25	0.21	0.29	-	-	-	-	-
Rh	0.37	1.07	0.93	0.26	1.46	2.33	1.39	1.39	0.31	0.32	1.35	0.33	2.65	0.36
Pd	0.62	0.44	0.64	-	2.30	1.25	0.34	0.37	-	-	-	-	1.62	-
Pt	89.79	89.11	87.12	88.97	87.56	89.85	91.31	91.89	93.36	93.52	92.98	90.72	89.40	83.41
Ir	-	-	1.44	0.73	-	-	0.39	0.69	-	0.30	0.27	5.50	-	8.01
Ni	-	-	-	-	-	0.08	0.11	0.07	0.10	-	0.08	-	-	-
Fe	8.59	8.43	8.38	8.33	7.76	6.29	4.79	4.63	4.25	3.99	3.86	2.38	5.34	6.69
Cu	0.64	0.81	0.56	0.87	0.54	0.59	0.29	0.23	0.11	0.15	0.23	1.10	0.89	0.56
Total	100.01	99.86	99.06	99.15	99.62	100.39	98.61	99.28	98.13	98.28	98.76	100.04	100.34	99.03
at.%														
Os	-	-	1.67	0.22	-	-	1.39	0.87	1.29	1.54	1.86	-	0.38	-
Ru	-	-	-	-	-	-	0.42	0.35	0.50	-	-	-	-	-
Rh	0.57	1.64	1.41	0.40	2.24	3.66	2.28	2.31	0.53	0.56	2.27	0.58	4.21	0.58
Pd	0.92	0.65	0.94	0.00	3.42	1.90	0.53	0.60	-	-	-	-	2.50	-
Pt	72.65	71.93	69.94	72.80	71.01	74.50	79.38	80.31	83.76	84.60	82.78	83.50	74.99	71.12
Ir	-	-	1.18	0.61	-	-	0.34	0.61	-	0.28	0.24	5.14	-	6.91
Ni	-	-	-	-	-	0.22	0.33	0.21	0.30	-	0.22	-	-	-
Fe	24.28	23.77	23.49	23.79	21.98	18.22	14.54	14.14	13.32	12.60	12.00	7.66	15.64	19.93
Cu	1.59	2.01	1.37	2.18	1.34	1.50	0.78	0.61	0.31	0.42	0.62	3.12	2.28	1.46
Total	100	100	100	100	100	100	100	100	100	100	100	100	100	100

Note: S, Pb, Bi, Sn, Sb, Te, As were not detected; - below detection limit

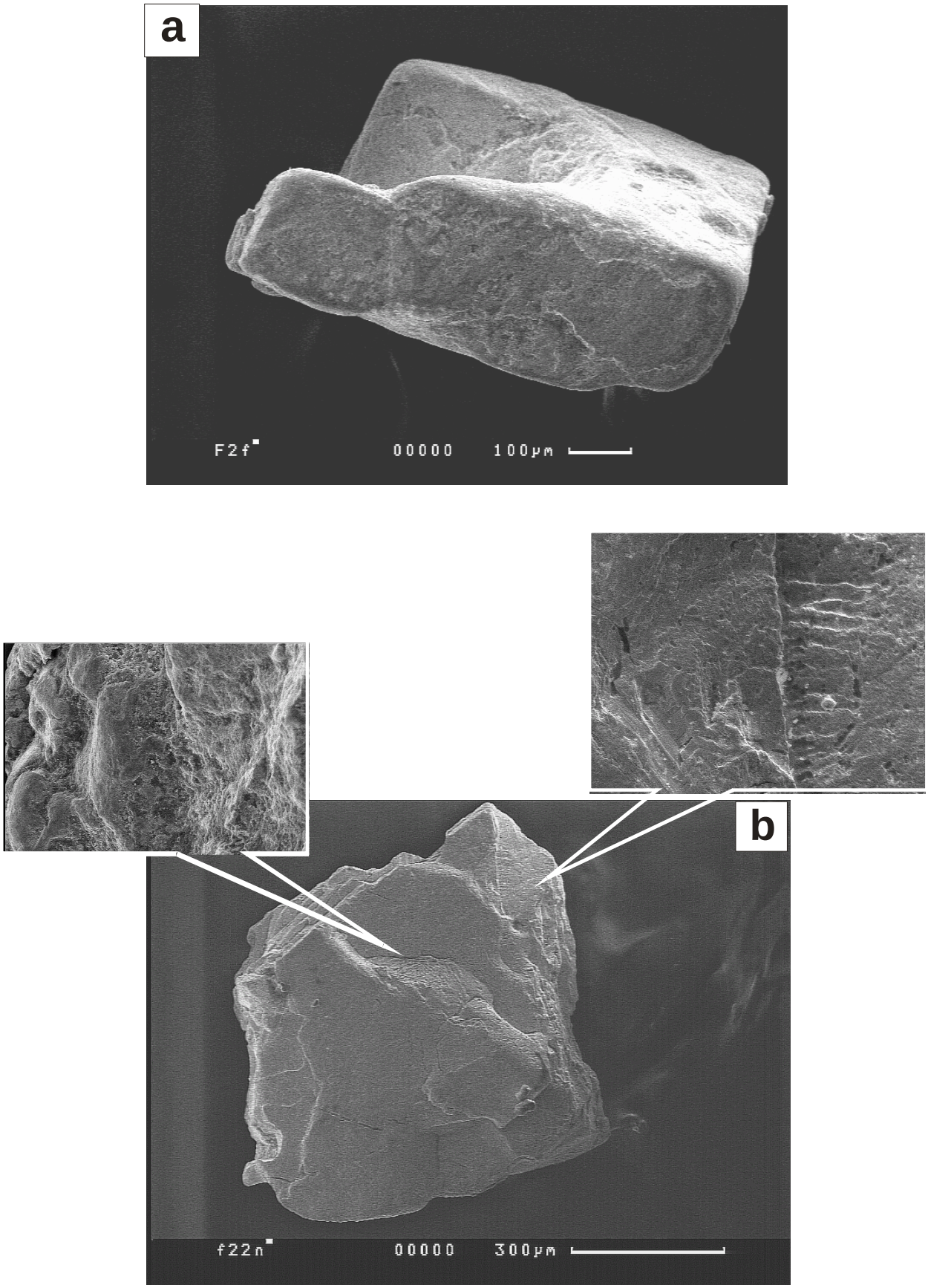

Fig. 12. *SEM photographs of Pt-Fe alloy crystals* ***(a)*** *and Os-Ir alloy* ***(b)*** *from Fadeevka river. Enlarged photos show the peculiarities of crystal growth.*

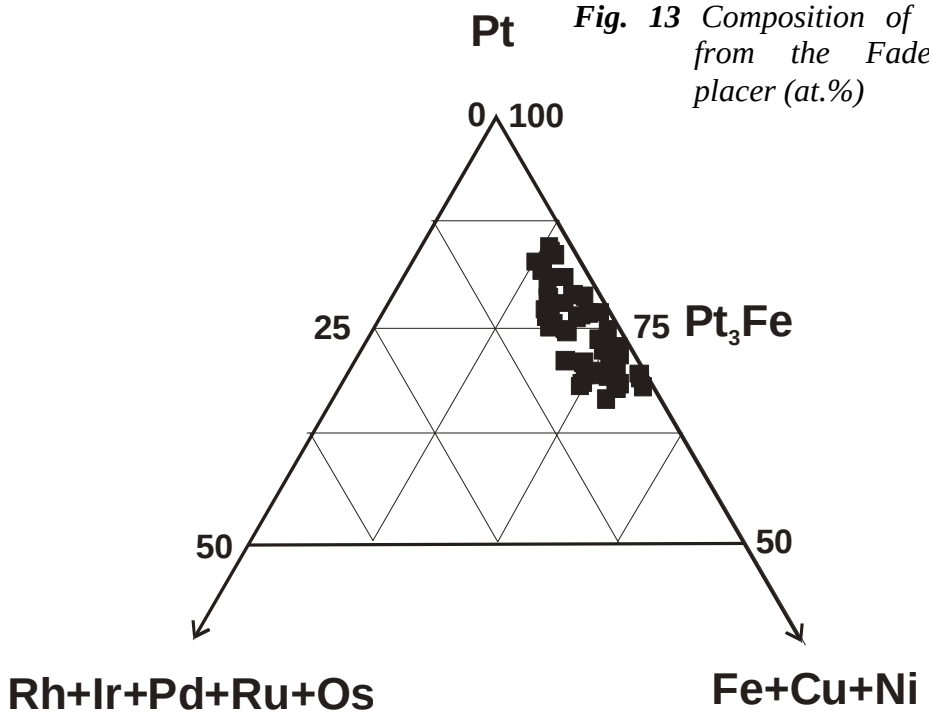

Fig. 13 *Composition of Pt-Fe alloy from the Fadeevka river placer (at.%)*

TABLE 8. CHEMICAL COMPOSITION OF LAURITE-ERLICHMANITE INCLUSIONS WITHIN Pt -Fe ALLOY OF THE FADEEVKA RIVER

	FD2-4		F1-63.2		F1-16.2		f3.20.3		F1-54in1
wt.%									
Os	16.80	25.72	19.76	24.48	32.10	29.65	41.77	46.88	51.28
S	33.74	31.25	34.25	33.76	28.29	30.17	30.11	30.25	27.13
Ru	37.63	29.45	37.87	35.30	19.33	25.16	21.15	18.40	9.06
Rh	4.89	5.33	4.70	3.73	5.80	4.27	2.39	2.37	1.49
Pt	1.11	1.29	1.24	1.60	0.75	1.13	1.61	0.79	1.77
Ir	4.93	4.69	2.24	1.85	10.25	7.46	2.46	2.33	9.93
Fe	-	-	-	0.13	-	-	0.11	0.08	0.23
Cu	0.08	-	-	-	-	-	-	-	-
As	2.32	2.21	-	-	3.68	2.36	0.10	0.06	0.46
Total	101.50	99.94	100.06	100.85	100.20	100.20	99.70	101.16	101.35
at.%									
Os	5.44	8.93	6.45	8.11	12.01	10.65	15.51	17.44	20.88
S	64.79	64.39	66.33	66.33	62.80	64.30	66.34	66.75	65.55
Ru	22.93	19.25	23.27	22.01	13.61	17.01	14.78	12.88	6.94
Rh	2.93	3.42	2.84	2.28	4.01	2.84	1.64	1.63	1.12
Pt	0.35	0.44	0.39	0.52	0.27	0.40	0.58	0.29	0.70
Ir	1.58	1.61	0.72	0.61	3.80	2.65	0.90	0.86	4.00
Fe	-	-	-	0.15	-	-	0.14	0.10	0.32
Cu	0.08	-	-	-	-	-	-	-	-
As	1.91	1.95	-	-	3.50	2.15	0.09	0.06	0.48
Total	100	100	100	100	100	100	100	100	100

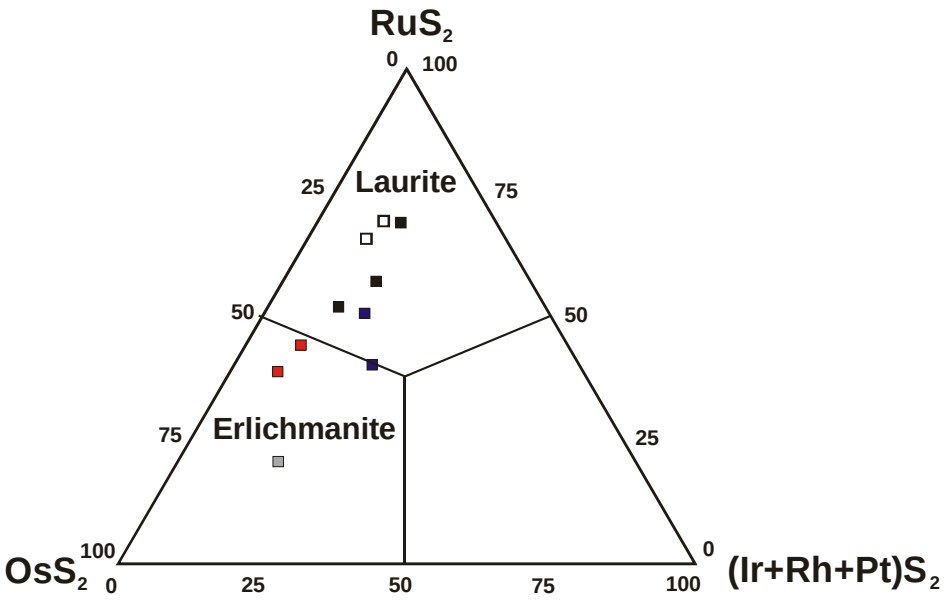

Fig. 14. *Mineral composition of the laurite-erlichmanite solid solution (at.%). Different colors of squares correspond to different inclusions.*

3.5.2. Primary Os-Ir-Ru-Pt alloy

Os-Ir alloy occurs as either (1) individual grains ranging from 0.3 up to 2-3 mm in size (Fig 12b); or (2) entrapped lath-like inclusions of ~ 20-30 μm in size (Fig. 15a), or (3) exsolution lamellae with 1-3 μm in size within Pt-Fe alloy (Fig.15b,c).

The alloy grains vary from iridium (nomenclature according to Harris and Cabri, 1991) with significant Pt content and low Ru content up to osmium with low Pt and high Ru content (Fig. 16; Table 9 Nos 1-9). Rh is a significant minor element with 0.10-4.85 wt.% (mean: 0.84 ± 0.94; n=53). The grains of the iridium group generally are enriched in Pt, and are often altered with formation of secondary rims and inclusions in contrast to the osmium group grains. The entrapped lath-like inclusions belong to the osmium field, but with significantly lower Ru content compare to the individual osmium grains (Table 9, Nos 10-11). The chemical composition of exsolution lamellae within the Pt-Fe alloy corresponds to native Os composition with only minor content of Ir (up to 1.76 wt.%) and Pt (up to 2.66 wt.%) (Table 9, Nos 12-14).

Inclusions of laurite-erlichmanite solid solution

Two Ru-rich (up to 16 wt.%) osmium grains contain laurite-erlichmanite inclusions [RuS_2-OsS_2] with Ir, Rh and As as main trace elements. One of the sulfide inclusions is zonal with the Os component increasing from the center of the laurite-erlichmanite grain towards the outermost part of the laurite-erlichmanite grain (Fig. 17; Table 10).

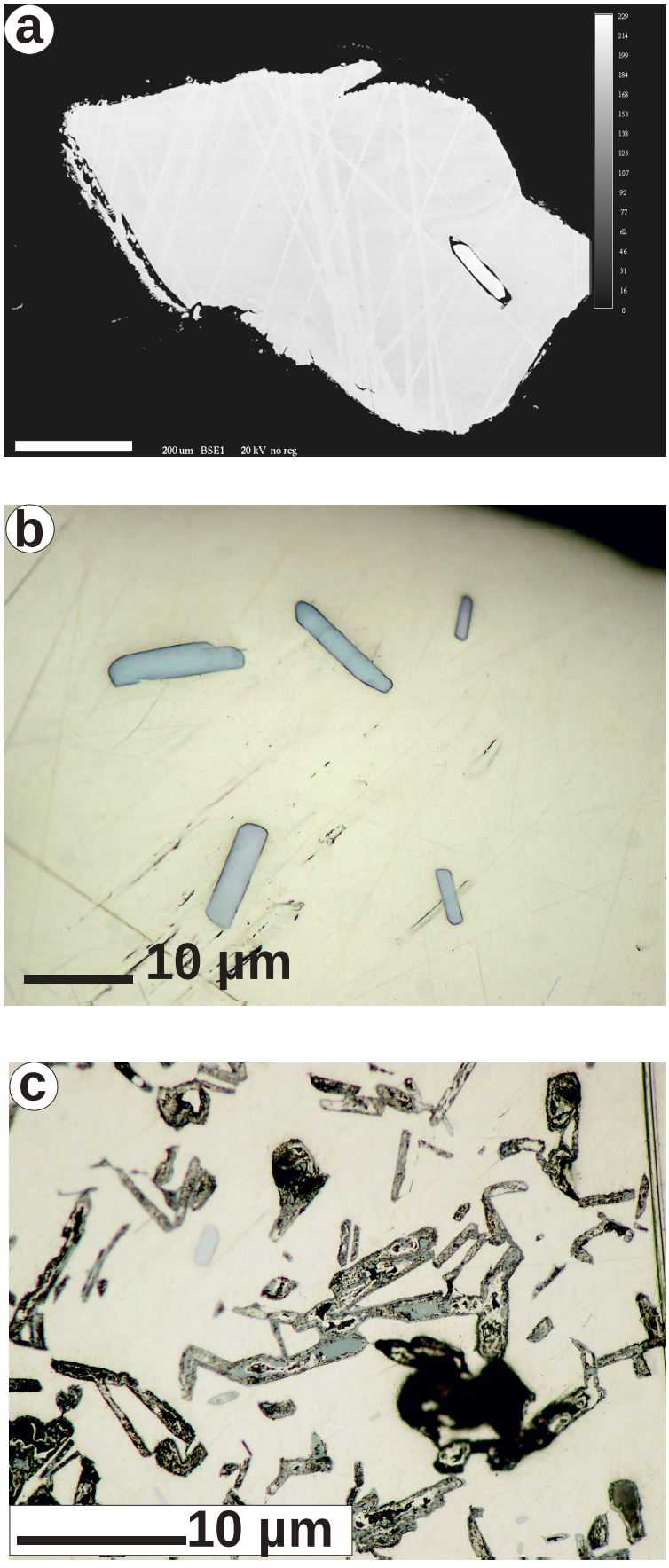

Fig. 15. (a) *BSE image of entrapped lath-like Os-Ir inclusion within Pt-Fe alloy grain;* ***(b)*** *microphotograph (oil immersion) of Os (+Ir) exsolution lamellae within Pt-Fe alloy grain;* ***(c)*** *microphotograph (oil immersion) of altered Os (+Ir) exsolution lamellae within Pt-Fe alloy grain.*

TABLE 9. SELECTED CHEMICAL ANALYSES OF Os-Ir ALLOY OF FADEEVKA RIVER

	1	2	3	4	5	6	7	8	9	10	11	12	13	14
	FD1-1	FD2-19	F3-9	F5	FD2-1	FD2-25	FD2-35	FD2-35	FD2-35	FD2-25	FD2-25	F1-1/11	F2-2/4	F2-1/8
wt.%														
Os	24.15	22.95	24.11	1.61	35.97	49.17	62.80	63.77	64.59	60.94	72.38	94.66	95.26	97.13
Ir	67.23	65.06	65.33	91.33	49.35	44.09	17.71	16.88	16.79	32.08	22.45	1.44	1.76	-
Ru	3.09	0.25	0.55	0.87	2.44	5.85	18.93	18.23	17.78	5.49	4.45	0.83	0.91	0.74
Rh	0.76	-	1.62	1.43	0.48	-	0.81	0.77	0.59	0.18	-	0.44	0.33	0.24
Pt	3.54	10.82	9.13	2.25	11.06	-	-	-	-	-	-	2.02	1.67	2.66
Ni	0.15	0.08	0.04	-	-	0.12	-	-	-	-	-	-	-	-
Fe	0.20	0.74	0.42	0.95	0.21	0.74	-	-	-	0.44	0.14	-	-	0.07
Cu	-	0.17	0.00	-	0.19	0.07	0.06	-	-		0.08	-	-	-
Total	99.12	100.07	101.20	98.44	99.70	100.04	100.31	99.65	99.75	99.13	99.50	99.39	99.92	100.84
at.%														
Os	23.56	22.58	23.35	1.58	35.14	45.98	53.39	54.87	55.80	58.12	69.80	94.25	94.38	95.41
Ir	64.90	63.34	62.61	88.87	47.71	40.80	14.90	14.38	14.35	30.28	21.43	1.42	1.72	-
Ru	5.67	0.46	1.00	1.61	4.49	10.30	30.29	29.53	28.91	9.85	8.08	1.55	1.69	1.37
Rh	1.37		2.90	2.60	0.87	-	1.27	1.22	0.94	0.32	-	0.82	0.60	0.43
Pt	3.37	10.38	8.62	2.16	10.54	-	-	-	-	-	-	1.96	1.61	2.55
Ni		0.26	0.13	-	-	0.36	-	-	-	-	-	-	-	-
Fe	0.66	2.48	1.39	3.18	0.70	2.36	-	-	-	1.43	0.46	-	-	0.24
Cu	-	0.50	0.00	-	0.56	0.20	0.15	-	-	-	0.23	-	-	-
Total	100	100	100	100	100	100	100	100	100	100	100	100	100	100

Note: S, Pb, Bi, Ag, Sn, Sb, Te, Au, Co, As were not detected; - below detection limit
No 1-9 individual grains; 10-11 entrapped lath-like inclusions; 12-14 exolution lammelaes

TABLE 10. CHEMICAL COMPOSITION OF LAURITE-ERLICHMANITE INCLUSIONS WITHIN Os-Ir ALLOY OF FADEEVKA RIVER

	FD2-35								FD2-36/3
wt.%									
Os	42.96	1.75	35.86	2.43	30.17	40.75	44.11	47.01	33.63
S	28.53	36.27	29.35	36.24	30.74	30.25	27.61	27.33	29.00
Ru	20.06	56.45	25.23	56.07	31.49	24.02	19.94	17.72	28.10
Rh	0.78	1.31	0.90	1.24	0.85	0.79	0.85	0.66	1.18
Ir	5.72	0.99	5.80	0.81	4.20	4.99	5.27	5.70	8.10
As	0.72	2.78	0.86	2.60	1.20	0.76	0.74	0.67	0.99
Total	98.77	99.55	98.00	99.39	98.65	101.56	98.52	99.09	101.00
at.%									
Os	16.59	0.52	13.43	0.73	10.75	14.89	17.36	18.72	12.40
S	65.37	64.49	65.20	64.63	65.00	65.56	64.46	64.58	63.42
Ru	14.58	31.85	17.78	31.72	21.12	16.52	14.77	13.28	19.50
Rh	0.56	0.73	0.62	0.69	0.56	0.53	0.62	0.49	0.80
Ir	2.19	0.29	2.15	0.24	1.48	1.80	2.05	2.25	2.96
As	0.71	2.12	0.82	1.98	1.09	0.70	0.74	0.68	0.93
Total	100	100	100	100	100	100	100	100	100

Note: Pd, Pt, Sb, Ni, Fe, Cu, Te below detection limit

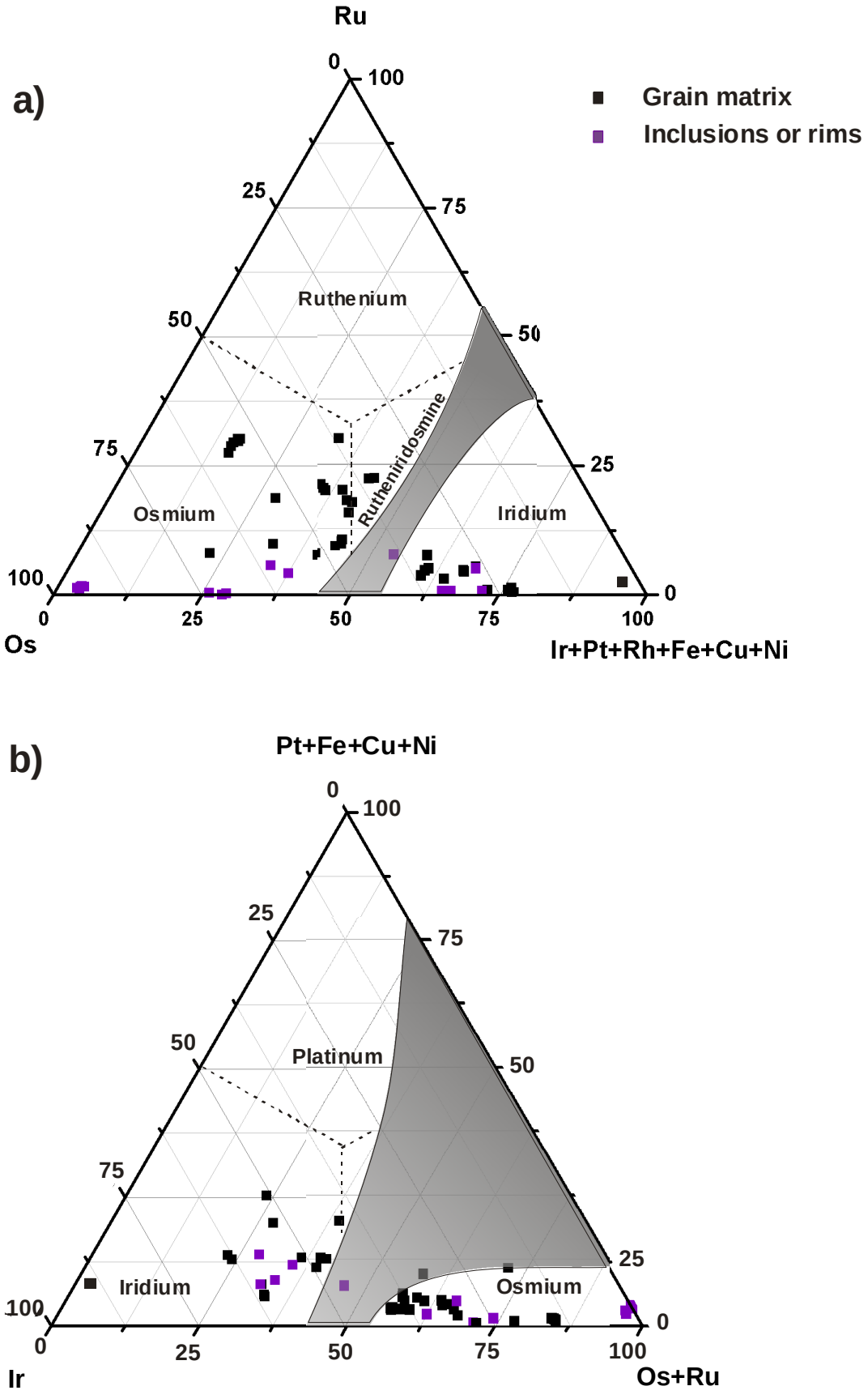

***Fig. 16**. Composition of Os-Ir-Ru-Pt alloy (at.%). The shaded area represents the miscibility gap according to Harris and Cabri (1991).*

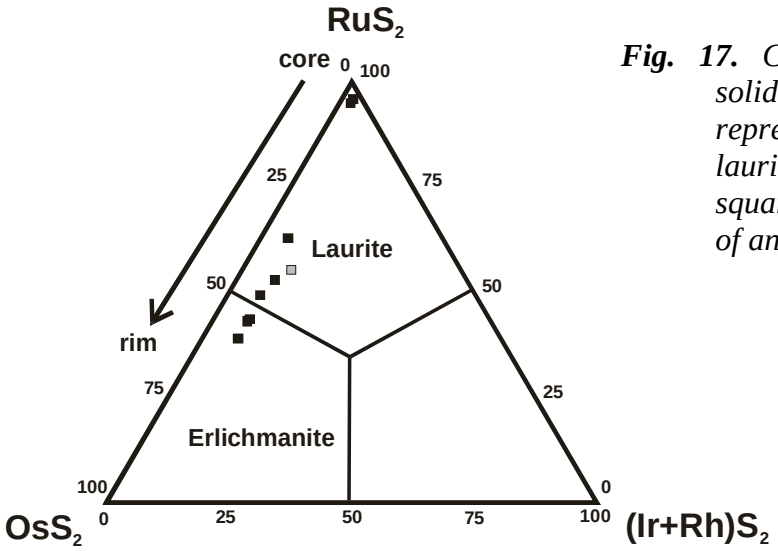

Fig. 17. *Composition of laurite-erlichmanite solid solution. The black squares represent the compositional zoning of one laurite-erlichmanite inclusion; the gray square represents chemical composition of another inclusion.*

3.5.3. Primary magmatic polymineralic sulfide inclusions

PGE sulfides in PGE-bearing deposits of chromite type (Uralian/Alaskan and ophiolite environments) are rare and mainly represented by minerals of laurite-erlichmanite solid solution [OsS_2-RuS_2] and cooperite [PtS]. Only zones of hydrothermal alteration are characterized by a wide spectrum of PGM with Ni, Cu, S, As, Te, Bi, Sn, Sb and Pb. Generally, the Cu-rich minerals are represented by minerals typical of hydrothermal paragenesis (bornite, cubanite, and chalcocite). Their secondary origin is proved by several factors, i.e. style of occurrence (as rims and veinlets in magmatic PGM), association with low-temperature minerals such as quartz, chlorite, actinolite, albite, fluorite, etc., and by close spatial association with contact and fracture zones in ultramafic rock with quartz veins and dikes of alkaline and felsic rocks. However, there are also doubtless magmatic but minor occurrences of pyrrhotite, pentlandite and chalcopyrite intergrown with PGM, chromite, olivine and Cr-bearing titanomagnetite. This chapter is on the compositional investigation of peculiar magmatic sulfide inclusions, found within several grains of Pt-Fe and Os-Ir alloys from the heavy mineral concentrate of the Fadeevka river placer, and comparison with published data from various other PGM localities.

Sample description

A number of PGM grains from the Fadeevka river contain small (<10 to 60 μm in size) roundish sulfide inclusions of complex mineral composition and with a specific very fine-grained internal fabric. Here we describe the two most representative multimineral inclusion types which occur both in Pt-Fe alloy and Os-Ir grains. Five less typical smaller composite inclusions are also studied.

Type 1: Composite sulfide inclusions in iridium matrix (sample FD2-1)

Composite inclusions of PGE and Cu-Ni sulfides were detected in a Pt-bearing iridium grain (1.2 mm across; Table 11).

TABLE 11. SELECTED ANALYSES OF THE MINERAL PHASES IN INCLUSION NO 1, SAMPLE FD2-1

Sample	Matrix	Pt-Pd-Ir-Fe alloy		Pyrrhotite	Cuprorhodsite		Vysotskite-braggite				Defocused
wt.%											
S	-	-	-	27.66	25.92	26.10	25.90	21.83	20.54	16.14	19.9
Os	35.97	0.55	0.49	-	-	-	-	-	-	0.83	
Ru	2.44	-	-	-	-	-	-	-	-	-	2.2
Rh	0.48	0.39	0.69	17.21	20.73	21.06	20.62	-	-	0.65	4.33
Pd	-	9.21	2.78	0.14	-	-	-	65.13	41.28	6.62	26.43
Pt	11.06	77.49	83.29	4.22	12.79	12.89	12.43	7.96	36.18	72.02	22.07
Ir	49.35	0.4	4.2	20.94	26.98	26.28	27.17	0.27	0.31	1.62	8.05
Ni	-	0.32	0.24	13.50	0.16	0.08	0.14	3.90	2.53	0.11	2.88
Fe	0.21	9.57	8.58	8.93	3.26	3.08	3.28	0.09	0.08	1.12	2.09
Cu	0.19	0.98	0.41	8.11	9.77	9.54	9.81	-	-	0.14	1.9
Co	-	-	-	-	-	-	-	-	-	-	0.06
Te	-	-	-	-	-	-	-	0.39	-	-	0.05
Total	99.70	98.91	100.68	100.71	99.61	99.03	99.35	99.57	100.92	99.25	89.96
at.%											
S	-	-	-	51.37	56.50	57.00	56.54	48.37	50.84	51.70	51.48
Os	35.14	0.42	0.40	-	-	-	-	0.10	-	-	
Ru	4.49	-	-	-	-	-	-	-	-	-	1.81
Rh	0.87	0.55	1.03	9.96	14.08	14.33	14.03	-	-	0.65	3.49
Pd	-	12.64	4.03	0.08	-	-	-	43.48	30.78	6.39	20.6
Pt	10.54	58.01	65.85	1.29	4.58	4.63	4.46	2.90	14.72	37.92	9.38
Ir	47.71	0.30	3.37	6.49	9.81	9.57	9.89	0.10	0.13	0.87	3.47
Ni	-	0.80	0.63	13.70	0.19	0.10	0.17	4.72	3.42	0.19	4.06
Fe	0.70	25.03	23.70	9.52	4.08	3.86	4.11	0.11	0.11	2.06	3.1
Cu	0.56	2.25	1.00	7.60	10.75	10.51	10.81	-	-	0.23	2.48
Co	-	-	-	-	-	-	-	-	-	-	0.09
Te	-	-	-	-	-	-	-	0.22	-	-	0.03
Total	100.00	100.00	100.00	100.00	100	100	100	100	100	100	100

Note: Pb, Au, Bi, Ag, Sn, Sb, As were not detected; - below detection limit

The largest inclusion is 60 μm across with smooth elliptical shape and sharp contacts to the iridium host (Fig. 18). The iridium matrix around the inclusion is optically and compositionally homogeneous without cracks and pipes. In the centre of the inclusion there is a pore surrounded by minerals of vysotskite-braggite solid solution [(Pd,Ni)S-(Pd,Pt,Ni)S] intergrown with cuprorhodsite [$CuRh_2S_4$]. Small inclusions of Rh-Ir bearing pyrrhotite and Pd-Ir bearing Pt-Fe alloy are located within this complex intergrowth.

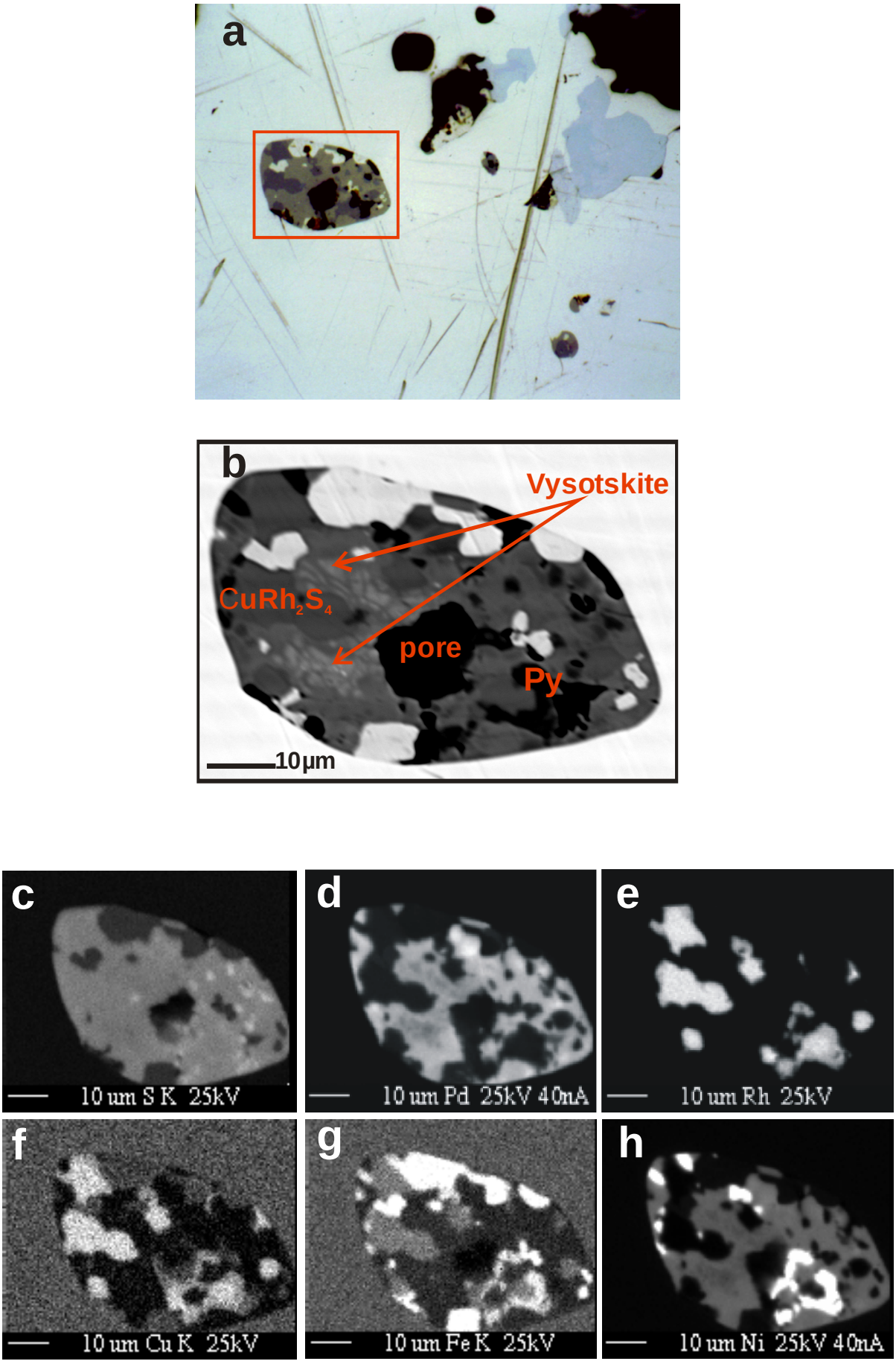

Fig. 18. ***(a)*** *Microphotograph (oil immersion) of Pt-rich Os-Ir grain with multiphase inclusions;* ***(b)*** *BSE image of the selected area;* ***(c-h)*** *Element-distribution maps showing S, Pd, Rh, Cu, Fe, Ni distributions within the multiphase inclusion. Sample FD2-1, polished section.*

Very small (1-3 μm) inclusions of laurite [RuS_2] were determined qualitatively. The analysis of this inclusion by defocused beam (40 μm in diameter) gives a pyrrhotite bulk-stoicheometry with unusually high Pd-content.

Type 2: Composite sulfide inclusions in Pt-Fe matrix (sample F3-15)

Pt-Fe alloy grains also contain multiphase sulfide inclusions. The most representative is a 40 μm-large roundish inclusion located close to the grain edge of Rh-Pd bearing Pt-Fe alloy (Fig. 19).

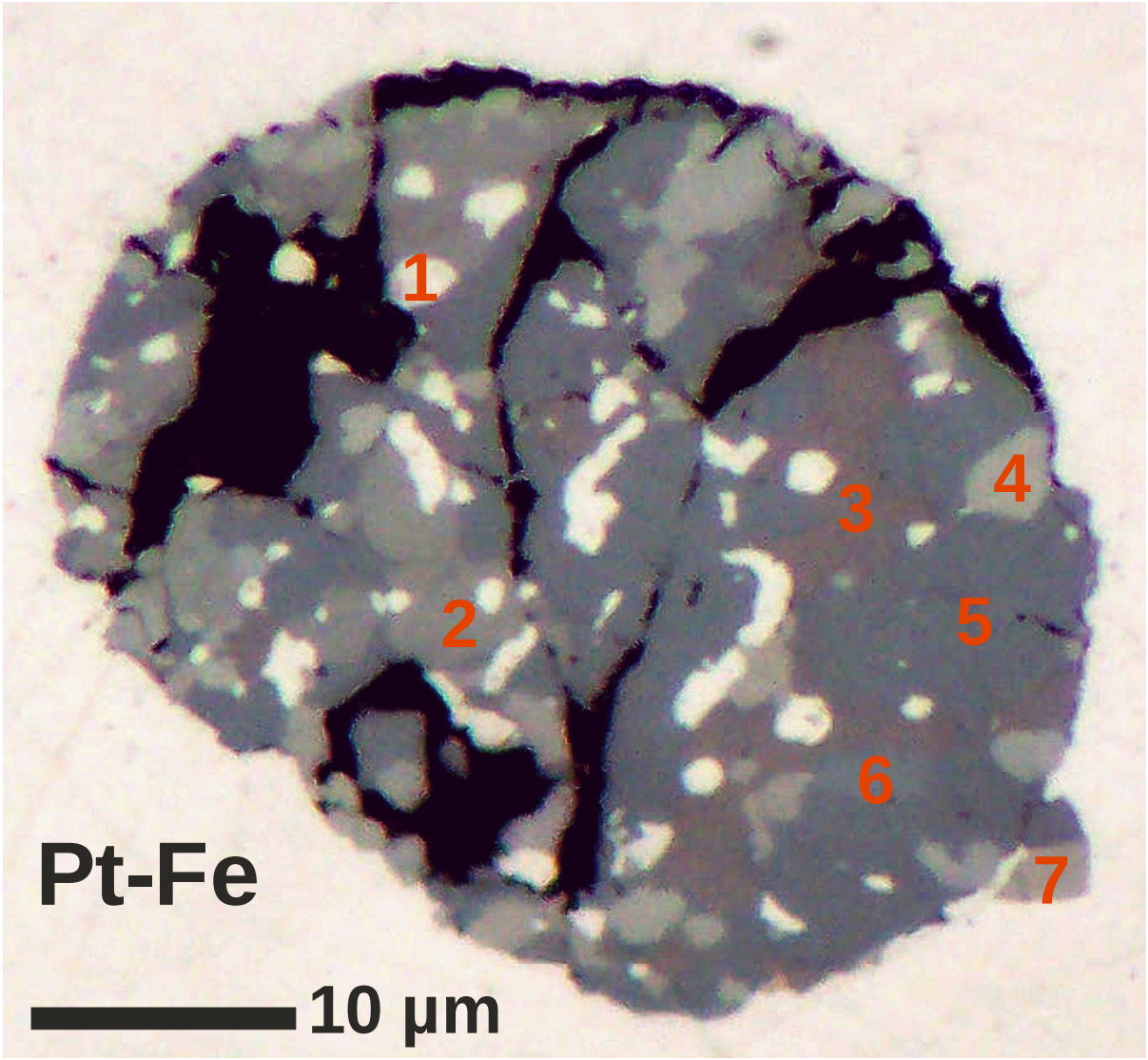

Fig. 19. *Microphotograph (oil immersion) of multiphase inclusion within Pt-Fe alloy:* ***(1)*** *Pd-rich Pt-Fe alloy;* ***(2)*** *Fe-rich vysotskite;* ***(3)*** *Cu-bearing vasilite/$(Pd,Cu)_7S_3$;* ***(4)*** *bowieite;* ***(5)*** *cuprorhodsite;* ***(6)*** *Rh-rich pyrrhotite;* ***(7)*** *keithconnite. Sample F3-15, polished section.*

There are at least six different minerals, which compose this inclusion: Fe-rich vysotskite [PdS], cuprorhodsite [$CuRh_2S_4$], bowieite [Rh_2S_3], Cu-bearing vasilite [$Pd_{16}S_7$], which is ideally calculated as $(Pd,Cu)_7S_3$, Pd-rich Pt-Fe alloy with a general formula of $(Pt,Pd,Rh)_3(Fe,Cu)_1$, and Rh-rich pyrrhotite (Table 12). At the very edge of the inclusion occurs keithconnite [$Pd_{3-x}Te$].

TABLE 12. SELECTED ANALYSES OF THE MINERAL PHASES IN INCLUSION NO 2, SAMPLE F3-15

	Matrix	Pt-Pd-Fe alloy		Pyrrhotite	Cuprorhodsite		Bowieite	Vysotskite	Vasilite	
wt.%										
S	-	-	-	29.49	30.66	30.00	30.80	22.65	12.31	12.25
Os	-	-	-	-	-	-	-	-	-	-
Ru	-	-	-	0.89	1.13	1.21	1.32	-	0.38	-
Rh	2.2	1.75	1.68	30.84	49.97	47.26	66.81	-	-	-
Pd	0.9	4.69	9.54	2.19	-	1.9	0.36	61.04	72.74	73.92
Pt	89.58	83.75	80.31	4.06	3.84	3.85	2.24	10.21	2.2	2.16
Ir	-	-	-	-	-	-	-	-	-	-
Ag	-	-	-	-	0.84	0.63	-	-	-	-
Ni	0.08	0.22	0.14	18.87	0.14	1.74	-	5.75	-	0.05
Fe	6.42	8.72	7.9	5.27	6.18	5.87	0.18	0.16	0.15	0.2
Cu	0.72	0.61	0.79	7.53	8.18	8.00	-	-	12.84	12.56
Co	-	-	-	0.84	-	-	-	-	-	-
Total	99.90	99.74	100.36	99.98	100.94	100.46	101.71	99.81	100.62	101.14
at.%										
S	-	-	-	50.58	55.52	54.68	57.16	49.29	29.82	29.62
Os	-	-	-	-	-	-	-	-	-	-
Ru	-	-	-	0.48	0.65	0.70	0.78	-	0.29	-
Rh	3.47	2.58	2.42	16.48	28.20	26.84	38.63	-	-	-
Pd	1.37	6.68	13.30	1.13	0.00	1.04	0.20	40.01	53.10	53.85
Pt	74.46	65.06	61.09	1.14	1.14	1.15	0.68	3.66	0.88	0.86
Ir	0.00	-	-	-	0.00	0.00	-	-	-	-
Ag	-	-	-	-	0.45	0.34	-	-	-	-
Ni	0.22	0.57	0.35	17.68	0.14	1.73	-	6.84	-	0.07
Fe	18.64	23.66	20.99	5.19	6.43	6.14	0.19	0.20	0.21	0.28
Cu	1.84	1.45	1.84	6.52	7.47	7.36	2.35	-	15.70	15.32
Co	-	-	-	0.78	-	-	-	-	-	-
Total	100	100	100	100	100	100	100	100	100	100

Note: Pb, Bi, Te, Sn, Sb, As were not detected; - below detection limit

Type 3: Other polymineralic sulfide inclusions

Three considerably smaller in size (10 μm in diameter) multiphase inclusions occur in the same Pt-bearing iridium grain, which hosts the above described Type 1 inclusions (Sample FD2/1) Among the minerals distinguished there are vysotskite, Pd-bearing Pt-Fe alloy and cuproiridsite (Table 13). Moreover, μm-sized Ir-Rh-Pd-bearing pyrrhotite occurs in the centre of the complex inclusion. The analysis of the 10 μm size inclusion by defocused beam gives a bulk composition of Pd, Pt, Rh, Ir- bearing pyrrhotite.

TABLE 13. SELECTED ANALYSES OF THE MINERAL PHASES IN INCLUSION NO 3, SAMPLE FD2-1

	Pt-Pd-Fe	Pyrrhotite	Cuproiridsite	Vysotskite	Vasilite
wt.%					
S	-	25.83	25.78	21.39	14.6
Os	1.27	-	-	-	0.47
Ru	-	-	-	-	0.21
Rh	0.43	10.06	19.14	-	-
Pd	11.95	7.59		53.03	70.29
Pt	73.43	3.58	2.25	22.44	5.93
Ir	3.32	26.55	39.81	1.56	1.06
Ni	0.38	14.23	2.5	2.79	0.95
Fe	8.62	4.46	1.39	-	0.03
Cu	0.43	5.82	8.1	0.08	7.12
Co	-	0.79	-	-	-
Total	99.83	98.91	98.97	101.29	100.66
at.%					
S	-	51.69	57.28	49.88	35.44
Os	0.98	-	-	-	0.19
Ru	-	-	-	-	0.17
Rh	0.61	6.27	13.25	-	-
Pd	16.41	4.58		37.26	51.39
Pt	55.00	1.18	0.82	8.60	2.37
Ir	2.52	8.86	14.76	0.61	0.43
Ni	0.95	15.56	3.03	3.55	1.25
Fe	22.55	5.12	1.77	-	0.04
Cu	0.99	5.88	9.08	0.09	8.72
Co	-	0.86	-	-	-
Total	100	100	100	100	100

Note: Pb, Au, Bi, Te, Sn, Sb, As were not detected; - below detection limit

Another Ru-Ir-Os grain with preserved hexagonal outline (sample FD2-25) contains several inclusions up to 30 μm size in the outermost part of the grain (Fig. 20). The inclusions consist of Ni pentlandite $(Ni_{5.42}Fe_{3.37}Rh_{0.04}Co_{0.04}Ir_{0.03}Cu_{0.02})_{8.92}S_{8.08}$ with only traces of PGE, occasionally intergrown with bornite and millerite (Table 14).

Another grain of Pd-Rh-bearing Pt-Fe alloy (sample F5-16) contains several multiphase inclusions of maximum 20 μm size located in the outermost part of the grain at relatively equal distance from the centre. The mineral assemblage is characterized by the following phases: vysotskite, cuprorhodsite, and Cu-vasilite $(Pd,Cu)_7S_3$ (Table 15).

Sample F1-8 consists of Pd, Rh-bearing Pt-Fe alloy and hosts small (8 μm in diameter) roundish inclusions which consist of vysotskite, bowieite, and Cu-vasilite/$(Pd,Cu)_7S_3$ (Table 16).

The polymineralic association of vysotskite, cuprorhodsite, bornite, and Rh,Ag,Pd-bearing pentlandite (?) occurs in a grain of Pt-Fe alloy (Sample F5-36) (Table 17).

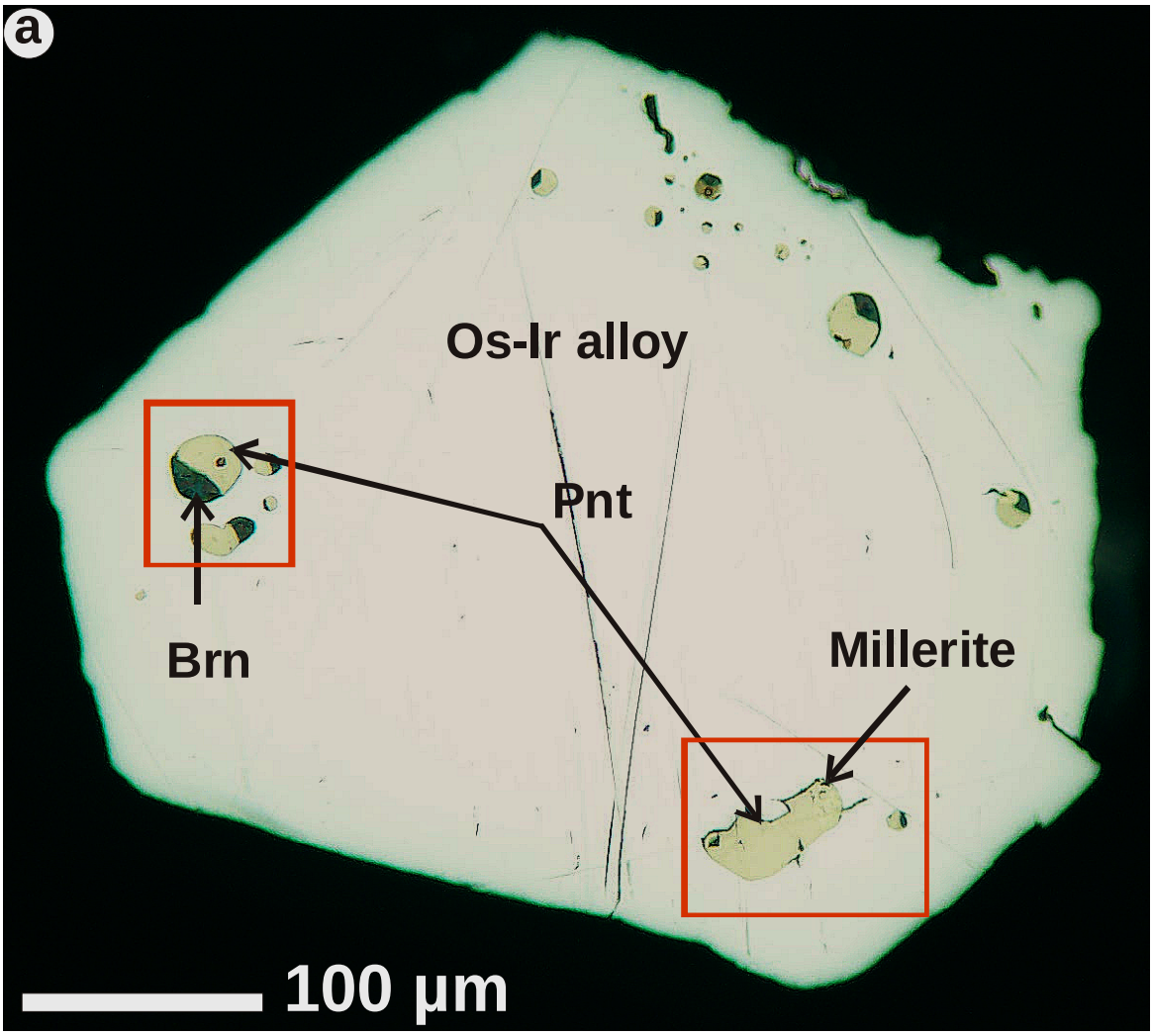

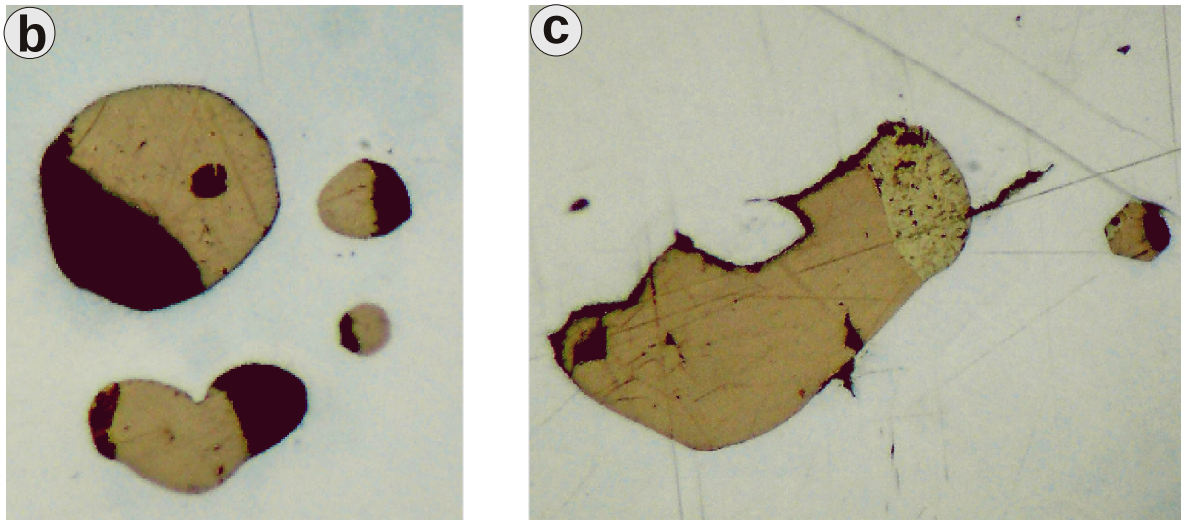

Fig. 20. a) *Microphotographs (oil immersion) of Ru-Os-Ir grain with preserved hexagonal outline and inclusions of Ni pentlandite intergrown with bornite and millerite;* ***b)*** *and* ***c)*** *enlarged parts of the grain. Sample FD2-25.*

TABLE 14. SELECTED ANALYSES OF THE MINERAL PHASES IN INCLUSION NO 4, SAMPLE FD2-25

	Matrix	Pentlandite	Bornite	Millerite
S	-	32.49	22.99	32.33
Os	46.44	-	-	-
Ru	5.86	0.29	-	-
Rh	-	0.53	-	-
Ir	45.63	0.82	-	0.67
Ni	-	39.88	0.46	62.65
Fe	0.74	23.59	9.56	0.43
Cu	0.07	0.16	68.19	-
Co	-	0.31	-	-
Total	98.74	98.07	101.20	96.08
S	-	47.51	36.41	48.35
Os	44.08	-	-	-
Ru	10.47	-	-	-
Rh	-	0.24	-	-
Ir	42.86	0.20	-	0.17
Ni	-	31.85	0.40	51.11
Fe	2.39	19.83	8.69	0.37
Cu	0.20	0.12	54.50	
Co	-	0.25	-	-
Total	100	100	100	100

Note: Pd, Pt, Ag, Pb, Bi, Te, Sn, Sb, As were not detected;

TABLE 15. SELECTED ANALYSES OF THE MINERAL PHASES IN INCLUSION NO 5, SAMPLE F5-16

	Matrix	Cuprorhodsite	Vysotskite	Vasilite
wt.%				
S	-	32.62	22.71	12.82
Ru	-	2.27	0.98	-
Rh	1.46	50.64	1.98	-
Pd	2.3	-	63.12	75.3
Pt	87.56	1.46	8.13	1.89
Ir	-	0.32	-	-
Ag	-	0.99	-	-
Ni	-	0.47	1.75	-
Fe	7.76	7.51	0.48	0.32
Cu	0.54	6.94	0.23	12.14
Total	99.62	103.22	99.38	102.47
at.%				
S	-	56.48	50.09	30.43
Ru	-	1.24	0.69	-
Rh	2.24	27.31	1.36	-
Pd	3.42	-	41.95	53.86
Pt	71.01	0.41	2.95	0.74
Ir	-	0.09	-	-
Ag	-	0.51	-	-
Ni	-	0.45	2.11	-
Fe	21.98	7.45	0.61	0.44
Cu	1.34	6.06	0.26	14.54
Total	100	100	100	100

Note: Os, Pb, Co, Bi, Te, Sn, Sb, As were not detected;
- below detection limit

TABLE 16. SELECTED ANALYSES OF THE MINERAL PHASES IN INCLUSION NO 6, SAMPLE F1-8

	Matrix	Bowieite	Braggite	Vasilite
	wt.%			
S	-	28.41	19.28	11.81
Os	0.78	-	-	-
Ru	-	1.07	-	-
Rh	2.52	55.37	1.19	-
Pd	4.51	10.75	46.68	80.44
Pt	85.35	4.38	34.35	4.54
Ir	-	0.45	-	-
Ag	-	0.76	-	-
Ni	0.04	0.07	0.38	-
Fe	5.31	0.13	0.14	0.09
Cu	0.50	0.28	0.38	4.45
Total	99.01	101.67	102.40	101.33
	at.%			
S	-	56.24	48.40	30.21
Os	0.67	-	-	-
Ru	-	0.67	-	-
Rh	4.00	34.15	0.93	-
Pd	6.92	6.41	35.29	62.00
Pt	71.34	1.43	14.18	1.91
Ir	-	0.15	-	-
Ag	-	0.45	-	-
Ni	0.12	0.08	0.52	-
Fe	15.65	0.15	0.21	0.13
Cu	1.30	0.28	0.47	5.74
Total	100	100	100	100

Note: Pb, Co, Bi, Te, Sn, Sb, As were not detected;
- below detection limit

TABLE 17. SELECTED ANALYSES OF THE MINERAL PHASES IN INCLUSION NO 7, SAMPLE F5-36

	Matrix	Bornite	Pentlandite	Cuprorhodsite	Vysotskite
	wt.%				
S	-	26.17	27.91	28.57	21.47
Ru	-	-	-	0.20	-
Rh	1.07	-	10.75	29.14	-
Pd	0.45	-	3.98	-	58.19
Pt	89.11	1.51	5.70	28.93	20.61
Ir	-	-	-	0.37	-
Ag	-	-	7.31	0.39	-
Ni	-	-	-	-	0.97
Fe	8.43	10.72	12.44	1.98	0.20
Cu	0.81	63.35	30.97	11.77	-
Total	99.87	101.75	99.06	101.35	101.44
	at.%				
S	-	40.55	47.84	57.46	49.73
Ru	-	-	-	0.13	-
Rh	1.64	-	5.74	18.26	-
Pd	0.67	-	2.06	-	40.61
Pt	71.92	0.38	1.61	9.56	7.85
Ir	-	-	-	0.12	-
Ag	-	-	3.72	0.23	-
Ni	-	-	-	-	1.23
Fe	23.77	9.54	12.24	2.29	0.27
Cu	2.01	49.53	26.79	11.94	-
Total	100	100	100	100	100

Note: Os, Pb, Co, Bi, Te, Sn, Sb, As were not detected; - below detection limit

3.5.4 Secondary PGE minerals developed after primary Pt-Fe alloy

The most common secondary PGM form mono-mineralic or complex rims on Pt-Fe alloy and consist of cooperite [PtS] with sperrylite [$PtAs_2$] (Fig. 21; Table 18).

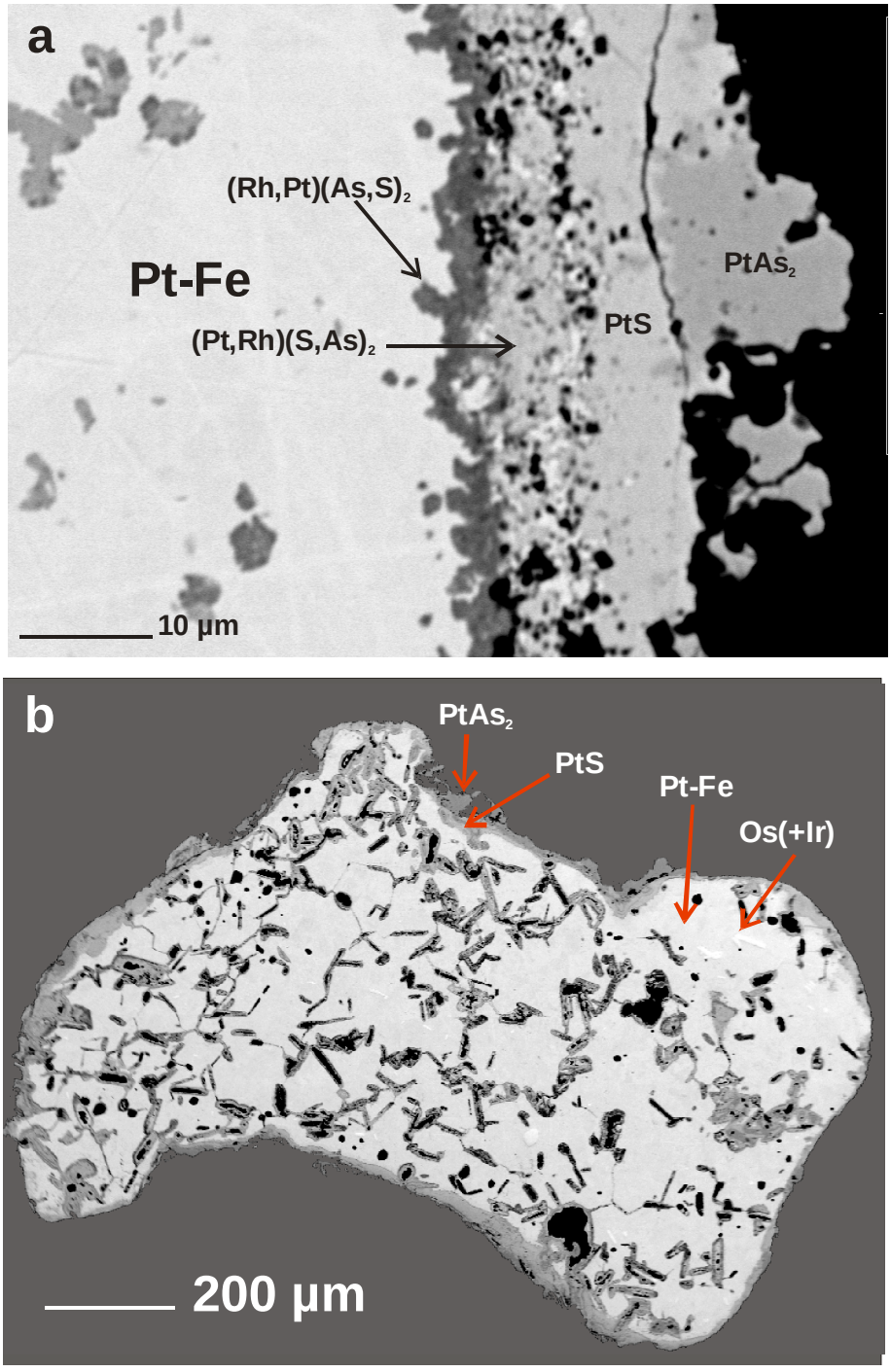

Fig. 21. *BSE image of Pt-Fe alloy grains mantled by complex rim, which consists of* ***(a)*** *hollingworthite [(Rh,Pt)(As,S)$_2$], platarsite [(Pt,Rh)(S,As)$_2$], cooperite [PtS] and sperrylite [$PtAs_2$]; **(b)** cooperite and sperrylite, formed as rim after Pt-Fe alloy and filling cavities after leached Os(+Ir) alloy inclusions.*

TABLE 18. SELECTED CHEMICAL ANALYSES OF SULFIDES, SULFARSENIDES AND ARSENIDES OF FADEEVKA RIVER

Mineral	PtS			Rh_3S_4	Ir_2S_3	Rh-Ir-Pt(As,S)$_2$							$PtAs_2$	
Sample	F2-9/7	f3.25.3	FD2-13/4	F6-39	F2-9/2	FD2_11	F1/5.13	FD2-4/6	F2-11	F2-8	F2-9	F2-14	F2-22	F1-24vr
wt.%														
Os	-	-	3.56	-	1.81	0.42	-	8.92	-	-	-	-	0.17	-
S	14.46	14.02	13.55	29.35	20.38	15.87	9.89	16.55	10.04	11.78	10.39	4.70	0.24	1.83
Bi	-	0.13	-	-	-	-	0.00	-	0.22	0.16	0.22	-	-	-
Ru	-	-	0.55	-	-	1.82	-	3.21	0.62	2.64	0.65	0.07	-	-
Rh	0.38	0.55	4.06	62.18	4.62	46.05	28.00	17.12	16.56	6.38	4.31	0.44	0.32	0.51
Pd	0.19	-	-	-	0.24	-	0.00	0.12	0.16	-	0.19	-	0.15	0.56
Ag	-	-	-	0.67	-	-	-	-	-	-	-	-	-	-
Sb	-	0.02	-	-	-	-	0.79	-	0.14	-	-	-	-	0.23
Te	-	-	-	-	-	-	-	-	-	-	-	-	0.18	
Pt	84.71	84.87	73.86	1.91	1.23	2.54	23.24	1.84	15.24	9.22	9.74	31.64	51.71	56.56
Ir	-	0.77	0.47	7.28	69.85	2.49	3.85	30.93	25.04	42.93	46.10	27.05	5.04	-
Fe	-	-	0.20	0.13	-	0.11	-	0.02	-	0.12	0.07	0.12	0.14	-
Cu	0.08	0.01	0.15	-	0.10	-	-	0.05	0.08	0.07	0.09	-	-	-
As	-	-	5.08	-	-	32.79	36.80	20.86	30.93	26.78	27.27	36.16	43.74	40.87
Total	99.82	100.37	101.48	101.52	98.23	102.09	102.57	99.62	99.03	100.08	99.03	100.18	101.69	100.56
at.%														
Os	-	-	1.99	-	0.89	0.15	-	3.87	-	-	-	-	0.10	-
S	50.56	49.54	44.91	58.09	59.77	34.66	25.34	42.58	28.30	33.78	31.41	15.61	0.84	6.31
Bi	-	0.07	-	-	-	-	-	-	0.10	0.07	0.10	-	-	-
Ru	-	-	0.58	-	-	1.26		2.62	0.55	2.40	0.62	0.07	-	-
Rh	0.41	0.61	4.19	38.34	4.22	31.33	22.35	13.72	14.54	5.70	4.06	0.46	0.35	0.55
Pd	0.20	-	-	-	0.21	-	-	0.09	0.14	-	0.17	-	0.16	0.58
Ag	-	-	-	0.39		-	-	-	-	-	-	-	-	-
Sb	-	0.02	-	-	-	-	0.53	-	0.10	-	-	-	-	0.21
Te	-	-	-	-	-	-	-	-	-	-	-	-	0.16	-
Pt	48.68	49.29	40.23	0.62	0.59	0.91	9.79	0.78	7.06	4.35	4.84	17.27	29.72	32.05
Ir	-	0.45	0.26	2.40	34.17	0.91	1.65	13.27	11.77	20.53	23.25	14.98	2.94	-
Fe	-	-	0.38	0.15	-	0.14	-	0.03	-	0.20	0.12	0.23	0.28	-
Cu	0.14	0.02	0.25	-	0.15	-	-	0.06	0.11	0.10	0.14	-	-	-
As	-	-	7.21	-	-	30.65	40.35	22.97	37.32	32.87	35.29	51.39	65.46	60.31
Total	100	100	100	100	100	100	100	100	100	100	100	100	100	100

Note: -: below analytical detection limit

The sulfarsenides are represented by minerals of hollingworthite-irarsite-platarsite solid solution with complete hollingworthite-irarsite series and rarer occurrence of platarsite (Fig. 21, 22). Cooperite and sperrylite occur as reaction rim and as inclusions within the Pt-Fe alloy grains, where they appear to fill cavities of leached osmium lammelae (Fig. 21).

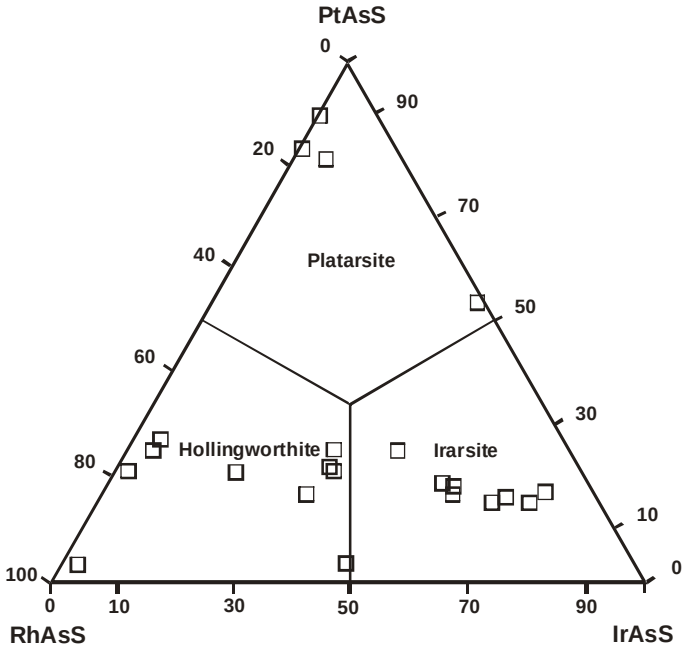

Fig. 22. *Chemical composition of platarsite-hollingworthite-irarsite solid solution (at.%) within Pt-Fe alloy grains of the Fadeevka river placer*

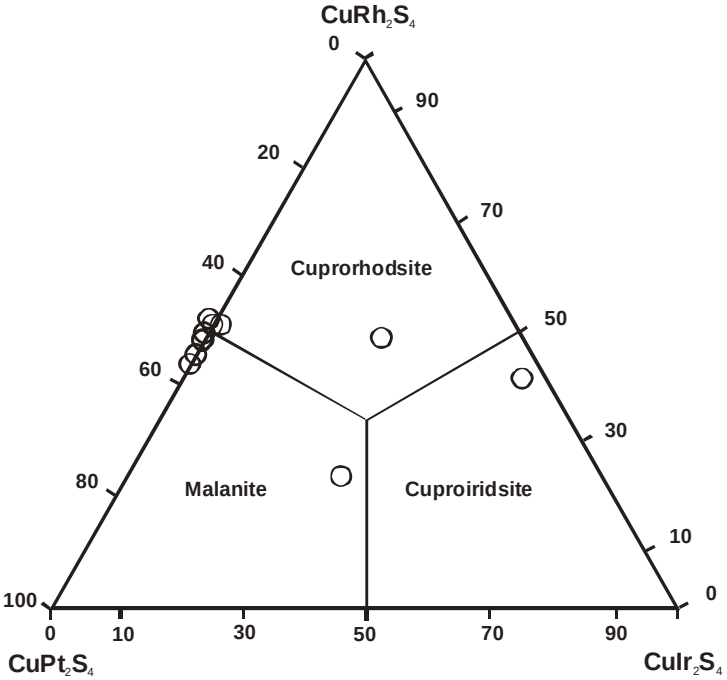

Fig. 23. *Chemical composition of cuprorhodsite-cuproiridsite-malanite solid solution (at.%) within Pt-Fe alloy grains of the Fadeevka river placer.*

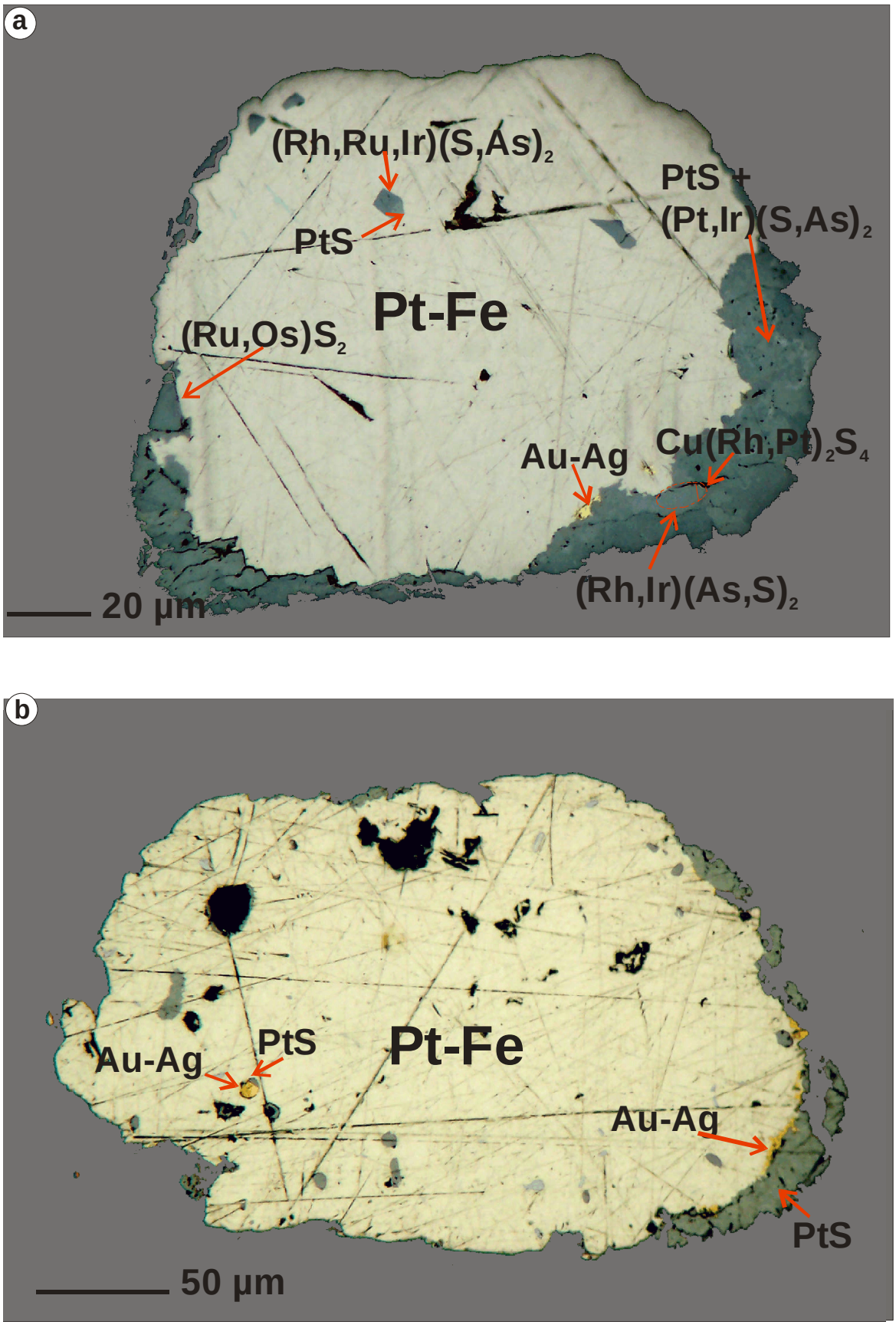

Fig. 24. *Microphotographs of Pt-Fe alloy grains rimmed by* ***(a)*** *complex rim of cooperite [PtS], platarsite [(Pt,Ir)(S,As)$_2$] and Au-Ag alloy. Within the grain occur inclusions of laurite-erlichmanite series [(Ru,Os,Ir)S$_2$], cuprorhodsite [CuRh$_2$S$_4$] and sulfarsenide [(Rh,Ir,Ru)(As,S)$_2$]; **(b)** complex Au-Ag alloy+cooperite rim. The same mineral assemblage also occurs as infill in cavities within the grain.*

Minerals of cuprorhodsite-cuproiridsite-malanite solid solution are also fairy common and occur either as inclusion at the periphery of the grains or as part of the complex rim with cooperite (Fig. 24a, Table 19). The malanite-cuprorhodsite minerals are the most abundant with single occurrence of cuproiridsite (Fig. 23).

TABLE 19. SELECTED ANALYSES OF MINERALS OF CUPRORHODSITE-CUPROIRIDSITE-MALANITE SOLID SOLUTION FROM FADEEVKA RIVER

Sample		FD2-4/7	FD2-22/7	FD2-22/7/3	FD2-22/10	F5_23	FD2-4/15	F3-25.3	f3.25.2
	wt.%								
Os		0.39	-	0.42	-	-	2.07	-	0.18
S		25.45	26.12	25.81	25.63	26.01	19.40	25.19	22.31
Bi		-	-	-	-	-	-	-	0.18
Ru		-	-	-	-	-	12.36	-	-
Rh		20.88	21.22	21.00	19.93	19.36	20.48	18.62	10.21
Pt		39.29	40.40	40.28	40.76	40.40	3.67	19.24	31.82
Ir		0.48	-	-	-	-	22.51	23.91	23.40
Ni		-	-	-	-	-	-	0.39	-
Fe		0.21	-	-	-	-	0.27	1.04	-
Cu		11.76	12.49	12.96	13.79	13.67	-	11.65	10.16
As		1.07	-	0.14	0.14	1.28	19.80	-	-
Total		99.53	100.23	100.61	100.25	100.72	100.56	100.04	98.26
	at.%								
Os		0.15	-	0.16	-	-	0.81	-	0.08
S		56.47	57.19	56.55	56.26	56.39	45.08	56.19	56.05
Bi		-	-	-	-	-	-	-	0.07
Ru		-	-	-	-	-	9.11	-	-
Rh		14.43	14.47	14.33	13.63	13.08	14.83	12.94	7.99
Pt		14.33	14.54	14.50	14.70	14.39	1.40	7.05	13.14
Ir		0.18	-	-	-	-	8.72	8.90	9.80
Ni		-	-	-	-	-	-	0.48	-
Fe		0.27	-	-	-	-	0.36	1.33	-
Cu		13.16	13.80	14.33	15.27	14.95	0.00	13.11	12.88
As		1.02	-	0.13	0.13	1.19	19.69	-	-
Total		100	100	100	100	100	100	100	100

Note: Pd, Ag, Sb, Te, and Au were not detected; -: below analytical detection limit

Kashinite [$(Ir,Rh)_2S_3$] and $(Rh,Pt)_3S_4$ phase occur only in single cases either as composite rim with cooperite or as fissure filling (Table 18).

The most interesting and unusual minerals developed within the Pt-Fe alloy grains are stumpflite [Pt(Sb,Bi)] and mertieite-II [Pd_8Sb_3].

Stumpflite occurs as inclusions (up to 50 μm) at the fissures along the crystallographic planes of sample F1-5 (Fig. 25; Table 20). Occasionally, it is overgrown by hollingworthite, which suggests the earlier formation of stumpflite (Fig. 25b,c).

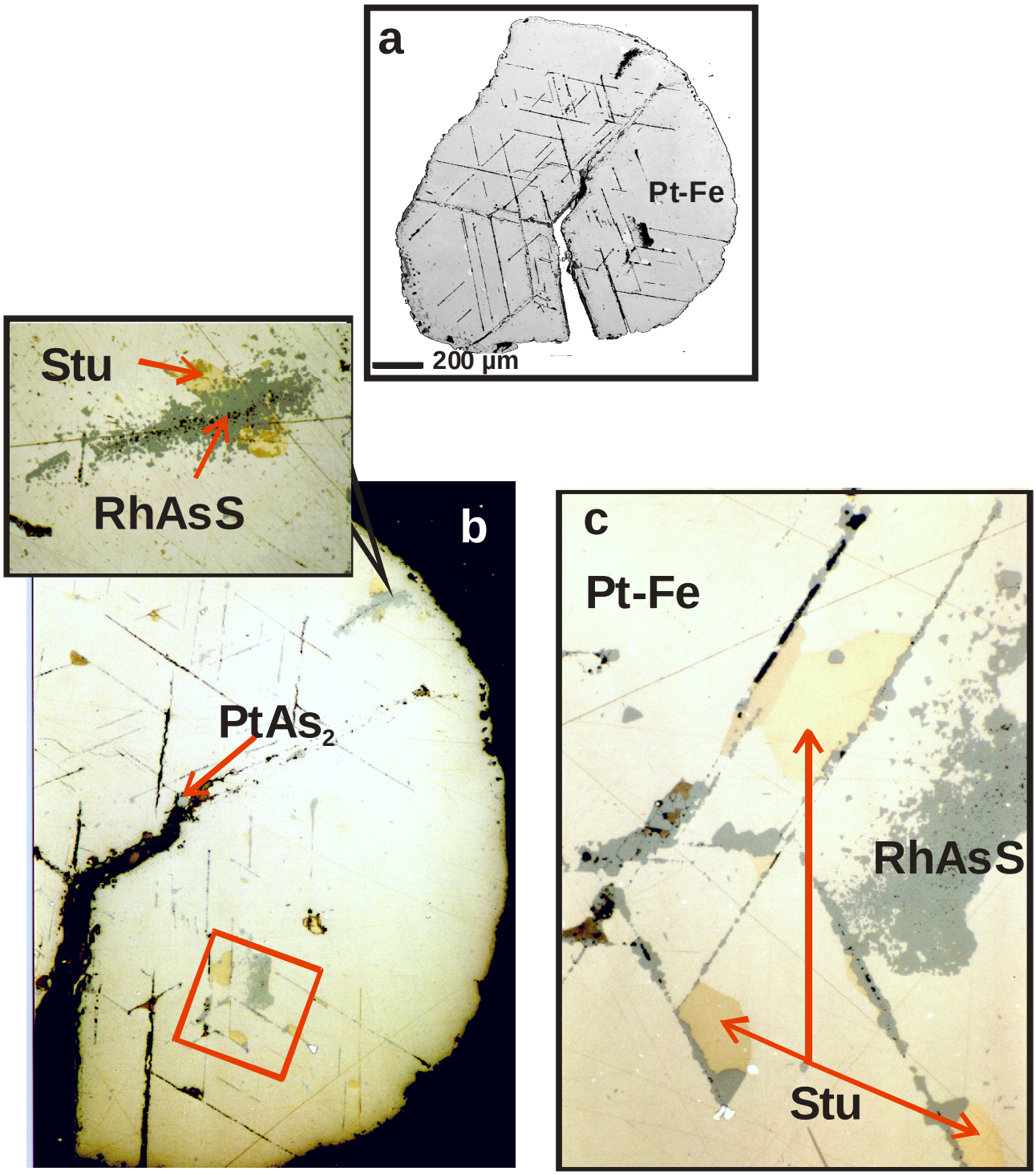

Fig. 25. ***(a)*** *BSE image of Pt-Fe alloy grain with fissures along the crystallographic planes;* ***(b)****,****(c)*** *microphotographs of the enlarged parts of the grain, which show inclusions of stumpflite (yellow) [Pt(Sb,Bi)] overgrown by hollingworthite [RhAsS] (gray).*

TABLE 20. SELECTED ANALYSES OF STUMPFLITE, MERTIEITE-II AND Au-BEARING ALLOY FROM FADEEVKA RIVER

		Stumpflite Pt(Sb,Bi)			Mertieite-II Pd_8Sb_3			Au-Ag alloy		
Sample		F1/5.5	F1/5.7	F1/5.12	F2-1	F2-5	F2-5/1	F5-30.2	F5-30.3	F5-30.4
	wt.%									
Bi		16.57	16.53	16.58	0.23	0.25	0.18	-	-	-
Rh		-	0.19	0.23	-	-	-	0.41		0.63
Pd		1.29	1.45	1.35	63.78	63.92	63.41	0.35	2.44	-
Ag		-	-	-	-	-	-	-	2.92	-
Sb		26.64	26.87	26.67	15.04	14.82	14.68	-	-	-
Te		-	-	-	0.37	0.22	0.27	-	-	-
Au		-	-	-	-	-	-	13.73	86.17	5.28
Pt		55.91	56.42	55.70	11.52	11.40	11.49	77.06	6.55	85.48
Fe		-	-	-	-	-	-	0.16	-	1.66
Cu		-	-	-	0.17	0.31	0.25	8.92	0.28	6.60
As		-	-	-	9.11	9.10	9.12	-	-	-
Total		100.41	101.46	100.53	100.22	100.02	99.40	100.63	98.36	99.65
	at.%									
Bi		13.29	13.09	13.25	0.12	0.13	0.10	-	-	-
Rh		-	0.31	0.37	-	-	-	0.65	-	1.01
Pd		2.03	2.25	2.12	65.85	66.00	65.91	0.53	4.36	-
Ag		-	-	-	-	-	-	-	5.15	-
Sb		36.66	36.51	36.58	13.57	13.38	13.34	-	-	-
Te		-	-	-	0.32	0.19	0.23	-	-	-
Au		-	-	-	-	-	-	11.33	83.26	4.43
Pt		48.02	47.84	47.68	6.49	6.42	6.52	64.21	6.39	72.46
Fe		-	-	-	-	-	-	0.47	-	4.92
Cu		-	-	-	0.29	0.54	0.44	22.81	0.84	17.18
As		-	-	-	13.36	13.35	13.47	-	-	-
Total		100	100	100	100	100	100	100	100	100

Note: Os, S, Ir were not detected; -: below analytical detection limit

Mertieite-II occurs as small (20 μm size) inclusions in the center of a roundish Pt-Fe alloy grain. The grain is altered and disseminated by number of different inclusions, mostly of platarsite-hollingworthite-irarsite solid solution. Inclusions of mertieite-II are occasionally covered by sulfarsenides (i.e. formed earlier) and are distinctly large in size (Fig. 26).

The Au-bearing minerals occur either as micron-size inclusions within the matrix of Pt-Fe grains or form extremely thin rims around these grains, overgrown by cooperite (Fig. 24). The chemical composition of the inclusions/intergrowths of Au-bearing alloy from the Fadeevka river placer is relatively constant and represented by Au-rich Au-Ag alloy (average mean: 89.06 ± 6.41 wt.% Au, 6.30 ± 5.83 wt.% Ag). All samples studied have traces of Pt (up to 6.55 wt.%; average mean is 3.21 ± 1.91 wt.% Pt). The content of other trace elements is extremely low: only one Au-Ag inclusion contains up to 2.44 wt.% Pd, and three samples contain up to 0.28 wt.% Cu.

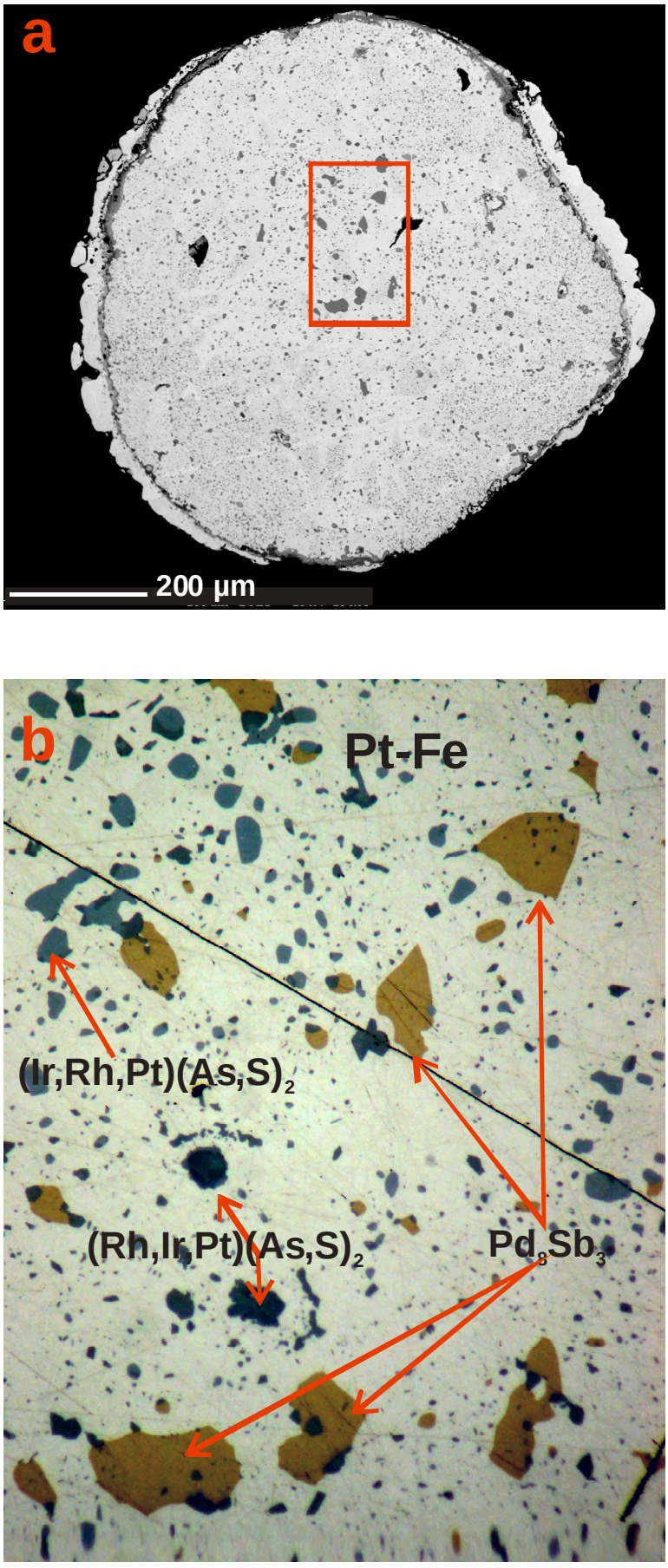

Fig. 26. (a) *BSE image of Pt-Fe alloy grain and* ***(b)*** *microphotograph of enlarged section of the grain with numerous inclusions of Ir-, Rh-, Pt-bearing sulfarsenides (dark-blue) and mertieite-II (yellow)[Pd_8Sb_3].*

3.5.5. Secondary PGE minerals developed after primary Os-Ir-Ru-Pt alloy

Reaction rim on Os-Ir alloy

A number of Os-Ir alloy grains display alteration textures. The most variable and complex sample is an iridium grain with 67 wt.% Ir, 24 wt.% Os, 3.5 wt.% Pt and 3.1 wt.% Ru (Sample FD1-1). This grain was earlier described by Shcheka et al. (1991), but because of micrometer-size intergrowth of several phases, some of them were identified incorrectly. Here we give new results on this grain. The sequence of minerals phases from the outermost part to the grain core is as follows (Fig. 27):

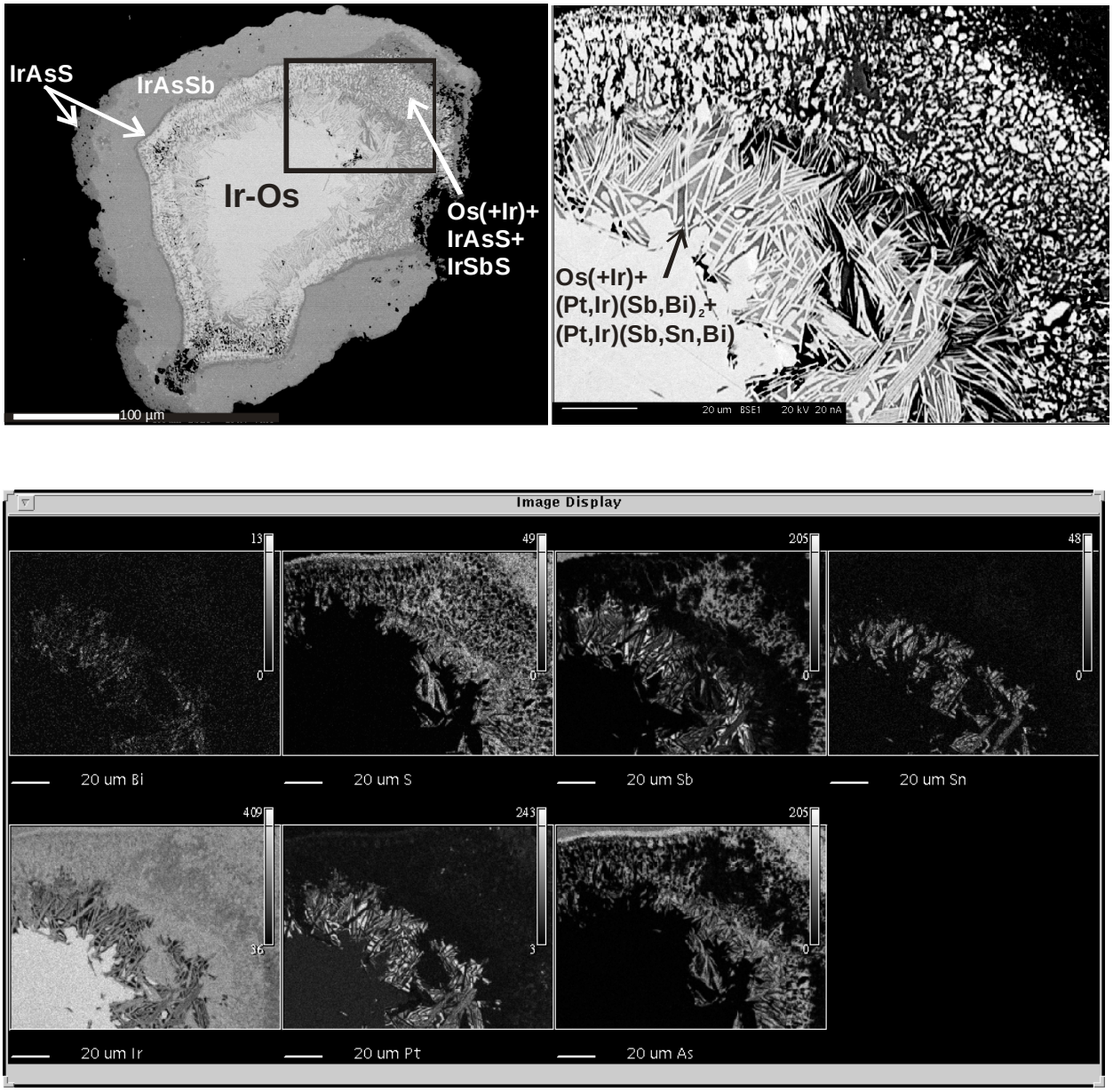

Fig. 27. *BSE images of sample FD1-1;* ***a)*** *general view of the grain;* ***b)*** *enlarged section of the grain;* ***c)*** *X-ray mapping of the section shown in picture b with Bi, S, Sb, Sn, Ir, Pt and As.*

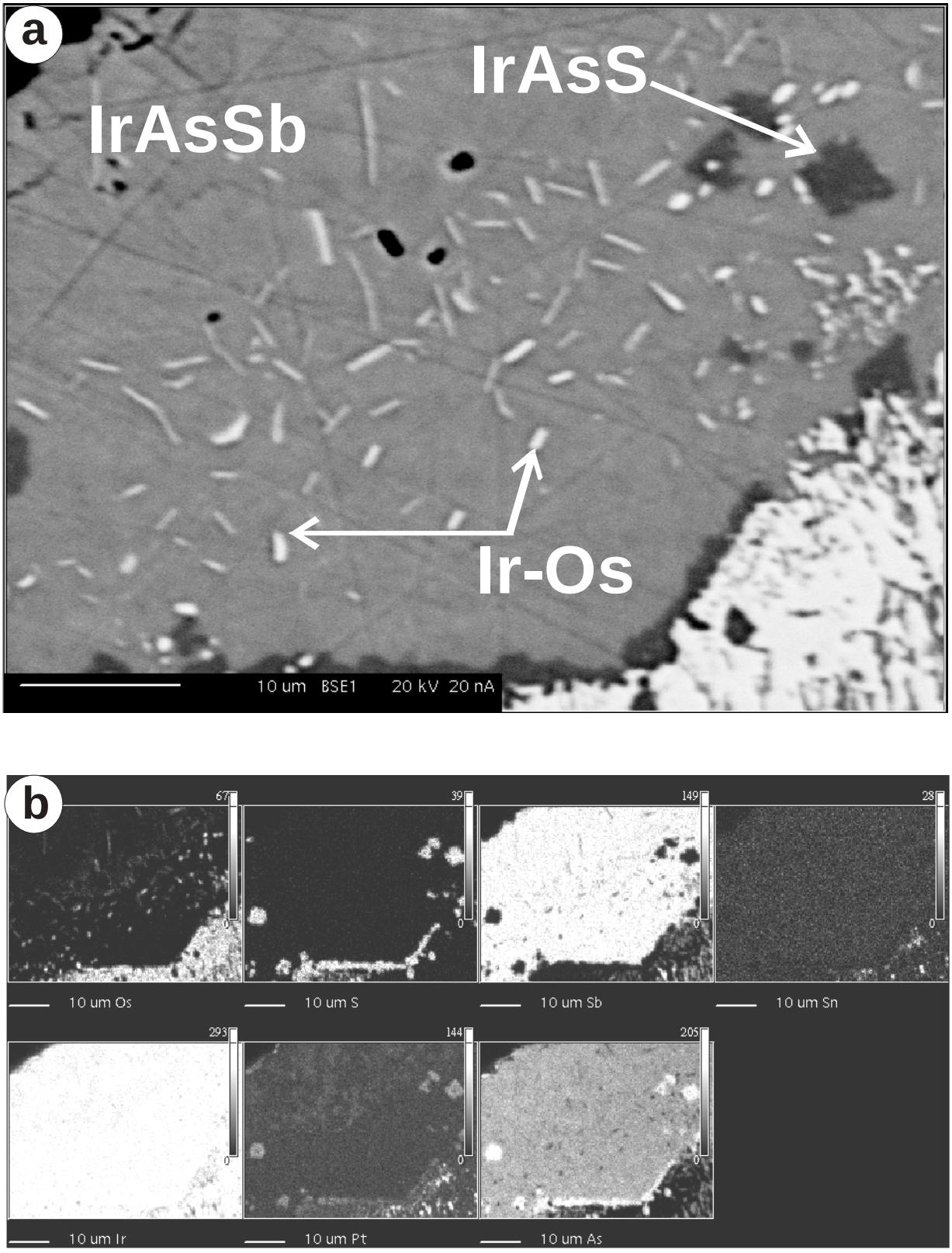

Fig. 28. *BSE image of IrAsSb rim with inclusions of (Pt,Os)AsS and Pt-Ir-Os alloy of FD1-1 sample* ***(a)****; X-ray mapping of this part of the grain* ***(b)****.*

1. Thin, μm-sized, discontinuous rim of irarsite [IrAsS];

2. Thick (50 μm) mantle of IrAsSb phase with μm-sized inclusions of Ir-Os and irarsite [(Ir,Pt)(As,S)] (Fig. 28);

3. Thin layer (5 μm) of irarsite;

4. Mixture of spotty Ir-Os alloy in irarsite and tolovkite [IrSbS] matrix (Fig. 27);

5. The spotty zone is followed by needle-shaped intergrowth of Ir-Os alloy with interstitial geversite [(Pt,Ir)$(Sb,Bi)_2$] and stumpflite [(Pt,Ir)(Sb,Sn,Bi)]. In the early study (Shcheka et al. 1991) the geversite and stumpflite were wrongly identified as new $Pt_3(Sb,Sn,Bi)_4$ and $Pt_2(Sb,Bi)_3$ phases because of their extremely small size in this intergrowth.

The textural evidence suggests the following sequence of formation:

I. Sb-Sn-Bi-bearing fluids react with the Pt and Ir component of Os-Ir alloy and form geversite [(Pt,Ir)$(Sb,Bi)_2$] and stumpflite [(Pt,Ir)(Sb,Sn,Bi)]. The osmium component recrystallizes to form needle-shaped Os alloy impoverished in Ir and Pt.

II. Ir from the matrix reacts with As-S-Sb-bearing fluids with rhythmic formation of :
Irarsite [IrAsS]
Tolovkite [IrSbS]
Irarsite [IrAsS]
IrAsSb phase
Irarsite[IrAsS]

Such a sequence can be understood as a function of decreasing temperature with increase of sulfide stabilities at lower temperature, and fluctuating As/Sb ratio in the fluid phase. Ir and Pt appear to be the most mobile phases, whereas Os is little transported.

Another example of hydrothermal alteration of an iridium grain (29 wt.% Os, 4 wt.% Pt, up to 4 wt.% Ru) is displayed by sample FD2-3. This alloy is mantled by a complex two-phase rim: the inner part of the rim is represented by graphic intergrowth of IrAsSb phase with Ir-Os alloy, the outermost part is rimmed by irarsite [IrAsS] (Fig. 29). This confirms the described general sequence of Sb-As-rich towards As-S-rich mineral assemblages.

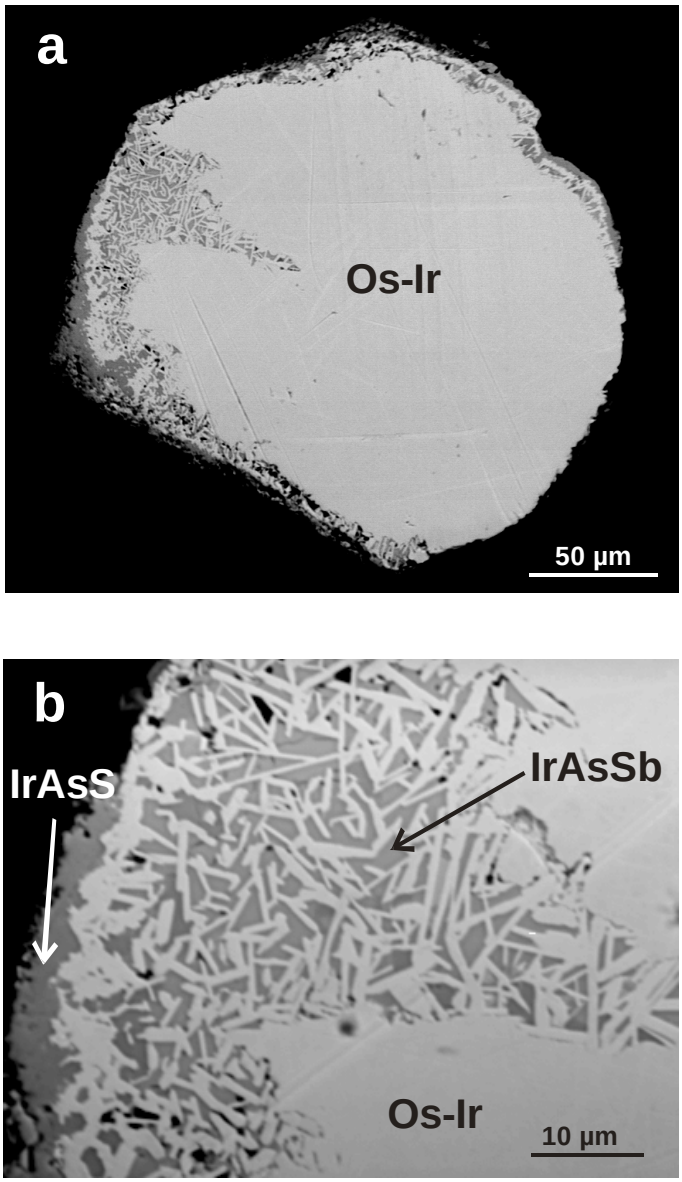

Fig. 29. *BSE images of sample FD2-3:* ***a)*** *general view of the grain;* ***b)*** *enlarged section of the grain, showing graphic intergrowth/replacement of IrAsSb with grain matrix and irarsite [IrAsSb] rim.*

A similar alteration pattern is seen in sample F6-16. This iridium grain (28 wt.% Os, with up to 16 wt.% Pt, and 0.5 wt.% Ru) has a great number of Pt-Fe alloy inclusions, which likely formed from solid solution breakdown. At the edge of the grain there is a complex intergrowth aggregate, consisting of Ru-Ir-Os alloy, two different arsenosulfides of (Ru,Os,Ir), tolovkite [IrSbS], As-bearing tolovkite [Ir(Sb,As)S] and irarsite [IrAsS]. The high Ru-content in this intergrowth aggregate (in the form of Ru-Ir-Os alloy and (Ru,Os,Ir) sulfarsenides with up to 27 wt.% Ru) points to the former existence of a primary Ru-rich metallic phase which has been altered. The Ru component is unlikely to come from the iridum alloy due to its low abundance of 0.5 wt.% Ru.

Sample F6-24 shows a two-phase rim on an iridium grain (up to 10 wt.% Pt, 1.6 wt.% Rh, 34 wt.% Os) (Fig. 30). The inner part of the reaction rim consists of $(Ir,Os)_7As_3$, the outer rim of $(Ir,Os)_2As_3$, suggesting progressive increase of As activity.

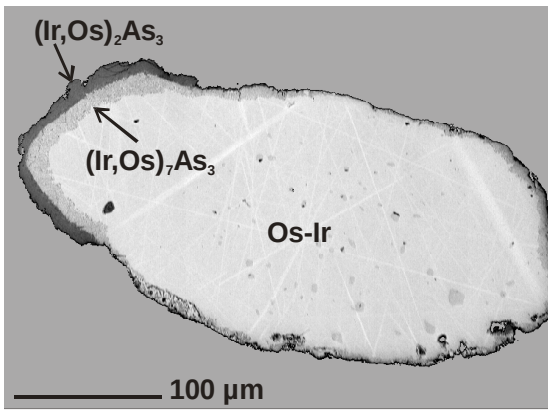

Fig. 30. *BSE image of two-phase rim developed on Os-Ir alloy. Sample F6-24.*

Secondary inclusions within Os-Ir alloy

Besides the complex reaction rims commonly developed at iridium grains, there are also a number of inclusions within the Os-Ir alloy matrix, whose composition is alien to the magmatic host mineral.

Sample FD2-19 is an iridium grain with high Pt content (11 wt.% Pt, 65 wt% Ir, 23 wt% Os) dappled with inclusions of Ir-bearing Pt-Fe alloy (Fig. 32), which are three to four times larger in size in the center of the grain than at the outermost part and present customary phenomenon of magmatic solid solution decay. In addition to the Pt-Fe inclusions the grain contains a number of other inclusions, such as stumpflite, Sb-bearing irarsite [IrAs(Sb)S], (Ir,Pt)(Te,Sb,As) phase, and Te-bearing sperrylite [$Pt(As,Te)_2$] (Fig 32; Table 21).

The entrapment of the inclusions during growth of the Pt-Os-Ir grain (and thus their earlier/concomitant formation) is unlikely. It appears more probable that the Pt-Fe inclusions acted as reactive weak points during the subsolidus evolution of the Pt-Os-Ir grains when late fluids affected and selectively replaced the magmatic Pt-Fe inclusions. The Pt-Fe inclusions are also selectively dissolved during weathering processes and then form cavities (Fig. 31, 32, 33).

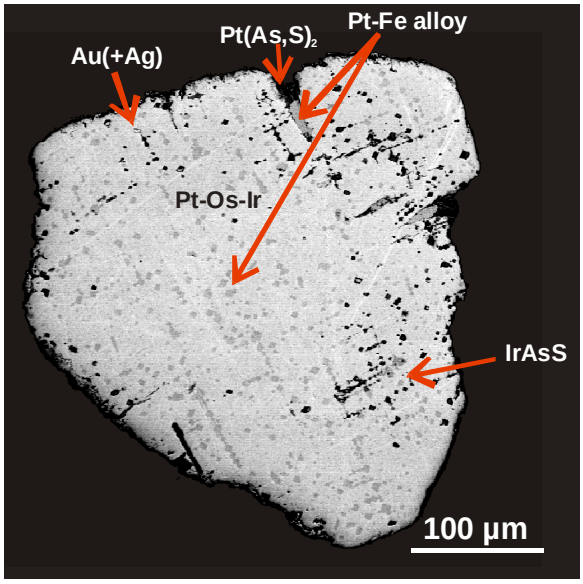

Fig. 31. *Back-scattered image of Pt-rich Os-Ir alloy with inclusions of Pt-Fe alloy, Au-rich Au-Ag alloy, irarsite [IrAsS] and $Pt(As,S)_2$. Sample F3-9.*

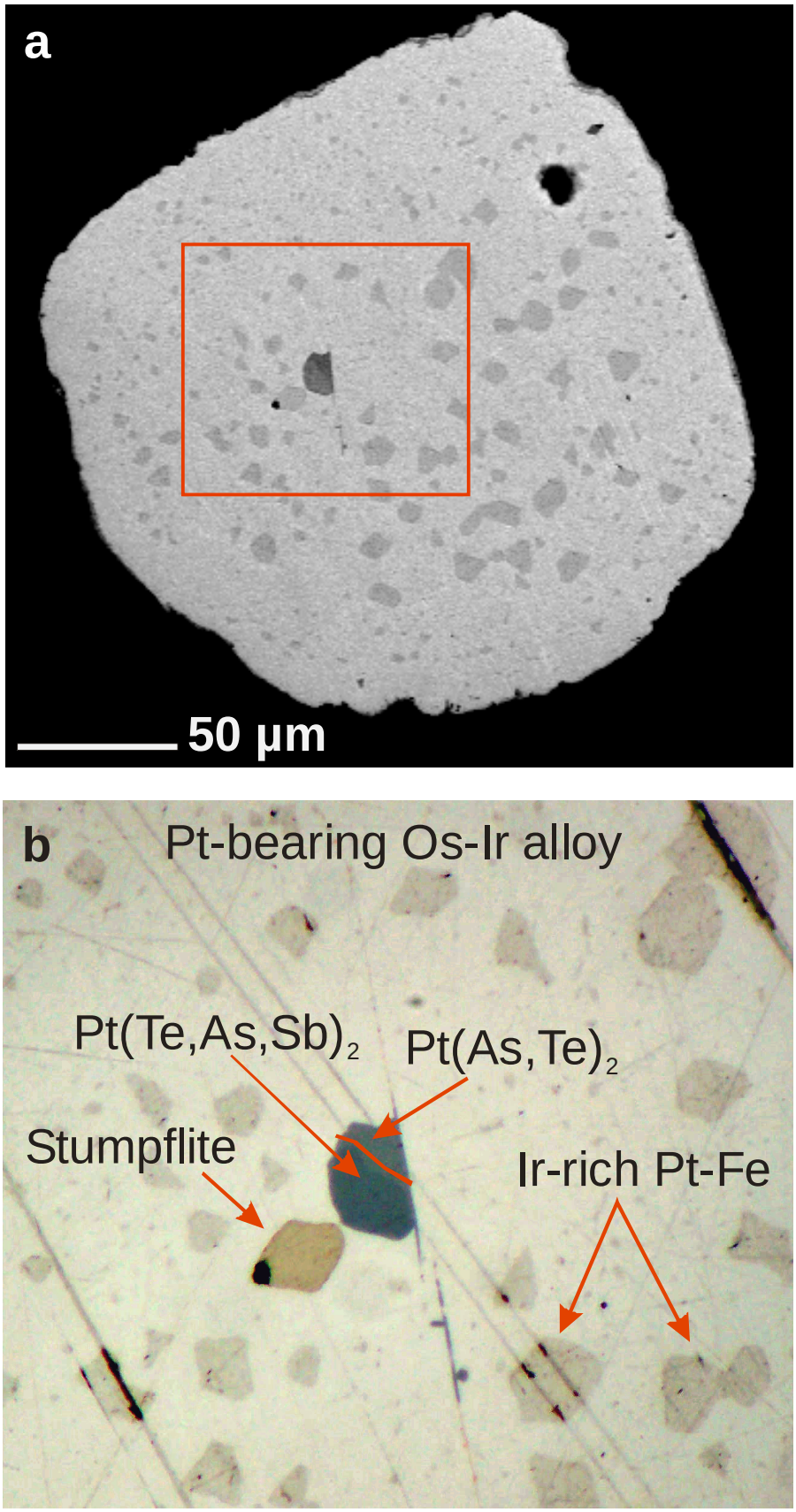

Fig. 32. (a) *BSE image of Pt-rich Os-Ir alloy (general view)* ***(b)*** *microphotograph (oil immersion) of enlarged section of the grain with inclusions of stumpflite; complex inclusion of Pt(Te,As,Sb)$_2$ and Te-bearing sperrylite, and Pt-Fe alloy. Sample FD2-19.*

TABLE 21. SELECTED CHEMICAL ANALYSES OF SECONDARY PGE MINERALS DEVELOPED AFTER Os-Ir ALLOY FROM FADEEVKA RIVER

	F6-16 IrAsS	FD1-1 IrAsSb	Ir(Sb,As)S	F6-16 IrSbS	FD1-1 $(Pr,Ir)(Sb,Bi)_2$	FD1-1 (Pt,Ir)(Sb,Sn,Bi)	FD2-19	FD2-19 $Ir(Te.Sb,As)_2$	FD2-19 Pt(Te,As,Sb)	F3-9 Au-Ag
wt.%										
Os	1.19	-	4.75	5.12	-	-	-	0.37	0.55	0.26
Ir	55.38	49.73	53.73	48.40	16.24	7.00	-	45.17	17.90	4.16
Ru	0.60	-	0.68	0.84	-	-	-	-	-	-
Pt	2.23	-	1.50	2.18	25.25	49.08	56.06	2.08	36.13	0.91
Rh	-	0.26	0.35	0.99		2.92	0.24	-	-	
Pd	-	-	-	-	-	-	1.41	-	-	0.15
Au	-	-	-	-	-	-	-	-	-	90.18
Ag	-	-	-	-	-	-	-	-	-	3.54
Bi	-	0.25	-	-	6.67	2.29	11.21	0.91	-	-
Sn	-	-	-	0.20	0.21	10.21	0.18	-	-	-
Sb	3.39	28.39	15.43	30.15	51.46	28.50	30.92	7.02	2.03	-
Te	-		-	-	-	-	-	30.58	8.68	-
Co	0.13	0.03	-	-	-	-	-	-	-	-
Cu	0.07	-	-	-	-	-	0.11	-	-	-
Fe	0.08	-	0.19	0.22	-	-		-	-	-
As	26.58	21.42	13.58	1.88	0.17	-	0.85	14.06	34.04	-
S	9.91	-	9.22	8.53	-	-	-	-	0.18	0.14
Total	99.56	100.08	99.43	98.51	100.00	100.00	100.98	100.19	99.51	99.34
at.%										
Os	0.62		2.71	3.16	-	-	-	0.26	0.35	0.26
Ir	28.58	33.08	30.34	29.55	12.56	5.62	-	31.89	11.28	4.13
Ru	0.59	-	0.73	0.97	-	-	-	-	-	-
Pt	1.13	-	0.83	1.31	19.25	38.86	45.97	1.45	22.43	0.89
Rh	-	0.32	0.37	1.13	-	4.39	0.37	0.00	-	
Pd	-	-	-	-	-	-	2.12	-	-	0.27
Au	-	-	-	-	-	-	-	-	-	87.36
Ag	-	-	-	-	-	-	-	-	-	6.26
Bi	-	0.15	-	-	4.75	1.69	8.58	0.59	-	-
Sn	-	-	-	0.20	0.27	13.29	0.24	0.00	-	-
Sb	2.76	29.82	13.76	29.06	62.85	36.15	40.62	7.82	2.02	-
Te	-	-	-	-	-	-	-	32.52	8.24	-
Co	0.22	0.07	-	-	-	-	-	-	-	-
Cu	0.11	-	-	-			0.28	-	-	-
Fe	0.14	-	0.37	0.46	-	-	-	-	-	-
As	35.19	36.56	19.68	2.94	0.34		1.81	25.47	55.01	-
S	30.66		31.21	31.22	-	-	-	-	0.68	0.83
Total	100	100	100	100	100	100	100	100	100	100

The same situation displays sample F3-9. This iridium grain with 24 wt% Os is Pt-rich (up to 9 wt.%), Rh-bearing (up to 1.66 wt.%) and hosts abundant Ir-bearing Pt-Fe alloy inclusions and cavities, which are filled with irarsite [IrAsS] and Au-rich Au-Ag alloy. The Pt-Fe alloys are occasionally altered to As-bearing cooperite [Pt(As,S)] (Fig. 31).

Sample F5-29 shows a beautiful alteration texture, which is somewhat similar on that of the already described Pt-rich Os-Ir alloy. It has numerous magmatic inclusions of Ir-bearing Pt-Fe alloy, which are altered into tolovkite [IrSbS], maslovite [PtTeBi] and Au-rich Au-Ag alloy (Fig. 33). The definition of a temporary sequence in this sample is difficult, but we suggest the simultaneous formation of Au-bearing phases with the Sb-Te-Bi-S minerals after the early inclusions of Ir-bearing Pt-Fe alloy.

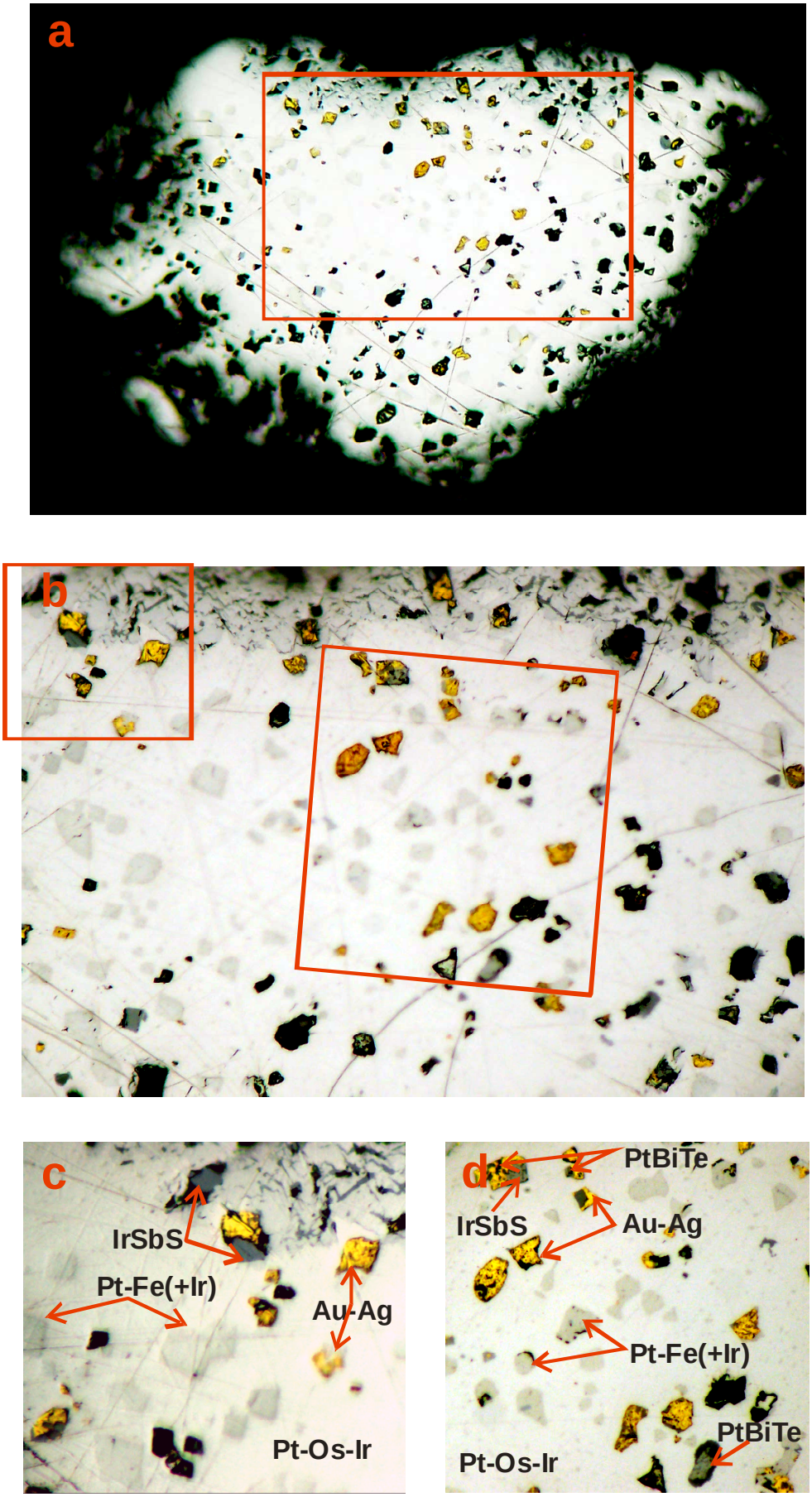

Fig. 33. *Microphotographs (oil immersion) of Pt-rich Os-Ir grain:* ***a)*** *general view;* ***b)*** *enlarged section of the grain;* ***c)*** *and* ***d)*** *enlarged section of the grain showing inclusions of Pt-Fe alloy, tolovkite [IrSbS], maslovite [PtBiTe] and Au-Ag alloy.*

3.5.6 Discussion and conclusions

The PGM assemblage of the Fadeevka river placer can be subdivided into primary (magmatic) and secondary (hydrothermal and supergene) minerals. The latter group formed by alteration of the magmatic assemblage. The mineral phases detected are listed in Table 22.

Primary mineral assemblage

The primary mineral assemblage consists of only two metal alloy phases which have minor sulfide inclusions. The alloy phases are:

(1) Pt-Fe alloy with a minor amount of Pd, Rh, Ir and Os;

(2) Os-Ir-Ru-Pt alloy with Rh as a significant minor element.

Iridium-rich alloy is generally enriched in Pt due to a greater solubility of Pt in Ir compared to the solubility of Pt in Os (Johan et al. 2002 and references therein). The Pt-Ir-rich alloy is often altered with formation of secondary rims and inclusions, in contrast to the osmium-dominant grains.

The dominance of Pt-Fe and Os-Ir-Ru-Pt alloy and the subordinate amounts of sulfides reflect the elevated $f(O_2)$ conditions of Uralian/Alaskan-type deposits. Platinum preferably enters Pt-Fe alloys, whereas Pd and Rh are concentrated in minor sulfide liquid as seen in sulfide inclusions (Peregoedova and Ohnenstetter, 2002; Fleet and Stone 1991, Fleet et al. 1993).

Inclusion phases are:

(1) Laurite-erlichmanite solid solution, which occurs as inclusions within Pt-Fe alloy (relatively enriched in Ir) or/and within Os-dominant Os-Ir-Ru-Pt alloy;

(2) Composite multimineral inclusions, which consist of BMS (pyrrhotite, pentlandite, chalcopyrite, millerite, bornite), vysotskite-braggite solid solution, cuprorhodsite-cuproiridsite-malanite solid solution, bowieite, vasilite and keithconnite. This group of complex sulfide inclusions is particularly interesting and discussed below.

TABLE 22. PGM ASSEMBLAGE OF FADEEVKA RIVER PLACER

	Pt-Fe ALLOY MATRIX		**Os-Ir-Ru-Pt ALLOY MATIX**	
	MAGMATIC	**SECONDARY**	**MAGMATIC**	**SECONDARY**
Pt-Fe alloy	+			
Ir-rich Pt-Fe alloy			+	
Iridium			+	
Osmium			+	
Laurite-erlichmanite [RuS_2-OsS_2]	+		+	
Cooperite [PtS]	+	+		
Cuprorhodsite [$CuRh_2S_4$] cuproiridsite [$CuIr_2S_4$]– malanite [$CuPt_2S_4$]	+	+	+	
Vysotskite-braggite [PdS-(Pt,Pd)S]	+		+	
Bowieite [Rh_2S_3]	+			
Vasilite [$Pd_{16}S_7$]	+		+	
Pyrrhotite	+		+	
Pentlandite	+		+	
Bornite	+		+	
Millerite			+	
Kashinite [$(Ir,Rh)_2S_3$]		+		
$(Rh,Pt)_3S_4$ phase		+		
Platarsite [$Pt(As,S)_2$]-hollingworthite [$Rh(As,S)_2$]-irarsite [$Ir(As,S)_2$]		+		
Irarsite [IrAsS]				+
Tolovkite [IrSbS]				+
IrSbAs				+
Geversite [$(Pt,Ir)(Sb,Bi)_2$]				+
Mertieite-II [Pd_8Sb_3]		+		
Stumpflite [(Pt,Ir)(Sb,Sn,Bi)]		+		+
Ir(Pt)Te(As,Sb)				+
Sperrylite [$PtAs_2$]		+		+
Au-rich Au-Ag alloy		+		+
As-bearing cooperite [Pt(As,S)]		+		+
Maslovite [PtTeBi]				+

Multimineral sulfide assemblage

The most abundant multimineral inclusion assemblage in the PGM grains studied consists of Pd-rich minerals (vysotskite-braggite-cooperite solid solution and vasilite), Rh-rich minerals (cuprorhodsite-malanite-cuproiridsite solid solution and bowieite), and BMS (bornite, pyrrhotite, pentlandite, millerite and chalcopyrite). A literature survey shows that such complex sulfide inclusions were also observed in other Uralian/Alaskan as well as in ophiolite settings, with very similar assemblages and small variations only (Table 23). The summary data indicate that pyrrhotite along with chalcopyrite are the most frequent BMS. Pd-Cu dominant sulfides, minerals of cuprorhodsite-cuproiridsite-malanite solid solution and keithconnite are found both in ophiolite and Uralian/Alaskan environments, while bornite and Rh-sulfides are distinctive minerals of Uralian/Alaskan deposits.

The spherical shape and brain-like intergrowth textures suggest an origin of the polymineralic sulfide inclusions from entrapment of a sulfide melt with subsequent exsolution and sub-solidus reequilibration. The original high-temperature bulk composition can be deduced from (1) microprobe analysis by defocused beam, integrating over the different inclusion phases, and (2) microprobe analysis of individual inclusion phases and recalculation according to modal inclusion composition from image analysis. Both methods have a large error margin due to matrix effects and problems in estimating phase proportions, which allow a semi-quantitative estimate only. Nevertheless, both methods arrive at approximately similar bulk compositions both for the PGE-rich sulfide inclusions (Table 24), and for the base-metal rich sulfide inclusions (Table 25).

The bulk composition of the PGE-rich sulfide inclusions is dominated by palladium, followed by rhodium and platinum. Base metals constitute a few percent only, with copper dominant. The stoichiometric composition is about $(Pd,Rh,Pt)_{0.46}(Cu,Ni,Fe)_{0.07}S_{0.47}$ for the data by defocused beam, and $(Pd,Rh,Pt)_{0.40}(Cu,Ni,Fe)_{0.11}S_{0.49}$ for the data by integration from image analysis (calculated from Table 24). This composition is likely to approximate the composition of the parental sulfide melt before recrystallization of individual mineral phases. These PGE-rich inclusions occur together with base-metal rich inclusions of Cu-rich pnss (pentlandite solid solution) composition $(Fe,Ni,Cu)_{54-56}S_{46-44}$ and Cu-free pnss $(Fe,Ni)_{51}S_{48}$.

TABLE 23. MINERAL ASSEMBLAGES IN MULTIPHASE INCLUSIONS FROM FADEEVKA RIVER PLACER COMPARED TO THOSE OF DIFFERENT TYPES OF PGE-DEPOSITS[1]

	FADEEVKA	**URALIAN/ALASKAN**	**OPHIOLITE**
Base-metal sulfides (BMS)			
Chalcopyrite		++	++
Pyrrhotite/PGE-bearing pyrrhotite	+++	++	+++++
Pentlandite/PGE-bearing pentlandite	++	+	+
Bornite	++	++	
Millerite	+		+
Rh-dominant minerals			
Cuprorhodsite-malanite-cuproiridsite	+++++	++++	++++++
Rh-sulfides (Prassoite+ Bowieite)	++	++	
Ir-dominant minerals			
Kashinite			+
Pd-Pt-bearing sulfides			
Vysotskite-braggite-cooperite and other Pd-S phases	++++++	+++++++	++
Laurite-erlichmanite	+	++	+++
Vasilite/$(Pd,Cu)_7S_3$/ Pd-Cu sulfides	++++	++++++	++
Pt-Fe-Cu alloys			
Pt-Pd-Au-Cu alloy		+	
Pt-Fe alloy	++	+	++
Te-bearing minerals			
Keithconnite	+	++	+
PGE-As-bearing minerals			
$(Pt,Pd)_{4+x}Cu_2As_{1-x}$, Pd-As-Te phase, platarsite; ruarsite; irarsit		++	++++

[1]The data for other Uralian/Alaskan and ophiolite deposits has been taken from Corrivaux and Laflamme (1990); Hagen et al. (1990); Johan et al. (1990); Augé and Legendre (1992); Weiser and Schmidt-Thomé (1993); Prichard et al. (1994); Garuti et al. (1995, 1999, 2002), Tolstykh et al. (2000); Malitch et al. (2001); Shcheka et al. 2004b.

TABLE 24. BULK COMPOSITION OF PGE-RICH SULFIDE INCLUSIONS (WT.%)

	Defocused beam	Modal calculation
Pd	31.9 ±8.8	20.4 ±6.4
Rh	7.8 ±4.3	11.5 ±5.2
Pt	6.4 ±2.4	7.6 ±4.6
Cu	3.4 ±2.0	5.1 ±2.3
Ni	2.3 ±2.2	2.4 ±1.7
Fe	1.5 ±1.3	3.7 ±1.8
S	46.7 ±5.1	49.4 ±2.2

TABLE 25. BULK COMPOSITION OF TWO-PHASE BASE-METAL RICH SULFIDE INCLUSIONS (WT.%)

	Pnl+Brn	Pnl+Mill	Measured Pnl+Brn
S	29.17	32.46	30.28
Ru	0.19	0.23	0.21
Rh	0.34	0.42	0.33
Ir	0.53	0.79	0.75
Ni	26.08	44.43	27.57
Fe	18.68	18.96	15.28
Cu	23.97	0.13	22.62
Co	0.20	0.25	0.19
Total	99.17	97.67	97.23
At.%			
S	43.80	47.63	45.93
Ru	0.09	0.11	0.10
Rh	0.16	0.19	0.16
Ir	0.13	0.19	0.19
Ni	21.39	35.61	22.84
Fe	16.10	15.97	13.31
Cu	18.16	0.09	17.31
Co	0.16	0.20	0.16
Total	100	100	100

Note: The first two columns are calculated from modal composition; the third one is from measurement by defocused beam. Pnl = pentlandite; Brn = bornite; Mill = millerite.

The occurrence of PGE-rich sulfide inclusions in Pt-Fe and Os-Ir alloy has been reported from various localities and was discussed with a number of concepts. Thus, Johan et al. (1990) described numerous droplet-like complex inclusions in Pt-Fe alloy grains from the Durance river alluvium, France, which comprise themselves intergrowths of bornite with cuprorhodsite, Pd-

telluride, Pd-Cu sulfide, guanglinite and $(Pt,Pd)_{4+x}Cu_2As_{1-x}$. The authors suggested the presence of a solid solution of Pt, Te, Ir, Rh, Pd, Cu, Ni, Au and S at high temperatures.

Augé and Legendre (1992) studied several multimineral inclusions ("globules") within alluvial Pt-Fe alloy grains from the Alaskan-type deposits of Eastern Madagaskar. The following mineral parageneses were observed:

(1) Keithconnite + Rh-bearing malanite + $(Pt,Pd,Rh,Os,Au,Cu)_3S_2$ + $(Pd,Pt)_3(Cu,Ni)S_2$ (vasilite)
(2) Keithconnite +Os + $(Pt,Pd, Au)_2Cu$ + $(Pd,Pt)_3(Cu,Ni)S_2$ (vasilite) + 3 unidentified minerals
(3) Keithconnite + undetermined Pd,Cu sulfide (vasilite?)
(4) Keithconnite + Pd_4S
(5) Keithconnite + $(Pd,Pt)_2S$
(6) Keithconnite Pd-Cu-S + braggite + laurite + Os-Ir

The authors stressed the absence of base-metal sulfides within these assemblages and suggest that the multimineral inclusions result from crystallization of trapped droplets of sulfide liquid in a closed system.

Weiser and Schmidt-Thomé (1993) describe a multimineral inclusion of about 10 µm size which consists of bowieite, braggite and Pd-As-Te phase within a Pt-Fe alloy grain from a heavy mineral concentrate from the Santiago river, Ecuador.

A detailed study of multiphase inclusions was done by Tolstykh et al. (2000) on material from the Pustaya river placer in Russia, derived from an Uralian/Alaskan-type intrusion. The mineral assemblage of these inclusions consists of vysotskite, palladian cooperite, vasilite, and other Pd-Pt sulfides in chalcopyrite-bornite matrix. The authors have interpreted the formation of the PGE-rich multiphase inclusions as product of crystallization of a residual melt with subsequent subsolidus transformation.

Several composite inclusions in chromian spinel were described by Garuti et al. (2002) from the Uralian/Alaskan-type Kytlym and Uktus complexes. They consist of Pt_3Fe alloy, erlichmanite, cuprorhodsite-cuproiridsite solid solution and PGE-bearing base-metal sulfides. The latter all have high Rh content and are enriched in Pt and Ir.

Multiphase inclusions (10-20 µm across) consisting of an intergrowth of cooperite with cuprorhodsite, and Pt-Pd bearing chalcopyrite in a Pt-Fe alloy matrix were also documented from the Zolotaya river placer (Shcheka et al. 2004b).

A complex inclusion, consisting of laurite + (Ni-Ir-Fe-Cu-S) + (Cu-Pt-S) + chalcopyrite was described by Corrivaux and Laflamme (1990) from chromitite of the Thetford Mine ophiolite in Québec.

Hagen et al. (1990) mentioned the occurrence of composite (vasilite + Pt-Fe alloy) inclusions within Ir-Os alloy from northern Birma.

Malanite, irarsite, Pd-S, pentlandite, chalcopyrite, millerite, $(Pt,Rh,Ir,Cu)_{1,9}S_3$, $(Ni,Fe,Cu)_2(Ir,Rh)S_3$, cuprorhodsite, laurite occur as primary composite inclusions in chromite of chromitite at Finero, Italy, and Ojén, Spain (Garuti et al. 1995).

Two-phase inclusions consisting of PGE-thiospinels + base-metal sulphides within the chromitite samples of New Caledonia ophiolite complex were discovered by Augé and Maurizot (1995).

Malich et al. (2001) described numerous multiphase inclusions from podiform chromitite, Kraubath, Austria. The mineral assemblages consist of:

(1) Keithconnite + rich in Pd Pt-Fe alloy + laurite

(2) Keithconnite + rich in Pd and Ir Pt-Fe alloy

(3) Keithconnite + Pt-Fe alloy + Rh-Ir-Pt bearing pyrrhotite

(4) Rich in Pd Pt-Fe alloy + Rh-Ir-Pt bearing pyrrhotite + laurite

(5) Cuprorhodsite + braggite + laurite

(6) Laurite-erlichmanite + cuprorhodsite

(7) Laurite-erlichmanite + platarsite – ruarsite - irarsite + irarsite - hollingworthite

The extreme enrichment of the sulfide melt in PGE and concomitant depletion in iron and base metals is a process not easily understandable and was discussed by several authors proposing a variety of processes. Prichard et al. (1994) summarized three possible mechanisms of PGE-enrichment in sulfide droplets:

1. Exsolution of extremely small amounts of sulfide melt could lead to high PGE concentration in the sulfide melt, with the partition coefficient of PGE many orders of magnitude higher than for base metals.
2. Involvement of C-H-O-bearing fluids which would enhance the solubility of the PGE in a sulfide-bearing BMS-, Pd- and Pt-rich melt.
3. Loss of base metals from the inclusions.

Prichard et al. (1994) conclude that the best explanation for the high PGE content is PGE accumulation in an immiscible volatile- and sulfur-rich melt separated from late-stage low-sulfur magma. Tolstykh et al. (2000) suggested that the cavities which some multiphase inclusions show derive from gas bubbles of the ore-forming residual melt enriched in volatile components, i.e. a C-H-O-rich sulfide melt.

The experimental work by Peregoedova and Ohnenstetter (2002) provides an explanation by liquid immiscibility. Their study suggested that anomalous PGE-Cu rich melt could form as a result of (1) fractionation of Mss from early-formed Fe-rich sulfide melt; (2) separation of sulfide melt into two liquids: (i) Fe-rich and (ii) Cu-rich, i.e. sulfide-sulfide immiscibility. The

coexistence of Cu-rich but S-poor and relatively Fe- and S-rich liquid at 1000°C (47-50 at.% S) was experimentally proved for the sulfur-undersaturated part of the system Fe-Ni-Cu-S by Peregoedova (1998). Under such conditions, Pt and Pd partition preferentially into Cu-rich liquid and Rh in the Fe-rich liquid.

Sulfide-sulfide liquid immiscibility is also suggested by our own observations, as seen in the coexistence of base-metal rich and PGE-rich sulfide inclusions. The constant mineral composition and similar intermineral proportions in the seven inclusions described, as well as in a larger number of inclusions studied qualitatively, suggest the existence of a sulfide melt unusually enriched in PGE, particularly in Pd and Rh. Such a melt is unlikely to form by simple sulfide exsolution from a silicate melt, because

$\mathbf{c}_{PGE}$(sulfide melt) = $\mathbf{D}_{PGE}$(sulfide/silicate) x $\mathbf{c}_{PGE}$(silicate melt), and

$\mathbf{c}_{BM}$(sulfide melt) = $\mathbf{D}_{BM}$(sulfide/silicate) x $\mathbf{c}_{BM}$(silicate melt).

The PGE/BM ratio in the sulfide melt is then dependent on the D_{PGE}/D_{BM} ratio times the concentration ratio of PGE/BM in the silicate melts. Given that the content of Fe+Ni+Cu in a silicate melt is in the percent range, while the concentration of PGE is commonly in the ppb range, a PGE/BM ratio of $< 10^{-6}$ in a silicate melt follows. The measured PGE/BM ratio in the sulfide inclusions is >3, which then requires a D_{PGE}/D_{BM} ratio of 10^5-10^6. Such a ratio appears extremely high, given the chalcophile affinity of base metals. Accepting empirical partition coefficients from mafic systems, the D value for Ni and Cu is about 100-200, and for Pt and Pd about 10^5 (Naldrett 1989), which would give a ratio of about 10^3 only. A further argument against direct exsolution of PGE-dominated sulfide melt is the composition of sulfide droplets in layered mafic intrusions, such as the Bushveld Complex, South Africa, or the Stillwater Complex, Montana (USA), where base metals contents are invariably higher than PGE contents, with the J-M Reef in the Stillwater Complex having the highest PGE contents in its magmatic sulfide fraction of up to 0.5 wt% Pd (Naldrett 1989).

The existence of a Pd-rich sulfide melt can be understood from phase relations in a hypothetical base metal-PGE-S system, as deduced from the individual Fe-Pd-S, Cu-Pd-S, Pd-Pt-S, Fe-Rh-S, and Pt-Fe-S systems (Makovicky 2002). These simple systems all have the characteristic of two immiscible sulfide liquids at high temperature (600-1000°C), one small field with pyrrhotite (or iss, by analogy) composition, the other much larger compositional field with high PGE content, which extends from ±isometric composition to the Pd-S join. The compositional field of the high-PGE sulfide melts shrinks with decreasing temperature, and a variety of individual PGE sulfides become stable. Copper and nickel strongly influence the solidus temperature of the PGE-rich sulfide melt which in simple ternary systems exists down to at least 550°C (Makovicky

2002). It is likely that this temperature is even lower in multicomponent systems. The solubility of Pt and Pd in pyrrhotite is strongly dependent on sulfur fugacity, with several wt.% Pd and several tenths of percent Pt at high sulfur fugacity at 800°C. The ubiquitous occurrence of Pt-Fe alloy, and no or minor PtS indicates very low sulfur fugacity under which both Pd and Pt are soluble in pyrrhotite at less than 0.1 wt.% only. This situation explains the PGE content of the base-metal sulfide inclusions below the analytical detection limit of the microprobe. On the other hand, copper is relatively soluble in the PGE-rich sulfide melt and is incorporated in vasilite.

Secondary PGE-bearing minerals

A complex secondary mineral assemblage is composed of Ir and Pt from the primary PGM, plus Sn, Sb, Bi, Te, As, S from a late fluid phase. These alteration PGM developed after primary Pt-Fe and Os-Ir alloys both as reaction rims and as inclusions within the primary grains.

The wide spectrum of secondary minerals developed within or after Pt-Fe grains can be divided in six groups: sulfides (cooperite [PtS], kashinite [$(Ir,Rh)_2S_3$] and $(Rh,Pt)_3S_4$ phase); arsenide (sperrylite [$PtAs_2$]); sulfarsenides (platarsite [$Pt(As,S)_2$]-hollingworthite [$Rh(As,S)_2$]-irarsite [$Ir(As,S)_2$] solid solution); cuprorhodsite [$CuRh_2S_4$]–cuproiridsite [$CuIr_2S_4$]–malanite [$CuPt_2S_4$] group; stibio-bismuthides (stumpflite [Pt(Sb,Bi)], mertieite-II [Pd_8Sb_3]) and Au-bearing alloy.
Textural relationships suggest the earliest formation of stibio-bismuthides, followed by Au-Ag alloy, cuprorhodsite-cuprorhodsite-malanite group, cooperite, sulfarsenides and arsenides.

A similar range of alteration minerals from Pt-Fe alloy was documented from the Tulameen complex by Nixon et al. (1990), who pointed out that Pt antimonides [$PtSb_2$], arsenides [$PtAs_2$], Rh-Ir sulfarsenides, and tulameenite developed in PGE-enriched rocks by metasomatic replacement and limited remobilization of primary PGE. The authors explain the alteration assemblage as a result of serpentinization and regional metamorphism.
Minerals of the irarsite-hollingworthite-platarsite-osarsite series as well as sperrylite-geversite series formed after Pt-Fe alloy have been described by Tolstykh et al. (2004) from lode and placer deposits associated with the Gal'moenan complex, Russia. Weiser and Schmidt-Thomé (1993) mentioned cooperite formed after Pt-Fe and partly replaced by sperrylite from the Santiago river placer, Ecuador.

The paragenetic sequence of alteration of Os-Ir-Ru-Pt alloy follows the general tendency of earliest occurrence of intermetallic compounds of Sn, Bi, Pt and Ir, followed by tellurides and

Sb-As phases, and terminated by As-S bearing phases. The late sulfide minerals are associated with gold. Typical alteration minerals for Os-Ir-Ru-Pt alloy from Fadeevka are IrSbAs, tolovkite [IrSbS] and irarsite [IrAsS].

Descriptions of alteration of Os-Ir alloy are rare in the literature. Tolstykh et al. (1997) studied secondary mineral assemblages developed on primary Ir-Os alloy from the Zolotaya river alluvium (Western Sayan, Russia). Exotic compounds with Se, Te and As [(Ir,Os)(As,Te), (Ir,Os)(Te,As), (Ru,Ir,Os)Te, $Ir(As,Se,S)_2$, $(Ir,Os)Te_2$, $(Ir,Os)(S,As,Te)_2$] were detected in the form of rims, meta-inclusions and net-like. These authors interpret the formation of the secondary PGM as related to hydrothermal overprint during a separate event of gold-quartz veining.

Two iridium grains with rims of irarsite and myrmekitic intergrowth of Ir-bearing iron and tolovkite, respectively, were described from the Nevyansk placer, Urals, Russia by Cabri et al. (1996).

Laurite, arsenide (irarsite) and antimonides (with composition close to tolovkite [IrSbS]) formed along cracks and as rims on Ir-Os-Ru alloy from a placer derived from ophiolite in the Horokanai area (Hokkaido, Japan) (Nakagawa and Franco 1997). The authors suggested the formation of these minerals in relation to overprint by fluids rich in S, As, Sb and other highly volatile elements introduced by abundant diorite dikes.

In summary, the primary PGM assemblage of the Fadeevka river placer, namely Pt-Fe alloy, Os-Ir-Ru-Pt alloy and minor laurite-erlichmanite, was overprinted by postmagmatic fluids which introduced Sn, Sb, Te, As, S, Ag and Au. The secondary mineral assemblage consists of cooperite [PtS], sperrylite [$PtAs_2$], kashinite [$(Ir,Rh)_2S_3$], $(Rh,Pt)_3S_4$ phase, cuprorhodsite-cuproiridsite-malanite group [$CuRh_2S_4$-$CuIr_2S_4$-$CuPt_2S_4$], platarsite-hollingworthite-irarsite solid solution [$Pt(As,S)_2$-$Rh(As,S)_2$-$Ir(As,S)_2$)], stumpflite [Pt(Sb,Bi)], mertieite-II [Pd_8Sb_3], Sb-bearing irarsite [IrAs(Sb)S], Ir(Pt)Te(As,Sb) phase, tolovkite [IrSbS], maslovite [PtTeBi], $(Ir,Os)_7As_3$, $(Ir,Os)_2As_3$, IrAsSb phase, and Au-Ag alloy. The hydrothermal overprint is probably related to the particular geological situation in the Fadeevka area, where the mafic rocks which probably host the primary PGM mineralization are intruded by abundant plagio- and granophyric granites. The latter could be the source for Au mineralization, which occurs in quartz-arsenopyrite-pyrite veins in the country rock. Quartz-cassiterite greisen mineralization is also known in this region.

The particular feature of disseminated gold in Os-Ir alloy can be explained by selective leaching of the primary Pt-Fe alloy inclusions and electrochemical precipitation of gold. The Pt-Fe alloy inclusions are much more sensitive to aqueous dissolution by hydrothermal or supergene fluids than the very immobile Or-Ir host, as can be seen by variable degree of dissolution and cavity

formation. The precipitation of gold during Pt-Fe dissolution results from the difference in electrochemical potential of platinum and gold, which is 1.2 V for the Pt/Pt^{2+} standard half-cell, and 1.5 V or 1.7 V for the Au/Au^{3+} or Au/Au^{1+} half cells, respectively. The more noble behavior of gold compared to PGE allows galvanical precipitation of gold on PGE metal surfaces from extremely low-gold solutions. This effect is probably enhanced by the Fe component in Pt-Fe alloy which has a negative electrochemical potential.

4 First occurrence OF PGM AT KEDROVKA RIVER PLACER, PRIMORYE

4.1 Introduction

The Kedrovka river gold placer in Central Sikhote-Alin was studied by numerous researchers, due to its unique mineral assemblage, but PGM were unknown so far. First geological investigations of the Bolshaya Ussurka river system were carried out by Russian mining engineer Butusov, French engineer Bordo and German mining engineer Kleis in 1910-1912 already. In the same time first data on the gold potential of this region was obtained (Annert 1928). Placer gold mining started in the 1920s. In the end of the 1970s, after more than 50 years of placer gold mining, corundum and zircon of gemstone quality were found. Their characteristics were comparable to sapphire and hyacinth from Australian and SE Asian deposits (Kaminskiy et al. 1978).

First analytical data on corundum, zircon, spinel and ilmenite from the Kedrovka placer were reported by Esin and Peretyatko (1992). They suggested the Cenozoic alkaline basalts as source rocks of these minerals. Other researchers, who studied the placer heavy mineral concentrates, came to similar conclusions (Anan'ev et al. 1998).

In 2000, during a field expedition in the Kedrovka gold placer, small metallic grains similar to PGM were found. Microprobe work in Clausthal confirmed the presence of osmium-iridium-ruthenium-platinum alloys. In the following, first mineralogical and chemical data on this new PGM discovery, are given, and an attempt is made to identify their primary source. The previously known PGM occurrences in the Primorye region have been estimated as of Uralian/Alaskan-type (Shcheka et al. 1991). They are characterized by platinum-iron alloys with minor osmium-iridium alloys (below 10 %).

4.2 GEOLOGICAL SETTING

The Kedrovka river is located in Central Sikhote-Alin and administratively belongs to the Krasnoarmeyskiy region of Primorskiy Kray (Fig.1). The Kedrovka river is part of the Bolshaya Ussurka drainage system situated within the Samarkinskiy terrane (Khanchuk et al. 1996). The general rock sequence consists of Middle Jurassic to lowermost Cretaceous turbidites and olistostromes with fragments of Paleozoic ophiolites, Upper Paleozoic limestones, Upper Paleozoic and Lower Mesozoic cherts and basalts (Fig. 34).

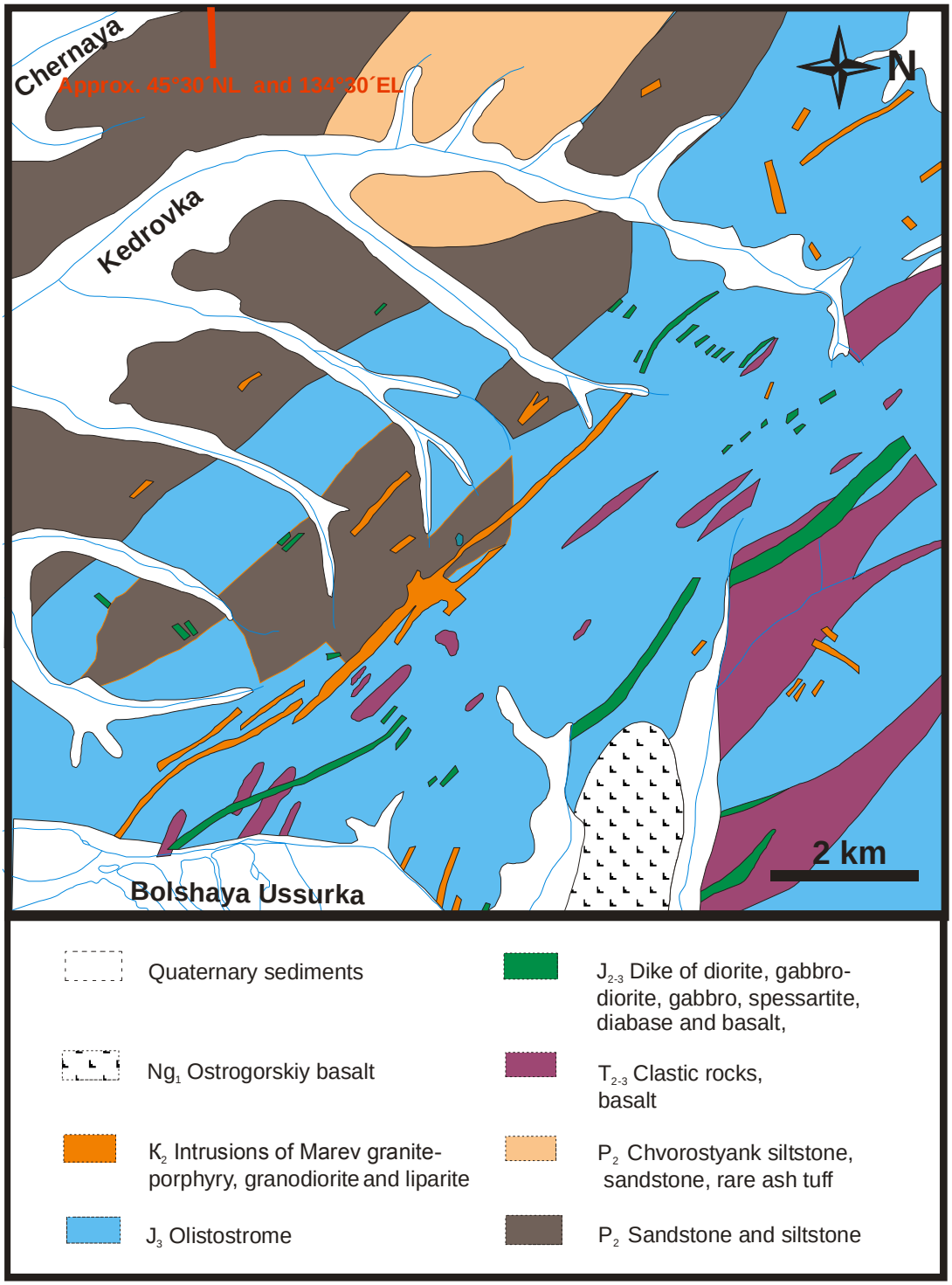

Fig. 34. *Geological sketch map of the Kedrovka area*

The Kedrovka river area is underlain by Lower to Middle Jurassic olistostrome-turbiditite series (sandstones, siltstones, and shales) in a mélange with fragments of Triassic to Lower Jurassic and Upper Permian cherts. The latter are characteristic for the lower structural level of the Samarkinskiy terrane (Elvadakskiy subterrane, according to Kemkin and Filippov 20010). All rocks in the study area suffered thermal overprint, i.e. terrigenious rocks are silicified and cherts turned into microquartzites. Igneous rocks are represented by dykes of Jurassic picrites, Lower Cretaceous granites, granite porphyries and gabbroides.

4.3 ASSOCIATION OF PGM OF KEDROVKA RIVER PLACER

In total 10 grains were examined by microprobe. The analytical results show that they consist of polycomponental alloys of refractory PGM: iridium, osmium, and ruthenium (Table 26). The composition of these alloys shows two distinct groupings, i.e. an iridium subgroup (7 grains) and an osmium subgroup (3 grains) according to the classification by Harris and Cabri 1991 (Fig. 35). The PGM grain size ranges from 50 μm up to 1 mm with the majority being around 0.5 mm. The grains have tabular to rounded or sub-rounded morphology without distinct crystallographic outlines. The iridium grains show smoother surface than those of osmium. The latter are characterized by large cavities and somewhat deformed texture. The ruthenium content ranges from 0.55 wt.% up to 10.21 wt.%.

TABLE 26. SELECTED ANALYSES OF PGM FROM KEDROVKA RIVER

N	sample	Os	Ru	Rh	Pt	Ir	Ni	Fe	S	As	Total
					wt. %						
1	V1-8	20.31	0.55	0.32	3.90	73.30	0.05	0.22	-	-	98.65
2	V1-5	30.83	0.57	0.07	3.49	63.17	0.10	0.48	-	-	98.71
3	V1-/1	31.77	4.72	0.86	3.50	58.89	0.05	0.19	-	-	99.98
4	V1-2	33.23	0.87	0.48	2.42	62.96	0.05	0.26	-	-	100.27
5	V2-1	34.29	2.03	0.68	1.88	61.67	0.07	0.19	-	-	100.81
6	V1-3	36.10	1.04	0.44	7.36	54.92	0.02	0.12	-	-	100.00
7	V1-7	37.24	1.02	0.13	3.11	58.96	0.04	0.22	-	-	100.72
8	V2-2	50.90	10.21	-	-	38.84	0.12	0.44	-	-	100.51
9	V1-6	54.67	3.52	0.33	0.93	40.91	0.06	0.23	-	-	100.65
10	V1-2/1	61.67	0.67	-	-	38.54	-	0.16	-	-	101.04
11	V1-2/2	35.97	23.74	-	-	9.22	-	-	29.97	0.18	99.08
					atomic proportion *(apfu)*						
1	V1-8	0.205	0.010	0.006	0.038	0.731	0.002	0.008	-	-	
2	V1-5	0.309	0.011	0.001	0.034	0.626	0.003	0.016	-	-	
3	V1-/1	0.303	0.085	0.015	0.033	0.556	0.002	0.006	-	-	
4	V1-2	0.327	0.016	0.009	0.023	0.614	0.002	0.009	-	-	
5	V2-1	0.333	0.037	0.012	0.018	0.592	0.002	0.006	-	-	
6	V1-3	0.358	0.019	0.008	0.071	0.539	0.001	0.004	-	-	
7	V1-7	0.366	0.019	0.002	0.030	0.574	0.001	0.007	-	-	
8	V2-2	0.461	0.174	-	-	0.348	0.004	0.014	-	-	
9	V1-6	0.524	0.064	0.006	0.009	0.388	0.002	0.008	-	-	
10	V1-2/1	0.607	0.012	-	-	0.375	-	0.005	-	-	
11	V1-2/2	0.134	0.167	-	-	0.034	-	-	0.663	0.002	

Note: - below detection limit; Pb, Bi, Pd, Ag, Sn, Sb, Te, Au, Co, Cu were tested for, but not detected;
No 1-7 - iridium grains, 8-10 - osmium grains, 11 - laurite inclusion

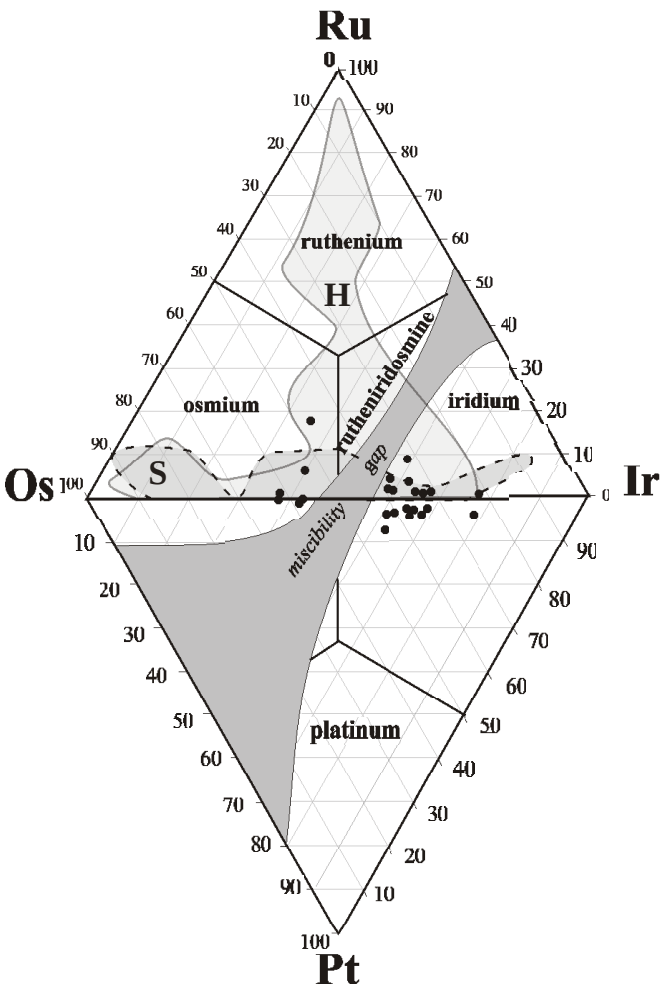

Fig. 35. *Chemical composition of PGE alloys from the Kedrovka placer (classification according to Harris and Cabri, 1991). Shadowed fields are after Nakagawa and Franco (1997):* ***H*** *- Hokkaido and* ***S*** *– Samar types.*

The iridium subgroup is enriched in Pt with an average content of 3 wt.% Pt. The rhodium content ranges up to 0.86 wt.%. Iridium samples are often inhomogeneous because of variation of Os content. Minerals of laurite-erlichmanite solid solution have been found both as intergrowth with PGE grains and as small (10x5 μm) idiomorphic inclusions with clear hexagonal habit in the center of the iridium grain (Fig. 36).

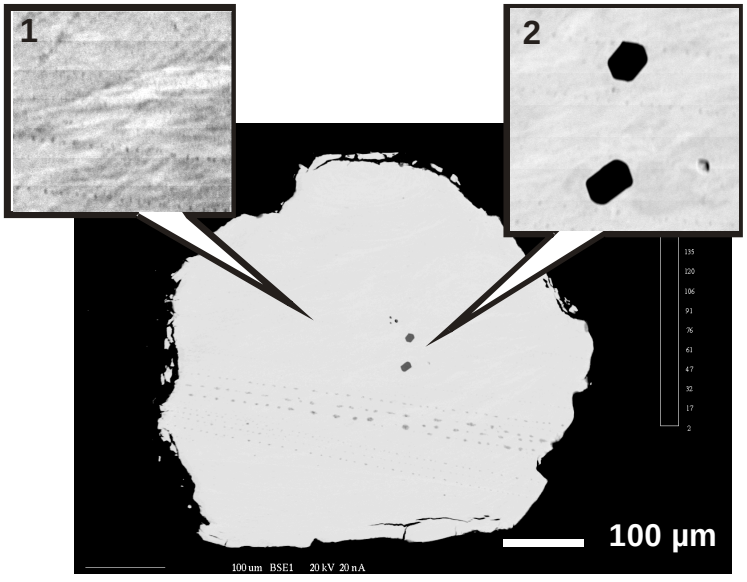

Fig. 36. *BSE image of iridium grain. Enlarged insets show example of the heterogeneiti of iridium (1) and laurite inclusions (2).*

In another case laurite has been observed intergrowth with an iridium grain. The highest Ir content in laurite is 9 wt.%. Two μm sized high Mg olivine inclusions were found within the PGM grains (Table 27).

TABLE 27. SELECTED ANALYSES OF OLIVINE INCLUSIONS WITHIN Os-Ir ALLOY FROM THE KEDROVKA PLACER (WT.%)

No	1	2
SiO_2	40.14	42.93
CaO	0.03	0.06
Al_2O_3	-	0.75
FeO	7.25	3.71
NiO	0.31	0.37
MnO	0.12	0.05
MgO	49.43	51.42
Total	97.28	99.30

Note: K, Ti, Cr, Na were tested for but not detected
- below detection limit

4.4 DISCUSSION AND CONCLUSIONS

What are the source rocks for the alluvial PGM? Numerous researchers have pointed out that the mineral association of PGM is diagnostic for different styles of PGM deposits (Tolstykh et al. 1996; Genkin and Evstegneeva 1986; Malitch 1999, and others): (1) Ophiolite complexes are characterized by Os-Ir alloy rich in ruthenium, with ferroplatinum in proportions of less than 5 %. (2) Sulfides of Pd and Pt, arsenides and metal alloys prevail in the sulfide deposit type, with osmiridium and ferroplatinum less than 2 %. (3) Ferroplatinum in excess of 90 % of the PGM spectrum, with minor Os-Ir alloy and laurite is typical for concentrically zoned Uralian/Alaskan type complexes.

The mineral association of the Kedrovka PGM is typical of rutheniridosmium or iridosmium placer formations (Mochalov 1997). The absence of platinum-iron alloys and the fact that the Kedrovka PGM consist of refractory PGE indicates their possible ophiolitic source. Laurite is present in all mineralization types of PGM, including ophiolites.

Nakagawa and Franco (1997), studying the PGM assemblages from Hokkaido (Japan) and Samar (Philippines), came to the conclusion that there are two types of Os-Ir-Ru mineral

assemblages of ophiolite origin: the first one (H) characterized by Os-Ir-Ru alloys of wide composition and absence of primary laurite; the second type (S) represented by Ru-poor Os-Ir-Ru alloys with laurite. The difference in the assemblages is explained by the order of crystallization of alloy and laurite that depends on $f(S_2)$. The majority of our samples have low Ru content and Os-Ir-Ru alloy compositions plot along the Ir-Os line. Hexagonal (magmatic) inclusions of laurite are present in the alloys. These two features allow us to conclude that the PGM assemblage of the Kedrovka river belongs to the S-type of the Os-Ir-Ru assemblage and formed under high $f(S_2)$. Ophiolites are presently not exposed and are probably hidden under Quaternary cover. But there are fragments of ophiolitic massifs located southwest and north from the Kedrovka river.

5 MACROCRYSTALS[2] OF PGM FROM DARYA RIVER PLACER, ALDAN SHIELD, KHABAROVSKIY KRAY

5.1 INTRODUCTION

The Darya Au-PGE placer is located within the southern margin of the Aldan Shield, which is a protrusion of Precambrian basement at the south-eastern part of the Siberian platform (Fig. 37).

***Fig. 37**. Location of the Darya PGE-Au placer, and of similar Uralian/Alaskan type PGE deposits.*

This area is known for several PGE deposits and occurrences genetically related to zoned ultramafic-alkaline massifs of Uralian-Alaskan-type, such as Kondyor[3], Inagli, Chad, Sybakh (Rozhkov et al. 1962; Gurovitch et al. 1994; Nekrasov et al. 1994; Malitch 1999). The Darya river, 75 km SW from the Kondyor PGE-Au placer was recently explored for alluvial PGE and gold. A field expedition in summer 2001 recovered a heavy-mineral concentrate from the Darya

[2]The term "macrocystal" is used here for crystals whose diameters exceed 1.0 mm, in line with the definition of macrocrystalline rock textures (Jackson 1997, p. 382).

[3]The English transliteration of the Russian name «Кондёр» has two variants: Konder and Kondyor (see Cabri and Laflamme 1997). Kondyor is closest to the Russian pronunciation and is preferred here.

river with pyroxene, amphibole, Fe-Ti-oxides, zircon, gold and PGM. The PGM assemblage is represented both by xenomorphic Pt-Fe alloy grains and by euhedral crystals. Formerly the PGE minerals of the Darya placer were briefly described by Mochalov (2001) who reported the occurrence of low-Ir Pt-Fe alloy, and crystals of sperrylite and cooperite. Thirty grains were selected from the heavy-mineral concentrate from Darya for detailed mineralogical study, and euhedral crystals of Pt-Fe alloy, cooperite and mertieite-II were identified. This is the first occurrence of mm-sized idiomorphic mertieite-II crystals, and the second occurrence of coarse-grained euhedral ferroan platinum and cooperite crystals.

5.2 GEOLOGICAL SETTING

The Darya alluvial Au-PGE placer is located in the Khabarovskiy Krai province (Siberia, Russia) (Fig. 38). It occurs in the right tributary of the Darya river which is in the western part of the Omninsko-Batomskiy uplift, SE Aldan Shield (Fig. 39; coordinates: 57° 23´ NL and 133° 23' EL), 75 km SW from the well known Kondyor PGE placer. The Omninsko-Batomskiy uplift has undergone repeated tectonic and magmatic reactivation with multiple intrusive complexes of positive morphostructures (Kondyor, Inagli, Chad, Sibakh, Fig. 37, 38). Numerous small stock-like ultramafic bodies are also known (El'yanov and Andreev, 1991). The age of this magmatic activity is obscure (Nekrasov et al. 1994; see chapter 7). The creek bed exposes alkaline clinopyroxenite which also occurs in boulders. Reconnaissance mapping defines a circular intrusion with a diameter of 1.2-1.5 km, hosted in updomed Archean gneisses surrounded by Upper Proterozoic sandstones with abundant sills, dikes and subvolcanic bodies of alkaline and felsic rocks. The clinopyroxenite is medium to coarse grained (pegmatoidal) and consists of aegirine-augite and biotite. Apatite, Ti-rich garnet and Ti-magnetite are present as accessory minerals. There are also many boulders and pebbles of magnetite-rich clinopyroxenite ("koswite") with ilmenite, apatite, and kaersutite. The clinopyroxenite from Darya is similar to that of the Kondyor dike complex (Nekrasov et al. 1994).

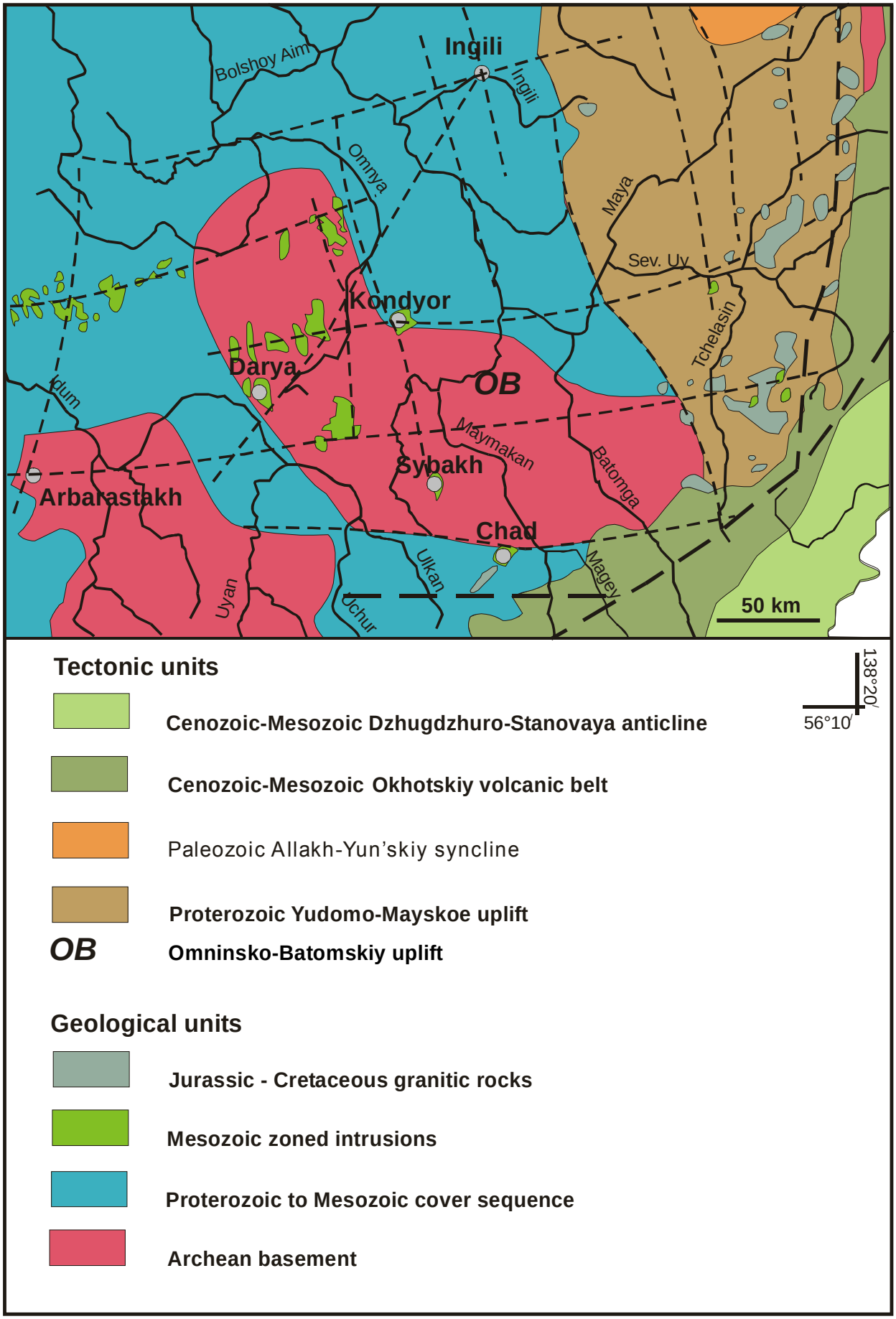

Fig. 38. *Geotectonic sketch map of the southeastern Aldan Shield (simplified from El'yanov and Andreev, 1991). Grey dots locate major PGE-bearing Uralian/Alaskan type intrusions.*

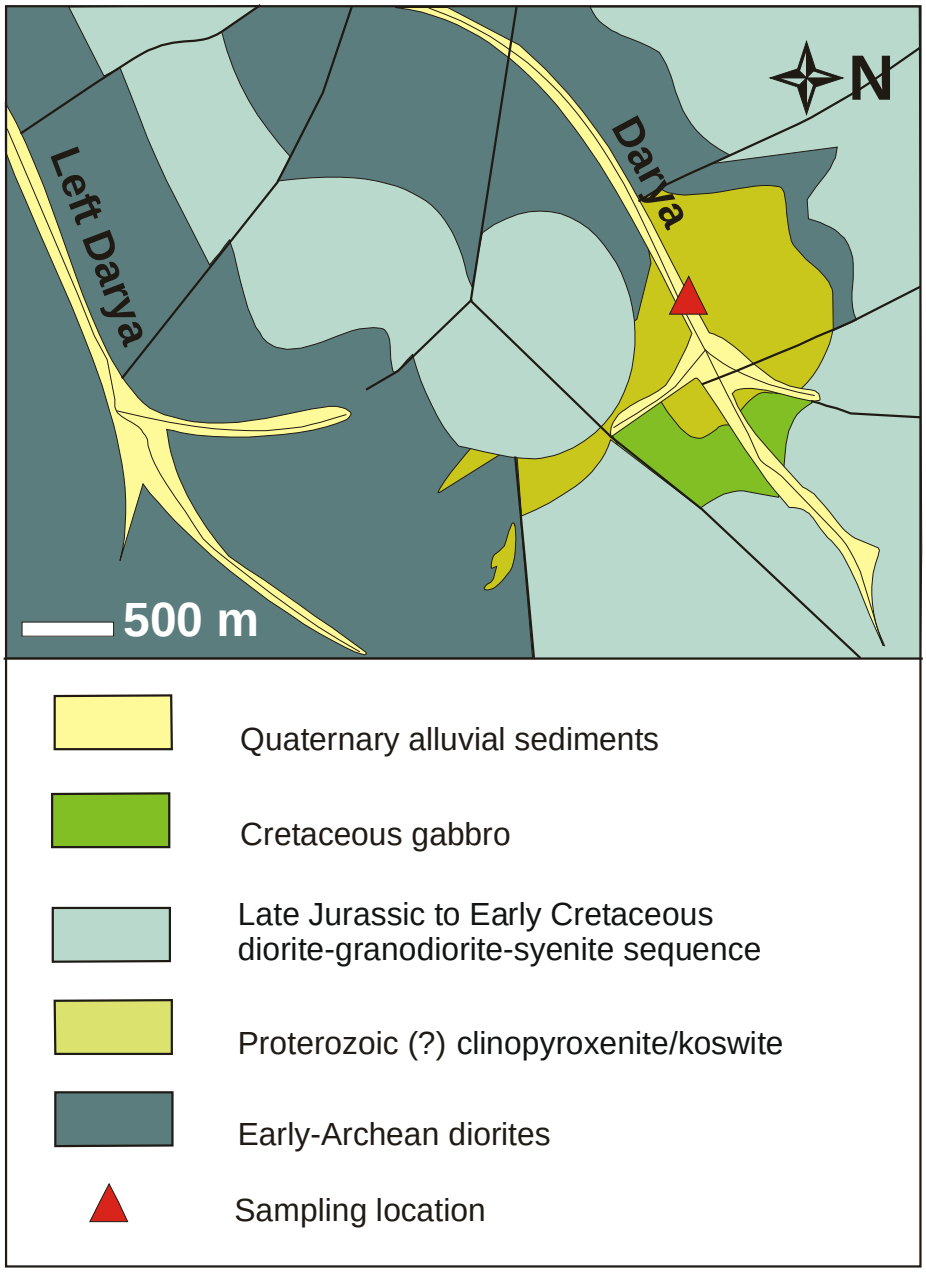

Fig. 39. *Geological map of Darya river area.*

5.3 MORPHOLOGY, CHEMICAL COMPOSITION, AND STRUCTURE OF THE PGM CRYSTALS

5.3.1 Pt-Fe alloy

Most of the 30 idiomorphic PGM crystals selected for this study are Pt-Fe alloy (60 %). This mineral phase forms relatively large crystals (up to 3.5 x 1.5 mm in size) with thin platy or elongated habit; one twinned crystal also was found (Fig. 40).

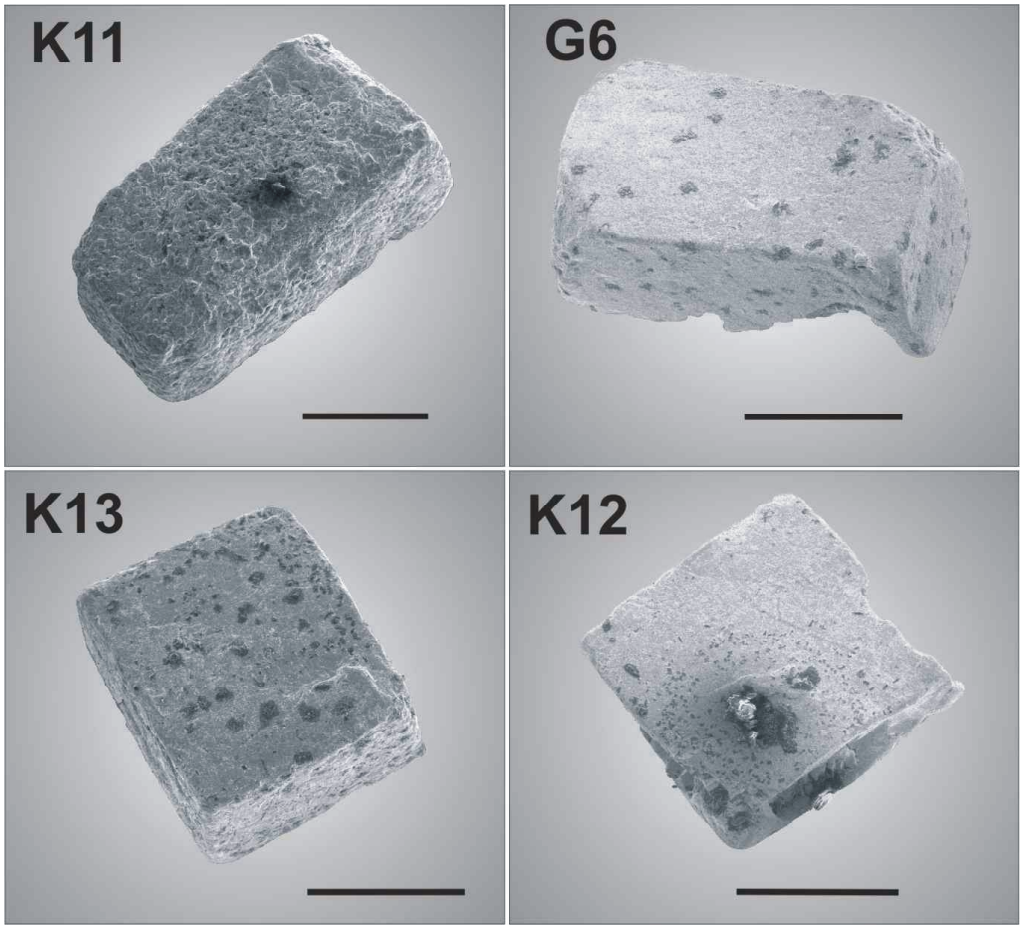

Fig. 40. *Scanning electron microscope (SEM) images of ferroan platinum crystals. The scale bar corresponds to 1 mm.*

The chemical composition corresponds to essentially pure Pt_3Fe with a compositional range from $Pt_{2.64}Fe_{1.00}$ to $Pt_{2.88}Fe_{1.00}$, and a minor copper component (up to 0.48 wt.%). Other PGE such as Os, Ru, Ir, Rh and Pd are below the analytical detection limit of the electron microprobe (0.10 wt.% for Os, 0.06 wt.% for Ru, 0.14 wt.% for Ir, 0.07 wt.% for Rh, and 0.14 wt.% for Pd) (Table 28).

Pt-Fe alloy of Pt_3Fe composition occurs in two structural states, i.e. isoferroplatinum with a primitive cubic structure (space group Pm3m), and ferroan platinum with a face-centered cubic structure (space group Fm3m) (Cabri and Feather, 1975).

We have taken powder diffraction diagrams from the Pt-Fe alloy in order to distinguish the cell type, but the strong texture in the samples prevented discrimination by this way. Therefore, we investigated a small piece of a crystal (0.14 x 0.11 x 0.09 mm^3) drilled from a polished section on a single-crystal diffractometer. Taking a rotation photograph, the complete diffracted powder rings can be displayed on the CCD-area detector avoiding the problems connected with texture. With a crystal-detector distance of 5 cm we thus recorded powder rings corresponding to Bragg-Brentano powder lines of 90° 2θ-CuKα.

TABLE 28. SELECTED ANALYSES OF FERROAN PLATINUM ALLOYS FROM DARYA RIVER

Sample	K12	DR3	Dr5	Dr4	Dr2	Dr1
wt.%						
Pt	89.63	89.66	90.2	90.59	90.45	90.29
Fe	8.83	8.83	8.71	8.61	8.58	8.68
Cu	0.34	0.26	0.23	0.29	0.25	0.28
Total	98.80	98.75	99.14	99.49	99.29	99.25
at.%						
Pt	73.76	73.81	74.34	74.52	74.62	74.33
Fe	25.38	25.39	25.08	24.74	24.74	24.97
Cu	0.86	0.66	0.58	0.73	0.64	0.70
Total	100	100	100	100	100	100

Note: Ru, Rh, Os, Ir, Pd, S, Au, Ni, Sn, Sb, As were not detected; - below detection limit

The sample gave just four lines, which could be indexed with a F-centered lattice type with a cell constant of 3.86(1) Å. These are the lines expected for ferroan platinum alloy (Cabri and Laflamme, 1997). Thus, within the experimental limitations, X-ray diffractometry suggests that the Pt-Fe alloy from the Darya area has F-centered lattice type (Table 29).

TABLE 29. X-RAY DIFFRACTION DATA OF FERROAN PLATINUM FROM DARYA RIVER

	a_o= 3.86(1) A	
hkl	d-value	Intensity
111	2.225	strong
200	1.935	medium
220	1.362	weak
311	1.164	weak

Occasionally, the ferroan platinum crystals have about 100 μm large cooperite overgrowth rims (Table 30, Fig. 41B) and contain μm-sized inclusions of bornite and minerals of the chalcocite group, probably digenite [Cu_9S_5] (Table 32).

One sample is covered by a gold-rich Au-Ag alloy (Fig. 41a). Sulfates and K-bearing silicates are often attached to the surface of the ferroan platinum crystals.

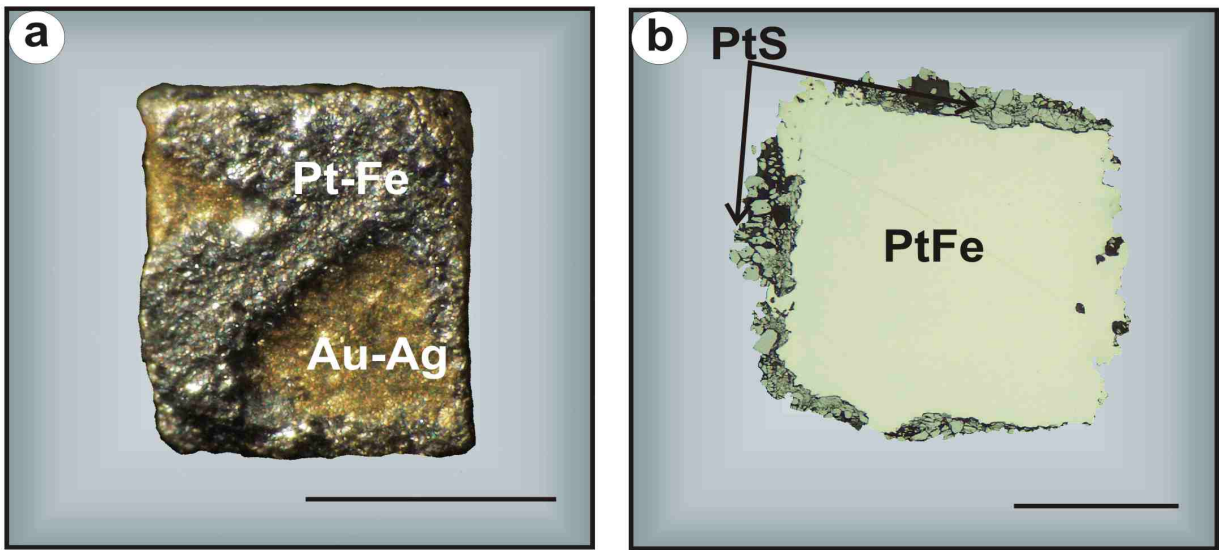

Fig. 41. *Photomicrograph of a crystal of Pt-Fe alloy covered by* ***a)*** *Au-Ag alloy (sample K2);* ***b)*** *cooperite (sample Dr3).*

5.3.2 Cooperite

Cooperite is also fairly common. It occurs both as large euhedral crystals (up to 3 mm across), partly twinned (Fig. 42), and as overgrowth aggregates on Pt-Fe crystals (Fig.41b).

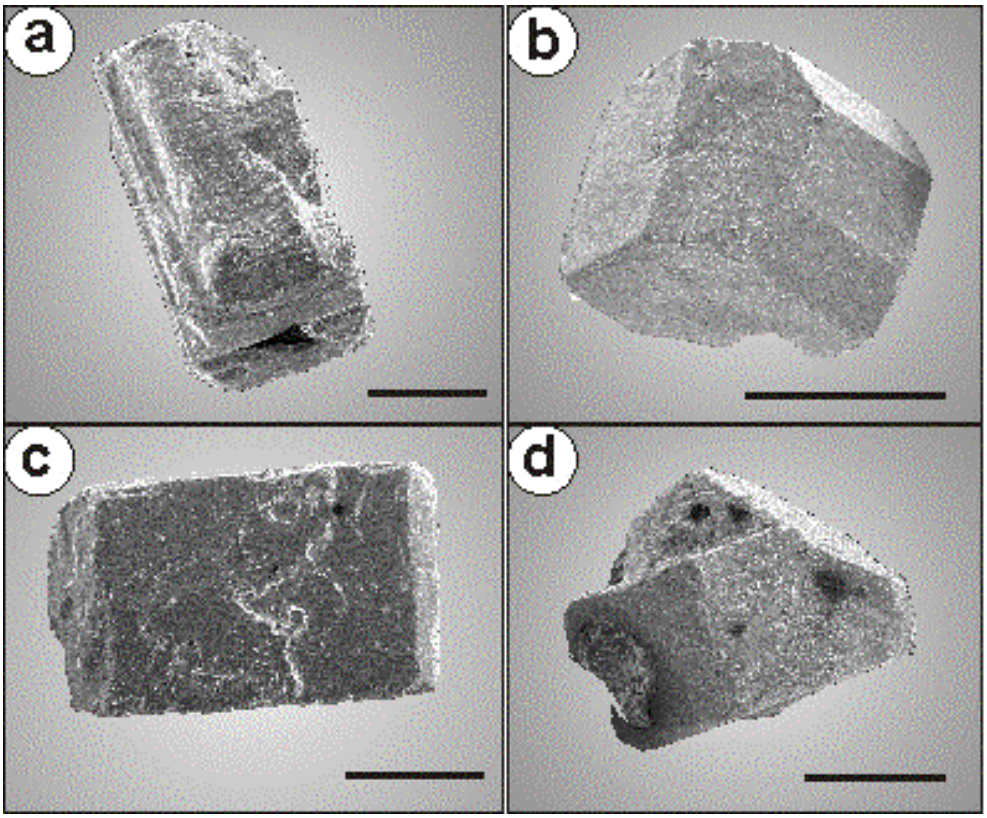

Fig. 42. *Scanning electron microscope (SEM) image of cooperite crystals (a-c) and cooperite twin (d). The scale bar corresponds to 1 mm. Samples: G3, K4, K1, G5.*

TABLE 30. SELECTED ANALYSES OF COOPERITE-BRAGGITE AND Pt-Pd-Hg PHASE

Sample	Cooperite-braggite								Pt-Pd-Hg	
	G1m	G3m	Dr6m	K1-2r	Dr3r	K9r	K7	Dr2	Dr2	Dr2
No	1	2	3	4	5	6	7	8	9	10
wt.%										
Pt	84.84	84.95	84.88	82.23	85.64	79.00	77.57	58.43	70.01	69.60
Pd	0.35	0.07	-	2.57	0.33	5.95	7.82	24.92	27.23	26.65
S	13.83	14.00	13.95	15.00	15.09	15.54	15.90	17.88	-	-
Fe	-	-	-	-	-	-	-	0.37	0.27	0.25
Hg	n.a.	n.a.	n.a.	n.a.	n.a.	n.a.	0.62	n.a.	3.56	3.24
Total	99.02	99.02	98.83	99.80	101.06	100.49	101.91	101.60	101.07	99.74
at.%										
Pt	50.02	49.90	50.00	46.15	48.10	42.83	40.99	27.28	56.31	56.83
Pd	0.38	0.08	-	2.64	0.34	5.91	7.57	21.33	40.15	39.89
S	49.60	50.03	50.00	51.21	51.56	51.26	51.12	50.79	-	-
Fe	-	-	-	-	-	-	-	0.60	0.76	0.71
Hg	n.a.	n.a.	n.a.	n.a.	n.a.	n.a.	0.32	n.a.	2.78	2.57
Total	100	100	100	100	100	100	100	100	100	100

Note: Au, Cu, Sn, Sb, As, Se were not detected; No 1-3 cooperite euhedral crystals,
No 4-5 cooperite overgrowth on Pt-Fe crystals; No 6-8 intergrowth with palladian antimonide
- below detection limit; n.a.-not analysed

It has constant chemical composition and has no detectable impurities (Fe and Ni below detection limit), except an appreciable palladium content of up to 5.95 wt.% Pd (intergrowth with mertieite-II) (Table 30). Occasionally, it contains chalcopyrite inclusions (Table 32) and inclusions of a new mineral phase of $Pt(Cu,Fe)S_3$ composition (Table 31).

5.3.3 Pt(Cu,Fe)S_3 phase

Three cooperite crystals contain relatively large inclusions of a new mineral phase with composition Pt(Cu,Fe)S_3 (Table 31). The largest inclusion with 300 µm in its long direction (Sample B1) has an irregular elongated form and remarkable "dendritic" internal texture with thread-like native platinum (Fig. 43a). This texture has probably developed by weathering. In two other cooperite grains the new phase occurs as inclusions (20 µm in sample B10 and 40 µm in sample D2) intergrown either with chalcopyrite (Fig. 43b) or both chalcopyrite and galena (Fig. 44).

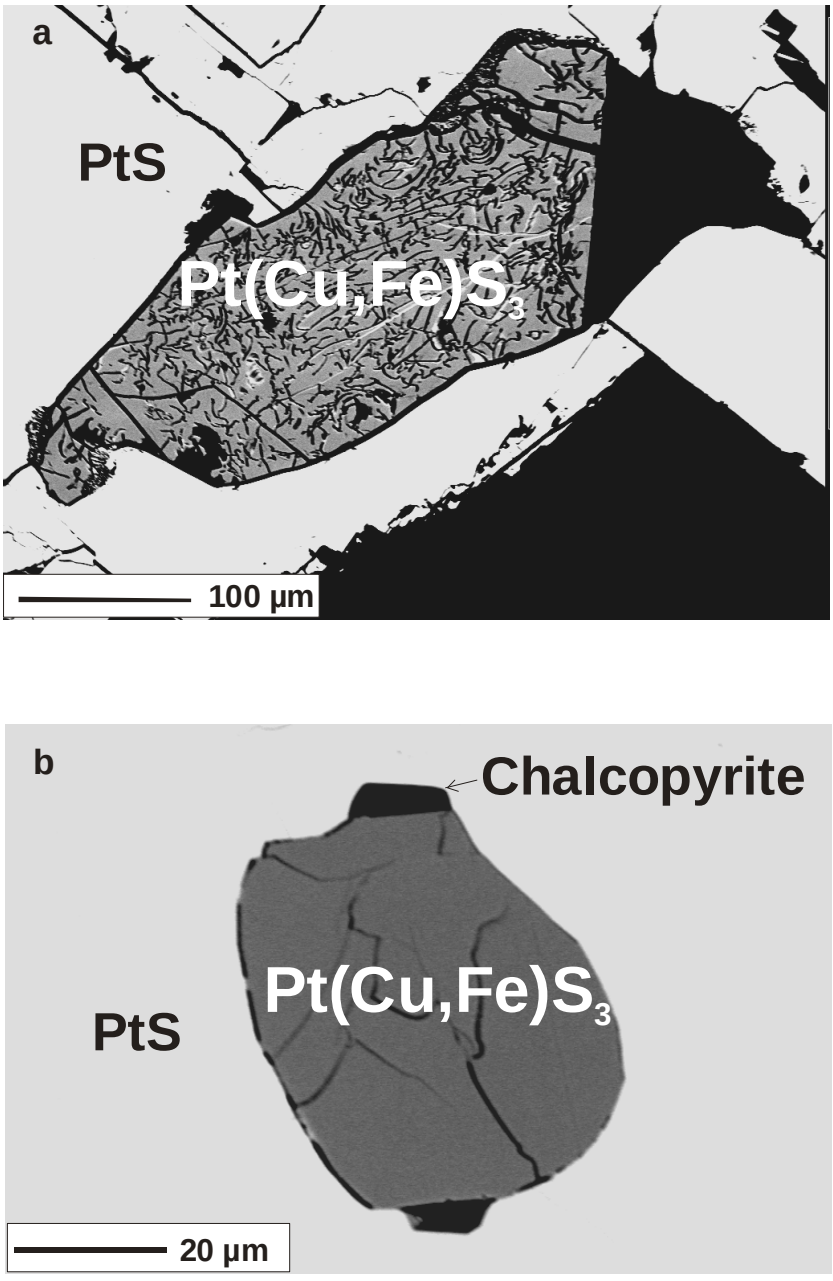

Fig. 43. *BSE images of Pt(Cu,Fe)S_3 inclusions in cooperite [PtS]:* ***a)*** *Sample B1;* ***b)*** *Sample Dr.*

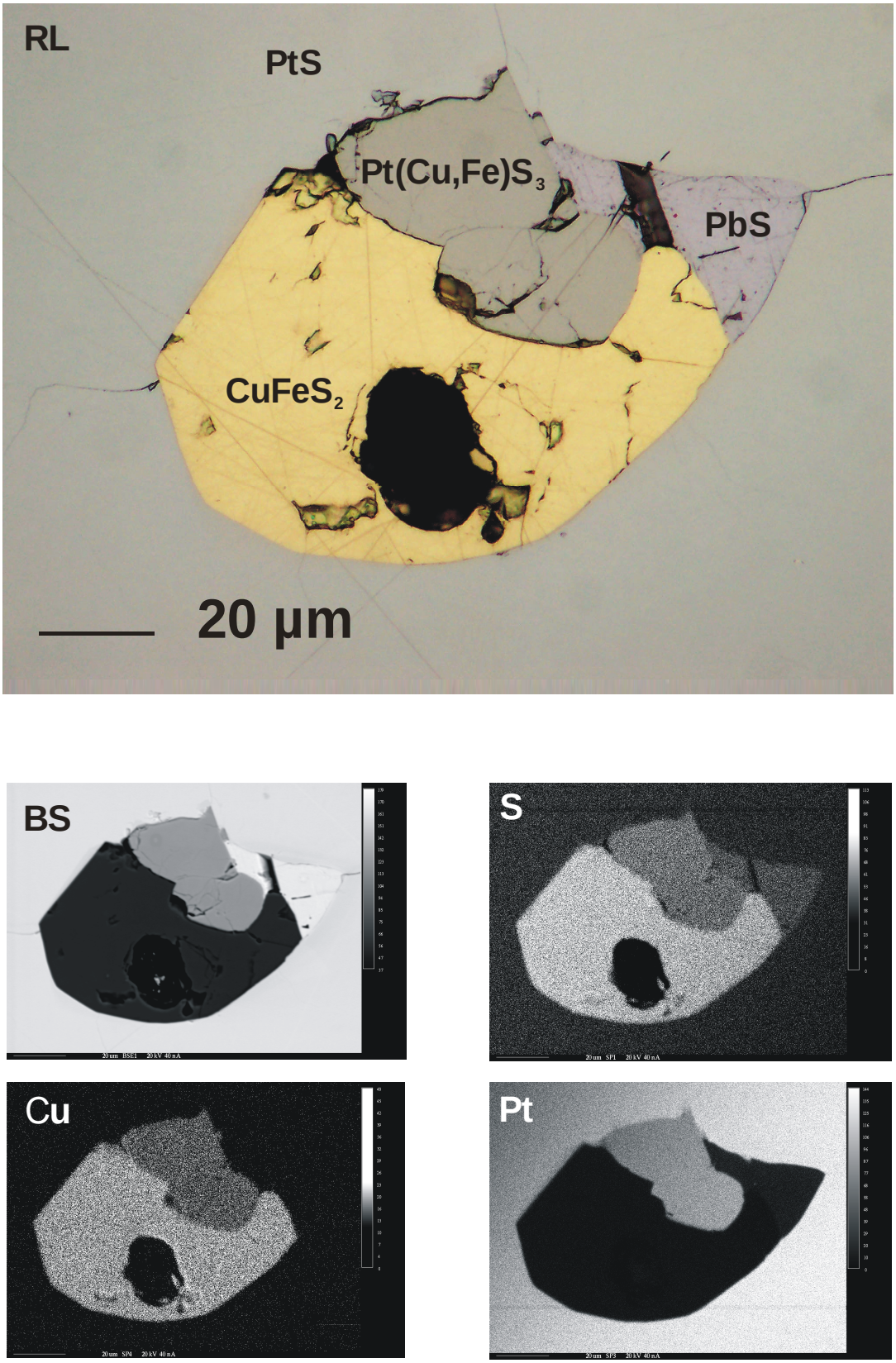

Fig. 44. *Inclusion of $Pt(Cu,Fe)S_3$ in cooperite [PtS] intergrown with chalcopyrite and galena:* ***RL*** *is photomicrograph (oil immersion);* ***BS*** *is back-scattered electron image (BSE);* ***S, Cu, Pt*** *are single-element scans.*

TABLE 31. SELECTED CHEMICAL ANALYSIS OF THE $Pt(Cu,Fe)S_3$ PHASE

Sample	B10					average	D2					average	B1					average
No	**1**	**2**	**3**	**4**	**5**	**N=17**	**6**	**7**	**8**	**9**	**10**	**N=15**	**11**	**12**	**13**	**14**	**15**	**N=30**
wt.%																		
Pt	54.40	54.16	53.35	53.13	54.47	**53.77 ± 0.58**	53.71	53.74	54.14	54.36	54.09	**54.09 ± 0.32**	56.09	55.67	56.34	57.14	56.24	**56.59 ± 0.61**
Cu	12.19	12.33	12.88	12.99	12.29	**12.77 ± 0.34**	12.60	12.64	12.45	12.36	12.43	**12.56 ± 0.11**	8.92	9.30	8.32	7.42	8.32	**8.42 ± 0.77**
Fe	6.78	6.75	6.86	7.11	6.52	**6.95 ± 0.23**	6.91	6.85	6.82	6.73	6.73	**6.86 ± 0.09**	7.16	7.16	7.10	7.18	7.16	**7.17 ± 0.06**
Ni	0.07	0.07	0.07	0.08	0.08	**0.07 ± 0.01**	0.06	0.06	0.06	0.06	0.06	**0.06 ± 0.01**	0.05	0.04	0.04	0.04	0.05	**0.04 ± 0.01**
S	27.56	27.67	27.26	27.66	27.74	**27.49 ± 0.23**	27.28	27.30	27.35	27.33	27.32	**27.40 ± 0.12**	28.27	28.34	28.74	29.56	28.89	**28.84 ± 0.38**
Total	101.00	100.98	100.42	100.97	101.10	**101.06 ± 0.34**	100.56	100.59	100.82	100.84	100.63	**100.97 ± 0.36**	100.49	100.51	100.54	101.34	100.66	**101.07 ± 0.38**
at.%																		
Pt	19.20	19.06	18.86	18.55	19.18	**18.88 ± 0.22**	19.00	19.00	19.15	19.26	19.17	**19.08 ± 0.11**	19.99	19.75	20.00	20.05	19.89	**19.99 ± 0.25**
Cu	13.20	13.33	13.97	13.92	13.28	**13.77 ± 0.36**	13.68	13.72	13.51	13.44	13.52	**13.60 ± 0.11**	9.74	10.13	9.06	8.00	9.03	**9.13 ± 0.83**
Fe	8.35	8.29	8.47	8.67	8.02	**8.53 ± 0.28**	8.54	8.47	8.42	8.32	8.33	**8.45 ± 0.10**	8.92	8.88	8.80	8.80	8.84	**8.85 ± 0.09**
Ni	0.08	0.08	0.09	0.10	0.09	**0.09 ± 0.01**	0.07	0.07	0.07	0.07	0.07	**0.07 ± 0.01**	0.06	0.05	0.05	0.05	0.06	**0.05 ± 0.01**
S	59.17	59.24	58.61	58.76	59.43	**58.73 ± 0.44**	58.71	58.74	58.85	58.91	58.91	**58.81 ± 0.11**	61.29	61.19	62.09	63.10	62.18	**61.98 ± 0.63**
Total	100	100	100	100	100		100	100	100	100	100		100	100	100	100	100	

1. $Pt_{0.960}(Cu_{0.660}Fe_{0.418}Ni_{0.004})_{\Sigma 1.082}S_{2.959}$

2. $Pt_{0.953}(Cu_{0.667}Fe_{0.415}Ni_{0.004})_{\Sigma 1.085}S_{2.962}$

3. $Pt_{0.943}(Cu_{0.669}Fe_{0.424}Ni_{0.005})_{\Sigma 1.127}S_{2.931}$

4. $Pt_{0.928}(Cu_{0.696}Fe_{0.434}Ni_{0.005})_{\Sigma 1.135}S_{2.938}$

5. $Pt_{0.959}(Cu_{0.664}Fe_{0.401}Ni_{0.005})_{\Sigma 1.070}S_{2.972}$

Average: $Pt_{0.944\pm0.011}(Cu_{0.688\pm0.018}Fe_{0.426\pm0.014}Ni_{0.004\pm0.000})_{\Sigma 1.118\pm0.032}S_{2.937\pm0.022}$

11. $Pt_{1.000}(Cu_{0.487}Fe_{0.446}Ni_{0.003})_{\Sigma 0936}S_{3.065}$

12. $Pt_{0.988}(Cu_{0.507}Fe_{0.444}Ni_{0.003})_{\Sigma 0.953}S_{3.060}$

13. $Pt_{1.000}(Cu_{0.453}Fe_{0.440}Ni_{0.003})_{\Sigma 0.896}S_{3.105}$

14. $Pt_{1.003}(Cu_{0.400}Fe_{0.440}Ni_{0.003})_{\Sigma 0.843}S_{3.155}$

15. $Pt_{0.995}(Cu_{0.452}Fe_{0.442}Ni_{0.003})_{\Sigma 0.897}S_{3.109}$

Average: $Pt_{1.005\pm0.031}(Cu_{0.456\pm0.041}Fe_{0.441\pm0.008}Ni_{0.002\pm0.000})_{\Sigma 0.899\pm0.049}S_{3.096\pm0.036}$

6. $Pt_{0.950}(Cu_{0.684}Fe_{0.427}Ni_{0.004})_{\Sigma 1.115}S_{2.936}$

7. $Pt_{0.950}(Cu_{0.686}Fe_{0.424}Ni_{0.004})_{\Sigma 1.113}S_{2.937}$

8. $Pt_{0.958}(Cu_{0.676}Fe_{0.421}Ni_{0.004})_{\Sigma 1.100}S_{2.943}$

9. $Pt_{0.963}(Cu_{0.672}Fe_{0.416}Ni_{0.004})_{\Sigma 1.092}S_{2.946}$

10. $Pt_{0.959}(Cu_{0.676}Fe_{0.417}Ni_{0.004})_{\Sigma 1.096}S_{2.946}$

Average: $Pt_{0.954\pm0.006}(Cu_{0.680\pm0.005}Fe_{0.422\pm0.005}Ni_{0.004\pm0.000})_{\Sigma 1.106\pm0.016}S_{2.940\pm0.006}$

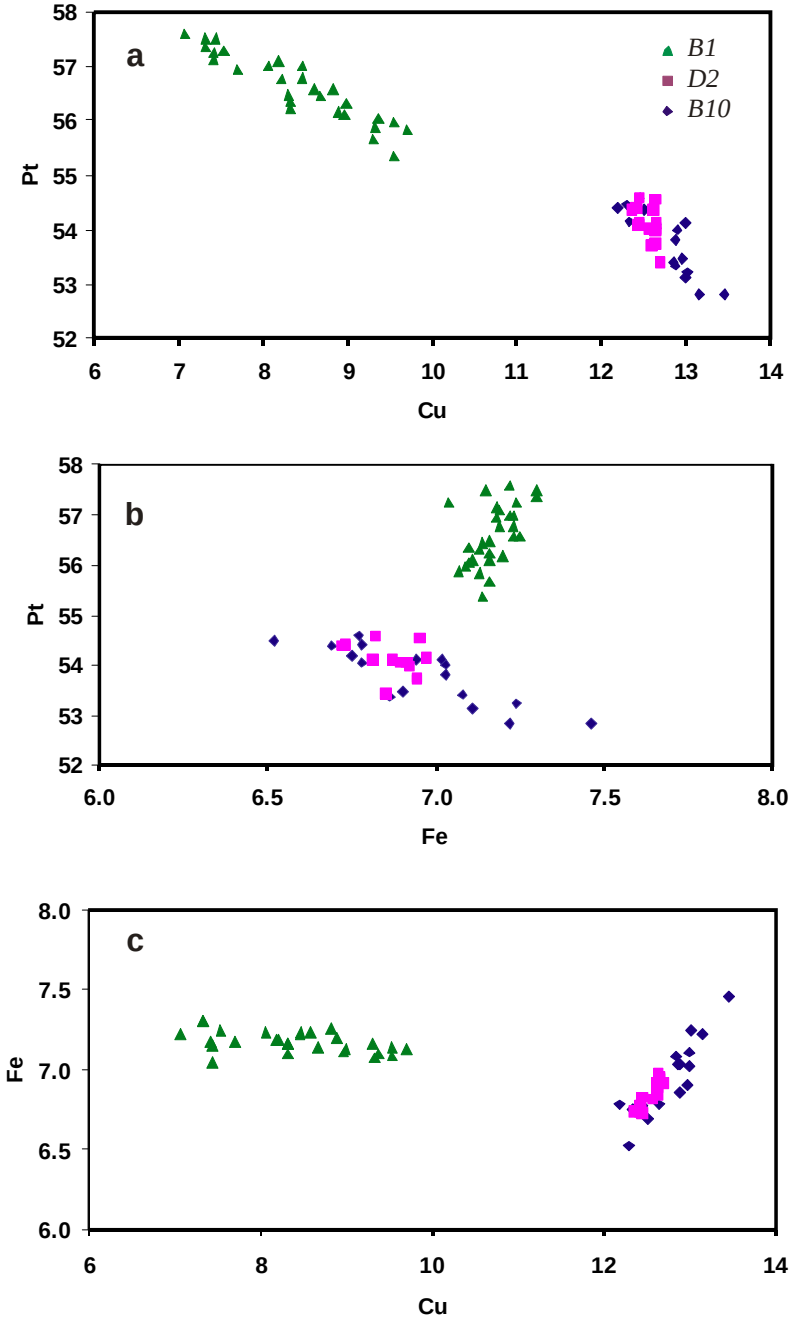

Fig. 45. *Binary element plots of* ***a)*** *Pt vs Cu;* ***b)*** *Pt vs Fe; and* ***c)*** *Fe vs Cu in new phase Pt(Cu,Fe)S_2.*

The three inclusions are generally identical in chemical composition, but form two groupings. Samples B10 and D2 display a slight deficiency in sulfur at distinctly lower Pt and higher Cu content (Fig. 45) compared to Sample B1. Sample B1 has practically constant Fe content with broad variation of Cu, while Fe and Cu in samples B10 and D2 are positively correlated within a narrow Cu interval. These trends probably reflect the distinct weathering overprint in Sample B1, where Cu is leached while iron remains immobile. The Pt enrichment in this sample is probably from the native Pt on cracks.

5.3.4 Mertieite-II

Palladium antimonides are also relatively abundant and occur in grain sizes from 1.3 to 2.5 mm (Fig. 46). The largest crystal (Sample K9) displays perfect hexagonal habit (Fig. 47a), and a sheetlike texture (Fig. 47b). It is brittle and shows perfect cleavage along (0001) (Fig. 47c). More than sixty analyses were done on different grains of palladium antimonide (Table 33). The chemical data were recalculated based on known mineral stoichiometries, i.e. on the basis of 11 atoms for mertieite-II $Pd_8(Sb,As)_3$, on the basis of 15 atoms for mertieite-I $Pd_{11}(Sb,As)_4$ - isomertieite $Pd_{11}Sb_2As_2$), and on the basis of 7 atoms for stibiopalladinite Pd_5Sb_2.

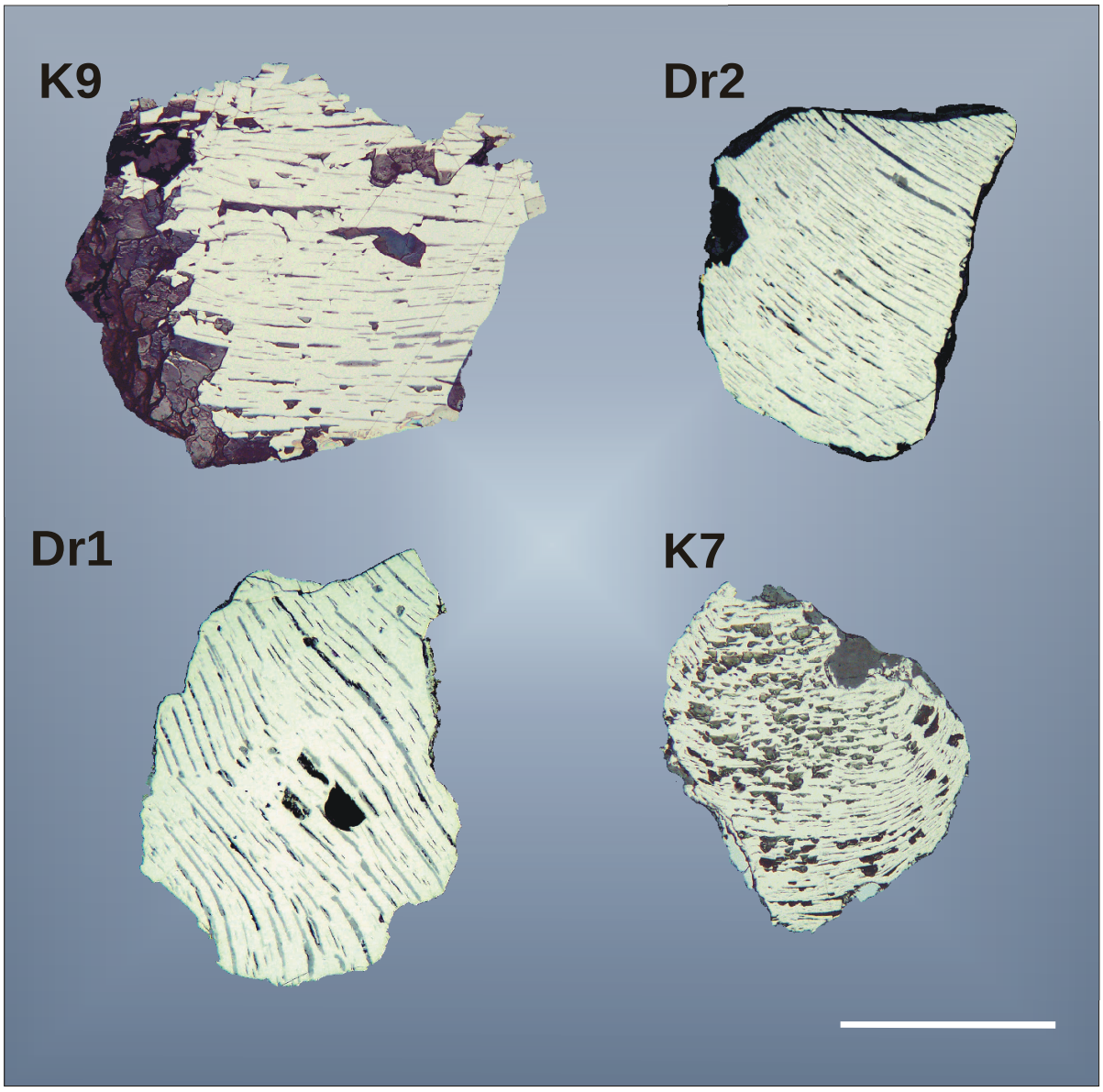

***Fig. 46**. Photomicrographs of mertieite-II grains. Note sheet-like grey phase of Pd-oxides along cleavage planes. Scale bar corresponds to 1 mm.*

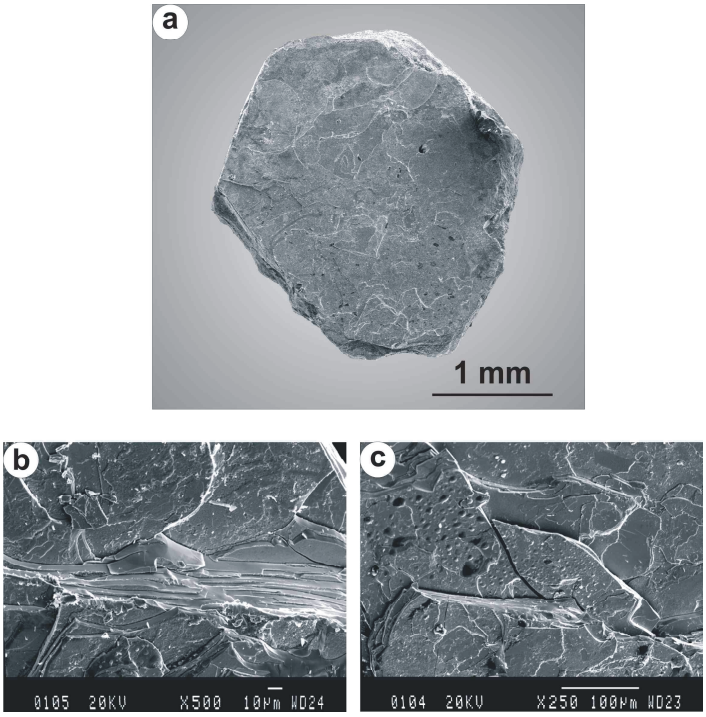

Fig. 47*. Scanning electron microscope (SEM) image of mertieite-II crystal:* ***a)*** *General view;* ***b)*** *Higher magnification that highlights sheet-like texture;* ***c)*** *Fracture/cleavage pattern of the crystal. Sample K9.*

TABLE 32. COMPOSITION OF INCLUSIONS WITHIN THE PGM CRYSTALS

Mineral	**Sperrylite**	**Chalcopyrite**	**Bornite**	**Chalcocite**
No	**1**	**2**	**3**	**4**
	wt.%			
Pd	0.37	-	-	-
Pt	53.74	2.56*	-	0.74*
Cu	-	34.50	68.80	74.09
Fe	-	29.49	7.21	2.28
S	-	33.42	23.84	21.42
Sb	0.15	-	-	-
As	43.11	-	-	-
Se	0.11	-	-	-
Total	97.48	99.98	99.85	97.79
	at.%			
Pd	0.41	-	-	-
Pt	32.15	0.62	-	0.20
Cu	-	25.53	55.37	62.06
Fe	-	24.83	6.60	2.17
S	-	49.02	38.02	35.56
Sb	0.14	-	-	-
As	67.14	-	-	-
Se	0.16	-	-	-
Total	100	100	100	100

Note: Ru, Rh, Ag, Os, Bi, Au, Ir, were not detected; - below detection limit
No 1 is inclusion within mertieite-II; No 2 inclusion within cooperite,
and Nos 3-4 inclusions within ferroan platinum
*Because of the small size of these inclusions, it is assumed that the Pt content found in chalcopyrite and chalcocite is due to secondary fluorescence from the host minerals (cooperite and ferroan platinum).

TABLE 33. AVERAGE ANALYSYS OF MERTIEITE-II CRYSTALS

wt.%	Dr1 n=16	Dr2 n=9	Dr2 defocused n=6	K9 n=11	K9* n=18	K7 n=12	K7 defocused n=9
Pd	71.85 ± 0.26	71.84 ± 0.15	69.97 ± 0.82	71.81 ± 0.31	71.22 ± 0.38	71.04 ± 0.46	66.89 ± 0.82
Sn	0.98 ± 0.34	1.28 ± 0.09	1.27 ± 0.06	1.51 ± 0.15	n.a.	1.58 ± 0.24	1.42 ± 0.04
Sb	22.51 ± 0.77	22.23 ± 0.26	21.79 ± 0.60	21.04 ± 0.17	21.77 ± 0.24	24.78 ± 0.51	22.47 ± 0.51
Pt	-	-	1.81 ± 0.83	-	-	0.12 ± 0.42	4.13 ± 0.78
Te	0.85 ± 0.06	0.67 ± 0.09	0.82 ± 0.12	2.01 ± 0.20	2.24 ± 0.23	0.44 ± 0.30	0.72 ± 0.13
As	3.8 ± 0.24	3.26 ± 0.12	4.31 ± 0.81	3.62 ± 0.11	3.92 ± 0.07	2.3 ± 0.39	4.80 ± 0.70
Cu	n.a.	n.a.	n.a.	n.a.	0.16 ± 0.01	n.a.	n.a.
Total	99.99 ± 1.67	99.28 ± 0.71	99.97 ± 3.24	99.99 ± 0.94	99.15 ± 0.92	100.26 ± 2.32	100.43 ± 2.98
apfu							
Calculation was made on the basis of 11 atoms - mertieite-II $Pd_8(Sb,As)_3$							
Pd	8.03 ± 0.11	8.10 ± 0.04	7.86 ± 0.16	8.03 ± 0.04	8.00 ± 0.02	7.99 ± 0.11	7.55 ± 0.13
Sn	0.10 ± 0.03	0.13 ± 0.01	0.13 ± 0.00	0.15 ± 0.01	-	0.16 ± 0.02	0.14 ± 0.00
Sb	2.20 ± 0.04	2.19 ± 0.01	2.14 ± 0.01	2.05 ± 0.00	2.14 ± 0.02	2.43 ± 0.00	2.21 ± 0.01
Pt	-	-	0.11 ± 0.05	-	-	0.01 ± 0.03	0.25 ± 0.04
Te	0.08 ± 0.01	0.06 ± 0.01	0.08 ± 0.01	0.19 ± 0.02	0.21 ± 0.02	0.04 ± 0.03	0.07 ± 0.01
As	0.60 ± 0.03	0.52 ± 0.02	0.69 ± 0.11	0.57 ± 0.01	0.62 ± 0.01	0.37 ± 0.04	0.77 ± 0.09
Cu	-	-	-	-	0.03 ± 0.00	-	-
Pd+Pt	**8.03 ± 0.11**	**8.10 ± 0.04**	**7.97 ± 0.11**	**8.03 ± 0.04**	**8.03 ± 0.02**	**8.00 ± 0.09**	**7.80 ± 0.09**
Sn+Sb+Te+As	**2.97 ± 0.11**	**2.90 ± 0.04**	**3.03 ± 0.11**	**2.97 ± 0.04**	**2.97 ± 0.02**	**3.00 ± 0.09**	**3.20 ± 0.09**
Calculation was made on the basis of 15 atoms - mertieite-I $Pd_{11}(Sb,As)_4$ - isomertieite $Pd_{11}Sb_2As_2$							
Pd	10.94 ± 0.14	11.04 ± 0.06	10.71 ± 0.22	10.95 ± 0.06	10.90 ± 0.03	10.89 ± 0.16	10.29 ± 0.18
Sn	0.13 ± 0.04	0.18 ± 0.01	0.17 ± 0.00	0.21 ± 0.02	-	0.22 ± 0.03	0.20 ± 0.00
Sb	2.99 ± 0.05	2.98 ± 0.01	2.91 ± 0.01	2.80 ± 0.00	2.91 ± 0.03	3.32 ± 0.00	3.02 ± 0.02
Pt	-	-	0.15 ± 0.07	-	-	0.01 ± 0.04	0.35 ± 0.06
Te	0.11 ± 0.01	0.09 ± 0.01	0.10 ± 0.01	0.26 ± 0.02	0.29 ± 0.03	0.06 ± 0.04	0.09 ± 0.01
As	0.82 ± 0.04	0.71 ± 0.02	0.94 ± 0.15	0.78 ± 0.02	0.85 ± 0.02	0.50 ± 0.05	1.05 ± 0.13
Cu					0.04 ± 0.00		
Pd+Pt	**10.94 ± 0.14**	**11.04 ± 0.06**	**10.86 ± 0.15**	**10.95 ± 0.06**	**10.94 ± 0.03**	**10.90 ± 0.12**	**10.64 ± 0.12**
Sn+Sb+Te+As	**4.06 ± 0.14**	**3.95 ± 0.06**	**4.14 ± 0.15**	**4.05 ± 0.06**	**4.05 ± 0.03**	**4.10 ± 0.12**	**4.36 ± 0.12**
Calculation was made on the basis of 7 atoms - stibiopalladinite Pd_5Sb_2							
Pd	5.11 ± 0.07	5.15 ± 0.03	5.00 ± 0.10	5.11 ± 0.03	5.09 ± 0.01	5.08 ± 0.07	4.80 ± 0.08
Sn	0.06 ± 0.02	0.08 ± 0.01	0.08 ± 0.00	0.10 ± 0.01	-	0.10 ± 0.01	0.09 ± 0.00
Sb	1.40 ± 0.03	1.39 ± 0.01	1.36 ± 0.01	1.31 ± 0.00	1.36 ± 0.02	1.55 ± 0.00	1.41 ± 0.01
Pt	-	-	0.07 ± 0.03	-	-	0.00 ± 0.02	0.16 ± 0.03
Te	0.05 ± 0.00	0.04 ± 0.01	0.05 ± 0.01	0.12 ± 0.01	0.13 ± 0.01	0.03 ± 0.02	0.04 ± 0.01
As	0.38 ± 0.02	0.33 ± 0.01	0.44 ± 0.07	0.37 ± 0.01	0.40 ± 0.01	0.23 ± 0.0.3	0.49 ± 0.06
					0.02 ± 0.00		
Pd+Pt	**5.11 ± 0.07**	**5.15 ± 0.03**	**5.07 ± 0.07**	**5.11 ± 0.03**	**5.11 ± 0.01**	**5.09 ± 0.06**	**4.97 ± 0.06**
Sn+Sb+Te+As	**1.89 ± 0.07**	**1.85 ± 0.03**	**1.93 ± 0.07**	**1.89 ± 0.03**	**1.89 ± 0.01**	**1.91 ± 0.09**	**2.03 ± 0.06**

Note: S, Fe, Hg, Bi, - below detection limit; n-a- not analysed
* The analyses have been made in the Centre for Mineral and Energy Technology, Canada
For K9* sample Ni, Fe, Ir, and Bi, were sought for but not detected.

A precise definition based on chemical composition only is difficult inasmuch as, according to Table 33 (including the control analyses for sample K9, done at CANMET, Ottawa), the grains could be mertieite-I, mertieite-II, or stibiopalladinite. The powder X-ray data of palladium antimonide did not allow to clearly distinguishing mertieite-I and mertieite-II (Table 34). In

order to clarify this vagueness small crystal fragment of the sample K9 were analyzed by single crystal diffractometry.

TABLE 34. X-RAY DIFFRACTION DATA OF MERTIEITE-II, SAMPLE K-9

No	2Θ	d	I	hkl
1	24.86	3.579	16	310
2	32.10	2.786	11	323
3	34.64	2.587	10	501
4	36.52	2.458	14	406
5	37.64	2.388	100	317
6	39.44	2.283	77	407
7	41.52	2.173	31	600
8	44.88	2.018	18	507
9	47.32	1.919	10	613
10	48.78	1.865	10	700
11	50.31	1.812	7	1112
12	50.92	1.792	12	607

This method showed trigonal symmetry with cell constants of a = 7.528(1) Å and c = 43.029(1) Å in a hexagonal lattice, which clearly proves that sample K9 is mertieite-II. The refinement of the structure was performed in space group R -3c (167).

Two samples of palladium antimonide (Dr2 and K7) are dappled with µm-sized sperrylite inclusions, which are distributed irregularly in grain Dr2, and which are uniformly dispersed in K7, suggesting an exsolution fabric. In order to learn about the high-temperature composition, analysis of the palladium antimonide crystals was done with defocused beam (Ø 50 µm). The primary composition of the K7 grain appears to be closer to stibiopalladinite whereas sample Dr2 could be interpreted both as mertieite-II and stibiopalladinite (Table 33).

The better preserved uniform exsolution texture in sample K7 makes the bulk analytical data for this sample more reliable, and one might speculate that the high-temperature primary state of both samples Dr2 and K7 was stibiopalladinite with a Pt content of up to ~5 wt.% Pt which then exsolved as sperrylite. A typical feature of the mertieite-II samples is the constant presence of tellurium as a trace element, with up to 2.64 wt.% Te in sample K9. Small inclusion/intergrowths of Au-Ag alloy with mertieite-II crystals are shown at the Fig. 48. Rare Pt-Pd-Hg alloy intergrown with mineral of cooperite-braggite solid solution attached to mertieite-II have been found in the Dr2 sample (Fig. 49).

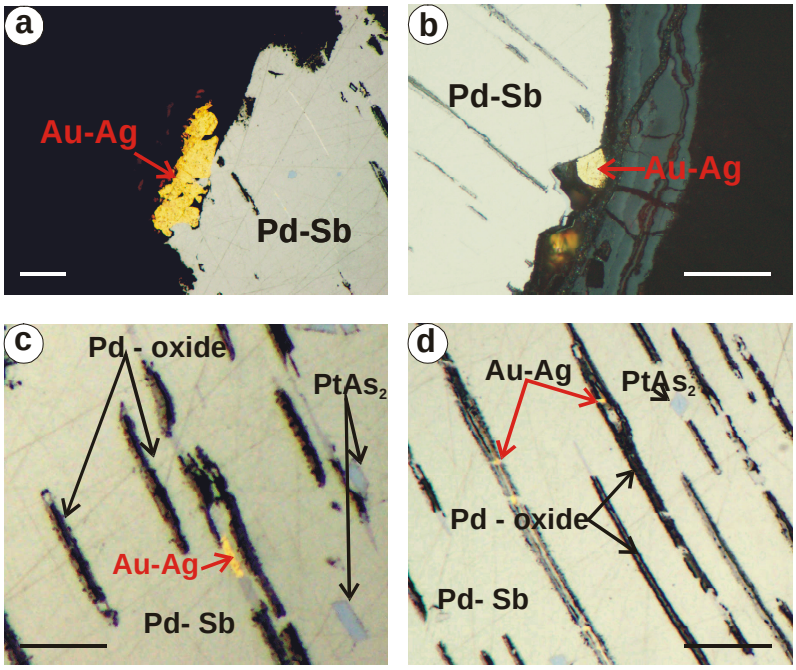

Fig. 48. *Photomicrographs of Au-Ag intergrowth (a, b) and inclusions (c, d) within mertieite-II crystal. Oil immersion. Sample Dr2. The scale bar corresponds to 20 µm.*

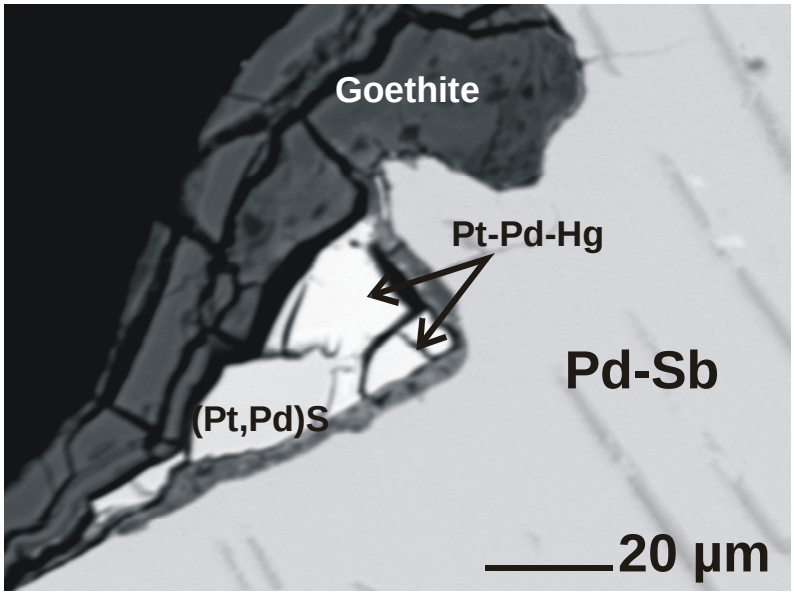

Fig. 49*. BSE image of braggite intergrown with Pt-Pd-Hg attached to mertieite-II crystal. Sample Dr2.*

5.4 DISCUSSION

Euhedral crystals of PGM are often reported in the literature, but they commonly have a size not exceeding 200 µm. The relatively large PGM crystals from the Darya placer are highly unusual. Due to the complexities of the Pd-Sb-As system with occurrence of at least five different phases of similar chemical composition of $Pd_{8\pm x}(Sb,As)_{3\pm y}$, i.e. triclinic arsenopalladinite [$Pd_8As_{2.5}Sb_{0.5}$], cubic isomertieite [$Pd_{11}Sb_2As_2$], hexagonal mertieite-I [$Pd_{11}(Sb,As)_4$], rhombohedral mertieite-II [$Pd_8(Sb,As)_3$], and hexagonal stibiopalladinite [$Pd_{5+x}Sb_{2-x}$], it is difficult to determine precisely the mineral species found. The chemical data of Pd-Sb phases

from the Darya river area are in favour of mertieite-II composition, although mertieite-I and stibiopalladinite cannot be excluded. The X-ray diffraction analysis obtained from sample K9 showed the mertieite-II structure, and the other three samples analyzed with very similar chemical composition are assumed to also be mertieite-II.

Mertieite-II has been found in numerous PGE-bearing deposits as free grain concentrate, as inclusions or as complex intergrowths of 0.1-0.5 mm size (mostly less than 0.25 mm) (Cabri, 2002, and references therein; Cabral et al. 2002a,b,c; Augé et al. 2002; Gervilla and Kojonen, 2002). The occurrence of an idiomorphic crystal of mertieite-II (mm-sized) is first reported here. The minor changes in stoichiometry of the samples studied probably reflect the amount of As dissolved in mertieite-II which appears to be controlled by the amount of Pt in the high-temperature solid solution. All four grains studied (except sample K7, where 3 analyses out of 12 have a Pt content of up to 0.61 wt.%), show absence of even traces of Pt by spot analysis. However, bulk analysis suggests that the primary high-temperature solid solution incorporated up to about 5 wt.% Pt, which completely exsolved to sperrylite on cooling. The more Pt was in the primary solid solution the less As will be left within the palladium antimonide structure.

A remarkable and characteristic feature of the palladium antimonide crystals from the Darya placer are complex Pd-oxides along crystallographically controlled fractures. These Pd-oxides are relatively high (several wt.%) in Pt, Sb, Fe, Te, Bi, with traces of Sn, As, and Cu. Some phases also contain Hg. Textural changes during microanalysis and low totals suggest the presence of H_2O/OH. The detailed study of these oxygenated compounds is a topic of Chapter 2. Hg-bearing Pt-Pd-alloy in association with mertieite-II has been detected very rarely so far. A very similar association of Hg-bearing Pt-Pd alloy with Pd-oxygenated compounds on isomertieite was previously described by Cabral et al. (2002c) from the Gongo Soco iron mine, Brazil. The authors suggested the formation from a low-temperature hydrothermal fluid. A single platinum nugget from Bom Sucesso stream, Brasil yielded about 78 wt.% of Pt, 20 wt.% of Pd, 2 wt.% of Hg, 2 wt.% of Ir, 1 wt.% of Ru and 1 wt.% of Au (Fleet et al. 2002). The authors noted that Ir and Ru occur likely in the form of microinclusions or within blackish precipitate in the interior. The formation was interpreted as episodic hydrothermal alteration of mafic and ultramafic rocks. In the case of the Darya samples the occurrence of Pt-Pd-Hg attached to cooperite-braggite and the compositional similarity in Pd content of both phases (note practically similar Pd content Table 30 No 8-10) allow to assume the formation of Hg-bearing palladian platinum as a result of cooperite-braggite alteration by Hg-bearing fluids.

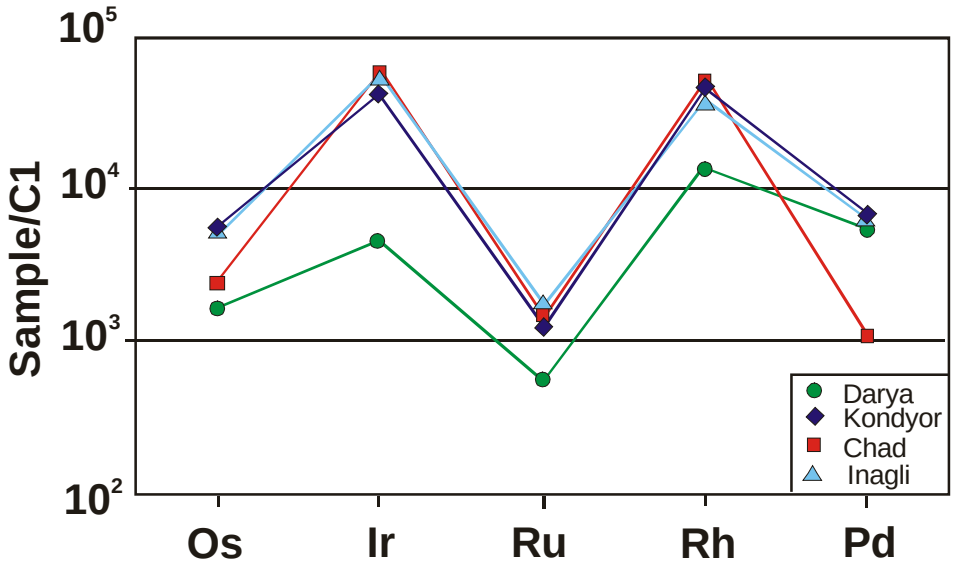

Fig. 50. *Chondrite-normalized PGE distribution of xenomorphic Pt-Fe alloy from Darya placer compared to xenomorphic Pt-Fe alloy from the Kondyor, Inagli, and Chad placers (Mochalov 2001).*

The Darya placer has two varieties of Pt-Fe alloy which is typical also for the Kondyor placer (Nekrasov et al. 1994). The first and more abundant variant is small xenomorphic grains of Pt-Fe alloy (not studied here) and the second is relatively large ferroan platinum crystals. Mochalov (2001) reported on the lack of IPGE (refractory PGE) minerals in the Darya river, as well as on the low trace-element content of the xenomorphic grains of Pt-Fe alloy. The plot of average PGE distribution (Fig. 50) of xenomorphic Pt-Fe alloy from the Darya placer shows a distribution pattern similar to Pt-Fe alloy from other zoned ultramafic-alkaline massifs of Alaskan-/Uralian-type.

Large (more than 1 mm across) Pt-Fe alloy crystals are very rare in nature. To our knowledge, the Kondyor PGE-Au placer is the only occurrence known so far. The euhedral Pt-Fe alloy from Kondyor consists of mm- to cm-sized ferroan platinum of F-centered cubic cell type (Cabri et al. 1997).

The present study reveals that all PGE besides Pt in the euhedral ferroan platinum crystals from Darya are below the electron-microprobe detection limit, similar to ferroan platinum crystals from Kondyor (Nekrasov et al. 1994; Cabri and Laflamme, 1997; Shcheka et al. 2004a). The lack of detectable PGE in ferroan platinum is a remarkable chemical signature which probably reflects uncommon conditions of crystallization. The absence of IPGE minerals in the mineral assemblage from the Darya placer indicates early PGE fractionation, which probably took place already during early stages of melt crystallization. The lower the temperature the less PGE can probably enter the structure of Pt-Fe alloy. It appears likely that the temperature of formation of the large PGM crystals was considerably lower than the temperature of average xenomorphic fine-grained Pt-Fe alloy. The Au-Ag rims on the ferroan platinum crystals and intergrowth

aggregates with mertieite-II suggest hydrothermal overprint, as also seen for the Pt-Fe alloy crystals from Kondyor (Shcheka et al. 2004a). Medium- to coarse-grained pegmatoidal clinopyroxenite bodies are associated both with the Darya and Kondyor PGM occurrences. The formation of the large euhedral PGM crystals could be related to residual pegmatitic fluids at much lower temperature than common in magmatic PGE deposits. A similar situation applies to the Tweefontein area, South Africa, where large euhedral crystals of sperrylite up to 1.85 cm across occur in granite pegmatite and on shear zones in ironstone country-rocks of the Platreef (Wagner 1929).

6 OXIDE/OXYHYDRATE ALTERATION OF MERTIEITE-II

6.1 INTRODUCTION

The present chapter aims to document the occurrence and chemical composition of Pd-bearing oxides/oxyhydrates developed within the mertieite-II crystals, as well as Pd-bearing oxygenated compounds resulting from alteration of keithconnite, Pd-Pt-Te grains and Hg-bearing phases intergrown with palladium antimonide crystals (Tables 33, 35).

The first record of PGE-oxygenated mineral phases dates back to the Brazilian gold rush in the late 17th century when gold with unusual blackish crusts (*ouro preto*) was mined in Minas Gerais, Brazil, much later only (Wollaston 1809) were identified as oxygen-bearing compounds of palladium, platinum, iron and manganese (see discussion in Jedwab and Cassedanne 1998 and Cabral et al. 2003 and references therein). The study of these "unconventional platinum-group minerals (UPGM)" (Jedwab Internet) is hampered due to their very fine grain size and low reflectance in optical microscopy, which makes them difficult to distinguish from commonly intergrown iron and manganese oxide/hydroxide phases, and which requires microanalytical techniques for proper identification. UPGM have been found in all geological environments where the more common PGM occur, but always in near-surface settings, and their occurrence appears to depend both on the nature of precursor PGM and supergene processes, with most advanced reaction progress in lateritic environments (see, among others, Augé and Legendre 1994; Prichard et al. 1994; Jedwab 1995; Garuti and Zaccarini 1997; Garuti et al. 1997; McDonald et al. 1999; Barkov et al. 1999; Gornostayev et al. 2000; Ahmed and Arai 2003; Oberthür et al. 2003; Clark et al. 1974; Olivo and Gauthier 1995; Cabral et al. 2002a, b, 2003; Cabral and Lehmann 2003). The low analytical totals of many UPGM and the specific dessication cracks which develop under the microprobe beam were always taken as indicating the existence of hydrated oxides of PGE, only recently confirmed by PIXE analysis of hydrogen in Pd-O-bearing *ouro preto* (Cabral et al. 2004).

The samples studied display abundant palladium oxide/oxyhydrate phases from a few µm up to 100 µm in size which occur along cystallographic planes and on grain boundaries (Fig. 46, 51). The four samples studied have the following characteristics.

6.2 SAMPLE DESCRIPTION

Sample K9

The oxidic PGE compounds of sample K9 are represented mainly by minerals with the analytical total close to 100%, i.e. “true” oxides with subordinate occurrence of hydrated oxides (Table 36). Oxygen displays a negative correlation with Pd (+Pt) (Fig 53a). Oxygen versus Pd/Sb and Pd/As (Fig.53b,c) gives positive trends with large scatter. Oxygen versus Pd/Sn shows a more restricted Pd/Sn range and no increase in Pd/Sn with increase in oxygen (Fig 53d). The correlation of O *vs* Te and As in this sample is negative (Fig. 53f).

Hg-bearing oxides/hydroxides form complex inhomogeneous intergrowth aggregates, distinctly visible on the back-scattered electron image, with Hg-bearing Pd-Sb-O phases of different oxidation stage and some element variations (enriched in Sb, Pt and H_2O) (Fig. 52). The oxide aggregates have heterogeneous composition and the microanalysis of invidual crystals is beyond the resolution of the electron microprobe. The stoicheometric bulk ratio of M (Pd, Pt, Sn, Sb, As, Te, Bi, Hg, Cu, Fe) to oxygen displays a continuum from 6 to 1.

Sample K7

All detected oxides of sample K7 are “true” oxides with a total close to 100 % (Table 37).

The relationships between the main components are similar to those of sample K9, i.e. Pd and Sb display negative correlation with oxygen (Fig. 53a,b), and Sn shows neutral behaviour (Fig. 53d). The trace elements (Pt, Bi, Cu and Fe), on the contrary, show positive correlation with oxygen (Fig. 53g). One analysed point has high Hg content (7.4 wt.%) which is attributed to local decay of a precursor Hg-bearing mineral.

Sample K7 contains a relatively large (~50 μm across) inhomogeneous inclusion of hexagonal shape (Fig. 51b) which contains a hydrated assemblage of (Sn-O)xnH_2O, (Pd-Fe-Sb-O)xnH_2O and (Pd-Fe-Sn-Bi-Te-O)xnH_2O. Shape and inclusion assemblage point to primary cassiterite.

The stoichiometric bulk ratio of the oxides of sample K7 of M (Pd, Pt, Sn, Sb, As, Te, Bi, Hg, Cu, Fe) to oxygen ranges from 4 to 2.

TABLE 35: COMPOSITION OF Pd-Te BEARING PHASES (SAMPLE Dr1)

		Keithconnite $Pd_{3-x}Te$			$(Pd,Pt)_9Te$
No		**1**	**2**	**3**	**4**
Pd	**wt.%**	68.52	69.94	69.11	58.95
Pt					29.74
Te		22.48	22.80	24.48	10.30
Hg		0.49	0.40	-	-
Bi		8.29	7.74	4.20	0.94
Sn		-	-	-	0.16
Sb		-	-	-	0.31
Cu		-	-	-	0.17
Fe		-	-	-	0.11
Total		99.78	100.88	97.79	100.68
	at.%				
Pd		74.68	75.12	75.39	69.30
Pt					19.07
Te		20.43	20.42	22.27	9.83
Hg		0.28	0.23	-	-
Bi		4.60	4.23	2.33	0.56
Sn		-	-	-	0.33
Sb		-	-	-	0.32
Cu		-	-	-	0.34
Fe		-	-	-	0.25
Total		100	100	100	100

Keithconnite:
Formulae are recalculated on the basis of 4 atoms

1. $Pd_{2.99}(Te_{0.82}Bi_{0.18}Hg_{0.01})_{?1.01}$

2. $Pd_{3.00}(Te_{0.82}Bi_{0.17}Hg_{0.01})_{?1.00}$

3. $Pd_{3.02}(Te_{0.89}Bi_{0.09})_{?0.98}$

$(Pd,Pt)_9Te$:
Formulae is recalculated on the basis of 10 atoms

4. $(Pd_{6.93}Pt_{1.91})_{?8.84}(Te_{0.98}Bi_{0.06}Sn_{0.03}Sb_{0.03}Cu_{0.03}Fe_{0.03})_{?1.16}$

Note: No 1, 2 intergrown with mertieite; No 3, 4 are inclusions witinin the Pd oxide
Au, As below detection limit

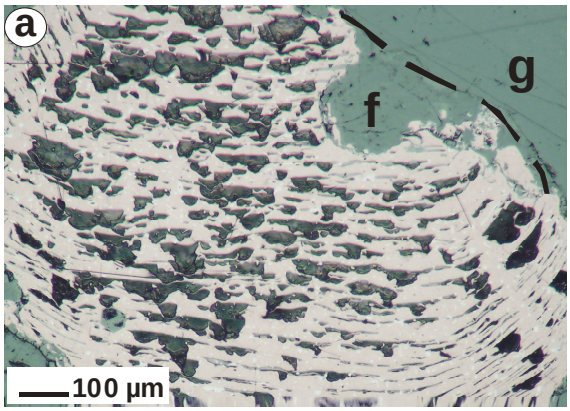
a
g
f
100 µm

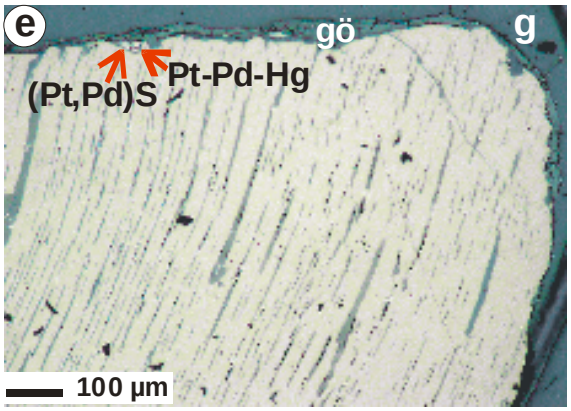
e
gö
g
(Pt,Pd)S
Pt-Pd-Hg
100 µm

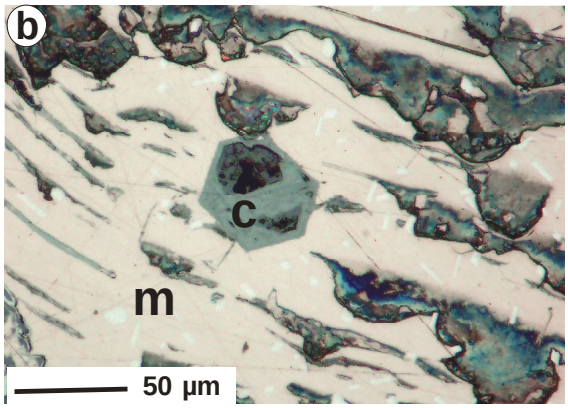
b
c
m
50 µm

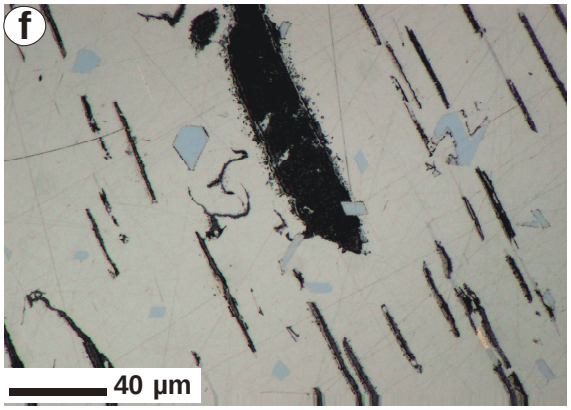
f
40 µm

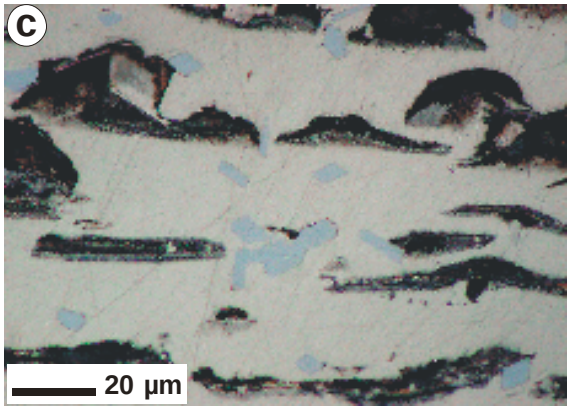
c
20 µm

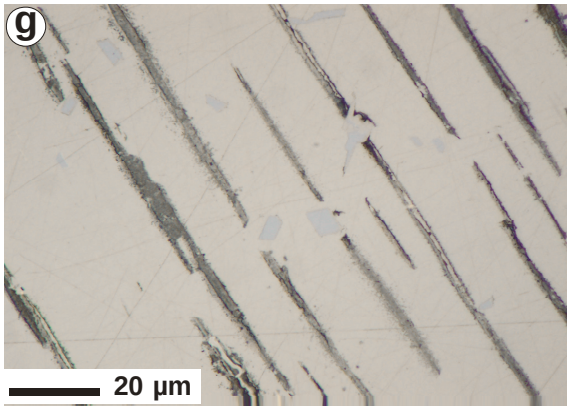
g
20 µm

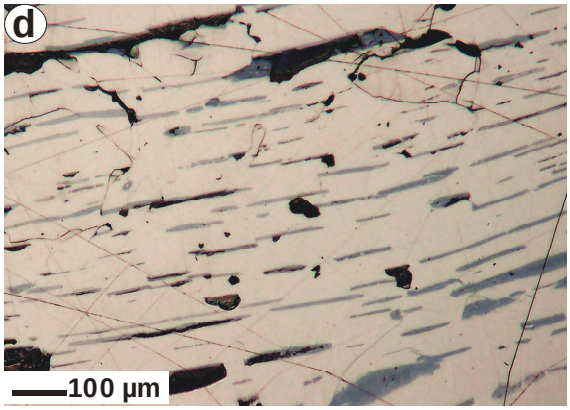
d
100 µm

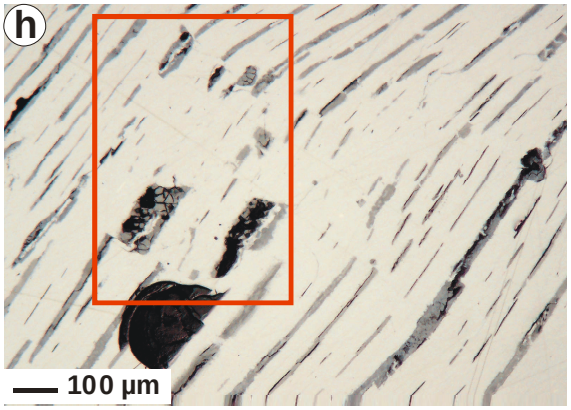
h
100 µm

Fig. 51. *(Previouse page) Photomicrographs (oil immersion) of Pd-bearing oxygenated phases developed within mertieite-II:* ***(a)*** *Slightly deformed mertieite-II grain (light grey) with a sheet-like texture, intergrown with feldspar (f) in glue (g). The dark-grey to black colour corresponds to the cavities and voids along the cleavage planes partly filled with Pd-O-bearing phases, Sample K7;* ***(b)*** *Idiomorphic hexagonal inclusion filled by hydrated cassiterite (c): Pd-Fe-Sb-OxnH_2O and Pd-Fe-Sn-Bi-Te-OxnH_2O phases in mertieite-II matrix (m). The dark grey to grey colour refers to cavities in the mertieite-II matrix, Sample K7;* ***(c)*** *Enlarged area of K7 sample shows sperrylite inclusions (bluish) in mertieite-II matrix (light-grey) with Pd-O-bearing phases (dark-grey) along cleavage planes;* ***(d)*** *Part of mertieite-II grain (light-grey) containing Pd-oxygenated phases (dark-blue) and cavities (black);* ***(e)*** *Part of mertieite-II grain (light-grey) in glue (g) with rim of goethite (gö). In between the mertieite-II matrix and goethite rim is an intergrowth of braggite-cooperite solid solution [(Pt,Pd)S] with Pt-Pd-Hg alloy. Light-grey elongated stripes are Pd-bearing oxygenated phases. Black colour indicates the cavities, Sample Dr2;* ***(f)*** *Enlarged area of mertieite-II of sample Dr2, which shows a large Pd-O-bearing aggregate along with thinner analogues (black) and bluish idiomorphic inclusions of sperrylite and micron-size yellowish inclusion of Au-Ag alloy;* ***(g)*** *Elongated thin stripes of Pd oxygenated compounds of sample Dr2;* ***(h)*** *Pd-bearing oxygenated phases (dark-grey) in mertieite-II matrix. The large black inclusion is a cavity. Red box delineates back-scattered electron image in the Fig.52. Sample Dr1*

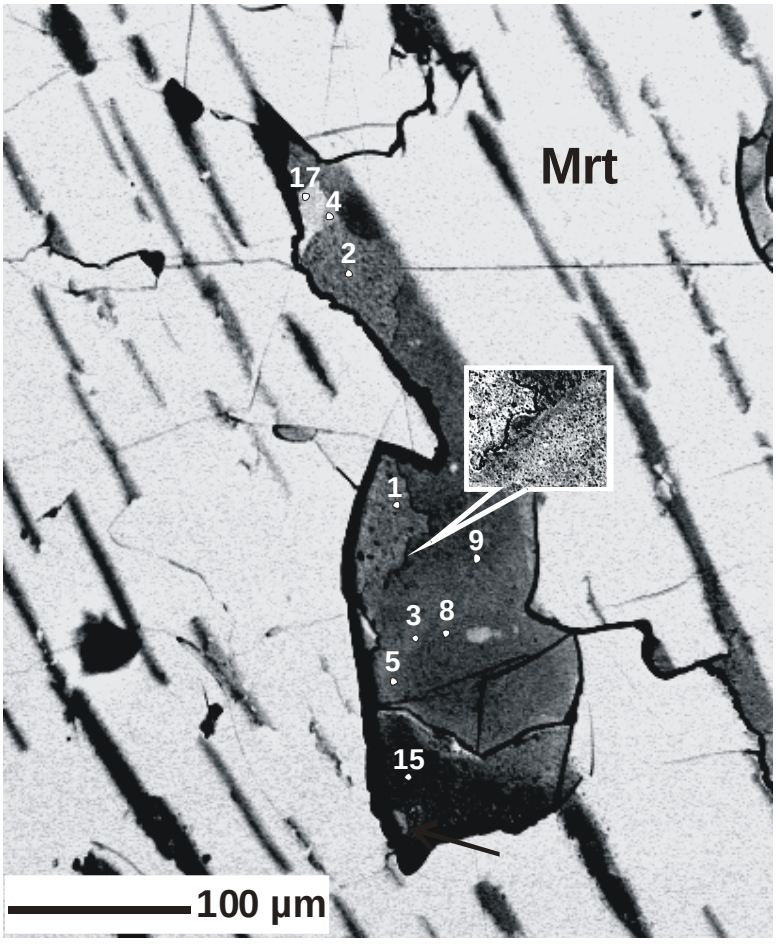

Fig. 52. *BSE image of complex Pd-O-(Hg)-bearing aggregate within the mertieite-II matrix (Mrt). Sample K9. The white spots mark the points of corresponding current number of analyses from Table 3. The small inset map shows highly inhomogeneous matrix of Pd-O-bearing aggregate.*

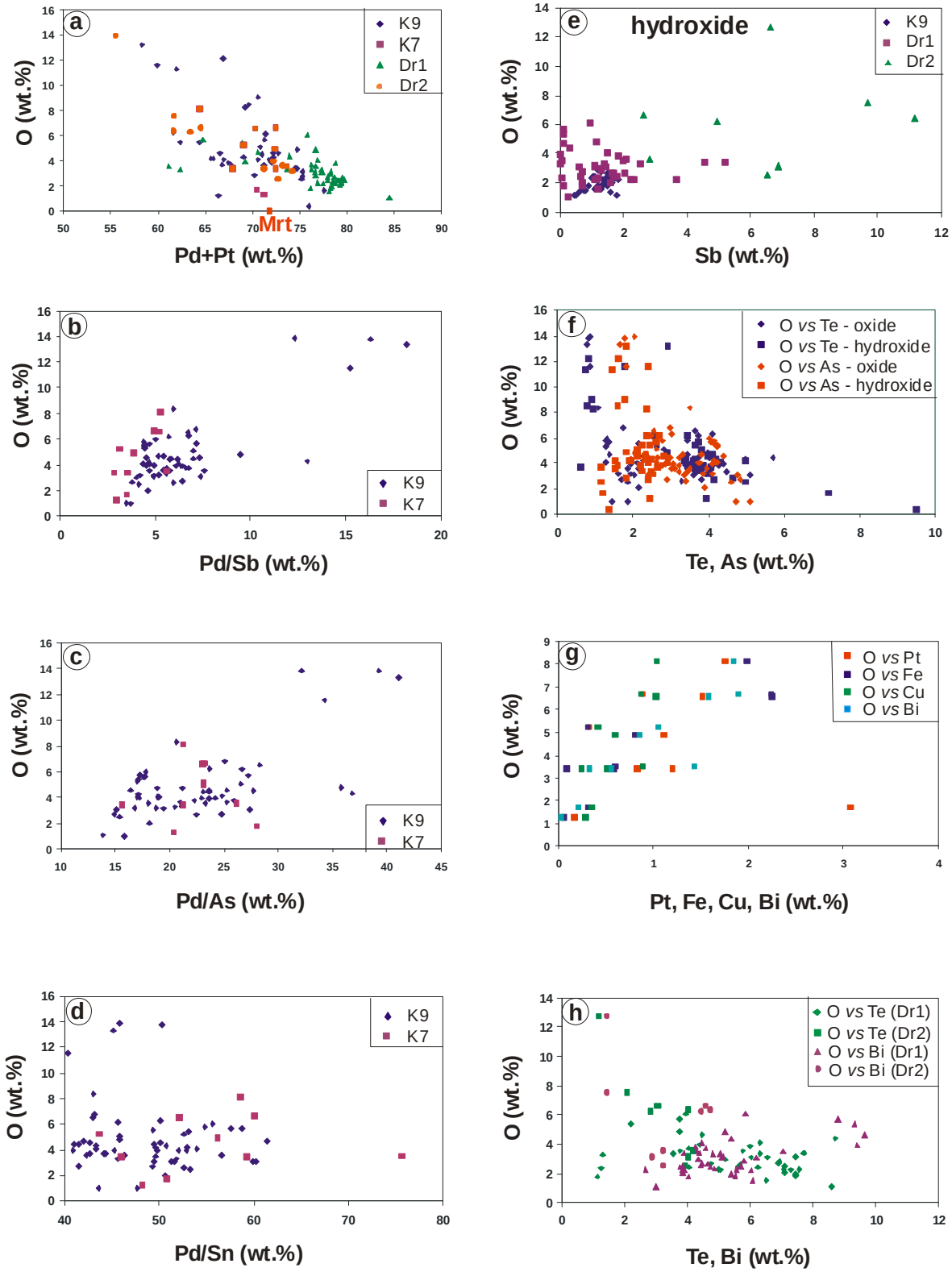

***Fig.53**. Binary element plots of **a)** O vs Pd+Pt in oxides/hydroxides developed within mertieite-II, samples K9, K7, Dr1, Dr2; **b)** O vs Pd/Sb ration in "true" oxide of K9 and K7 samples; **c)** O vs Pd/As ratio in "true" oxides of K9 and K7 samples; **d)** O vs Pd/Sn ration in "true" oxides of K9 and K7 samples; **e)** O vs Sb in hydroxides of K9, Dr1 and Dr2 samples; **f)** O vs Te and As in oxides/hydroxides of K9 sample; **g)** O vs Pt, Fe, Cu, and Bi in sample K7; **h)** O vs Te and Bi in hydroxides of samples Dr1 and Dr2.*

TABLE 36. SELECTED ANALYSES OF OXIDES/HYDROXIDES OF SAMPLE K9

	M_6O		M_5O	M_4O			M_3O			M_2O		MO		$MOxnH_2O$	M_2OxnH_2O	M_3OxnH_2O	M_4OxnH_2O
No	**1**	**2**	**3**	**4**	**5**	**6**	**7**	**8**	**9**	**10**	**11**	**12**	**13**	**14**	**15**	**16**	**17**
No an.	***K9/5n16***	***K9/21***	***K9/5n1***	***K9/5n25***	***K9/5n3***	***K9/24***	***K9/5n21***	***K9/5n4***	***K9/5n11***	***K9/7***	***K9/17***	***K9/31***	***K9/ox1***	***K9/5***	***K9/5n35***	***K9/5n42***	***K9/5n26***
wt.%																	
Pd	70.92	76.28	71.47	65.56	71.71	78.14	71.25	69.88	71.04	71.81	71.23	67.78	65.90	58.37	65.44	67.75	62.29
Sn	1.33	1.45	1.72	1.28	1.62	1.38	1.35	1.53	1.67	1.67	1.28	1.50	1.44	1.48	1.42	0.74	1.10
Sb	17.13	12.76	11.15	13.38	12.80	10.32	15.36	9.99	9.68	10.71	14.24	3.73	5.35	9.63	10.45	3.23	10.02
Te	1.85	3.28	3.79	3.60	3.38	1.87	2.29	2.80	4.09	3.64	1.29	0.79	0.86	2.93	3.66	3.63	3.77
Cu	0.28	0.44	0.39	0.25	0.38	0.45	0.30	0.42	0.42	0.46	0.46	0.71	0.90	0.40	0.37	0.58	0.24
Pt	-	-	-	6.86	-	-	-	0.19	-	-	-	-	-	-	-	-	12.17
Hg	1.87	-	4.63	0.29	3.86	-	1.11	5.82	4.63	0.98	1.90	-	-	0.68	7.24	10.60	0.44
Bi	0.00	-	0.19	0.40	-	-	-	-	-	0.38	-	-	-	-	-	0.11	1.05
Fe	0.14	0.18	0.21	0.14	0.21	1.26	0.19	0.27	0.29	0.25	1.05	10.93	11.05	0.30	0.28	0.30	0.16
As	4.59	3.40	2.89	3.37	3.22	3.10	4.15	2.63	2.81	2.54	4.00	1.65	2.05	1.84	2.22	1.50	2.50
O	2.53	2.61	2.70	3.09	3.75	3.57	4.23	5.09	4.58	6.52	5.99	13.33	13.86	13.20	5.43	3.64	3.39
Total	100.63	100.40	99.14	98.22	100.93	100.09	100.23	98.62	99.21	98.96	101.44	100.42	101.41	88.83	96.51	92.07	97.13
at.%																	
Pd	62.39	66.48	64.04	58.78	59.86	64.44	57.80	56.22	57.96	53.33	52.68	36.43	34.64	31.89	51.28	57.86	55.31
Sn	1.05	1.13	1.38	1.03	1.21	1.02	0.98	1.10	1.22	1.11	0.85	0.72	0.68	0.72	1.00	0.57	0.88
Sb	13.17	9.72	8.73	10.49	9.34	7.44	10.89	7.03	6.90	6.95	9.21	1.75	2.46	4.60	7.16	2.41	7.78
Te	1.36	2.38	2.83	2.69	2.36	1.29	1.55	1.88	2.78	2.25	0.80	0.35	0.38	1.34	2.39	2.58	2.79
Cu	0.42	0.64	0.58	0.38	0.53	0.62	0.41	0.56	0.57	0.57	0.57	0.64	0.79	0.37	0.49	0.83	0.36
Pt	-	-	-	3.36	-	-	-	0.08	-	-	-	-	-	-	-	-	5.89
Hg	0.87	-	2.20	0.14	1.71		0.48	2.48	2.00	0.39	0.75	-	-	0.20	3.01	4.80	0.21
Bi	-	-	0.09	0.18	-	-	-	-	-	0.14	-	-	-	-	-	0.05	0.47
Fe	0.23	0.30	0.35	0.24	0.33	1.98	0.29	0.42	0.45	0.35	1.48	11.19	11.07	0.31	0.42	0.49	0.27
As	5.74	4.21	3.67	4.29	3.82	3.63	4.78	3.01	3.26	2.68	4.20	1.26	1.53	1.43	2.47	1.82	3.15
O	14.79	15.13	16.12	18.43	20.84	19.58	22.82	27.21	24.85	32.21	29.47	47.65	48.46	47.97	28.30	20.67	20.02
Total	100	100	100	100	100	100	100	100	100	100	100	100	100	89	97	92	97

Note: M is sum of Pd, Sn, Sb, Te, Cu, Pt, Hg, Bi, Fe and As; -below detection limit

TABLE 37. SELECTED ANALYSES OF OXIDES OF SAMPLE K7

		M_4O		M_2O	
No		**1**	**2**	**3**	**4**
No an.		***K7/8***	***K7/polos***	***K7/10***	***K7/11***
	wt.%				
Pd		66.68	72.67	68.82	62.71
Sn		1.45	0.96	1.32	1.07
Sb		23.77	13.01	13.27	11.91
Te		0.55	1.56	1.2	1.1
Cu		0.24	0.89	1.03	1.04
Pt		1.2	0.89	1.51	1.75
Hg		-	-	0.31	7.39
Bi		0.32	1.43	1.58	1.84
Fe		0.08	0.6	2.25	1.98
As		4.27	2.78	2.99	2.95
O		3.41	3.53	6.58	8.11
Total		101.97	98.32	100.86	101.85
	at.%				
Pd		55.88	61.86	49.72	43.41
Sn		1.09	0.73	0.85	0.66
Sb		17.41	9.68	8.38	7.21
Te		0.38	1.11	0.72	0.64
Cu		0.34	1.27	1.25	1.21
Pt		0.55	0.41	0.60	0.66
Hg		-	-	0.12	2.71
Bi		0.14	0.62	0.58	0.65
Fe		0.13	0.97	3.10	2.61
As		5.08	3.36	3.07	2.90
O		19.01	19.99	31.62	37.34
Total		100	100	100	100

Note: M is sum of Pd, Sn, Sb, Te, Cu, Pt, Hg, Bi, Fe and As;
-below detection limit

Sample Dr1

The characteristic features of the oxygenated compounds of sample Dr1 are: (1) the empirical total of all analysed points is always <100 wt%, which indicates the presence of water; (2) all Pd hydroxides have elevated Te and Bi at low Sb, Sn and As content with uniform distribution (Table 38); (3) complex overgrowth rims with elevated Hg content. The standard deviation of the mean for all elements in Pd-oxide/hydrioxide phases intergrown with mertieite-II, calculated on the basis of more than 30 points, is very small, which reflects little compositional fluctuation. The high Te and Bi contents exclude an origin of these elements from mertieite-II oxidation, and

require Te- and Bi-rich precursor minerals. These are probably keithconnite, and Pd-Pt-Te-bearing phase intergrown with mertieite-II (Fig 54).

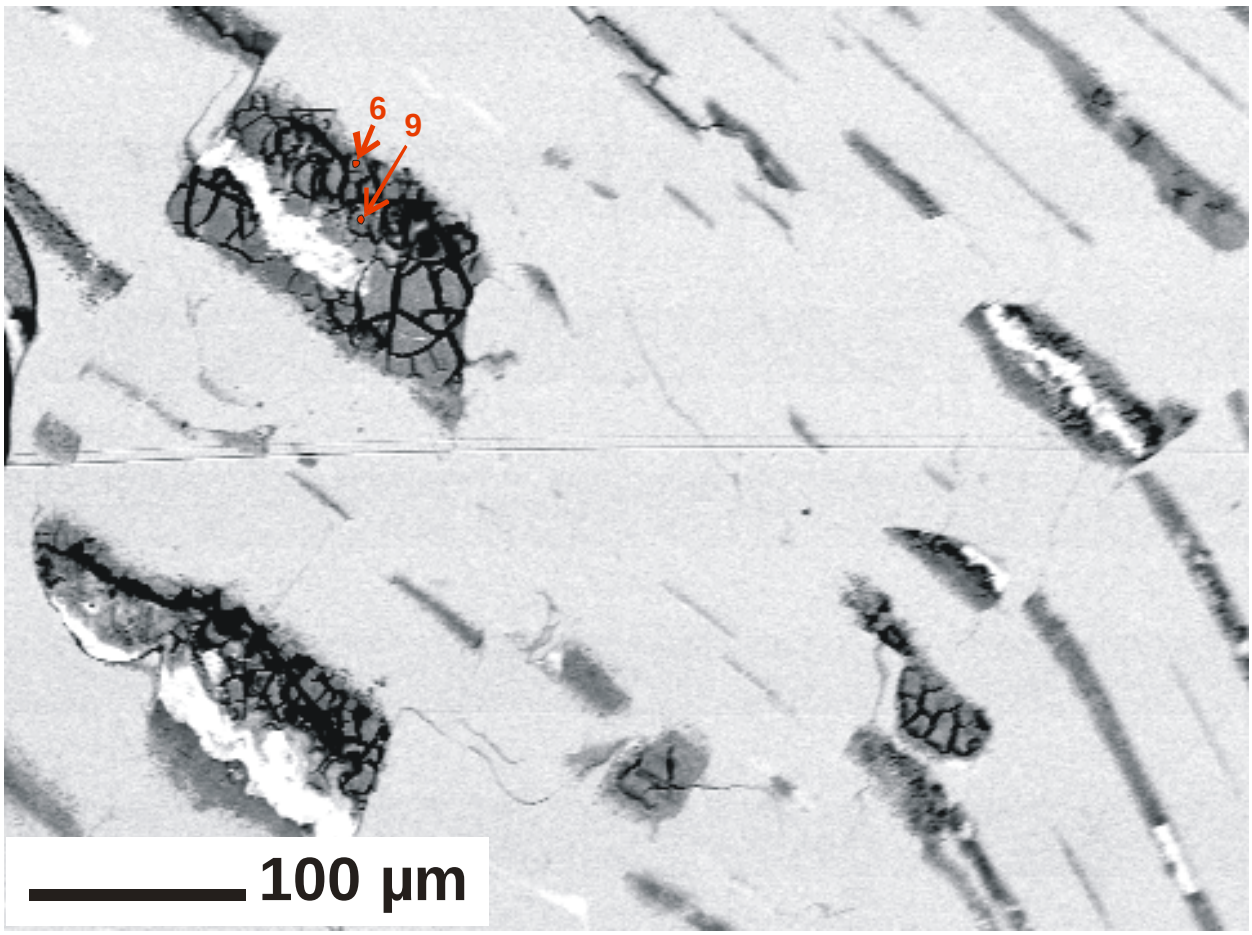

Fig. 54. *BSE image of Pd-bearing oxygenated phases with typical cracking texture from volume reduction (dessication?)(ark-grey) developed after Pd-Te-bearing minerals (white) in mertieite-II matrix (light-grey). Sample Dr1. The red arrows locate points of microanalyses in Table 38.*

TABLE 38. SELECTED ANALYSES OF HYDROXIDES OF SAMPLE DR1

	$M_6OxnH2O$					M_5xnH_2O				M_4xnH_2O			M_3xnH_2O	
No	***1***	***2***	***3***	***4***	***5***	***6***	***7***	***8***	***9***	***10***	***11***	***12***	***13***	
No an.	***Dr1/16***	***Dr1/30***	***Dr1/18***	***Dr1/32***	***Dr1/24***	***Dr1/11***	***Dr1/31***	***Dr1/34***	***Dr1/13***	***Dr1/21***	***Dr1/40***	***Dr1/33***	***Dr1/23***	***Average, n=32***
wt.%														
Pd	77.47	79.42	78.47	79.00	79.74	77.56	79.40	77.95	76.74	78.31	75.85	78.80	76.84	77.33 ± 1.85
Sn	0.60	0.65	0.70	0.67	0.46	0.62	0.87	0.63	0.61	0.48	0.88	0.39	0.77	0.58 ± 0.21
Sb	1.16	2.23	1.11	1.69	1.77	0.67	2.06	1.64	0.73	1.09	2.53	1.84	1.53	1.7 ± 1.07
Te	7.31	5.08	7.07	6.26	5.66	7.09	5.69	6.88	6.92	7.43	6.33	6.00	6.33	6.15 ± 1.34
Cu	1.02	1.69	1.00	1.60	1.83	1.07	1.32	1.32	1.12	0.87	0.88	1.54	1.25	1.39 ± 0.50
Pt	-	-	-	-	-	0.33	-	-	-	-	0.36	-	-	0.07 ± 0.26
Bi	6.03	3.93	5.57	3.78	3.87	5.72	4.45	4.47	5.79	5.13	4.83	4.28	4.46	4.8 ± 0.83
Fe	0.05	0.02	0.04	0.04	0.03	0.02	0.04	0.04	0.03	0.03	0.04	0.17	0.03	0.05 ± 0.05
As	0.71	1.25	0.69	1.07	1.08	0.66	1.25	1.02	0.70	0.88	1.34	1.19	1.10	1.03 ± 0.26
O	2.22	2.26	2.32	2.41	2.45	2.49	2.63	2.73	2.82	3.13	3.32	3.81	4.09	2.98 ± 0.94
Total	96.57	96.51	96.93	96.52	96.86	96.21	97.67	96.64	95.43	97.35	96.36	98.02	96.40	
at.%														
Pd	70.73	71.06	71.11	70.26	70.64	69.71	70.15	68.57	67.60	68.01	65.07	65.53	63.13	
Sn	0.49	0.52	0.57	0.53	0.37	0.50	0.69	0.50	0.48	0.37	0.68	0.29	0.57	
Sb	0.93	1.74	0.88	1.31	1.37	0.53	1.59	1.26	0.56	0.83	1.90	1.34	1.10	
Te	5.57	3.79	5.34	4.64	4.18	5.31	4.19	5.05	5.08	5.38	4.53	4.16	4.34	
Cu	1.56	2.53	1.52	2.38	2.71	1.61	1.95	1.94	1.65	1.27	1.26	2.14	1.72	
Pt	0.00	0.00	0.00	0.00	0.00	0.16	0.00	0.00	0.00	0.00	0.17	0.00	0.00	
Bi	2.80	1.79	2.57	1.71	1.75	2.62	2.00	2.00	2.60	2.27	2.11	1.81	1.87	
Fe	0.09	0.03	0.07	0.07	0.05	0.03	0.07	0.07	0.05	0.05	0.07	0.27	0.05	
As	0.92	1.59	0.89	1.35	1.36	0.84	1.57	1.27	0.88	1.09	1.63	1.41	1.28	
O	13.48	13.45	13.98	14.26	14.44	14.89	15.46	15.97	16.52	18.08	18.95	21.07	22.35	
Total	97	97	97	97	97	96	98	97	95	97	96	98	96	

Note: M is sum of Pd, Sn, Sb, Te, Cu, Pt, Hg, Bi, Fe and As;
-below detection limit

Pd-bearing oxygenated phases developed also within cracks and as rims on keithconnite (Fig. 55). Keithconnite overgrown by Pd-bearing oxide/hydroxide phases shows a remarkable content of Hg (up to 25 wt.%, Table 39), some parts of the rim are enriched in Pt (up to 44 wt.%). The overgrowth phases are characterized by a low empirical total, which points to the presence of water. The recalculated formulae show different stages of hydration of keithconnite. The stoichiometric bulk ratio of the oxyhydrates of sample Dr1 of M (Pd, Pt, Sn, Sb, As, Te, Bi, Hg, Cu, Fe) to oxygen ranges from 6 to 2.

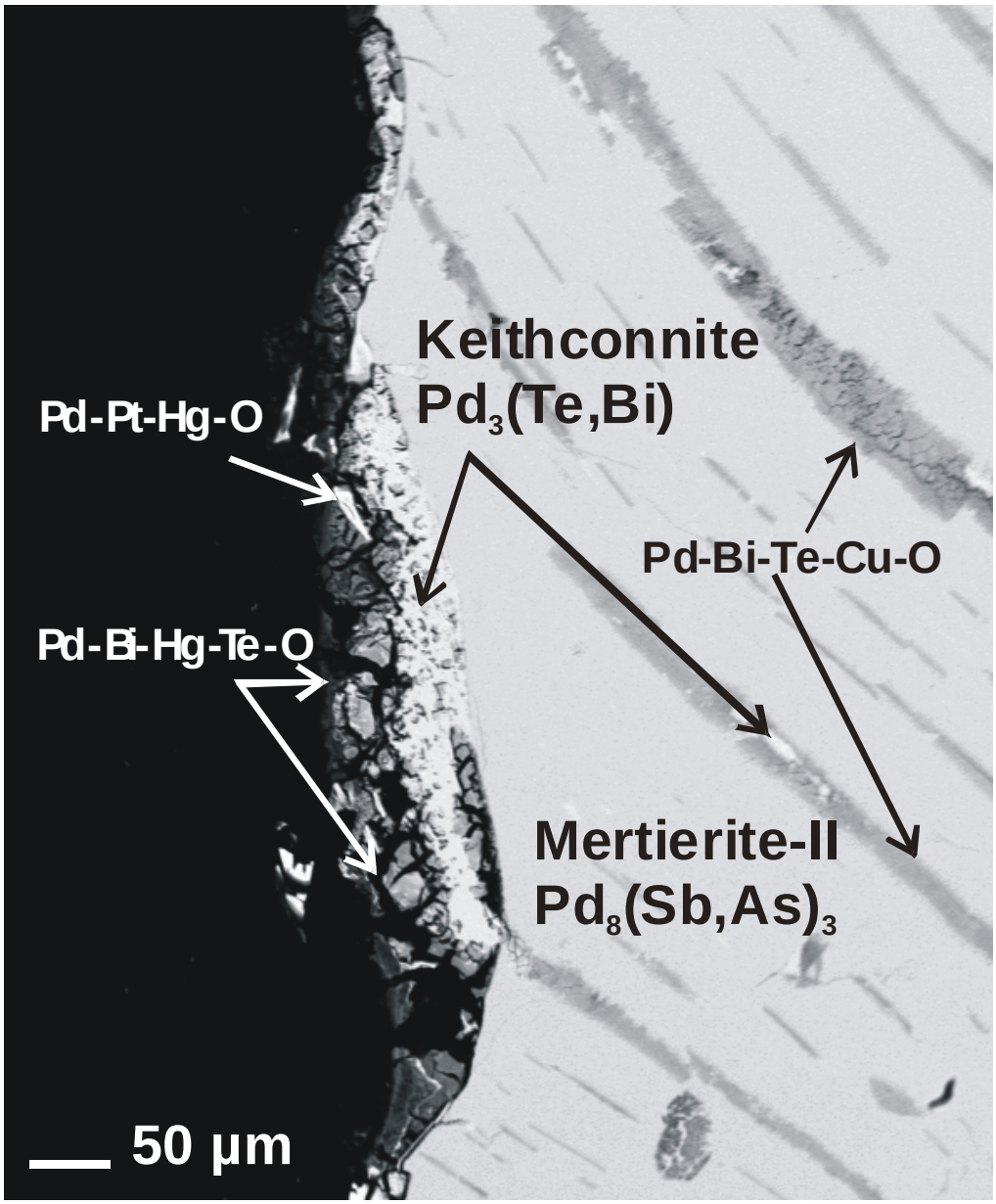

Fig.55. *Back-scattered electron image of Pd-Hg-oxygenated compounds developed within cracks and on keithconnite associated with mertieite-II. Sample Dr1.*

Another Pd-bearing oxyhydrate intergrowth aggregate on mertieite-II has a zoned composition, with a Pd-Bi-Fe-Te-Cu-bearing core, mantled by aggregates rich in Hg (up to 35 wt.%, Table 39 No12,13) (Fig. 56a) with strong negative correlation of Hg *vs* Te and Pd (Fig. 56 b,c).

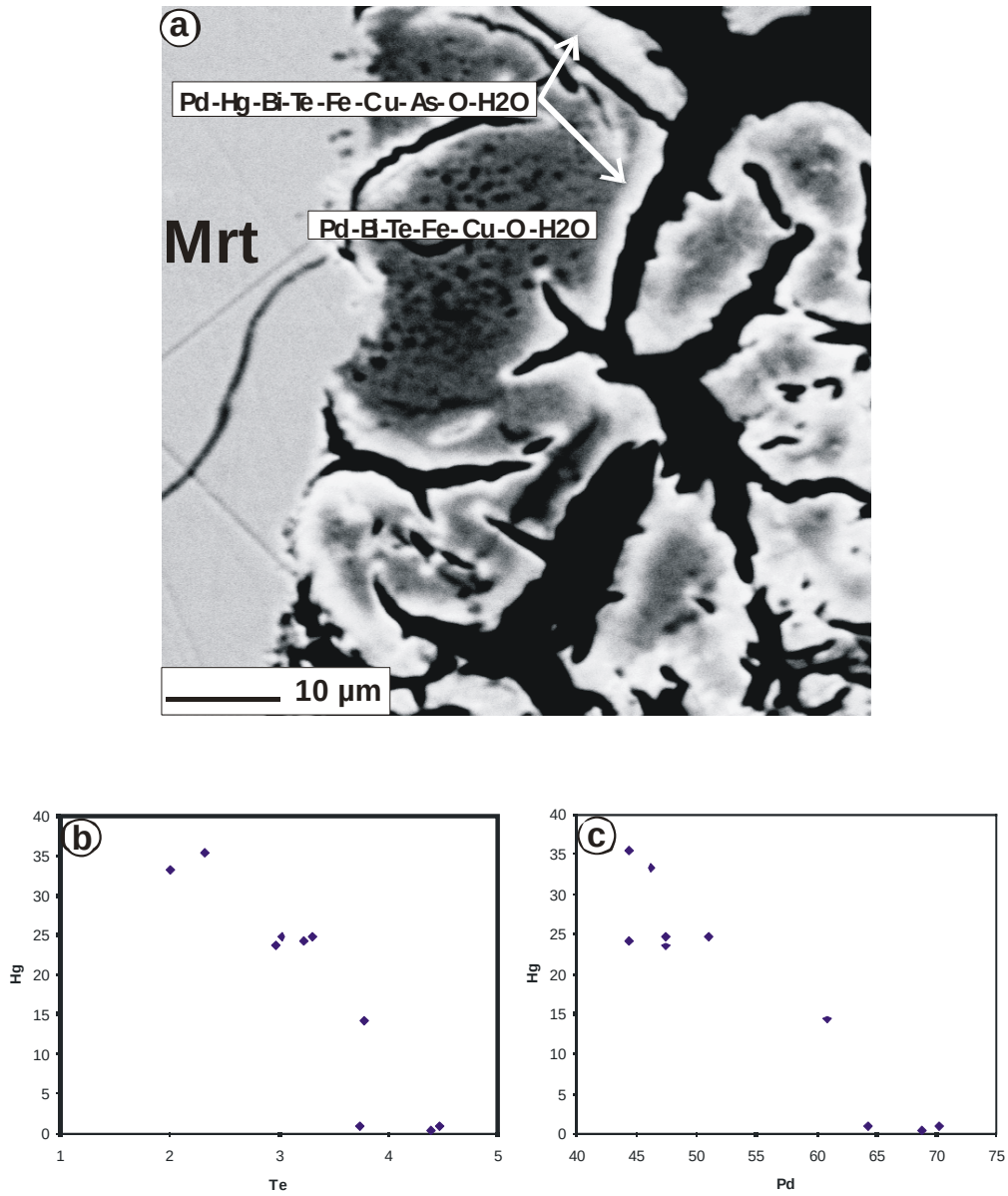

Fig. 56. *BSE image of* ***(a)*** *zoned aggregate of Pd-Bi-Te – bearing hydroxide rimmed by Hg-rich hydroxide overgrown on mertieite-II (Mrt);* ***(b)*** *Correlation between Hg and Te and* ***(c)*** *Hg and Pd. Sample Dr1.*

The Hg-bearing oxyhydrate has likely been formed after one of the Hg-Pd-bearing minerals. With regard to high Hg and relatively low Te and Bi contents one could speculate that the pristine Hg-bearing mineral was potarite [PdHg].

The Hg-rich oxygenated phases as well as previously documented intergrowth aggregates of Pt-Pd-Hg alloy with mertieite-II, imply hydrothermal overprint by a Hg-bearing fluid.

TABLE 39. SELECTED ANALYSES OF HYDROXIDE DEVELOPED AT THE KEITHCONNITE AND Pd-Pt-Te-Bi PHASE. SAMPLE DR1

No		1	2	3	4	5	6	7	8	9	10	11	12	13
	wt.%													
Pd		41.10	47.16	50.96	61.68	57.90	65.38	64.48	63.72	24.12	31.78	15.88	44.33	46.28
Sn		0.07	0.26	0.07	-	0.09	0.13	0.11	0.13	-	0.04	0.21	-	0.06
Sb		0.09	-	0.10	-	-	0.11	-	-	0.26	0.09	0.01	0.18	3.42
Te		5.58	2.86	3.50	2.30	2.38	2.73	2.02	2.75	0.67	1.16	1.33	2.32	2.00
Cu		0.38	0.37	0.78	0.56	1.62	1.51	1.26	0.87	0.14	0.23	0.10	0.63	0.33
Pt		0.97	3.72	1.77	3.23	3.50	3.45	3.30	3.51	40.48	44.35	46.51	0.34	1.15
Hg		23.89	20.53	20.63	10.66	5.23	4.45	5.27	4.32	11.49	10.33	3.83	35.36	33.30
Bi		6.83	7.96	9.41	7.59	11.22	8.85	8.92	9.23	2.69	4.05	4.82	6.17	5.19
Fe		5.62	3.92	1.39	3.20	0.51	1.72	1.99	1.73	4.06	2.87	4.44	0.78	1.08
As		0.21	0.15	-	0.23	-	-	-	-	6.23	0.25	0.55	1.21	0.60
O		7.88	6.03	4.14	3.93	7.26	5.02	5.01	5.02	4.48	1.80	3.31	2.03	1.57
Total		92.62	92.96	92.75	93.38	89.71	93.35	92.36	91.28	94.62	96.95	80.98	93.35	95.00
	at.%													
Pd		30.06	38.07	46.23	53.14	42.46	52.70	51.95	51.39	22.58	37.22	16.39	47.97	51.20
Sn		0.05	0.19	0.06	-	0.06	0.09	0.08	0.09	-	0.04	0.20	-	0.06
Sb		0.06	-	0.08	-	-	0.08	-	-	0.22	0.09	0.01	0.17	3.31
Te		3.40	1.93	2.65	1.65	1.46	1.84	1.36	1.85	0.52	1.13	1.15	2.09	1.84
Cu		0.47	0.50	1.18	0.81	1.99	2.04	1.70	1.18	0.22	0.45	0.16	1.14	0.61
Pt		0.39	1.64	0.87	1.52	1.40	1.52	1.45	1.54	20.67	28.34	26.19	0.20	0.69
Hg		9.27	8.79	9.93	4.87	2.03	1.90	2.25	1.85	5.71	6.42	2.10	20.30	19.55
Bi		2.54	3.27	4.35	3.33	4.19	3.63	3.66	3.79	1.28	2.41	2.53	3.40	2.93
Fe		7.84	6.03	2.41	5.25	0.71	2.64	3.06	2.66	7.24	6.41	8.73	1.61	2.28
As		0.22	0.17	-	0.28	-	-	-	-	8.28	0.42	0.80	1.86	0.95
O		38.33	32.38	25.00	22.52	35.41	26.91	26.85	26.93	27.90	14.02	22.73	14.60	11.58
Total		92.62	92.96	92.76	93.38	89.71	93.36	92.36	91.28	94.63	96.95	80.98	93.35	95.00

Note: No 1- 8 are hydroxide, rimmed keithconnite intergrown with sample Dr1;
No 9-11 developed on Pd-Pt-Te-Be phase; No 12-13 is outermost rim at Pd-Te-Bi hydroxide intergrown with mertieite-II sample Dr1.

Sample Dr2

TABLE 40. SELECTED ANALYSES OF HYDROXIDES OF SAMPLE DR2

	M_4OxnH_2O				M_2OxnH_2O		$MOxnH_2O$
No	***1***	***2***	***3***	***4***	***5***	***6***	***7***
No an.	***Dr2/7***	***Dr2/2***	***Dr2/3***	***Dr2/1***	***Dr2/15***	***Dr2/10***	***Dr2/14***
wt.%							
Pd	74.17	71.15	73.16	71.95	64.05	61.73	49.31
Sn	1.03	0.74	0.75	0.78	0.59	0.75	0.7
Sb	6.9	8.9	2.81	8.2	2.65	9.65	6.62
Te	4.05	3.55	4.22	3.49	3.07	2.09	1.19
Cu	1.53	0.62	0.95	0.62	0.34	0.23	0.22
Pt	-	-	-	0.23	0.51	-	-
Bi	2.88	2.43	3.24	1.72	4.58	1.44	1.43
Fe	1.54	4.55	5.98	4.3	12.1	11.63	21.63
As	1.35	1.93	1.28	1.99	1.21	2.46	2.15
O	3.14	3.36	3.57	3.93	6.63	7.53	12.74
Total	96.59	97.23	95.96	97.21	95.73	97.51	95.99
at.%							
Pd	62.69	58.33	62.69	57.36	43.33	40.28	25.33
Sn	0.78	0.54	0.78	0.56	0.36	0.44	0.32
Sb	5.10	6.38	5.10	5.71	1.57	5.50	2.97
Te	2.86	2.43	2.86	2.32	1.73	1.14	0.51
Cu	2.17	0.85	2.17	0.83	0.39	0.25	0.19
Pt	-	-	-	0.10	0.19	-	-
Bi	1.24	1.01	1.24	0.70	1.58	0.48	0.37
Fe	2.48	7.11	2.48	6.53	15.60	14.46	21.18
As	1.62	2.25	1.62	2.25	1.16	2.28	1.57
O	17.65	18.32	17.65	20.84	29.83	32.68	43.54
Total	96.59	97.23	96.59	97.21	95.73	97.51	95.99

Note: M is sum of Pd, Sn, Sb, Te, Cu, Pt, Hg, Bi, Fe and As;
-below detection limit

The chemical composition of the oxygenated compounds of sample Dr2 is close to that of Dr1, with low empirical totals and somewhat high Te and Bi contents, although the Sb (Sn, As) content is slightly higher than that of Dr1 sample (Table 40). It probably indicates the transition stage between formation of Te-bearing phases after mertieite-II. The element distribution patterns have trends similar to sample Dr1 and display negative correlation of oxygen and Pd, Te, and Bi (Fig. 53a,h). Hydroxides of the following formulae have been detected in sample Dr1 sample: M_4OxnH_2O, M_2OxnH_2O, and $MOxnH_2O$.

6.3 DISCUSSION AND CONCLUSION

The mineralogical observation indicates that the PGE-O-bearing compounds in mertieite-II crystals from the Darya river closely reflect their host mineralogy and variable degree of element leaching. Texture and mineralogy suggest the following evolution of the mertieite-II crystals and their intergrowth and reaction mineral assemblages: (1) hydrothermal formation of mertieite-II and exsolution of idiomorphic micron-sized inclusions of sperrylite; rare cassiterite appears to be trapped during mertieite-II growth; (2) overprint by Te-Bi rich hydrothermal fluids and formation of keithconnite, Pd-Pt-Te phase, Pt-Pd-Hg alloy, Pd-rich cooperite-braggite solid solution together with Au-Ag alloy as overgrowth aggregates on mertieite-II and along crystallographic planes within mertieite-II; (3) formation of oxygenated and variably hydrated compounds as a result of weathering preferentially along grain boundaries and crystallographic planes. The very variable composition of the oxide/oxyhydrate phases can be related to either decomposition of mertieite-II, which gives the most abundant low-Te and low-Bi oxide phases, or keithconnite, which is reflected in high Te and Bi content of the oxidic alteration product, or Pd-Pt-Te phase, which is expressed in elevated Pt content, or Hg-bearing minerals with remarkable high Hg content. Progressive oxidation is accompanied by progressive leaching of Sb and As, while the abundance of Sn is relatively constant. Copper, bismuth and iron content increase with oxygen, indicating small-scale redistribution and mixing of the element inventory from the decay of mertieite-II and its hydrothermal inter- and overgrowth mineral assemblage. Locally high mercury content in outermost rims of oxide/oxyhydrate aggregates refelcts the relatively mobile behavior of mercury. Goethite is commonly associated with the Pd-bearing oxide-/oxyhydrate phases and indicates their low-temperature formation, i.e. weathering processes.

The PGE-O-bearing phases form two main compositional groups:

(I) PGE-O bearing minerals with total close to 100%, *i.e.*”true” oxides

(II) PGE-O bearing compounds with distinctly low total, *i.e.* hydrated oxides

The variable degree of oxidation is expressed in the stoichiometric bulk ratios of metals to oxygen which ranges from 6 to 1. The individual characterization of these oxide/oxyhydrate phases is not possible due to the very small grain size beyond the resolution of the electron microprobe.

7 Pt-Fe ALLOY MACROCRYSTALS FROM THE KONDYOR PGE-Au PLACER DEPOSIT, KHABAROVSKIY KRAY

7.1 INTRODUCTION

The Kondyor PGE-Au placer deposit currently has a production of about 4 t PGE+500 kg Au/year, second in Russia to the Norils'k Ni-PGE district, with about 100 t PGE/year. The main PGM in the Kondyor deposit is Pt-Fe alloy of xenomorphic shape and of primitive cubic cell type (Nekrasov et al. 1994), which in the classification scheme of Cabri and Feather (1975) is isoferroplatinum. However, the Kondyor placer is also known for spectacular euhedral Pt-Fe alloy crystals, which can reach up to several cm across (Sushkin 1995; Cabri and Laflamme 1997; Szymañski et al. 1997). These coarse crystals have a face-centered cubic cell and are ferroan platinum (Nekrasov et al. 1994; Cabri and Laflamme 1997). In the following we will use the general term of Pt-Fe alloy for both variants.

Coarse-grained Pt-Fe alloy crystals are known only from the Kondyor deposit, and have attracted much attention by mineral collectors (Fehr et al. 1995; Gebhard and Schlüter 1996; Weiss et al. 2002) and scientists alike (Mochalov 1994; Sushkin 1995; Nekrasov et al. 1994, 1997, 1999; Cabri and Laflamme 1997). An intriguing feature of the macrocrystals of Pt-Fe alloy is their unusually low content of the minor PGE elements (Nekrasov et al. 1994). An ion-microprobe reconnaissance study by Cabri et al. (1998) revealed Re and Os concentrations below the limits of detection in one large crystal (<<1 ppm Os).

Another feature of the Kondyor deposit is the large spectrum of mineral inclusions and alteration minerals associated with the large Pt-Fe alloy crystals. The description of mineral-inclusion and mineral-reaction assemblage of some macrocrystals, taken from the original collection of the Far East Geological Institute (FEGI), Vladivostok, Russia, and report some compositional data is given in this chapter.

7.2 GEOLOGICAL SETTING

The Kondyor PGE-Au placer deposit is located in the southern part of the Precambrian Aldan Shield (Ajano-Maiskiy region of Khabarovskiy Kray), eastern Siberia (Fig. 37, 38, 57).

The deposit is genetically related to the zoned ultramafic-alkaline Kondyor intrusion of Uralian/Alaskan type. The 6-km large intrusion with positive morphostructure is a perfectly circular, concentrically zoned massif (Fig. 58, 59) with a dunitic core and external rings of pyroxenite and peridotite (Fig. 60).

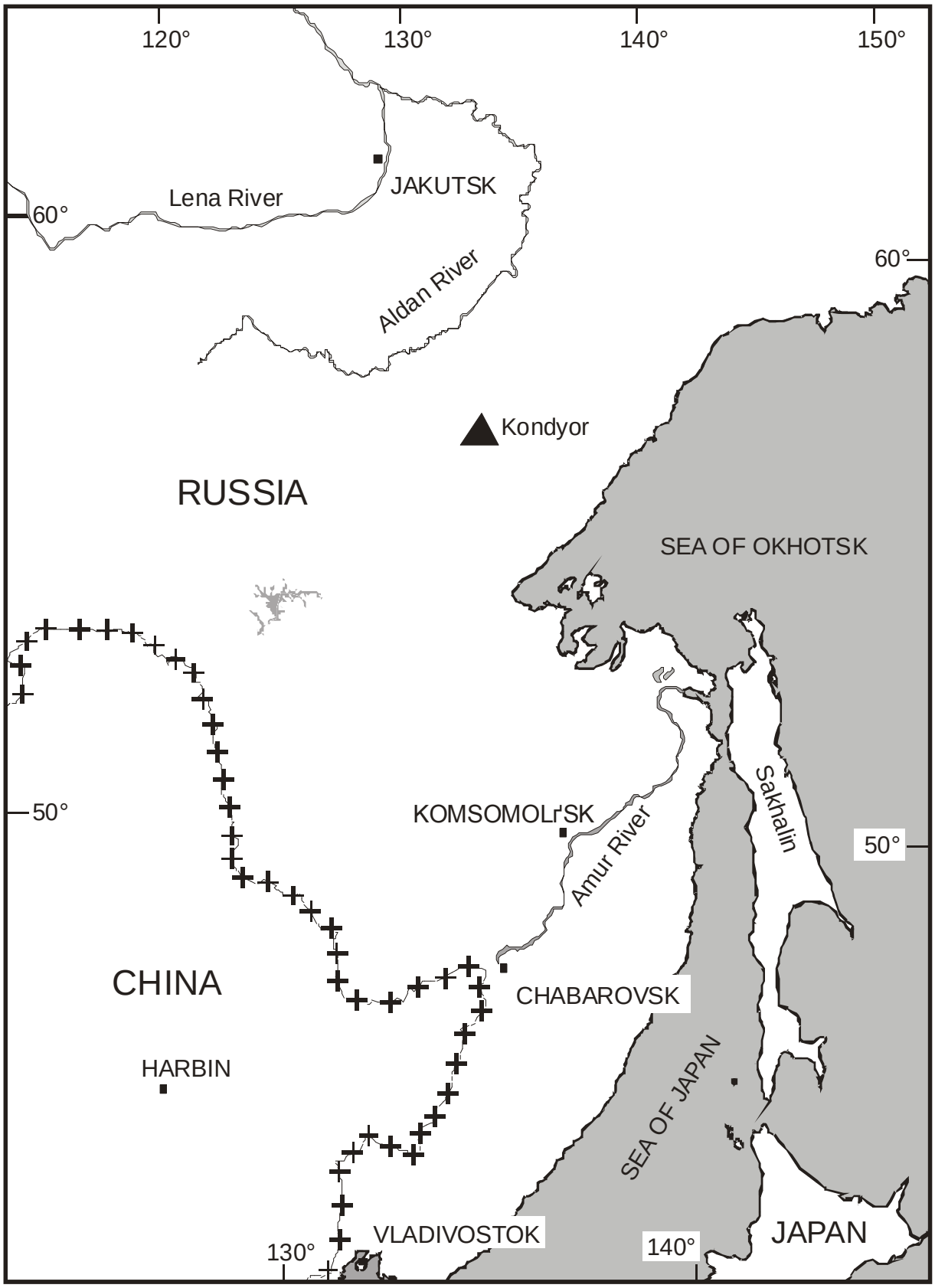

***Fig. 57**. Location map of the Kondyor deposit*

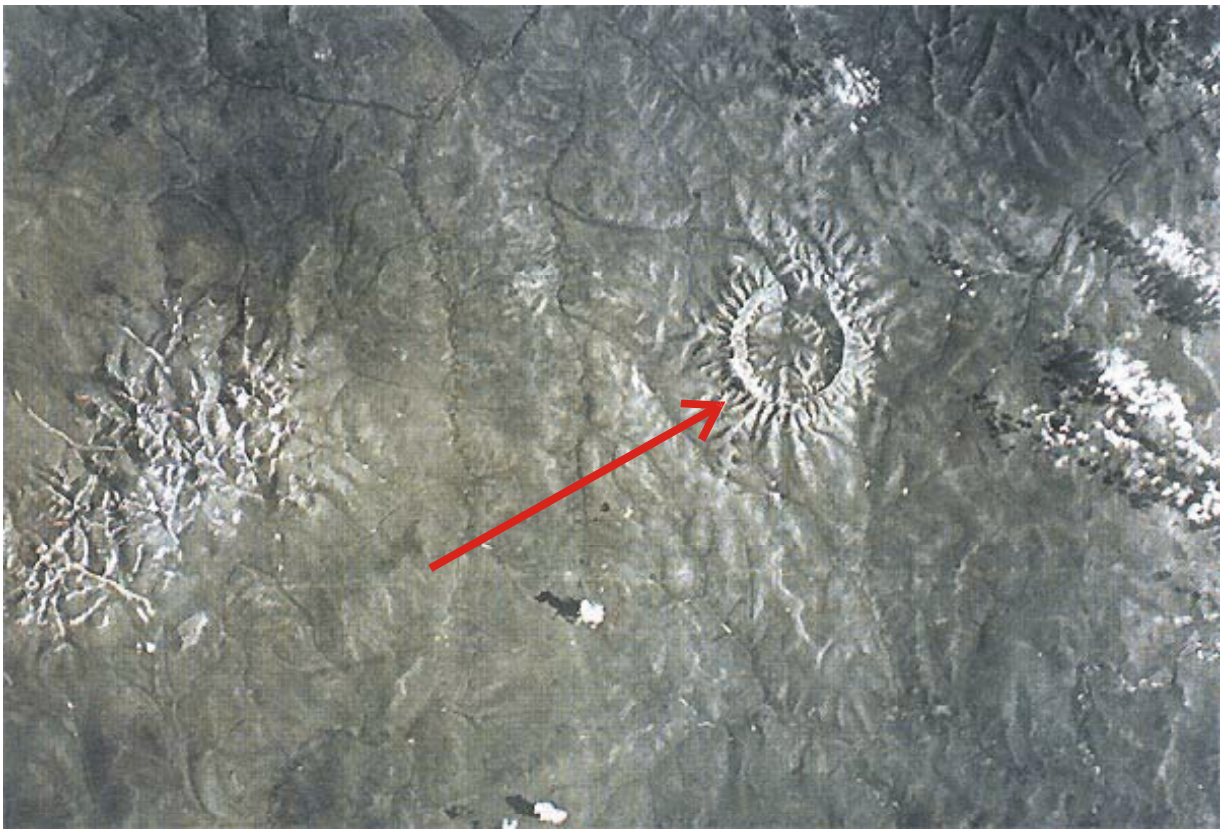

Fig. 58. *Satellite image of the Kondyor Uralian/Alaskan-type intrusion (6 km in diameter). The alluvial PGE-Au placer along the northward draining Kondyor river stretches for 50 km. http://astravel.rosnet.ru*

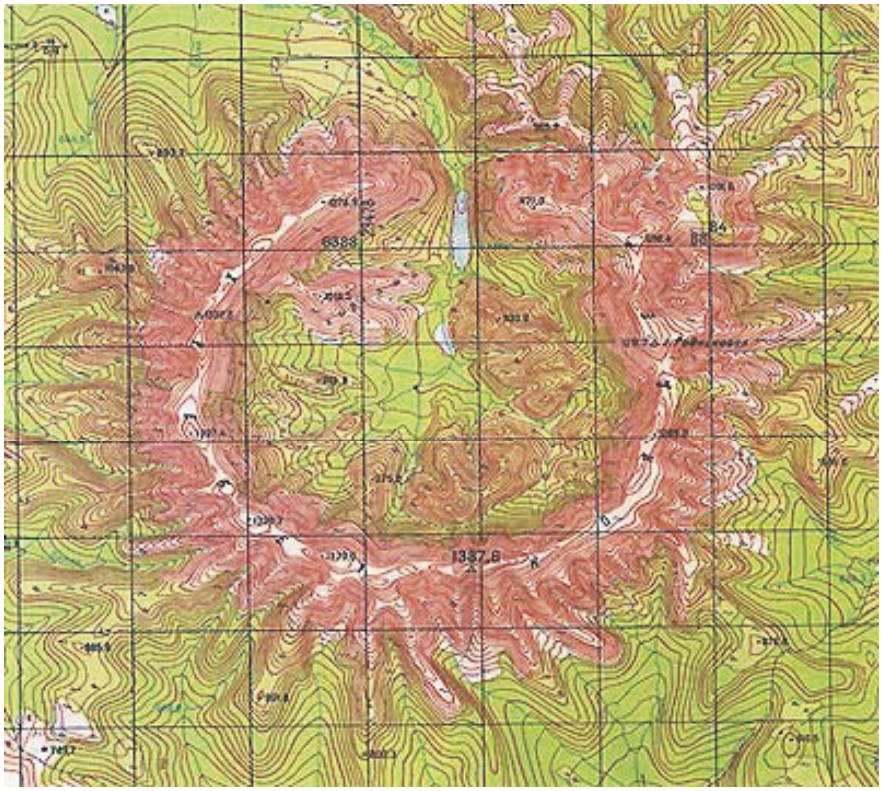

Fig. 59. *Topographic map of Kondyor intrusion. Grid width is 1 km. http://astravel.rosnet.ru*

Apatite-magnetite-biotite clinopyroxenite with Ti-bearing magnetite veins is located in the southwestern part of the massif (Sushkin 1995). Dunites and host rocks are penetrated by veins and veinlets of Mesozoic alkaline rocks, accompanied by contact and metasomatic transformations (Emelynenko et al. 1989).

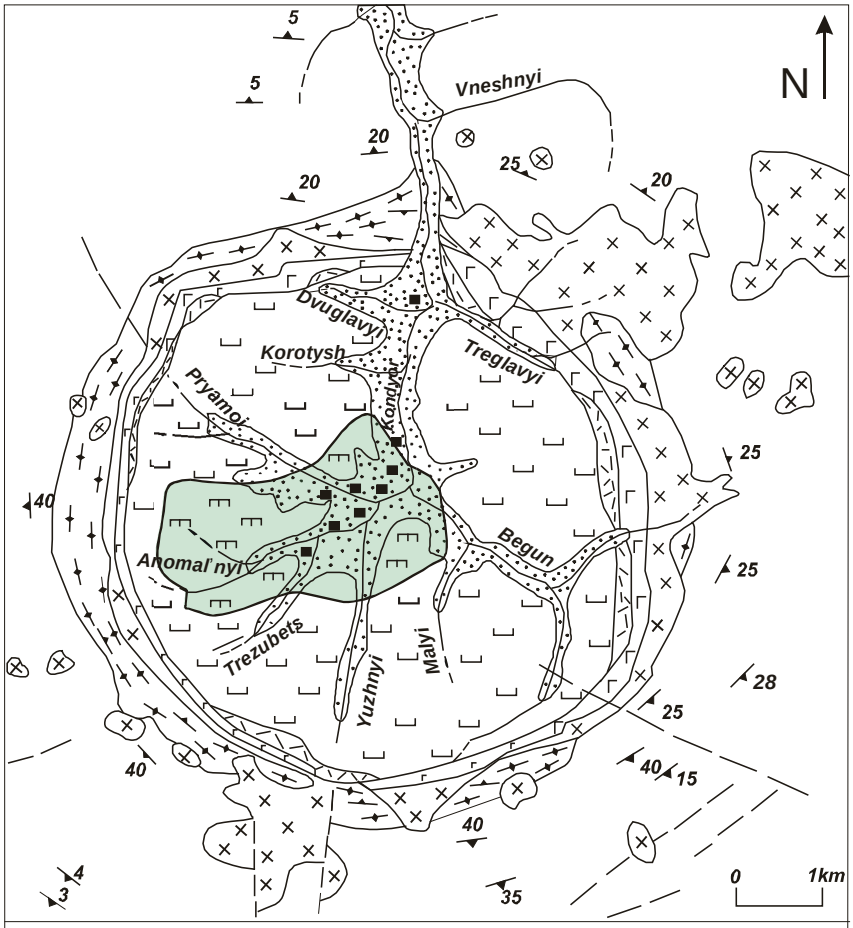

Fig. 60. *Geological map of the Kondyor deposit (modified from Sushkin 1995). Note occurrence of coarse Pt-Fe alloy crystals in the outcrop area of the magnetite-apatite-phlogopite clinopyroxenite.*

The Kondyor massif intrudes Archean and Proterozoic metasedimentary rocks of the Siberian Platform. The age of the intrusion is not well constrained. A parallel study by Malitch and Thalhammer (2002) and Pushkarev et al. (2002) defined the osmium isotope composition of inclusions of Os-Ir alloy in xenomorphic Pt-Fe alloy and found a $^{187}Os/^{188}Os$ ratio of 0.1250 ±0.002 (n=5) which gives a mantle model age of 330 ±30 Ma. Biotite from cross-cutting dikes yielded an $^{40}Ar/^{39}Ar$ age of 120 ± 1 Ma (data by G.K. Czamanske, given in Cabri et al. 1998). Pushkarev et al. (2002) measured K-Ar ages on biotite of 132 ± 8 Ma and 115 ±6 Ma for ultramafic and gabbro units, respectively, and a discordant Rb-Sr age of 123 ±2 Ma for pyroxenite and 93 ± 47 Ma for gabbro-pegmatite, respectively.

Fig.61. *Valley of Kondyor River*

Alluvial PGM placers developed inside the intrusion with basin morphology, along the northern valley of the Kondyor river and its tributaries (Sushkin 1995) (Fig. 61).

The main metal resources are concentrated in flood-plain placers with 1-1.5 m up to 7 m in thickness (Malitch 1999). Exploitation of the placers began in 1984 by the Amur mining company (Fig. 62).

Fig. 62. *Settlement of Amur mining company*

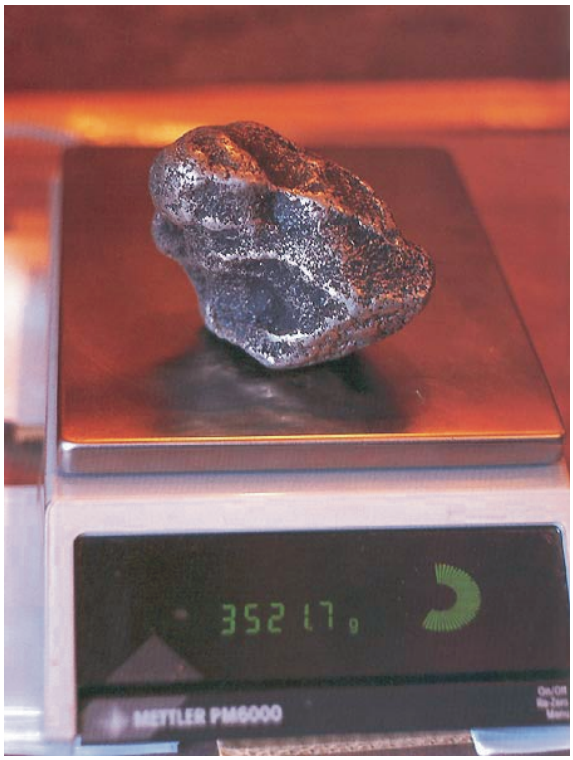

Fig. 63. *A 3.5 kg platinum nugget from Kondyor placer.*

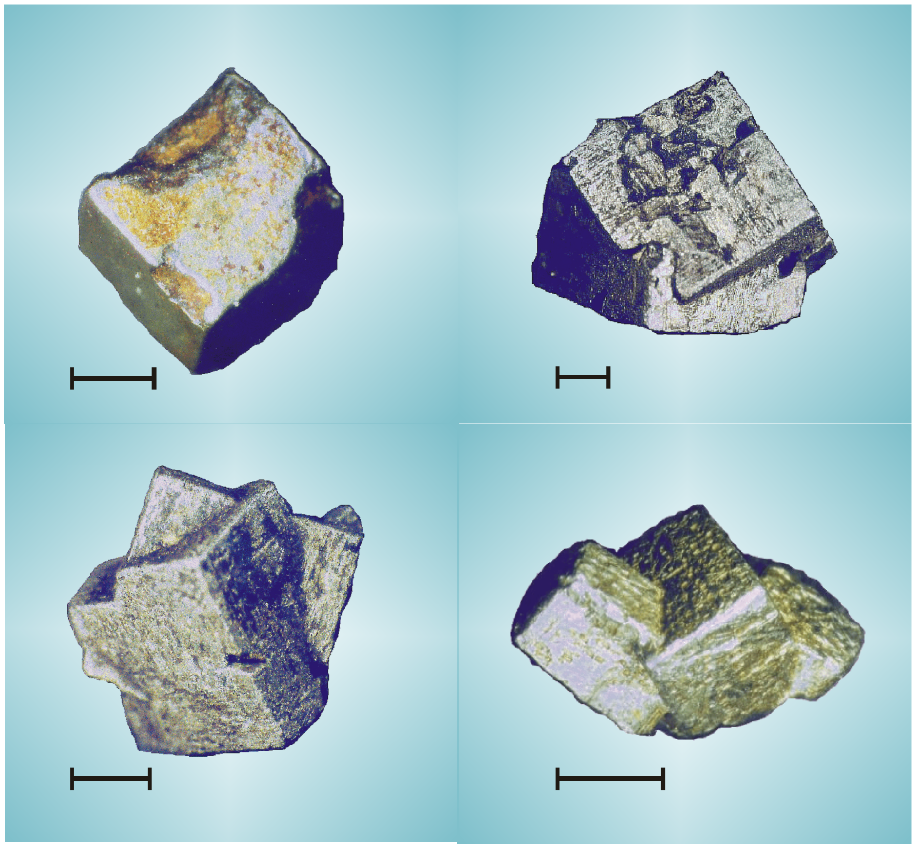

Fig. 64. *Examples of coarse Pt-Fe alloy crystals from the Kondyor placer. Scale bar is 1 mm. Yellowish tint is from gold-rich mineral assemblages.*

About 40 % of the total resource of around 60 t PGE have been mined so far; the average ore grade is 1.6 g PGE/m^3, decreasing from 4 g/cm^3 in drainages within the intrusive body to 0.5 g/m^3 at its downstream extremity, over a total length of about 50 km (Yakubchuk and Edwards 2002).

Platinum-iron alloy is characteristic of the Kondyor placer. Iridium-osmium alloy and gold are present as minor components. The largest nugget found at Kondyor had a weight of 3521 g (Fig 63). The Kondyor deposit belongs to the iridium-platinum type (Mochaov et al. 1991), with about 85 % Pt, 1.7 % Ir, 0.7 % Os, 0.5 % Pd, 0.4 % Rh, 0.1 % Ru, and other elements, including Au, 9 % (Yakubchuk and Edwards 2002).

7.3 OCCURRENCE OF Pt-Fe ALLOY MACROCRYSTALS

A remarkable and very unusual mineralogical feature of the Kondyor deposit is the presence of coarse idiomorphic crystals of Pt-Fe alloy up to 1.5 cm in size. The area of confluence of the Anomal'nyi and Trezubets creeks and the left bank of the Kondyor river between the Pryamoi and Korotish creeks is characterized by the occurrence of such idiomorphic Pt-Fe alloy crystals (Fig. 60) (Sushkin 1995). The same area around Anomal'nyi creek also shows enrichment in gold. In general, the gold content in heavy-mineral concentrates from Kondyor is about 1 wt. %. But heavy-mineral concentrates from the Anomal'nyi and Trezubets creeks have around 3-5 wt.% Au (Nekrasov et al. 1999).

The coarse crystals from Kondyor are hexahedral in shape. Penetration twins and intergrowth aggregates of two and more crystals are common, especially among the larger crystals (Fig. 64). The crystals often display a gold-rich reaction rim.

7.4 SAMPLE DESCRIPTION AND ANALYTICAL RESULTS

Over the last two decades, the Far East Geological Institute has been actively participating in the investigation of the geology, geochemistry and mineralogy of the Kondyor deposit. A large amount of representative rocks and minerals of the Kondyor placer has been collected under the leadership of I.Ya. Nekrasov, formerly the director of the institute, in collaboration with researchers B.L. Zalishchak and V.P. Molchanov. The samples studied belong to this collection. Four alluvial euhedral Pt-Fe alloy crystals of about 2-4 mm across have been chosen. Their origin is from the Anomal'nyi creek area (Fig. 60). The crystals were first documented by

scanning electron microcopy, then prepared in polished sections, and studied by ore microscopy and electron-microprobe analysis. In addition, a large number of xenomorphic Pt-Fe grains from a composite heavy-mineral concentrate were studied in order to compare their composition to the euhedral macrocrystals.

Sample I

Sample I is an irregular cube of 4.3 x 3.1 mm size. The crystal consists of Pt-Fe alloy with a composition of $Pt_{2.5}Fe$ (Table 41). Copper, nickel and tin occur as minor elements. There were no other platinum-group elements besides Pt detectable by electron-microprobe analysis. Reconnaissance proton-microprobe analysis detected zinc, germanium and antimony in the 100-1,000 ppm range (Table 42). Palladium gave 154 ppm, rhodium 99 ppm, and ruthenium 22 ppm.

TABLE 41. CHEMICAL COMPOSITION (ELECTRON MICROPROBE) OF THE FERROPLATINUM MATRIX OF THE Pt-Fe MACROCRYSTALS FROM THE KONDYOR PLACER

Sample	I n=3	II n=2	III n=4	IV n=3
wt.%				
Sn	0.30 ± 0.13	0.19 ± 0.04	-	0.22 ± 0.06
Sb	-	-	0.23 ± 0.10	0.11 ± 0.01
Pt	89.77 ± 0.43	88.58 ± 0.09	89.74 ± 0.78	89.01 ± 0.55
Ni	0.09 ± 0.02	0.07 ± 0	0.09 ± 0.02	0.09 ± 0.01
Fe	9.31 ± 0.04	9.04 ± 0.01	8.92 ± 0.36	9.42 ± 0.20
Cu	0.77 ± 0.13	0.60 ± 0.01	0.52 ± 0.07	0.79 ± 0.11
Total	100.23 ± 0.23	98.51 ± 0.18	99.77 ± 1.23	99.87 ± 0.67
at.%				
Sn	0.39 ± 0.16	0.25 ± 0.05	-	0.29 ± 0.08
Sb	-	-	0.29 ± 0.13	0.14 ± 0.01
Pt	71.57 ± 0.38	72.25 ± 0.06	72.69 ± 0.79	71.10 ± 0.54
Ni	0.23 ± 0.06	0.19 ± 0	0.23 ± 0.05	0.25 ± 0.02
Fe	25.92 ± 0.13	25.76 ± 0.09	25.27± 0.63	26.27 ± 0.33
Cu	1.89 ± 0.32	1.50 ± 0.03	1.32 ± 0.17	1.97 ± 0.26
Total	100	100	100	100

Note: Os, Ru, Ir, Rh, Pd, Pb, Ag, Te, Au, Co, Bi, As, S, were not detected
- below detection limit

TABLE 42. COMPARISON OF THE TRACE ELEMENT COMPOSITION (PPM) IN Pt-Fe ALLOY OF MACROCRYSTALS (A) AND XENOMORPHIC GRAINS (B)

A. Macrocrystals			**B. Xenomorphic grains**		
PIXE	**Sample I**		**EMPA**	**n=56**	
Element	**Concentration**	**LOD**	**Element**	**Concentration**	**LOD**
Ru	22 ± 8	15	**Ru**	< 1600	
Rh	99 ± 14	20	**Rh**	6900 ± 2900	1200
Pd	154 ± 14	25	**Pd**	3300 ± 2700	2400
Ni	1025 ± 84	102	**Ni**	2000 ± 1400	300
Cu	7287 ± 206	174	**Cu**	6000 ± 3000	900
Zn	367 ± 141	281	**Zn**	n.a.	
Ge	577 ± 107	231	**Ge**	n.a.	
Sn	2257 ± 54	33	**Sn**	< 1600	
Sb	568 ± 36	42	**Sb**	< 800	
Te	61 ± 27	53	**Te**	< 900	
Os	< 1448		**Os**	1700 ± 600	1500
Ir	< 1624		**Ir**	21500 ± 17200	1500
Cs	88 ± 44	73	**Cs**	n.a.	

Other elements below analytical detection limit:

Ga	< 2720
As	< 163
Au	< 1270
Hg	<567
Br	< 117
Rb	< 564
Sr	< 32
Y	< 24
Zr	< 14
Nb	< 21
Mo	< 13
Ag	< 126
Cd	< 44
In	< 131
Ba	< 164
W	< 2430
Re	< 642
Tl	< 253
Pb	< 326
Bi	< 3533
U	< 296

Note: Cabri et al. (1998) found Re and Os values in a macrocrystal from Kondyor below the SIMS detection limit (<< 1ppm); n.a. - not analyzed

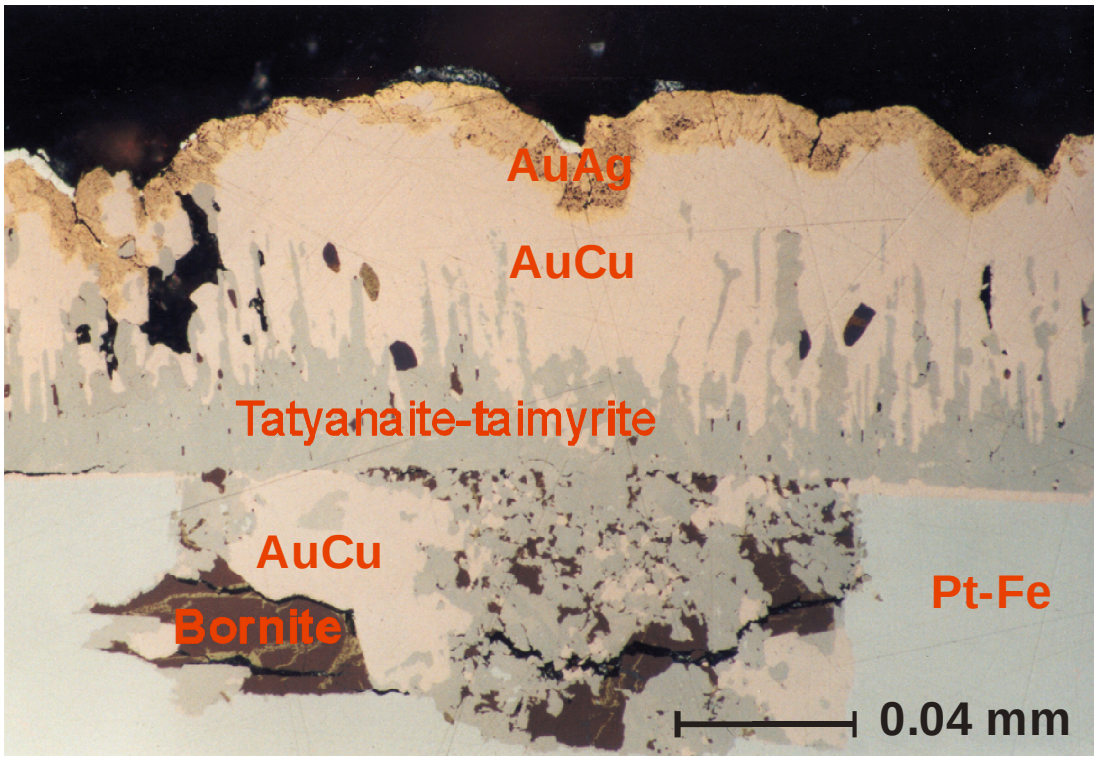

Fig. 65. *Photomicrograph (oil immersion) of fine-grained intergrowth aggregate of bornite and tatyanaite-taimyrite in Pt-Fe alloy, with flame-like rim of tatyanaite-taimyrite grading outwards into tetra-auricupride and overgrown by Au-Ag alloy. Sample I.*

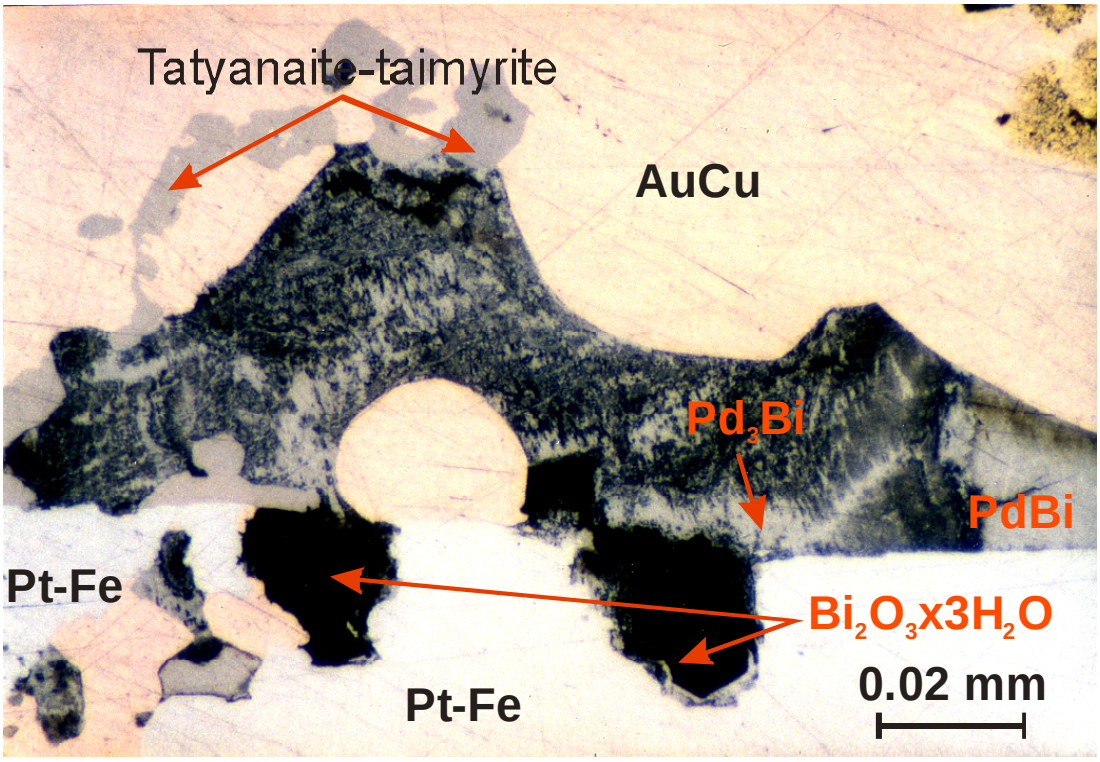

Fig. 66. *Photomicrograph (oil immersion) of the complex Pd-Bi mineral assemblage at the interface between ferroplatinum and tetra-auricupride. Sample I.*

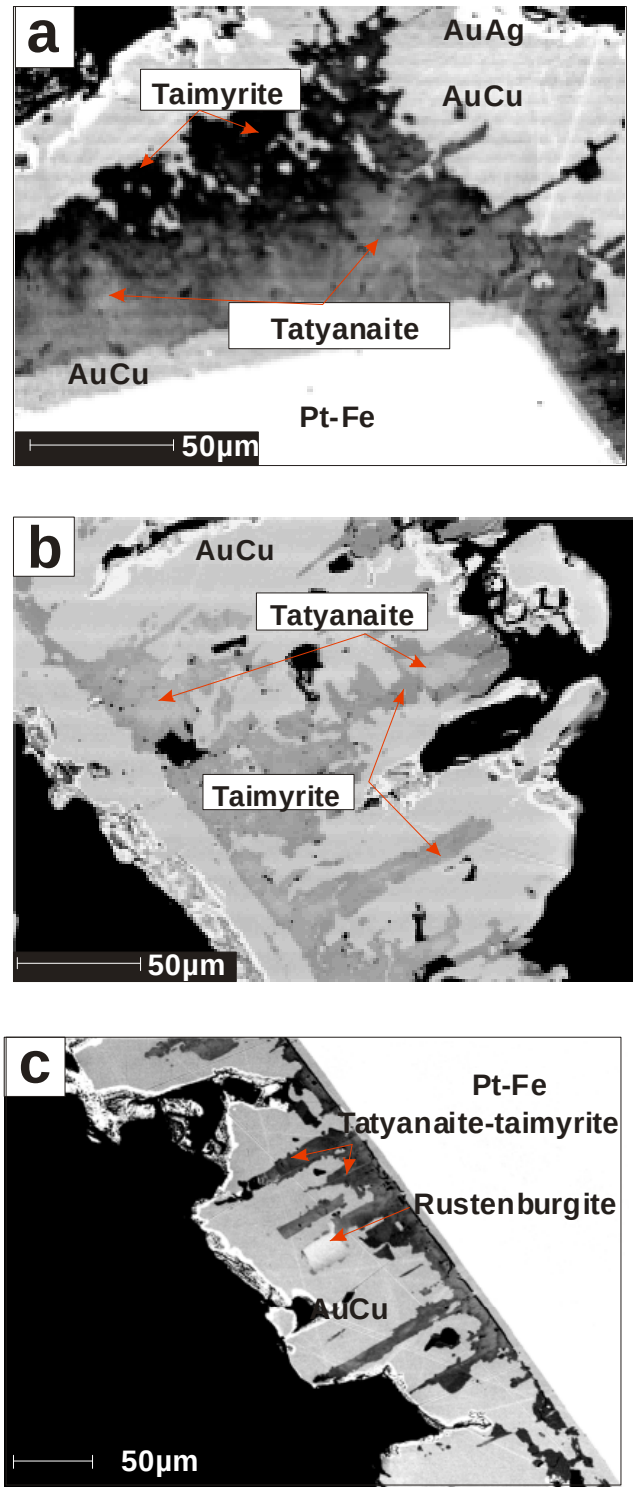

***Fig. 67**. Back-scattered electron images showing: **a)** tatyanaite grading outwards into taimyrite within tetra-auricupride; **b)** tatyanaite inclusion in taimyrite; **c)** inclusions of rustenburgite intergrown with taimyrite-tatyanaite aggregates. Sample I.*

The crystal contains several inclusions of chromian titanian magnetite up to 0.9 mm in size with up to 8 wt.% TiO_2 and 3 wt.% CrO_2 (Table 43).

The magnetite is altered along fractures to a titanite-like phase with high chlorine content (2.2-7.9 wt.% Cl). The chlorine-rich rim is surrounded by perovskite (Table 44) and chlorite (Table 45). Chlorite is represented both by clinochlore and chamosite. A 10 μm inclusion of fluorapatite was found inside of a clinochlore rim (Table 44). Phlogopite is present as an inclusion inside of a magnetite grain, surrounded by clinochlore.

TABLE 43. CHEMICAL COMPOSITION OF TITANIAN MAGNETITE AND ILMENITE INCLUSIONS (WT.%) WITHIN THE MATRIX OF Pt-Fe MACROCRYSTALS

	Titananian magnetite					Ilmenite	
	1	2	3	4	5	6	7
CaO	-	-	-	-	-	0.62	0.48
Cr_2O_3	3.02	3.02	3.12	3.02	3.01	-	-
TiO_2	7.87	8.00	7.75	7.71	7.91	50.83	50.33
Fe_2O_3	49.99	57.36	57.77	58.25	57.26	1.86	1.84
FeO	32.76	26.18	25.43	25.28	25.19	37.28	37.69
MnO	1.06	1.18	1.03	1.08	0.99	5.44	5.73
MgO	2.87	2.49	3.14	3.21	3.18	0.75	0.65
Al_2O_3	1.39	1.41	1.60	1.42	1.62	-	-
Total	98.95	99.65	99.84	99.96	99.16	96.78	96.72

Formulae:

1. $(Fe^{2+}_{1.025}Mg_{0.160}Mn_{0,034})_{1.219}(Fe^{3+}_{1.408}Ti_{0.222}Cr_{0.089}Al_{0.061})_{1.780}O_4$
2. $(Fe^{2+}_{0.800}Mg_{0.136}Mn_{0,037})_{0.973}(Fe^{3+}_{1.577}Ti_{0.220}Cr_{0.087}Al_{0.061})_{1.945}O_4$
3. $(Fe^{2+}_{0.772}Mg_{0.170}Mn_{0,032})_{0.974}(Fe^{3+}_{1.578}Ti_{0.212}Cr_{0.090}Al_{0.068})_{1.948}O_4$
4. $(Fe^{2+}_{0.767}Mg_{0.174}Mn_{0,033})_{0.974}(Fe^{3+}_{1.590}Ti_{0.210}Cr_{0.087}Al_{0.061})_{1.948}O_4$
5. $(Fe^{2+}_{0.769}Mg_{0.173}Mn_{0,031})_{0.973}(Fe^{3+}_{1.572}Ti_{0.217}Cr_{0.087}Al_{0.070})_{1.946}O_4$
6. $(Fe^{2+}_{0,805}Ca_{0,017}Mn_{0,119}Mg_{0,029})_{0,970}(Fe^{3+}_{0,036}Ti_{0,988})_{1,024}$
7. $(Fe^{2+}_{0,818}Ca_{0,013}Mn_{0,126}Mg_{0,025})_{0,982}(Fe^{3+}_{0,036}Ti_{0,982})_{1,018}$

Note: FeO and Fe_2O_3 are calculated according to stoichiometry.
Si, P, K, S, Cl, Zn, F, Na were not detected

The Pt-Fe alloy crystal is rimmed by a complex and irregular gold-rich zone (locally up to 0.4 mm wide) with high contents of gold, copper, platinum, palladium, bismuth and tin. The main mineral phase in the inner part of the gold-rich rim is Pd-Pt-bearing tetra-auricupride [(Au,Pt,Pd)Cu] (Table 46).

The outer part of the rim is formed by Au-Ag alloy of $Au_{0.47}Ag_{0.52}Cu_{0.01}$ composition as well as by small aggregates of very pure native gold in the outermost rim (Fig. 65, Table 46). There are flame-like composite aggregates of tatyanaite [$(Pt,Pd,Cu)_3Sn$] - taimyrite [$(Pd,Pt,Cu)_3Sn$] solid solution (Table 48) within the tetra-auricupride (Fig. 65). Tatyanaite also grades outwards into taimyrite or occurs as inclusion in taimyrite (Fig. 67a,b). There are rare inclusions of rustenburgite [$(Pt,Pd)_3Sn$] intergrown with taimyrite-tatyanaite aggregates (Fig. 67c; Table 48). Chalcopyrite and bornite relics are present both on the boundary between Pt-Fe alloy and the gold-bearing rim, and inside the gold rim (Fig. 65).

TABLE 44. CHEMICAL COMPOSITION (WT.%) OF FLUORAPATITE AND PEROVSKITE INCLUSIONS IN Pt-Fe MACROCRYSTALS

	Apatite						Perovskite
	1	**2**	**3**	**4**	**5**	**6**	**7**
SiO_2	1.03	0.56	1.03	-	0.64	0.62	-
P_2O_5	42.26	40.95	40.52	43.22	42.58	41.04	-
CaO	56.11	57.44	55.35	56.79	56	56.22	41.61
Cr_2O_3	-	-	-	-	-	-	0.15
TiO_2	-	-	-	-	-	-	55.75
SO_2	-	0.27	0.47	-	0.62	0.72	0.66
Cl	-	-	-	-	-	-	0.08
F	3.3	2.26	1.74	2.83	2.17	3.23	-
FeO	0.26	-	0.1	-	-	-	0.78
Na_2O	-	-	-	-	-	-	0.14
MgO	0.17	-	-	-	-	-	-
Total	103.13	101.48	99.21	102.84	102.01	101.83	99.17
-O=F	1.39	0.95	0.73	1.19	0.91	1.36	
Real Total	101.74	100.53	98.48	101.65	101.1	100.47	

Formulae:

1. $Ca_{9.554}Fe_{0.035}Mg_{0.04}(PO_4)_{5.686}(SiO4)_{0.164}F_{1.659}$
2. $Ca_{10.062}(PO_4)_{5.668}(SiO_4)_{0.192}F_{1.169}$
3. $Ca_{9.886}Fe_{0.014}(PO_4)_{5.719}(SiO_4)_{0.172}F_{0.917}(OH)_{0.083}$
4. $Ca_{9.701}(PO_4)_{5.834}F_{1.427}$
5. $Ca_{9.688}(PO_4)_{5.821}(SiO_4)_{0.103}F_{1.108}$
6. $Ca_{9.812}(PO_4)_{5.661}(SiO_4)_{0.101}F_{1.664}$
7. $(Ca_{1.034}\ Fe_{0.015}Na_{0.006})_{1.055}(Ti_{0.972}Cr_{0.003})_{0.975}O_3$

Note: Calculation of the true total in the case of apatite has been made by substracting an oxygen equivalent of the fluorine atoms by using the following formula:

$$\frac{\text{F wt.\% x atomic weight of oxygen}}{\text{2 x atomic weight of fluorine}}$$

[Deer et al. 1998]

- below detection limit; K, Mn, Zn, Al were not detected

Complex Pd-Bi mineral assemblage occurs lacally at the interface between Pt-Fe alloy and tetra-auricupride. This assemblage consists of an intergrowth aggregate of a Pd_3Bi phase, an unknown Pd_7Bi_3 phase and sobolevskite [PdBi] developing at the edge. Interstices are filled by late bismuth oxide hydrate $Bi_2O_3 \times 3H_2O$ (Table 50) (Fig. 66).

TABLE 45. CHEMICAL COMPOSITION (WT.%) OF SILICATE MINERALS IN Pt-Fe MACROCRYSTALS

	Quartz	Aegirine	Aegirine-augite	Ab100 albite	Ab80 oligoclase	Ab60 andesine	Orthoclase	Biotite	Titanite	Chamosite	Clino-chlore
	1	2	3	4	5	6	7	8	9	10	11
SiO2	99.06	53.22	55.42	71.01	67.10	60.55	68.16	40.7	31.23	47.91	31.55
P2O5	-	0.13	-	-	-	-	-	-	-	-	-
K2O	-	-	0.83	-	0.17	0.2	14.12	7.58	-	0.68	-
CaO	-	4.18	9.14	0.18	4.10	7.25	-	-	29.23	0.13	-
Cr2O3	-	-	0.16	-	-	-	-	0.28	-	-	0.80
TiO2	-	2.94	0.63	-	-	-	-	1.23	37.88	0.17	-
FeO	0.45	22.00	8.82	0.14	0.33	0.2	0.21	6.77	0.91	21.12	2.11
MnO	-	0.10	-	-	-	-	-	-	-	-	-
Na2O	-	11.19	3.80	9.15	8.30	7.08	0.67	1.85	-	0.26	-
MgO	-	3.37	18.32	-	-	-	-	24.89	-	5.07	35.04
Al2O3	-	1.80	2.46	19.2	21.77	24.39	18.37	15.59	0.77	7.98	15.14
Total	99.51	98.93	99.58	99.68	101.77	99.67	101.53	98.89	100.02	83.32	84.64

Note: S, Cl, Zn, F were not detected; - below detection limit

Sample II

The sample is an irregular cube of 2 x 3 mm size with a matrix composition of $Pt_{2.6}Fe$ (Table 41). It has inclusions of titanite, manganoan ilmenite, chalcopyrite-bornite intergrowth aggregates and fluorapatite (Tables 43, 44). A gold-rich rim zone, 50 to 130 μm wide, consists of tetra-auricupride [(Au,Pt,Pd)Cu] together with Pt-rich taimyrite [$(Pd,Pt,Cu)_3Sn$], commonly intergrown with atokite [$(Pd,Pt)_3Sn$] (Fig. 68). The latter occasionally forms aggregates with mertieite-II [Pd_8Sb_3] and Te-sobolevskite [(Pd,Pt)(Bi,Te)] (Tables 49 and 51; Fig. 69).

The tetra-auricupride has a constant palladium content of 1.4 wt.%. The platinum content varies from 6.9 up to 12.4 wt.%. A complex Au-Ag-Cu alloy with the composition of $Au_{0.50}Ag_{0.36}Cu_{0.12}Pd_{0.01}Pt_{0.01}$ occurs as inclusion in the tetra-auricupride rim. The outer part of the rim is formed by Au-Ag alloy of composition $Au_{0.51\text{-}0.37}Ag_{0.48\text{-}0.63}Cu_{0.01}$ and is overgrown by pure gold [$Au_{0.97}Ag_{0.03}$] (Table 46). The gold-bearing rim has anhedral quartz inclusions intergrown with albite, andesine and orthoclase as well as aegirine-augite, smectite and chamosite aggregates (Table 45).

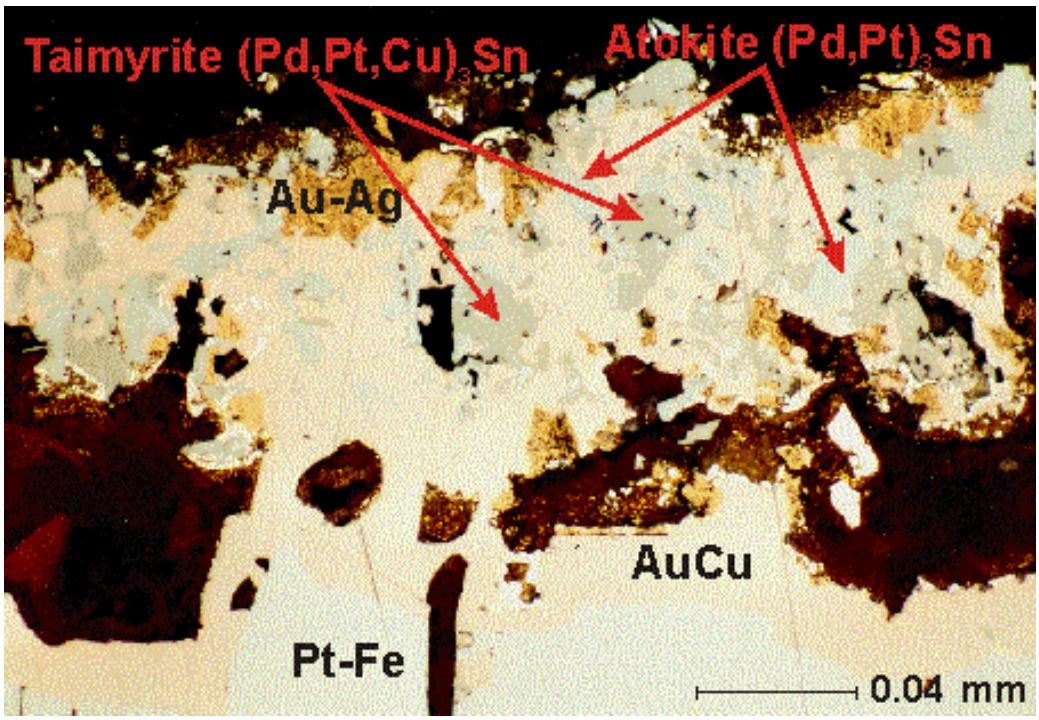

Fig. 68. *Photomicrograph (oil immersion) of atokite and taimyrite intergrowth inside tetra-auricupride reaction rim on Pt-Fe alloy. Outlined section shows atokite relics within taimyrite. Sample II.*

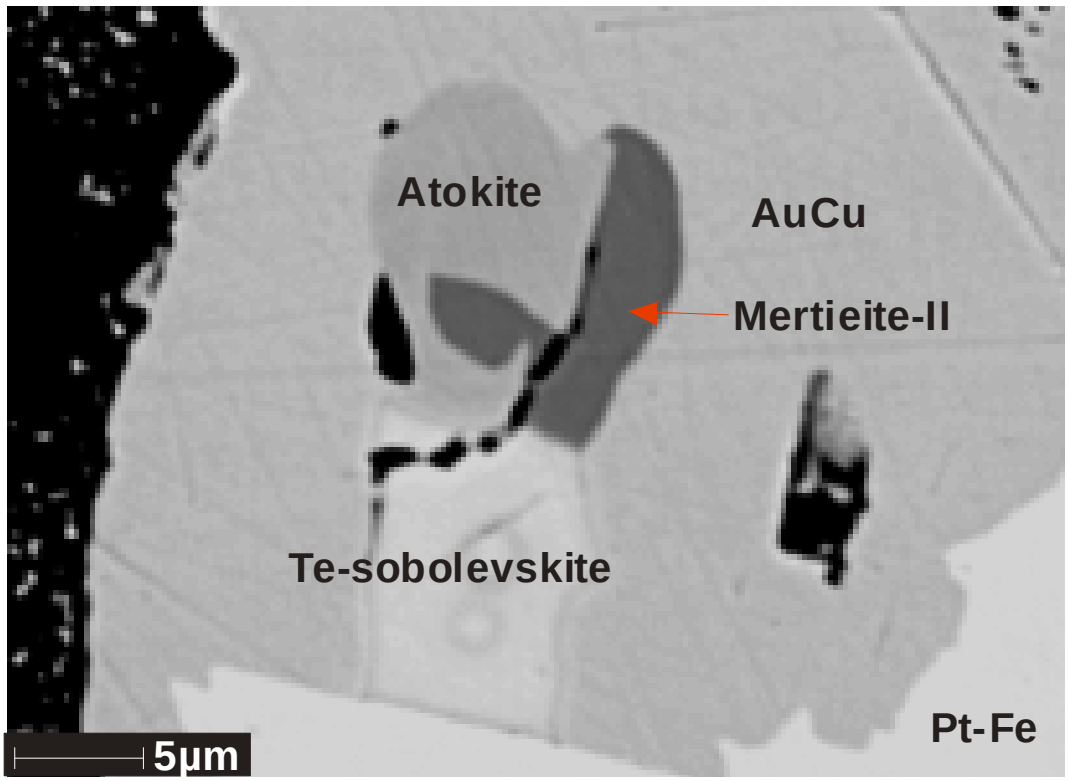

Fig 69*. Back-scattered electron image, showing intergrowth of atokite, mertieite-II [Pd_8Sb_3] and Te-sobolevskite [(Pd,Pt)(Bi,Te)] within tetra-auricupride rim on Pt-Fe alloy crystal. Sample II.*

Sample III

The sample is an irregular cube of Pt-Fe alloy [$Pt_{2.6}Fe$] of 4.5 x 3 mm size (Fig. 70). The crystal is affected by leaching and pervasive alteration to chamosite, along crystallographic planes (001). Thin Pt-Fe alloy laminae show contorted microdeformation (?)/dissolution fabrics. Chalcopyrite inclusions are intergrown with bornite and chalcocite. The outer part of the crystal has rounded inclusions of fractured mertieite-II, up to 0.1 mm across (Table 50, Fig. 71).

The narrow gold-bearing rim, with average thickness of around 80 μm, consists of a complex Au-Ag-Cu alloy with minor palladium. The rim composition is heterogeneous and changes from native gold [$Au_{0.98}Ag_{0.02}$] through Au-Ag alloy [$Au_{0.49}Ag_{0.51}$] to very fine-grained intergrowth aggregates with bulk composition of $Au_{0.66\text{-}0.68}Ag_{0.07\text{-}0.10}Cu_{0.18\text{-}0.21}Pd_{0.04\text{-}0.06}$ to $Au_{0.69}Ag_{0.13}Cu_{0.15}Pd_{0.03}$. Minor inclusions of tetra-auricupride [$Au_{0.44}Cu_{0.50}Pd_{0.05}Pt_{0.01}$] and atokite [$(Pd,Pt)_3Sn$] are present in the reaction rim.

Silicate inclusions in the gold-rich rim consist of aegirine, quartz, chamosite, clinochlore, smectite, and serpentine (Table 45).

TABLE 46. CHEMICAL COMPOSITION OF TETRA-AURICUPRIDE AND Au-Ag ALLOY

	Tetra-auricupride				Au-Ag alloy			
	1	2	3	4	5	6	7	8
wt.%								
Bi	-	-	-	-	0.23	-	-	-
Pb	-	-	-	-	0.13	-	-	-
Pd	3.86	1.55	2.71	0.78	0.15	1.10	-	-
Ag	-	-	0.28	-	1.71	29.66	33.96	54.11
Au	70.76	69.55	67.31	61.50	97.92	70.43	65.63	47.34
Pt	1.87	3.91	5.33	13.91	0.15	0.00	0.30	-
Fe	-	-	0.10	0.16	-	-	-	-
Cu	25.32	24.91	25.02	24.83	-	0.44	0.27	-
Total	101.81	99.92	100.75	101.18	100.29	101.63	100.16	101.45
at.%								
Bi	-	-	-	-	0.21	-	-	-
Pb	-	-	-	-	0.12	-	-	-
Pd	4.51	1.88	3.19	0.93	0.28	1.59	-	-
Ag	-	-	0.33	-	3.07	42.26	48.16	67.61
Au	44.71	45.28	43.12	39.80	96.17	55.07	50.94	32.39
Pt	1.19	2.57	3.45	9.10	0.15	-	0.24	-
Fe	-	-	0.22	0.36	-	-	-	-
Cu	49.59	50.27	49.69	49.81	-	1.08	0.66	-
Total	100	100	100	100	100	100	100	100

Note: Os, S, Ru, Rh, Sn, Sb, Te, Bi, Ir, Ni, Co, Fe were not detected

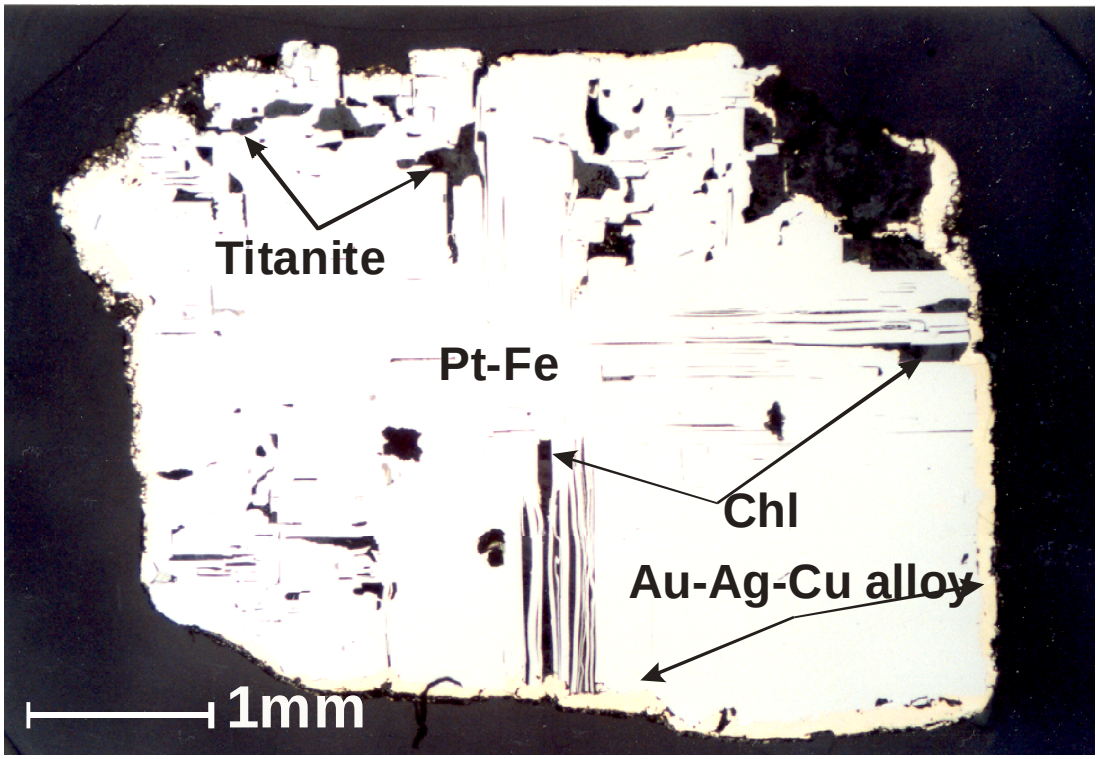

Fig. 70. *Photomicrograph (oil immersion) of coarse Pt-Fe alloy crystal with microdeformation (?)/dissolution fabrics along crystallographic planes. Sample III.*

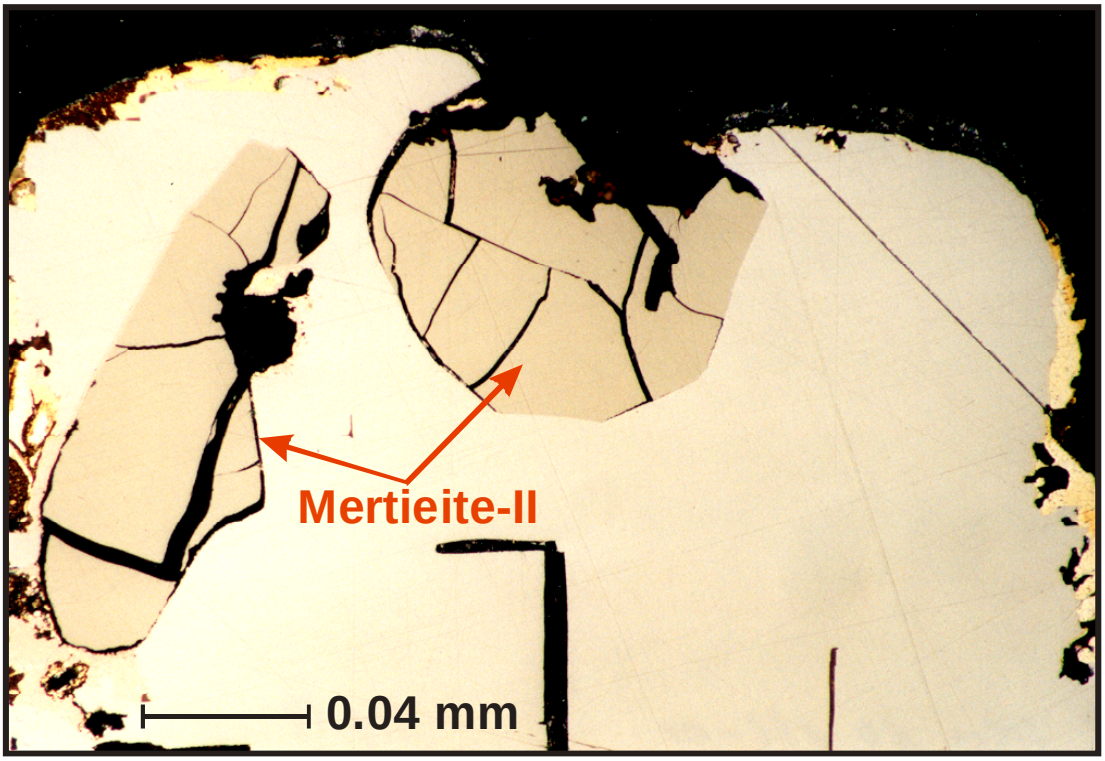

Fig. 71. *Inclusions of mertieite-II in matrix of Pt-Fe alloy with Au-bearing alloy on rim. Sample III (oil immersion).*

Sample IV

The sample is a regular cube of Pt-Fe alloy [$Pt_{2.4}Fe$] with a crystal face of 3 mm (Fig. 72) and is characterized by a variety of sulfide inclusions.

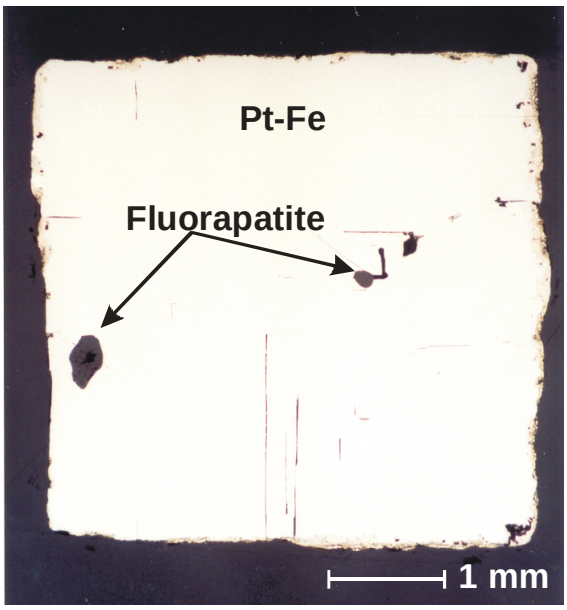

Fig. 72. *Inclusions of fluorapatite in Pt-Fe alloy. Sample IV (oil immersion).*

Chalcopyrite and bornite inclusions are dominant; one single inclusion (~120 μm large) of Co-bearing pentlandite was found. Several inclusions (up to 330 x 200 μm) of fluorapatite occur within the Pt-Fe matrix (Fig. 72). Inside the fluorapatite, small (≤5 μm) rounded inclusions of an unknown Th phosphocarbonate [$(Ca_{0.422}Th_{0.504}Si_{0.074})((PO_4)_{0.248}(CO_3)_{1.697}Cl_{0.055})_2$] and plumboan aragonite/tarnowitzite (?) [$(Ca_{0.848}Pb_{0.124}Si_{0.028})CO_3$] are present.

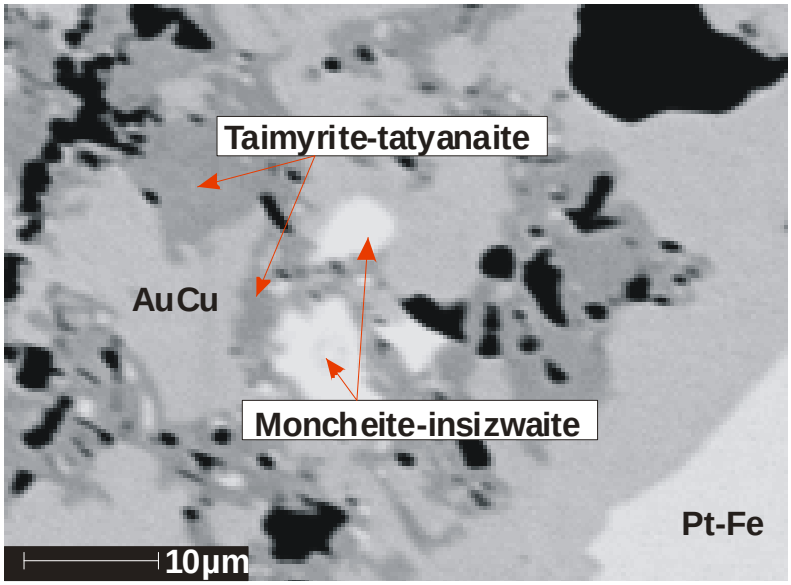

Fig 73*. Back-scattered electron images, showing intergrowth of taimyrite-tatyanaite with moncheite-insizwaite. Sample IV.*

The heterogeneous gold-bearing rim is dominated by terta-auricupride with 1.10 to 1.55 wt.% Pd and 2.67 to 10.92 wt.% Pt. Within the tetra-auricupride there are thin aggregates (exsolution lamellae?) of Au-Ag-Cu alloy [$Au_{0.48}Ag_{0.33}Cu_{0.19}$]. The outer part of the rim consists of Au-Ag alloy with a composition of [$Ag_{0.67}Au_{0.33}$].

The main PGM inclusions in the rim zone are represented by taimyrite-tatyanaite solid solution (Table 48) intergrown with minerals of the moncheite-insizwaite solid solution (Fig. 73; Table 49). The rim zone also hosts inclusions of aegirine, chamosite and goethite.

TABLE 47.CHEMICAL COMPOSITION OF Au-Ag-Cu-Pd-Pt ALLOY IN Pt-Fe MACROCRYSTALS

		1	2	3	4	5	6	7	8
	wt.%								
Bi		-	0.54	-	-	-	-	0.78	0.93
Pd		1.69	2.62	1.54	0.73	1.45	0.69	3.95	4.29
Ag		6.96	3.16	20.32	27.18	13.08	24.87	-	0.69
Au		90.66	82.77	76.52	66.18	61.87	67.33	92.38	72.42
Pt		-	0.47	-	0.76	5.93	0.4	-	0.12
Cu		1.73	11.10	2.83	5.10	19.49	8.15	1.35	23.06
Sn		-	-	-	-	-	-	0.38	0.29
Total		101.04	100.66	101.21	99.95	101.82	101.44	98.46	101.51
	at.%								
Bi		-	0.40	-	-	-	-	0.70	0.57
Pd		2.80	3.76	2.27	1.01	1.75	0.91	6.97	5.14
Ag		11.37	4.46	29.63	37.11	15.42	32.51	-	0.81
Au		81.05	64.28	61.08	49.49	39.96	48.21	88.01	46.91
Pt		-	0.37	-	0.58	3.87	0.29	-	0.08
Cu		4.78	26.73	7.02	11.81	39.00	18.08	3.98	46.31
Sn		-	-	-	-	-	-	0.34	0.18
Total		100	100	100	100	100	100	100	100

Note: Os, S, Ru, Rh, Sb, Te, Ir, Ni, Pb, Co, Fe, As were not detected
- below detection limit

TABLE 48. CHEMICAL COMPOSITION OF Pd-Pt-Cu-Sn-BEARING MINERALS

Mineral	Pt-rich taimyrite		Tatyanaite		Rustenburgite		Atokite	
No	1	2	3	4	5	6	7	8
wt.%								
Pd	35.86	35.57	22.24	21.87	17.42	25.27	30.94	33.84
Pt	24.72	26.47	41.96	42.22	61.42	51.55	45.29	42.70
Cu	12.31	12.10	11.40	12.23	0.84	0.59	1.03	0.59
Fe	-	-	-	0.09	-	-	0.33	-
Ni	-	-	0.13	0.09	-	-	-	0.07
Sn	25.34	25.23	22.05	21.83	19.51	20.77	21.03	21.41
Sb	0.89	0.73	0.22	0.20	0.20	0.57	0.55	0.85
Total	99.12	100.09	100.18	99.16	99.39	98.75	99.17	99.46
at%								
Pd	38.37	38.03	26.35	25.59	24.89	34.38	40.01	43.28
Pt	14.43	15.44	27.12	26.95	47.87	38.26	31.95	29.79
Cu	22.07	21.66	22.61	23.97	2.01	1.34	2.23	1.26
Fe	-	-	-	0.20	-	-	0.81	-
Ni	-	-	0.28	0.19	-	-	-	0.16
Sn	24.31	24.18	23.42	22.90	24.99	25.33	24.38	24.55
Sb	0.83	0.68	0.23	0.20	0.25	0.68	0.62	0.95
Total	100	100	100	100	100	100	100	100

Formulae recalculated on the basis of 4 atoms:

1. $(Pd_{1.54}Pt_{0.58}Cu_{0.88})_{3.00}(Sn_{0.97}Sb_{0.03})_{1.00}$
2. $(Pd_{1.52}Pt_{0.62}Cu_{0.87})_{3.01}(Sn_{0.97}Sb_{0.02})_{0.99}$
3. $(Pt_{1.08}Pd_{1.05}Cu_{0.90}Ni_{0.02})_{3.05}(Sn_{0.94}Sb_{0.01})_{0.95}$
4. $(Pt_{1.08}Pd_{1.02}Cu_{0.96}Fe_{0.01}Ni_{0.01})_{3.08}(Sn_{0.92}Sb_{0.01})_{0.92}$
5. $(Pt_{1.91}Pd_{1.00}Cu_{0.08})_{2.99}(Sn_{1.00}Sb_{0.01})_{1.01}$
6. $(Pt_{1.53}Pd_{1.38}Cu_{0.05})_{2.96}(Sn_{1.01}Sb_{0.03})_{1.04}$
7. $(Pd_{1.60}Pt_{1.28}Cu_{0.09}Fe_{0.03})_{3.00}(Sn_{0.97}Sb_{0.03})_{1.00}$
8. $(Pd_{1.73}Pt_{1.19}Cu_{0.05}Ni_{0.01})_{2.98}(Sn_{0.98}Sb_{0.04})_{1.02}$

Note: Os, S, Pb, Bi, Ru, Ag, Te, Ir, Co, As were not detected;
- below detection limit

TABLE 49. CHEMICAL COMPOSITION OF TELLURIDE AND BISMUTHIDE INCLUSIONS IN Pt-Fe MACROCRYSTALS

	Pd_7Bi_3		Pd_3Bi	Sobolevskite		Moncheite-insizwaite	Bi oxide $Bi_2O_3x3H_2O$
	1	2	3	4	5	6	7
wt.%							
Pd	52.11	52.51	56.47	33.92	33.44	0.16	-
Pt	2.40	1.92	2.66	2.67	4.07	36.13	1.69
Ag	-	-	-	-	-	0.44	0.77
Au	-	0.62	0.63	0.77	1.27	0.39	-
Cu	0.33	-	0.15	0.20	-	-	0.15
Bi	43.20	43.70	37.09	57.14	52.04	33.44	80.02
Te	1.07	0.18	1.30	4.65	10.27	28.66	0.56
Sb	0.12	-	0.23	0.64	0.53	0.24	-
O	-	-	-	-	-	-	9.13
							H_2O= 7.68*
Total	99.23	98.93	98.53	99.99	101.62	99.46	100.00
at.%							
Pd	67.70	68.83	71.77	48.70	46.54	0.26	-
Pt	1.70	1.37	1.85	2.09	3.09	31.96	0.62
Ag	-	-	-	-	-	0.70	0.51
Au	-	0.44	0.43	0.60	0.95	0.34	-
Cu	0.72	-	0.31	0.48	-	-	0.17
Bi	28.58	29.16	24.00	41.76	36.87	27.62	27.30
Te	1.16	0.20	1.38	5.57	11.91	38.77	0.31
Sb	0.14	-	0.26	0.80	0.64	0.35	-
O	-	-	-	-	-	-	40.67
H	-	-	-	-	-	-	H_2O=30.42
Total	100.00	100.00	100.00	100.00	100.00	100.00	100.00

Formulae:

Unknown Pd_7Bi_3 phase

1. $(Pd_{6.77}Pt_{0.17}Cu_{0.07})_{7.01}(Bi_{2.86}Te_{0.12}Sb_{0.01})_{2.99}$
2. $(Pd_{6.85}Pt_{0.14}Au_{0.04})_{7.06}(Bi_{2.92}Te_{0.02})_{2.94}$

Unknown Pd_3Bi phase

3. $(Pd_{2.97}Pt_{0.07}Cu_{0.01})_{2.97}(Bi_{0.96}Te_{0.06}Sb_{0.01})_{1.03}$

Sobolevskite Pd(Bi,Te)

4. $(Pd_{0.97}Pt_{0.04}Au_{0.01}Cu_{0.01})_{1.03}(Bi_{0.84}Te_{0.12}Sb_{0.01})_{0.97}$
5. $(Pd_{0.94}Pt_{0.06}Au_{0.02})_{1.02}(Bi_{0.73}Te_{0.24}Sb_{0.01})_{0.98}$

Moncheite - insizwaite Pt $(Te,Bi)_2$

6. $(Pt_{0.95}Ag_{0.02}Pd_{0.01}Au_{0.01})_{0.99}(Te_{1.17}Bi_{0.83}Sb_{0.01})_{2.01}$

Note: Rh, Os, Ru, Ir, S, Pb, Sn, Ni, Co, Fe, As were not detected;
- below detection limit;
No 1-2 calculated on basis of 10 atoms
No 3 calculated on basis of 4 atoms
No 4-5 calculated on basis of 2 atoms
No 6 calculated on basis of 3 atoms
* H_2O calculated by difference

TABLE 50. CHEMICAL COMPOSITION OF MERTIEITE-II INCLUSIONS IN Pt-Fe MACROCRYSTALS

	Mertieite-II		
	1	2	3
wt.%			
Rh	0.14	0.25	-
Pd	66.33	66.52	67.57
Sn	2.27	2.33	0.13
Sb	27.07	27.00	28.77
Te	0.18	0.14	0.11
Au	-	0.49	-
Pt	3.00	1.81	2.86
Cu	0.90	1.53	1.02
As	0.20	0.19	0.64
Total	100.09	100.26	101.10
at.%			
Rh	0.15	0.26	-
Pd	69.27	68.81	69.59
Sn	2.12	2.16	0.12
Sb	24.71	24.41	25.89
Te	0.16	0.12	0.10
Au	-	0.28	-
Pt	1.71	1.02	1.60
Cu	1.58	2.64	1.76
As	0.30	0.30	0.94
Total	100	100	100

Formulae

Mertieite-II

1. $(Pd_{7.62}Pt_{0.19}Cu_{0.17}Rh_{0.02})_{8.00}(Sb_{2.72}Sn_{0.23}As_{0.03}Te_{0.02})_{3.00}$
2. $(Pd_{7.57}Pt_{0.11}Cu_{0.29}Rh_{0.03}Au_{0.03})_{8.03}(Sb_{2.69}Sn_{0.24}As_{0.03}Te_{0.01})_{2.97}$
3. $(Pd_{7.66}Pt_{0.18}Cu_{0.19})_{8.03}(Sb_{2.85}Sn_{0.01}Te_{0.01}As_{0.10})_{2.97}$

Note: Fe, S, Os, Bi, Ru, Ag, Ir, Co were not detected;
- below detection limit

TABLE 51. CHEMICAL COMPOSITION OF SULFIDE INCLUSIONS IN Pt-Fe MACROCRYSTALS

Mineral	Bornite		Chalcopyrite		Chalcocine		Co-pentlandite	
No	1	2	3	4	5	6	7	8
wt.%								
S	25.72	25.49	33.81	34.17	20.34	20.63	33.07	32.19
Fe	10.56	9.72	28.79	28.71	1.64	0.73	26.50	26.54
Cu	64.02	64.33	35.37	35.94	77.68	80.07	-	-
Ni	-	-	-	-	-	-	33.80	33.06
Co	-	-	-	-	-	-	6.25	6.36
Au	-	0.66	-	-	-	-	-	-
Pt	-	-	-	-	0.54	-	-	-
Total	100.30	100.20	97.97	98.82	100.20	101.43	99.62	98.15
apfu								
on basis of 10 atoms			*of 4 atoms*		*of 3 atoms*		*of 17 atoms*	
S	4.01	4.01	1.98	1.99	1.01	1.01	8.01	7.94
Fe	0.95	0.88	0.97	0.96	0.05	0.02	3.69	3.76
Cu	5.04	5.10	1.05	1.05	1.94	1.97	-	-
Ni	-	-	-	-	-	-	4.48	4.45
Co	-	-	-	-	-	-	0.82	0.85
Au	-	0.02	-	-	-	-	-	-
Pt	-	-	-	-	0.01	-	-	-

Note: Pb, Bi, Ru, Rh, Pd, Ag, Sn, Sb, Te, Ir, As were not detected
- below detection limit

7.5 DISCUSSION

There is a distinct difference between small xenomorphic and coarse idiomorphic Pt-Fe alloy crystals of the Kondyor massif, both in terms of chemical composition and mineral inclusions. Xenomorphic Pt-Fe alloy grains contain microinclusions of Ir, Ru, Os and Pt solid solutions rimmed by erlichmanite-laurite and irarsite-hollingworthite (Nekrasov et al. 1999). The main oxide inclusion in matrix Pt-Fe alloy is chromite. The characteristic chemical and mineralogical features of the coarse crystals are different, as noted below.

1. Very low abundances of PGE impurities

The PGE concentrations other than platinum are very low. Our reconnaissance proton-microprobe data indicate around 150 ppm Pd, 100 ppm Rh, and 20 ppm Ru. Osmium and iridium are below the analytical detection limit of the electron microprobe, i.e., <1500 ppm. The earlier ion microprobe study by Cabri et al. (1998) gave <<1 ppm Os.

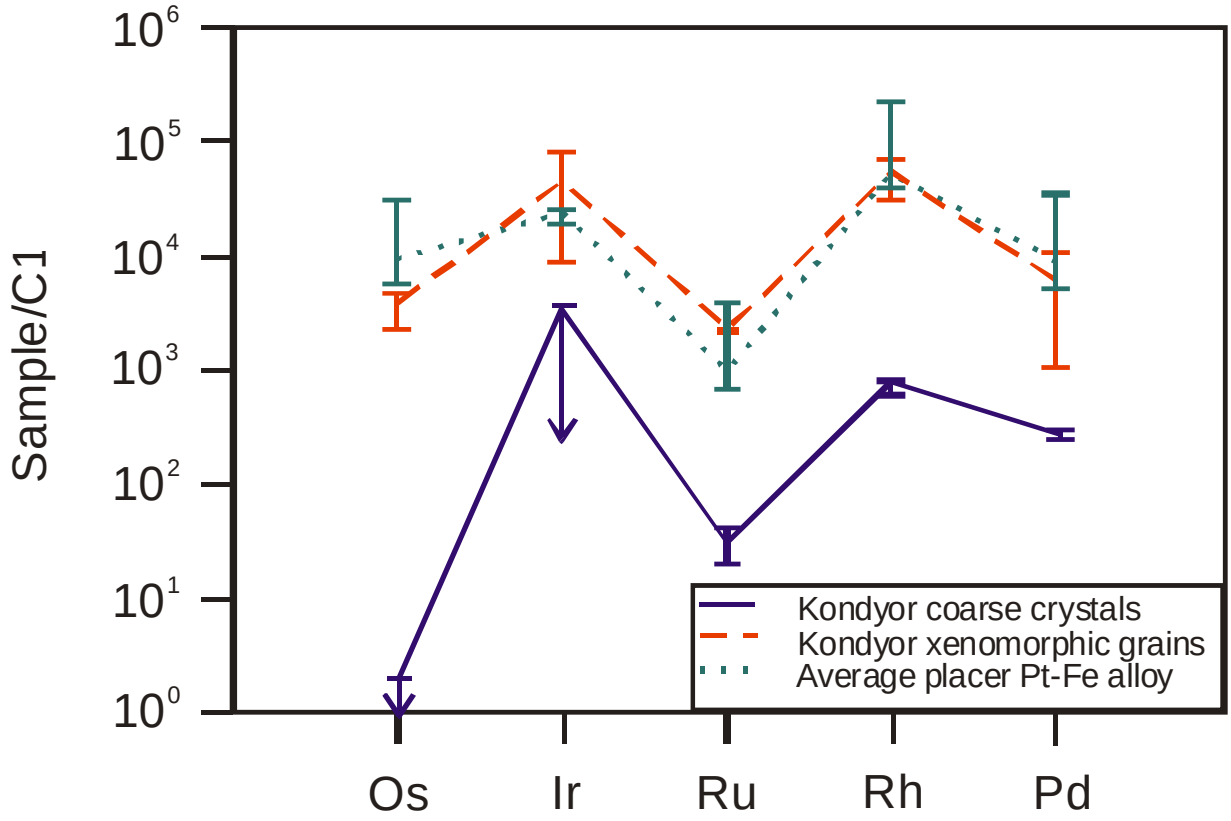

Fig. 74. *Chondrite-normalized PGE distribution of euhedral Pt-Fe alloy macrocrystals from Kondyor compared to the composition of xenomorphic Pt-Fe alloy grains from Kondyor (n=56) and average placer Pt-Fe alloys (n=1700) from the worldwide compilation of Cabri et al. (1996). Bar graphs show geometric mean ±1 standard deviation. These parameters were generated from log-normal probability graphs which allow limited extrapolation below the analytical detection limit.*
Note that the euhedral macrocrystals from Kondyor have all PGE (except Pt) below the analytical detection limit of the electron microprobe, but also are below the detection limit of ion microprobe analysis for osmium (arrow) (Cabri et al. 1998). The Ru, Rh and Pd data are from proton microprobe analysis (this study). The detection limit for Ir (arrow) is around 1500 ppm for both electron and proton microprobe analysis.

A compilation of about 1700 compositional data on Pt-Fe alloy from about 30 occurrences worldwide shows that only 55 samples have Os values below the detection limit of electron-microprobe analysis (Cabri et al. 1996). However, such samples are invariably high in Ir, Rh, Pd and Cu. The evaluation of the data set from Cabri et al. (1996) with a log-normal probability graph technique which allows limited extrapolation below detection limits. The geometric means and one standard deviation range are: 0.45 wt.% Os (0.3-1.0), 1.0 wt.% Ir (0.3-3.0), 0.07 wt.% Ru (0.02-0.2), 1.1 wt.% Rh (0.4-1.7) and 0.65 wt.% Pd (0.2-1.2). The trace-element composition

of the coarse Pt-Fe alloy crystals is at least one order of magnitude lower than from all other Pt-Fe alloy occurrences (Fig. 74).

Evaluation of the data set for the xenomorphic Pt-Fe alloy from Kondyor (n=56) in log-normal probability graphs is also done. The geometric means and one standard variation ranges are: ≈0.1 wt.% Os (<0.1-0.2), 1.2 wt.% Ir (0.1-4.5; bimodal), <<0.1 wt.% Ru, 0.6 wt.% Rh (0.45-1.2), 0.18 wt.% Pd (<0.1-0.5). These data indicate that the xenomorphic Pt-Fe alloy is relatively low in PGE when compared to the world average, but still at least one order of magnitude higher than in the macrocrystals.

2. Enrichment in tin and antimony

The macrocrystals studied have a composition in the range $Pt_{2.4-2.6}Fe$, with 0.66 ± 0.15 wt.% Cu, 0.07 ± 0.02 wt.% Ni, 0.11 ± 0.11 wt.% Sb, and 0.19 ± 0.11 wt.% Sn (arithmetic mean ± 1 standard deviation). The presence of the trace elements Ge, Zn, Te, and Cs at the ppm to hundred ppm levels is indicated by proton microprobe analysis. Most remarkable are the high contents of Sb and Sn, with around 2000 ppm Sn and up to 3600 ppm Sb. These two elements are consistently below the detection limit of the electron microprobe for xenomorphic Pt-Fe alloy.

3. Absence of Ir-, Rh-, Os- bearing minerals

Microinclusions of Ir, Ru, Os and Pt solid solutions are typical of the xenomorphic Pt-Fe alloy (Nekrasov et al. 1999), but completely absent from the coarse Pt-Fe crystals. This mineralogical observation is reflected in the very low PGE abundances in the Pt-Fe crystals.

4. Absence of chromite inclusions

Chromite inclusions are typical of the xenomorphic Pt-Fe alloy and indicate a dunite affiliation (Nekrasov et al. 1999). Such inclusions have not been seen in the macrocrystals. Instead, fluorapatite was repeatedly observed, together with chromian titanian magnetite, titanite, manganoan ilmenite, and chalcopyrite-bornite intergrowth aggregates. This mineral association is unusual for dunites, but characterizes pyroxenites and contact zones between pyroxenites and dunites (Nekrasov et al. 1994).

5. Fluorapatite inclusions

The apatite inclusions in the macrocrystals have 2-3 wt.% F and chlorine content below the analytical detection limit (0.05 wt.% Cl), indicating a high F/Cl environment of crystal growth, typical of evolved magmatic environments. Fluoapatite was described as a cumulus phase from the Stillwater and Bushveld layered mafic intrusions (Boudreau et al. 1986). By contrast, Cl-rich

apatite is typical of interstitial and vein occurrences in both intrusions and characterizes a hydrothermal environment (Boudreau et al. 1986). The complementary distribution pattern of chlorine and fluorine results from the contrasting partitioning behavior of these two elements, with strong preference of Cl for aqueous fluid phases, whereas F partitions preferentially into the melt phase (Holland 1972; Manning and Pichavant 1988). Thus, the fluorapatite inclusions suggest formation of the Pt-Fe alloy crystals in a non-hydrothermal environment, i.e. in a melt system.

6. Hydrothermal overprint by chlorine- and alkali-rich Au-Pd-base metal-bearing fluids

The complex gold-rich rim mainly consists of four varieties of gold alloy: tetra-auricupride, Au-Ag alloy, Au-Ag-Pd-Cu alloy, Au-Pd-Cu alloy. Tetra-auricupride is the main gold-bearing phase, characterized by Pd (0.78-3.86 wt.%) and Pt (0.67-13.9 wt.%) content. Gold-silver alloy has a variable composition from native gold (97 wt.% Au) up to Au-Ag alloy (47 wt.% Au). Myrmekitic intergrowth structures of Au-Ag-Cu-Pd alloys are typical.

Cupriferous gold is very rare in nature and seems to be associated with hydrothermal alteration or weathering of mafic-ultramafic rocks (Knipe and Fleet 1997). The formation of tetra-auricupride is accompanied by hydrothermal alteration of titanian magnetite to a Cl-rich titanite-like phase on fractures in titanian magnetite (Sample I), which suggests a chlorine-rich environment. The precious- and base-metal assemblage is intergrown with the hydrothermal mineral assemblage of quartz, albite, orthoclase, andesine as well as aegirine-augite, clinochlore, smectite and chamosite.

The secondary rim hosts a great variety of PGM phases. They are mainly represented by Pd stannides, antimonides and tellurobismuthides. Copper-bearing and Cu-free Pd stannides occur as complex zonal aggregates of tatyanaite rimmed by taimyrite and intergrown with minerals of the atokite-rustenburgite series. Genkin and Evstegneeva (1986) described a similar mineral paragenesis at the Noril’sk complex, Russia, namely formation of stannopaladinite (Pd-Sn-Cu) after rustenburgite (Pt-Sn) through atokite (Pd-Sn). The detailed study by Barkov et al. (2000) of the zoned intergrowth of Pt-Pd-Cu compounds from the same occurrence shows the following sequence of crystallization: atokite – rustenburgite → tatyanaite → Pt-rich taimyrite → Pt-poor taimyrite, and inferred that this process was controlled by a decrease in temperature and increase in Cu activity. The observations on natural samples are in a agreement with the experimental work of Evstigneeva and Nekrasov (1980) who studied the hydrothermal Pd-Cu-Sn-Cl system at 300-400°C and found that Pd-(Pt)-Cu stannides formed later than Cu-free compounds. A similar situation applies to the reaction assemblages studied from Kondyor. The gold-rich rim of sample II has relics of the atokite-rustenburgite series within minerals of the taimyrite-tatyanaite solid

solution (Fig. 68). Sample I shows the formation of tatyanaite (Pt-rich compound) followed by later taimyrite (Pd-rich compound) (Fig. 67a,b).

Antimonides, represented by mertieite-II, generally occur as relatively large inclusions in the gold-bearing rims. Occasionally, intergrowths with atokite and Te-sobolevskite developed along fractures (Fig. 69). Tellurobismuthides consist of Te-sobolevskite and an intermediate member of the moncheite-insizwaite solid solution.

7.6 CONCLUSIONS

The above observations and interpretations allow to tentatively propose a genetic model for the formation of the Pt-Fe alloy macrocrystals. One important geological constraint is the fact that these crystals are confined to the outcrop area of apatite-magnetite-phlogopite clinopyroxenite dikes within dunite in the Anomal'niy Creek and its secondary dispersion pattern (Nekrasov et al. 1999). The inclusion assemblage of the coarse Pt-Fe alloy crystals also suggests a petrogenetic association with the late apatite-magnetite-phlogopite clinopyroxenite bodies, but not with the dunite main intrusion. The latter is in agreement with the suggestion by Malitch and Thalhammer (2002) that the cell type of Pt_3Fe minerals depends on the host rock and that ferroan platinum is characteristic for clinopyroxenite.

The large size of the crystals could be related to crystal growth in a pegmatitic environment with a protracted magmatic evolution, i.e. from residual liquids which eventually reached fluid saturation. The latter possibly promoted the formation of miaroles or interstitial space where coarse-grained idiomorphic PGM could form at relatively low temperature. A similar setting applies to the Tweefontein area in South Africa, where large euhedral crystals of sperrylite up to 1.85 cm across occur in granite pegmatite and on shear zones in ironstone country-rocks of the Platreef (Wagner 1929). The coarse sperrylite crystals were interpreted as of late-stage magmatic-hydrothermal origin (Cawthorn et al. 1998).

The extreme fractionation of platinum from the other PGE in the coarse Pt-Fe alloy crystals is a matter of speculation. The solubilities of Pt and Os, Ir or Rh in a sulfur-free silicate melt are not dramatically different (Borisov and Palme 1997; Borisov and Walker 2000; Ertel et al. 1999). However, experimental data on the metal/silicate melt partition coefficient indicate that D (Pt) is 3-4 orders of magnitude higher than D (Os) at 1300-1400°C (Borisov and Walker 2000). This effect may be even larger at lower temperature and could possibly produce the huge separation of platinum from osmium (and the geochemically similar Ir, Ru, Rh). The low Pd content could be explained by the much higher solubility of Pd, compared to all other PGE, in silicate melt

which is similar to the solubility of Au (Borisov and Palme 1996). The Pd-Au component and base metals is then fractionated into the aqueous fluid phase on fluid saturation.

The coarse Pt-Fe alloy crystals have undergone hydrothermal overprint by NaCl-rich gold-silver-palladium-copper-bearing solutions, which produced intermetallic aggregates of gold-bearing alloy (tetra-auricupride) as well as Pd-bearing intermetallides. The aqueous solutions also had a minor but characteristic bismuth-tin-antimony-tellurium component. The element spectrum of this overprint and alteration stage is typical of late magmatic-hydrothermal fluids.

EPILOGUE AND OUTLOOK

The present mineralogical study aims providing new data on very selected platinum-group minerals from five occurrences of different geological setting. This work is largely descriptive, and severely limited by the sample material studied from the collections of the Far East Geological Institute in Vladivostok, as well as by fragmentary information on the geological field situation. All samples are handpicked mineral grains from alluvial heavy-mineral concentrates, which involves a problem of representativety and mineral survival during weathering and alluvial transport. Nevertheless, given the relatively low level of knowledge on the PGM mineralogy of Uralian/Alaskan-type intrusions, and those of the Russian Far East in particular, some new findings of regional and broader interest are:

- Identification of Uralian/Alaskan-style PGM mineralization in Primorye (Zolotaya and Fadeevka rivers):

  The primary PGM mineralogy, i.e. mainly Pt-Fe alloy, minor Os-Ir alloy, diagnostic Rh signature (as minor element in Pt-Fe alloy and in the mineral inclusion assemblage in laurite-erlichmanite) and inclusions of low-Ni cooperite, point to a Uralian/Alaskan primary source for PGM mineralization.

  The composition of chromian spinel from the Fadeevka and Zolotaya placers, both as inclusions in PGM and in individual crystals in heavy mineral concentrates, is identical with chromian spinel from the little exposed Late Permian dunite-hornblendite-gabbro complex within the same area (high-Cr, low-Ti), which identifies this zoned intrusion as PGM source.
- Primary PGM composition in both placers is strongly affected by hydrothermal alteration: The magmatic platinum-group minerals (Pt-Fe alloy, Os-Ir alloy; and inclusions of laurite-erlichmanite solid solution [OsS_2-RuS_2], cherepanovite-ruthenarsenite solid-solution series [RhAs-(Ru,Ni)As], cooperite, vysotskite-braggite solid solution, cuprorhodsite-cuproiridsite-malanite solid solution, bowieite, vasilite and keithconnite) are affected by fluid overprint during which As, Sb, Bi, Au and S are introduced. The secondary mineral assemblage is characterized by cooperite (II), irarsite, sperrylite, kashinite, $(Rh,Pt)_3S_4$ phase, platarsite-hollingworthite-irarsite solid solution, stumpflite, mertieite-II, IrSbAs phase, tolovkite, maslovite, $(Ir,Os)_7As_3$ phase, $(Ir,Os)_2As_3$ phase, and Au-bearing alloy. Intermetallic compounds of Sn, Bi, Pt and Ir formed first, followed by tellurides and Sb-As phases, and terminated by As-S bearing phases. Several of these phases are yet unknown minerals, but their crystallographic characterization is hindered by the small grain size in the µm range. The hydrothermal overprint is probably related to the particular geological situation in the

Zolotaya and Fadeevka area, where the ultramafic-mafic host rocks of primary PGM mineralization are intruded by abundant granite magmatism.

- Discovery of PGE mineralization in the Kedrovka river alluvium, Primorye: The first PGM found in the drainage system of the Kedrovka river consist of dominantly iridium alloy with subordinate osmium alloy and inclusions of the laurite-erlichmanite solid solution series. The absence of Pt-Fe alloy and chemical composition of chromian spinel suggest an ophiolitic PGM source.
- Multiphase inclusion assemblage consists of Pd-rich minerals (vysotskite-braggite-cooperite solid solution and vasilite), Rh-rich minerals (cuprorhodsite-malanite-cuproiridsite solid solution and bowieite), and BMS (bornite, pyrrhotite, pentlandite, millerite and chalcopyrite) within the primary Pt-Fe and Os-Ir alloy grains prove existence of a sulfide melt unusually enriched in PGE, particularly in Pd and Rh, which formation caused by sulfide-sulfide liquid immiscibility.

The mineralogical study of PGM from the Aldan Shield (Kondyor and Darya) was focussed on an intriguing style of mineralization, i.e. the exotic occurrence of PGM macrocrystals. Macrocrystals of Pt-Fe alloy were known so far from Kondyor only, and the complex inclusion and reaction assemblage was never described. A heavy-mineral concentrate from Darya proved to have many similarities to the Kondyor PGM mineralization, which both are related to Uralian/Alaskan-style zoned alkaline intrusions, 75 km apart.

- PGM macrocrystals (>1 mm in size) in the Darya PGE-Au placer: The occurrence (second in the world, after Kondyor) of Pt-Fe alloy macrocrystals is confirmed. Further exotic macrocrystals from Darya are mertieite-II and cooperite (both occurrences are unique so far).
- Composition of PGM macrocrystals from Darya and Kondyor: A particular feature of the Pt-Fe alloy macrocrystals is their extremely low content in PGE besides Pt, which is distinctly different from the common xenomorphic and clearly magmatic Pt-Fe alloy. The origin of these macrocrystals is not known, but medium- to coarse-grained pegmatoidal clinopyroxenite bodies were suggested as source. The formation of the large euhedral PGM crystals could then be related to residual pegmatitic fluids at much lower temperature than in typical magmatic PGE deposits.
- Hydrothermal overprint of PGM macrocrystals: A complex reaction assemblage was identified which includes variable Au-rich alloy phases (basically the very rare tetra-auricupride), which contain Pd stannides, antimonides and tellurobismuthides (inclusions of tatyanaite rimmed by taimyrite and intergrown with minerals of the atokite-rustenburgite

series and moncheite-insizwaite series, and inclusions of mertieite-II occasionally intergrown with atokite and Te-sobolevskite).

- Weathering of PGM macrocrystals: Mertieite-II crystals display a broad variation range of unusual and complex Pd-oxides/hydroxides which are located in the distinct crystallographical planes of mertieite-II. These Pd-oxides are relatively high (several wt.%) in Pt, Sb, Fe, Te, Bi, with traces of Sn, As, and Cu. Some phases also contain Hg. Another interesting textural feature is the dissolution of inclusions of Pt-Fe alloy in Os-Ir alloy and replacement by gold. This process could be of hydrothermal or supergene origin, and appears to be controlled by elctrochemistry, i.e. the more noble character of gold compared to Pt (and Fe).

The minerogenetic interpretation of the many observations and data on the five PGM occurrences studied would require petrological information and an understanding of the petrogenesis of the PGM host rocks which is beyond the scope of this thesis. However, the subject of formation of Uralian/Alaskan-type zoned alkaline intrusions, and of PGE-Au mineralization is such intrusions, as well as in the better known Bushveld-type layered mafic intrusions, is still much under debate. Particularly, the role of sulfide saturation for PGE enrichment is an important and conversely discussed topic, because Uralian/Alaskan-type intrusions with their PGM inventory dominated by metal alloys do not have sulfide levels indicative of sulfide saturation. Therefore, the PGE enrichment process in such intrusions is enigmatic. However, the much better known Bushveld Complex also is distinctly undersaturated in sulfur and it may well be that the sulfur deficiency in these intrusions is related to degassing (Cawthorn 2005), in which case the magmatic PGM composition could dramatically change. The combination of textural observation by ore microscopy/microprobe analysis with experimental petrology will be critical in unravelling the evolution of PGE-bearing systems. The complex mineralogy and reaction assemblages of some PGM documented here, point to a similarly complex petrological evolution of their host rocks.

8 REFERENCES

Ahmed, A.H. and Arai, S. (2003) Platinum-group minerals in podiform chromitites of the Oman ophiolite. *Can. Mineral.*, **41**, 597-616.

Anan'ev, S.A., Anan'eva, T.A., Garanin, V.K. and Kudryavzeva, G.P. (1998) Precious corundums and zircons from the Primorye's placers. *Zap. Vsesouzn. Mineral. Obshch.*, **4**, 120-124 (in Russ.).

Annert, E.E. (1928) *Natural resources of the Far East.* Akz. o-vo "Knizchnoe delo", Khabarovsk-Vladivostok, 930 p. (in Russ.).

Augé, T. and Legendre, O. (1992) Alluvial platinum-group minerals from alluvial deposits in eastern Madagascar. *Can. Mineral.*, **30**, 983-1004.

Augé, T. and Legendre, O. (1994) Platinum-group element oxides from the Pirogues ophiolitic mineralization, New Caledonia: origin and significance. *Econ. Geol.*, **89**, 1454-1468.

Augé, T. and Maurizot, P. (1995) Stratiform and alluvial platinum mineralization in the New Caledonia ophiolite complex. *Can. Mineral.*, **33**, 1023-1045.

Augé, T., Salpeteur, I., Bailly, L., Mukherjee, M. and Patra, R.N. (2002) Magmatic and hydrothermal platinum-group minerals and base-metal sulfides in Baula complex, India. *Can. Mineral.*, **40**, 277-309.

Barkov, A.Y., Halkoaho, T.A.A., Laajoki, K.V.O., Alapieti, T.T. and Peura, R.A. (1997) Ruthenian pyrite and nickeloan malanite from the Imandra layered complex, northwestern Russia. *Can. Mineral.*, **35**, 887-897.

Barkov, A.Y., Halkoaho, T.A.A., Roberts, A.C., Criddle, A.J., Martin, R.F., Papunen, H. (1999) New Pd-Pb and Pb-V oxides from a bonanza-type PGE-rich, nearly BMS-free deposit in the Penikat layered complex, Finland. *Can. Mineral.*, **37**, 1507-1524.

Barkov, A.Y., Martin, R.F., Halkoaho, T.A.A. and Poirier, G. (2000) The mechanism of charge compensation in Cu-Fe-PGE thiospinels from the Penikat layered intrusion, Finland. *Am. Mineral.*, **85**, 694-698.

Barnes, S.J. and Roeder, P.L. (2001) The range of spinel composition in terrestrial mafic and ultramafic rocks. *Jour. Petrol.*, **42**, 2279-2302.

Borisov, A. and Palme, H. (1996) Experimental determination of the solubility of Au in silicate melts. *Mineral. Petrol.*, **56**, 297-312.

Borisov, A. and Palme, H. (1997) Experimental determination of the solubility of platinum in silicate melts. *Geochim. Cosmochim. Acta*, **61**, 4349-4357.

Borisov, A. and Walker, R.J. (2000) Os solubility in silicate melts: New efforts and results. *Am. Mineral.*, **85**, 912-917.

Bottrill, R. S. (1993) Update to the Minerals of Tasmania, Part 2: Sulphides and Related Minerals. *J. Mineral. Soc. Tasmania,* **5**.

Boudreau, A.E., Mathez, E.A. and McCallum, I.S. (1986) Halogen geochemistry of the Stillwater and Bushveld Complexes: evidence for transport of the platinum-group elements by Cl-rich fluids. *J. Petrol.,* **27**, 967-986.

Britvin, S.N., Rudashevskiy, N.S., Bogdanova, A.N. and Shcherbachev, D.K. (1999) Palladodimite $(Pd,Rh)_2As$ — a new mineral from the River Miass (Ural) placer. *Zap. VMO*, **128** (2), 39-42 (in Russ,).

Cabral, A.R. and Lehmann, B. (2003) A two-stage process of native palladium formation at low temperatures: evidence from a palladian gold nugget (Gongo Soco iron ore mine, Minas Gerais, Brazil). *Mineral. Mag.*, **67**, 453-463.

Cabral, A.R., Lehmann, B., Kwitko, R., and Cravo Costa, C.H. (2002a) Palladium and platinum minerals from the Serra Pelada Au-Pd-Pt deposit, Carajás mineral province, Northern Brazil. *Can. Mineral.*, **40**, 1451-1463.

Cabral, A.R., Lehmann, B., Kwitko, R., Galbiatti, H.F. and Pereira, M.C. (2002b) Palladseite and its oxidation: evidence from Au-Pd vein-type mineralization (jacutinga), Cauê iron-mine, Quadrilátero Ferrifero, Minas Gerais, Brazil. *Mineral. Mag.*, **66(2)**, 327-336.

Cabral, A.R., Lehmann, B., Kwitko, R., and Jones, R.D. (2002c) Palladian gold and palladium arsenide-antimonide minerals from Gongo Soco iron ore mine, Quadrilátero Ferrifero, Minas Gerais, Brazil. *Transac. Inst. Min. Metall., Sec. B: Applied Earth Science*, **111**, B74-B80.

Cabral, A.R., Lehmann, B., Kwitko-Ribeiro, R., Jones, R.D. and Rocha Filho, O.G. (2003) On the association of palladium-bearing gold, hematite and gypsum in an *ouro preto* nugget. *Can. Mineral.*, **41**, 473-478.

Cabral, A.R., Lehmann, B., Grambole, D., Herrmann, F. (2004) Hydrogen in natural Pd-O compounds from Gongo Soco, Minas Gerais, Brazil. *Can. Mineral.*, **42**, 689-694.Cabri, L.J. (2002) The platinum-group minerals. *The geology, geochemistry, mineralogy and mineral beneficiation of platinum-group elements* (L.J. Cabri, ed.). Can. Inst. Min. Metall. Petrol., Spec. Vol., **54**, 13-129.

Cabri, L.J. and Feather, C.E. (1975) Platinum-iron alloys: a nomenclature based on a study of natural and synthetic alloys. *Can. Mineral.*, **13**, 117-126.

Cabri, L.J. and Laflamme, J.H.G. (1997) Platinum-group minerals from the Konder Massif, Russ. Far East. *Mineral. Rec.*, **28**, March-April, 97-106.

Cabri, L.J., Griddle, A.J., Laflamme, J.H.G., Bearne, G.S. and Harris, D.C. (1981) Mineralogical study of complex Pt-Fe nuggets from Ethiopia. *Bull. Minéral.* **104**, 508-525.

Cabri, L.J., Harris, D.C. and Weiser, T.W. (1996) Mineralogy and distribution of platinum mineral (PGM) placer deposits of the world. *Explor. Min. Geol.*, **5**, 73-167.

Cabri, L.J., Stern, R.A. and Czamanske, G.K. (1998) Osmium isotope measurements of Pt-Fe alloy placer nuggets from the Konder intrusion using a Shrimp II ion microprobe. *8th Intern. Platinum Symp., Abstracts*, 55-58.

Cawthorn, G (2005) Contrasting sulphide contents of the Bushveld and Sudbury igneous complexes. *Mineral. Depos*., in print.

Cawthorn, G., Lee, C., McDonald, I., Tredoux, M. and White, J. (1998) Field excursion to the Bushveld Complex 3-9 July 1998. *Excursion Guide, 8th Plat. Symp.*

Clark, A.M., Griddle, A.J., Fejer, E.E. (1974) Palladium arsenide-antimonides from Itabira, Minas Gerais, Brazil. *Mineral. Mag.*, **39**, 528-543.

Corrivaux, L. and Laflamme, J.H.G. (1990) Mineralogy of platinum-group elements in chromitites in ophiolites at Thetford Mines, Quebec. *Can. Mineral.*, **28**, 579-595.

Deer, W.A., Howie, R.A., and Zussman, J. (1998) *An introduction to the rock-forming minerals.* Longman, Hong Kong, 549 p.

El'yanov, A.A. and Andreev, G.B. (1991) *Magmatism and metallogeny of the platform provinces of multistage activation.* Novosibirsk, Nauka, 168 p. (in Russ.).

Emelyanenko, E.P., Maslovskiy, A.N., Zalishchak, B.L., Kamaeva, L.V. and Fomenko, A.S. (1989) Regularities of the location of ore mineralization at the Kondyor massif. In: *Geologicheskie usloviya localizatzii endogennogo orudeneniya*, Far Eastern Branch, Academy of Sciences, Vladivostok, 100-113 p. (in Russ.).

Ertel, W., O'Neill, H.S.C., Sylvester, P.J. and Dingwell, D.B. (1999) Solubilities of Pt and Rh in haplobasaltic silicate melt at 1300°C. *Geochim. Cosmochim. Acta,* **63**, 2439-2449.

Esin, S.V. and Peretyatko, Y.V. (1992) Identification of the primary sources of zircons and corundums from the Neozoic friable deposits of the Central Sikhote-Alin. *Geol. Geoph.*, **12**, 93-102. (in Russ.).

Evstigneeva, T.L. and Nekrasov, I.Ya. (1980) Synthesis conditions and phase relationships in the systems Pd-Sn-Cu-HCl and Pd_3Sn-Cu_3Sn. In: *Essays of physicochemical petrology* (Zharikov, V. and Fed'kin, V., eds), 20-35, Nauka, Moscow (in Russ.).

Fehr, T., Hochleiter, R. and Weiss, S. (1995) Sensationell: natürliche Platin-Kristalle aus Sibirien. *Lapis* **20** (10), 44-46.

Fleet, M.E. and Stone, W.E. (1991) Partioning of platinum-group elements in the Fe-Ni-S system and their fractionation in nature. *Geochim. Cosmochim. Acta*, **55**, 245-253.

Fleet, M.E., Chryssoulis, S.L., Stone, W.E. and Weiser, C.G., (1993) Partioning of platinum-group elements and Au in the Fe-Ni-Cu-S system: Experiments on fractional crystallization of sulfide melt. *Contr. Mineral. Petrol.,* **115**, 36-44.

Fleet, M.E., De Almera, C.M. and Angeli, N. (2002) Botryoidal platinum, palladium and potarite from the Bom Sucesso stream, Minas Gerais, Brazil: Compositional zoning and origin. *Can. Mineral.*, **40**, 341-355.

Garuti, G. and Zaccarini, F (1997) In situ alteration of platinum-group minerals at low temperature: evidence from serpentinized and weathered chromitite of the Vourinos complex, Greece. *Can. Mineral.*, **35**, 611-626.

Garuti, G., Gazzotti, M. and Torres-Ruiz, J. (1995) Iridium, rhodium and platinum sulfides in chromitites from the ultramafic massifs of Finero, Italy and Ojen, Spain. *Can. Mineral.*, **33**, 509-520.

Garuti, G., Zaccarini, F., Cabella, R., Fershtater, G. (1997) Occurrence of unknown Ru-Os-Ir-Fe oxides in the chromitites of the Nurali ultramafic complex, Southern Urals, Russia. *Can. Mineral.*, **35**, 1431-1439.

Garuti, G., Zaccarini, F., Moloshag, V. and Alomov, V. (1999) Platinum-group minerals as indicators of sulfur fugacity in ophiolitic upper mantle: an example from chromitites of the Ray-Iz ultramafic complex, polar Urals, Russia. *Can. Mineral.*, **37**, 1099-1115.

Garuti, G., Pushkarev, E. and Zaccarini, F. (2002) Composition and paragenesis of Pt alloys from chromitites of the Uralian-Alaskan-type Kytlym and Uktus complexes, Northern and Central Urals, Russia. *Can. Mineral.*, **40**, 357-376.Gebhard, G., and Schlüter, J. (1996) Zvyagintsevit aus Sibirien: der erste Fund grosser Kristalle eines Palladium-Minerals. *Lapis,* **21** (10), 47-48.

Genkin, A.D. and Evstegneeva, T.L. (1986) Associations of Platinum-Group Minerals of the Noril'sk Copper-Nickel Sulfide Ores. *Econ. Geol.*, **81**, 1203-1212.

Gervilla, F. and Kojonen, K. (2002) The platinum-group minerals in the upper section of the Keivitsansarvi Ni-Cu-PGE deposit, Northern Finland. *Can. Mineral.*, **40**, 377-394.

Gornostayev, S.S., Dodatko, A.D., Laajoki, K.V.O. and Mochalov, A.G. (2000) Origin of platinum-bearing placer in the Aluchin Horst, Russ. Far East. *Econ. Geol.*, **95**, 549-558.

Gurovitch, V.G., Zemlyanukhin, V.N., Emelyanenko, E.P., Karetnikov, A.S., Kvasov, A.I., Lazarenkov, V.G., Malitch, K.N., Mochalov, A.G., Prikhod'ko, V.S., and Stepashenko, A.A. (1994) *Geology, petrology and ore presence of the Kondyor massif.* (Kosigin, Yu.A. and Prikhod'ko, V.S. eds.) Moscow, Nauka, 176 p. (in Russ.).

Hagen, D., Weiser, Th. and Than Htay, (1990) Platinum-group minerals in Quaternary gold placers in the upper Chinwin area of northern Burma. *Mineral. Petrol.*, **42**, 265-286.

Harris, D.C. and Cabri, L.J. (1991) Nomenclature of platinum-group-element alloys: review and revision. *Can. Mineral.*, **29**, 231-237.

Himmelberg, G.R. and Loney, R.A. (1995) Characteristics and petrogenesis of Alaskan-type ultramafic-mafic intrusions, Southeastern Alaska. *US Geol. Surv. Prof. Paper*, **1564**, 1-47.

Holland, H.D. (1972) Granites, solutions and base metal deposits. *Econ. Geol.*, **67**, 281-301.

Ivanov, O.K. (1997) *Concentrically zoned pyroxenite-dunite massifs of Ural.* Ekaterinburg, Ural University, 488 p. (in Russ.).

Jackson, J.A., ed. (1997) *Glossary of geology*. Fourth edition. American Geological Institute, Washington.

Jedwab, J. (1995) Oxygenated platinum-group-element and transition-metal (Ti, Cr, Mn, Fe, Co, Ni) compounds in the supergene domain. *Chron. rech. min*., **520**, 47-53.

Jedwab, J. (1999) *Unconventional Platinum Group Minerals (UPGM).* http://www.ulb.ac.be/sciences/upgm/intro.html

Jedwab, J. and Cassedanne, J. (1998) Historical observations on oxygen-bearing compounds of platinum and palladium in Minas Gerais, Brazil. *Can. Mineral.*, **36**, 887-893.

Jochum, K.P., Dingwell, D.B., Rocholl, A., Stoll, B., Hofman, A.W., Becker, S., Besmehn, A., Bessette, D., Dietze, H.J., Dulski, P., Erzinger, J., Hellebrand, E., Hoppe, P., Horn, I., Janssens, K., Jenner, G.A., Klein, M., McDonough, W.F., Maetz, M., Mezger, K., Muenker, C., Nikogosian, I.K., Pickhardt, C., Raczek, I., Rhede, D., Seufert, H.M., Simakin, S.G., Sobolev, A.V., Spettel, B., Straub, S., Vincze, L., Wallianos, A., Weckwerth, G., Weyer, S., Wolf, D. and Zimmer, M. (2000) The preparation and preliminary characterisation of eight geological MPI-DING reference glasses for in-situ microanalysis. *Geostand. Newsl.*, **24**, 1, 87-133.

Johan, Z. (2002) Alaskan-type complexes and their platinum-group element mineralization. In: *The geology, geochemistry, mineralogy and mineral beneficiation of platinum-group elements* (L.J. Cabri, ed.). Can. Inst. Min., Metall. Petrol., Spec. Vol. **54**, 669-719.

Johan, Z., Ohnenstetter, M., Fisher, W. and Amosse, J. (1990) Platinum-group minerals from the Durance River alluvium, France. *Mineral. Petrol.*, **42**, 287-306.

Johan, Z., Ohnenstetter, M., Slansky, E., Barron, L.M. and Suppel, D. (1989) Platinum mineralization in Alaskan-type intrusive complexes near Fifield, New South Wales, Australia. Part 1. Platinum-group minerals in clinopyroxenites of the Kelvin Grove prospect, Owendale intrusion. *Mineral. Petrol.*, **40**, 289-309.

Johnson Matthey (2004) *Platinum 2004*. London, Johnson Matthey, 56 p.

Kaminskiy, F.V., Kluev, Yu.I., Prokopchuk, B.I., Shcheka, S.A., Smirnov, V.I., Ivanovskaya, I.N. (1978) First carbonado and new ballas find in the Soviet Union. *Transact. Doklady USSR*, **242 (**1-6), 152-155.

Kemkin, I.V. and Filippov, A.N. (2001) Structure and genesis of the lower structural unit of the Samarka Jurassic accretionary prism (Sikhote-Alin, Russia). *Geodiversitas*., **23**, (3). 323-339.

Khanchuk, A.I., Ratkin, V.V., Ryazantseva, M.D., Golozubov, V.V., and Gorokhova N.G. (1996) *Geology and mineral deposits of Primorskiy krai (Territory).* Vladivostok, Dalnauka, 61 p.

Knipe, S.W. and Fleet, M.E. (1997) Gold-copper alloy from the Kerr mine, Ontario. *Can. Mineral.*, **35**, 573-586.

Makovicky, E. (2002) Ternary and quaternary phase systems with PGE. *In The geology, geochemistry, mineralogy and mineral beneficiation of platinum-group elements* (L.J. Cabri, ed.). Can. Inst. Min., Metall. Petrol., Spec. Vol. **54**, 131-175.

Malitch, K.N. (1999) *Platinum-group elements in clinopyroxenite-dunite massifs of East Siberia (geochemistry, mineralogy, and genesis).* St-Petersburg, Saint Petersburg Cartographic Factory VSEGEI Press, 296 p. (in Russ.)

Malitch, K.N. and Thalhammer, O.A.R. (2002) Pt-Fe nuggets derived from clinopyroxenite-dunite massifs, Russia: a structural, compositional and osmium-isotope study. *Can. Mineral.*, **40**, 395-418.

Malitch, K.N., Melcher, F. and Mallhaus, H. (2001) Palladium and gold mineralization in podiform chromitite at Kraubath, Austria. *Mineral. Petrol.*, **73**, 247-277.

Manning, D.A.C. and Pichavant, M. (1988) Volatiles and their bearing on the behavior of metals in granitic systems. In: *Recent advances in the geology of granite-related mineral deposits* (Taylor, R.P. and Strong, D.F. eds). Can. Inst. Min. Metall. Petrol., Spec. Vol. **39**, 13-24.

Maxwell, J.A., Campbell, J.L. and Teesdale, W.J. (1989) The Guelph software package. *Nucl. Instrum. Meth. Phys. Resear.*, **B43**, 218-230.

Maxwell, J.A., Teesdale, W.J. and Campbell, J.L.(1995) The Guelph software package II. *Nucl. Instrum. Meth. Phys. Resear.*, **B95**, 407-421.

McElduff, B. and Stumpfl, E.F. (1990) Platinum-group minerals from the Troodos ophiolite, Cyprus. *Mineral. Petrol.* **42**, 211-232.

McDonald, I., Ohnenstetter, D., Ohnenstetter, M. and Vaughan, D.J. (1999) Palladium oxides in ultramafic complexes near Lavatrafo, Western Andriamena, Madagascar. *Mineral. Mag.*, **63(3)**, 345-352.

Mochalov, A. G. (1994) Mineralogy of platinum-group elements from dunite. In: *Geology, petrology and ore presence of the Kondyor massif* (Kosigin, Y.A., ed.), Moscow, Nauka 92-106 (in Russ.).

Mochalov, A.G. (1997) Platinum metals placers. In: *Placer deposits of Russia and CIS countries.* (Laverov, N.P. and Patyk-Kara, N.G. eds), Moscow, Nauch. Mir, 27-163 (in Russ.).

Mochalov, A.G. (2001) "Heavy concentrate platinum" from the placers of the Russ. Far East. Abstract of doctoral thesis. Moscow, IGEM, 48 p. (in Russ.)

Molchanov, V.P., Sapin, V.I. and Khomich, V.G. (2001) On types of gold and platinum sources from the Fadeevka ore district, Primorye. *Genesis mestorozhdeniy zolota i metodi dobichi blagorodnikh metallov.* Blagoveshchensk, Abstract, 74-76 (in Russ.).

Nakagawa, M. and Franco, H.E.A. (1997) Placer Os-Ir-Ru alloys and sulfides: indicators of sulphur fugacity in an ophiolite? *Can. Mineral.,* **35**, 1441-1452.

Naldrett, A.J. (1989) Stratiform PGE deposits in layered intrusions. *Rev. Econ. Geol.* **4**, 135-166.

Nekrasov, I.Ya., Ivanov, V.V., Lennikov, A.M., Sapin, V.I., Safronov, P.P., Oktyabrsky, R.A. and Molchanova, G.B. (1999) Native alloys of gold, copper, silver, palladium and platinum from the Kondyor alkali-ultrabasic massif. *Geodyn. Metallog.,* Vladivostok, Dalnauka (in Russ.).

Nekrasov, I.Ya., Lennikov, A.M, Ivanov, V.V., Oktyabrsky, R.A., Zalishchak, B.L. and Sapin, B.I. (1997) Unique nature museum of new and rare minerals of precious metals. *Vest.* Dal'nevostoch. Otdel. *RAN*, **3**, 135-152 (in Russ.).

Nekrasov, I.Ya, Lennikov, A.M, Oktyabrsky, R.A., Zalishchak, B.L. and Sapin, B.I. (1994) *Petrology and platinum mineralization of the alkaline-ultramafic ring complexes* (Laverov, N.P. ed.). Moscow, Nauka, 381 p. (in Russ.).

Nixon, G.T., Cabri, L.J. and Laflamme, J.H.G. (1990) Platinum-group element mineralization in lode and placer deposits associated with Tulameen Alaskan-type complex, British Columbia. *Can. Mineral.,* **28**, 503-535.

Oberthür, T., Weiser, T.W., Gast, L. and Kojonen, K. (2003) Geochemistry and mineralogy of platinum-group elements at Hartley platinum mine, Zimbabwe. Part 2: Supergene redistribution in the oxidized ´main Sulfide Zone of the Great Dyke, and alluvial platinum-group minerals. *Mineral. Depos.*, **38**, 3, 344-355.

Olivo, G.R. and Gauthier, M. (1995) Palladium minerals from the Cauê iron-mine, Itabira District, Minas Gerais, Brazil. *Mineral. Mag.*, **59**, 455-463.

Peregoedova, A. (1998) The experimental study of the Pt-Pd-partitioning between monosulfide solid-solution and Cu-Ni-siulfide melt at 900-840°C. *8th Int. Platinum Symp. (Johannesburg), Abstr.*, 325-327.

Peregoedova, A. and Ohnenstetter, M. (2002) Collectors of Pt, Pd and Rh in S-poor Fe-Ni-Cu sulfide system at 760°C: experimental data and application to ore deposits. *Can Mineral*., **40**, 527-561.

Prichard, M.H., Ixer, R.A., Lord, R.A., Maynard, J. and Williams, N. (1994) Assemblages of platinum-group minerals and sulphides in silicate lithologies and chromite-rich rocks within the Shetland ophiolite. *Can. Mineral.*, **32**, 271-294.

Pushkarev, Yu.D., Kostoyanov, A.I., Orlova, M.P., and Bogomolov, E.S. (2002) Peculiarities of the Rb-Sr, Sm-Nd, Re-Os and K-Ar isotope systems in the Kondyor massif: mantle substratum, enriched by PGE. *Reg. Geol. Metall,* **16**, 80-91, (in Russ.).

Railton, G.L. and Watters, W.A. (1990) Minerals of New Zealand. *New Zealand Geol. Surv. Bull.* **104**.

Rozhkov, I.S., Kitsul, V.I., Razin, L.V., and Borishanskaya, S.S (1962) *Platinum of Aldan Shield*. Academy of Sciences of the USSR Press, Moscow, 119 p. (in Russ.).

Rudashevkiy, N.S., Men'shikov, Y.A., Mochalov, A.G., Trubkin, N.V., Shumskaya, I.I. and Zhdanov, V.V. (1985a) Cuprorhodsite $CuRh_2S_4$ and cuproiridsite $CuIr_2S_4$ – a new natural PGE thiospinel. *Zap. VMO*, **114**, 187-195 (in Russ.).

Rudashevkiy, N.S., Mochalov, A.G., Trubkin, N.V., Shumskaya, I.I. Shkurovskiy, V.I. and Evstigneeva, T.L. (1985b) Cherepanovite RhAs – a new mineral. *Zap. VMO*, **114**, 464-469 (in Russ.).

Shcheka, G.G., Lehmann, B., Gierth, E., Goemann, K., and Wallianos, A. (2004a) Macrocrystals of Fe-Pt alloy from the Kondyor PGE placer deposit, Khabarovskiy Kray, Russia: Trace element content, mineral inclusions and reaction assemblages. *Can. Mineral.,* **42**, 601-617.

Shcheka, G.G., Vrzhosek, A.A., Lehmann, B., Tolstykh, N.D. (2004b) Associations of platinum-group minerals from the Zolotaya gold placer, Primorye, Russian Far East. *Can. Mineral.*, **42**, 583-599.

Shcheka, S.A., Ishiwatari, A. and Vrzhosek, A.A. (2001) Geology and petrology of Cambrian Khanka ophiolite in Primorye (Far East Russia) with notes on its manganese-rich chromian spinel. *Earth Science,* **55,** 265-274.

Shcheka, S.A., Vrzhosek, A.A. and Chubarov, V.M. (1990) Troctolite-cortlandite Ni-bearing formation of the Far East. *Geologia medno-nikelevykh mestorozhdeniy SSSR.* Leningrad, Nauka, 247-255 (in Russ.).

Shcheka, S.A., Vrzhosek, A.A., Sapin, V.I. and Kirukhina, N.I. (1991) Transformations of the PGM from the Primorye placers. *Mineral. Zh.* **13**, 1, 31-40 (in Russ.).

Slansky, E., Johan, Z., Ohnenstetter, M., Barron, L.M., and Suppel, D. (1991) Platinum mineralization in the Alaskan-type intrusive complexes near Fifield, N.S.W., Australia. Part 2. Platinum-group minerals in placer deposits at Fifield. *Mineral. Petrol.* **43**, 161-180.

Sushkin, L.V. (1995) Characteristic features of the native elements of the Kondyor deposit. *Tikhook. Geol.*, **14**, 97-102 (in Russ.).

Szymañski, J.T., Cabri, L.J. and Laflamme, J.H.G. (1997) The crystal structure and calculated powder-diffraction data for zvyagintsevite, Pd_3Pb. *Can. Mineral.*, **35**, 773-776.

Taylor, H.P. (1967) The zoned ultramafic complexes of southeastern Alaska. In: *Ultramafic and related rocks.* (Wyllie, P.J. ed.). J. Willey and Sons Inc. New York-London-Sydney, 97-121.

Taylor, H.P. and Noble J.A. (1969) Origin of magnetite in the zoned ultramafic complexes of southeastern Alaska. In: *Magmatic ore deposits* (Wilson, H.D.B. ed.), Econ. Geol. Monogr., **4**, 209-230.

Tolstykh, N.D. and Krivenko, A.P. (1997) Platinum-group minerals in the Inagli placer (Aldan shield). *Russ. Geol. Geophys.*, **38**, 765-774 (in Russ.).

Tolstykh, N.D., Foley, J.Y., Sidorov, E.G. and Laajoki, K.V.O. (2002) Composition of the platinum-group minerals in the Salmon River placer deposit, Goodnews Bay, Alaska. *Can. Mineral.*, **40**, 463-471.

Tolstykh, N.D., Krivenko, A.P. and Baturin, S.G. (1996) Peculiarities of the platinum composition from different PGM mineral assemblages. *Russ. Geol. Geophys.*, **37**, 3, 39-46 (in Russ.).

Tolstykh, N.D., Krivenko, A.P., Pospelova, L.N. (1997) Unusual compounds of iridium, osmium, and ruthenium with selenium, tellurium, and arsenic from the Zolotaya river placer (Western Sayan). *Zap. VMO*, **6**, CXXVI, 23-34 (in Russ.).

Tolstykh, N.D., Lapukhov, A.S., Krivenko, A.P. and Lazareva, E.V. (1999) Minerals of platinum group elements from gold placers of northeast Salair. *Russ. Geol. Geophys.*, **40**, 900-910 (in Russ.).

Tolstykh, N.D., Sidorov, E.G. and Kozlov A.P. (2004) Platinum-group minerals in lode and placer deposits associated with the Ural-Alaskan-type Gal'moenan complex, Koryak-Kamchatka platinum belt, Russia. *Can. Mineral.*, **42**, 619-630.

Tolstykh, N.D., Sidorov, E.G., Laajoki, K.V.O. Krivenko, A.P. and Podlipskiy, M. (2000) The association of platinum-group minerals in placers of the Pustaya river, Kamchatka, Russia. *Can. Mineral.*, **38**, 1251-1264.

Torres-Ruiz, J., Garuti, G., Gazzotti, M., Gervilla, F. and Fenoll Hach-Ali, P. (1996) Platinum minerals in chromitites from the Ojen lherzolite massif (Serrania de Ronda, Betic Cordillera, Southern Spain). *Mineral. Petrol.*, **56**, 25-50.

Traxel, K., Arndt, P., Bohsung, J., Braun Dullaeus, K.U., Maetz, M., Reimold, D., Schiebler, H. and Wallianos, A. (1995) The new Heidelberg proton microprobe: The success of a minimal concept. *Nucl. Instrum. Meth. Phys. Resear.*, **B104**, 19-25.

Vysotskiy, N.K. (1925) *Platinum and its mining fields.* Petrograd, 692 (in Russ.).

Wagner, P.A. (1929) *The platinum deposits and mines of South Africa.* Oliver and Boyd, London, 326 p.

Wallianos, A., Arndt, P., Maetz, M., Schneider, T. and Traxel, K. (1997) Accurate quantification resulting from precise beam monitoring and calibration. *Nucl. Instrum. Meth. Phys. Resear.*, **B130**, 144-148.

Weiser, T. and Schmidt-Thomé, M. (1993) Platinum-group minerals from the Santiago river, Esmeraldas province, Ecuador. *Can. Mineral.*, **31**, 61-73.

Weiss, S., Möckel, S. and Kolesar, P. (2002) Seltene Palladium-Mineralien und die besten Platinkristalle aus Konder, Jakutien. *Lapis*, **11,** 19-27.

Wollaston, W.H. (1809) On platina and native palladium from Brazil. *Philosoph. Transact.*, **99**, 189-194.

Yakubchuk, A. and Edwards, A. (2002) Russia's PGM potential. *Mining Jour.*, May 17, 358-359.

Yakubchuk, A. and Nikishin, A. (2004) Noril'sk-Tanakh Cu-Ni-PGE deposits: a revised tectonic model. *Mineral. Deposita*, **39**, 125-142.